

# Developmental cell lineage dynamics in Bicuspid Aortic Valve disease

Peterson, J.C.

#### Citation

Peterson, J. C. (2022, September 13). *Developmental cell lineage dynamics in Bicuspid Aortic Valve disease*. Retrieved from https://hdl.handle.net/1887/3455679

Version: Publisher's Version

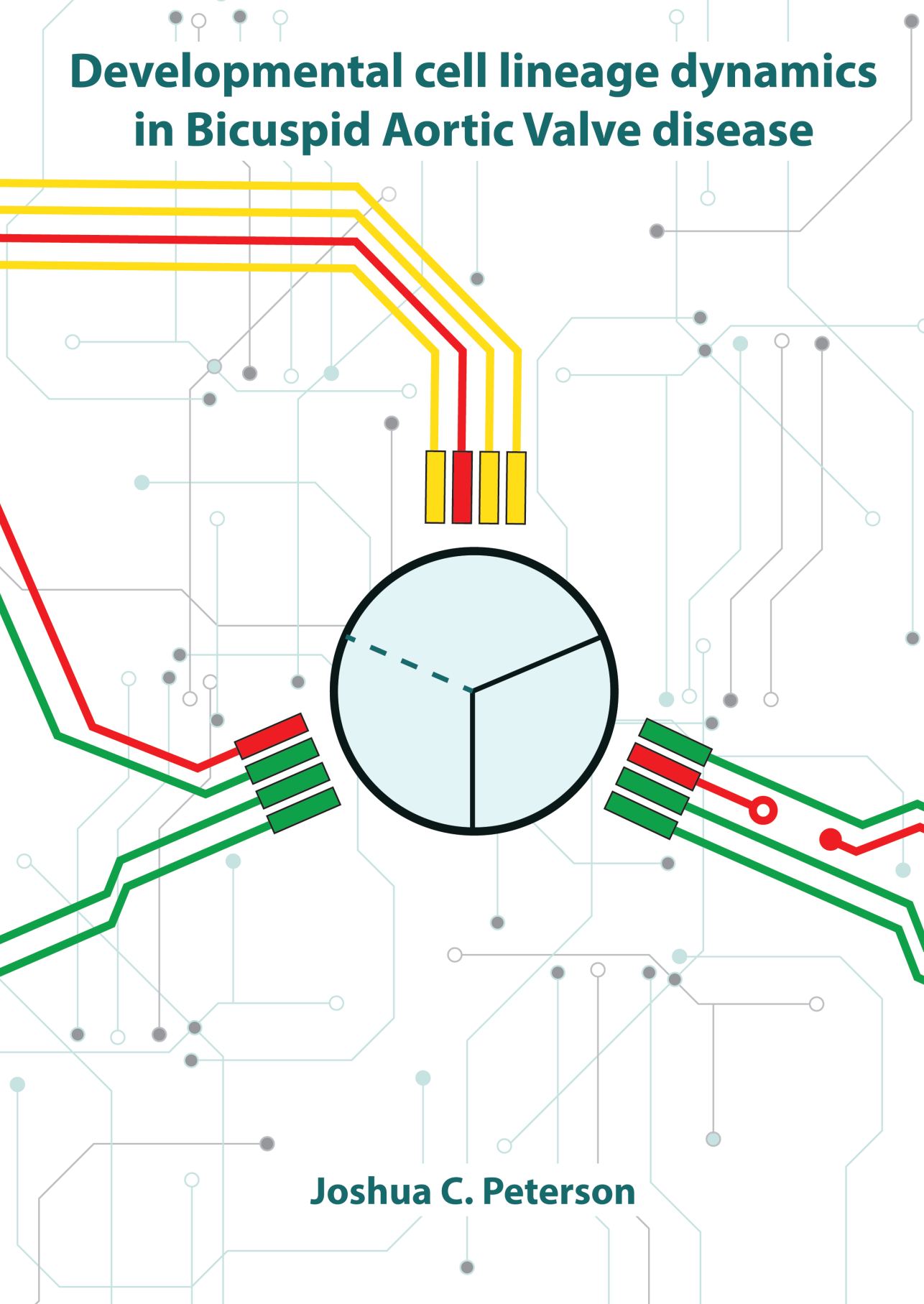
Licence agreement concerning inclusion of doctoral

License: thesis in the Institutional Repository of the University

of Leiden

Downloaded from: <a href="https://hdl.handle.net/1887/3455679">https://hdl.handle.net/1887/3455679</a>

**Note:** To cite this publication please use the final published version (if applicable).



# Developmental cell lineage dynamics in Bicuspid Aortic Valve disease

Joshua C. Peterson

Copyright © Joshua C. Peterson, 2022

All rights reserved. No part of this book may be reproduced, stored in a retrieval system, or transmitted, in any form or by any means, without the written permission of the author.

ISBN 978-94-6421-813-8

Cover design: Joshua C. Peterson

Layout: Esther Plomp-Peterson

Printing: Proefschriften.nl

# Developmental cell lineage dynamics in Bicuspid Aortic Valve disease

#### Proefschrift

ter verkrijging van de graad van doctor aan de Universiteit Leiden, op gezag van rector magnificus prof.dr.ir. H. Bijl, volgens besluit van het college voor promoties te verdedigen op dinsdag 13 september 2022 klokke 16.15 uur

door

Joshua Craiger Peterson geboren te Utrecht in 1990 **Promotor:** Prof. dr. M.C. de Ruiter

Co-promotor: Prof. dr. M.J.T.H. Goumans

Promotiecommissie:

Prof. Dr. R.J.M. Klautz

Dr. A. Alemany

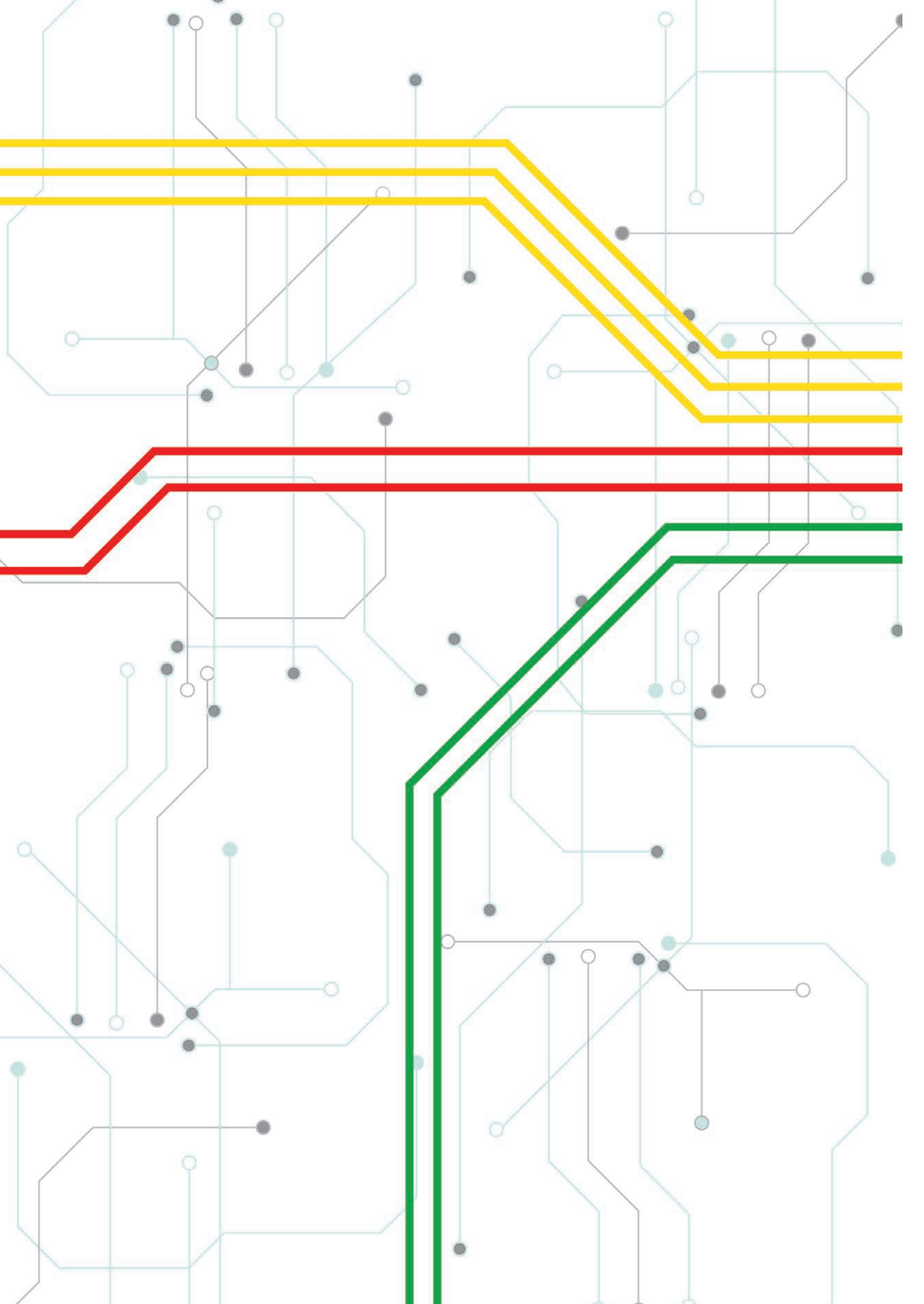
Prof. Dr. A.C. Zwijsen (Katholieke Universiteit van Leuven, België)

Prof. Dr. B. Loeys (Universiteit van Antwerpen, België. RadboudUMC, Nijmegen)

Prof. Dr. M.K. Richardson (Institute of Biology, Leiden)

## **Contents**

Introduction	7
The role of cell tracing and fate mapping experiments in cardiac outflow tract development, new opportunities through emerging technologies	19
Fluorescent Nuclei Measurements Macro (FNMM), a tool for automated cell quantification in ImageJ	49
Nos3 mutation leads to abnormal neural crest cell and second heart field lineage patterning in bicuspid aortic valve formation	57
Disturbed NO signalling gives rise to congenital bicuspid aortic valve and aortopathy	87
Pulmonary ductal coarctation and left pulmonary artery interruption; pathology and role of neural crest and second heart field during development	117
Discussion and future perspectives	141
s	148
	152
ments/Dankwoord	170
menvatting	173
ations and Curriculum Vitae	182
	in cardiac outflow tract development, new opportunities through emerging technologies  Fluorescent Nuclei Measurements Macro (FNMM), a tool for automated cell quantification in ImageJ  Nos3 mutation leads to abnormal neural crest cell and second heart field lineage patterning in bicuspid aortic valve formation  Disturbed NO signalling gives rise to congenital bicuspid aortic valve and aortopathy  Pulmonary ductal coarctation and left pulmonary artery interruption; pathology and role of neural crest and second heart field during development  Discussion and future perspectives  ments/Dankwoord  menvatting



# **Chapter 1**

Introduction

## 1.1 Background

Bicuspid aortic valve (BAV) is a congenital heart defect in which the aortic valve contains only two instead of three cusps. BAV is the most common congenital heart defect, estimated to affect 1-2% of the general population (Hoffman and Kaplan, 2002) and occurs three to four times more frequent in males than females (Kong et al., 2020). BAV can have multiple configurations depending on the fusion of the aortic leaflets (Fig. 1). As such, BAV can be classified into three categories; fusion of the right and left coronary cusps (RC/LC) (Fig. 1C) which occurs in ~60% of patients, fusion of the right and non-coronary cusps (RC/NC) (Fig. 1D) occurring in ~30% of patients, and finally fusion of the left and non-coronary cusp (LC/NC) (Fig. 1E) occurring in ~4% of patients (Fernandes et al., 2004; Sievers and Schmidtke, 2007; Sun et al., 2018). Patients with BAV have an increased risk of aortic valve stenosis, which is a result of the narrowing of the outflow tract due to insufficient opening of the aortic cusps (Aydin et al., 2013; Verma and Siu, 2014). Moreover, inadequate functioning of the aortic valves can also lead to aortic regurgitation (Braverman et al., 2005). Another complication, is the increased risk of developing a dilation in the aortic vessel known as an aortic aneurysm which can lead to aortic rupture or dissection (Fedak et al., 2002). Aortic aneurysms can develop in the thorax or the abdominal part of the aorta. Within this thesis we use the terms thoracic aortic aneurysm and aortic aneurysms interchangeably because within the context of BAV, patients are more prone to develop thoracic aortic aneurysms over abdominal aortic aneurysms than the general population (Ward, 2000; Shim et al., 2011; Aydin et al., 2013; van de Pol et al., 2017).

Whilst aortic valve stenosis and aortic regurgitation are often considered a direct result of the aberrations in aortic valve morphology, the mechanisms through which BAV affect the integrity of the aortic wall in aortic aneurysms and dissection are less well understood. Such gaps in knowledge affect clinical decision making and have direct consequences for patient management and intervention strategies. Given the unpredictable lifetime risk of acute aortic emergencies related to aortic wall pathology in BAV, there has been much debate regarding common guidelines for surgical intervention (*Boodhwani et al., 2014*; *Michelena et al., 2014*). Historically, aortopathy observed in BAV patients was treated identical to aortopathy in patients with a normal tricuspid aortic valve (TAV). However, as more research supported a strong genetic component underlying BAV-associated aortopathy, the risk of acute aortic complications was estimated substantially higher in BAV (*Fedak et al., 2005*; *Biner et al., 2009*). Such insights led to recommendations for a more aggressive surgical approach similar to guidelines for patients with Marfan syndrome (*Hiratzka et al., 2010*). More recent studies and

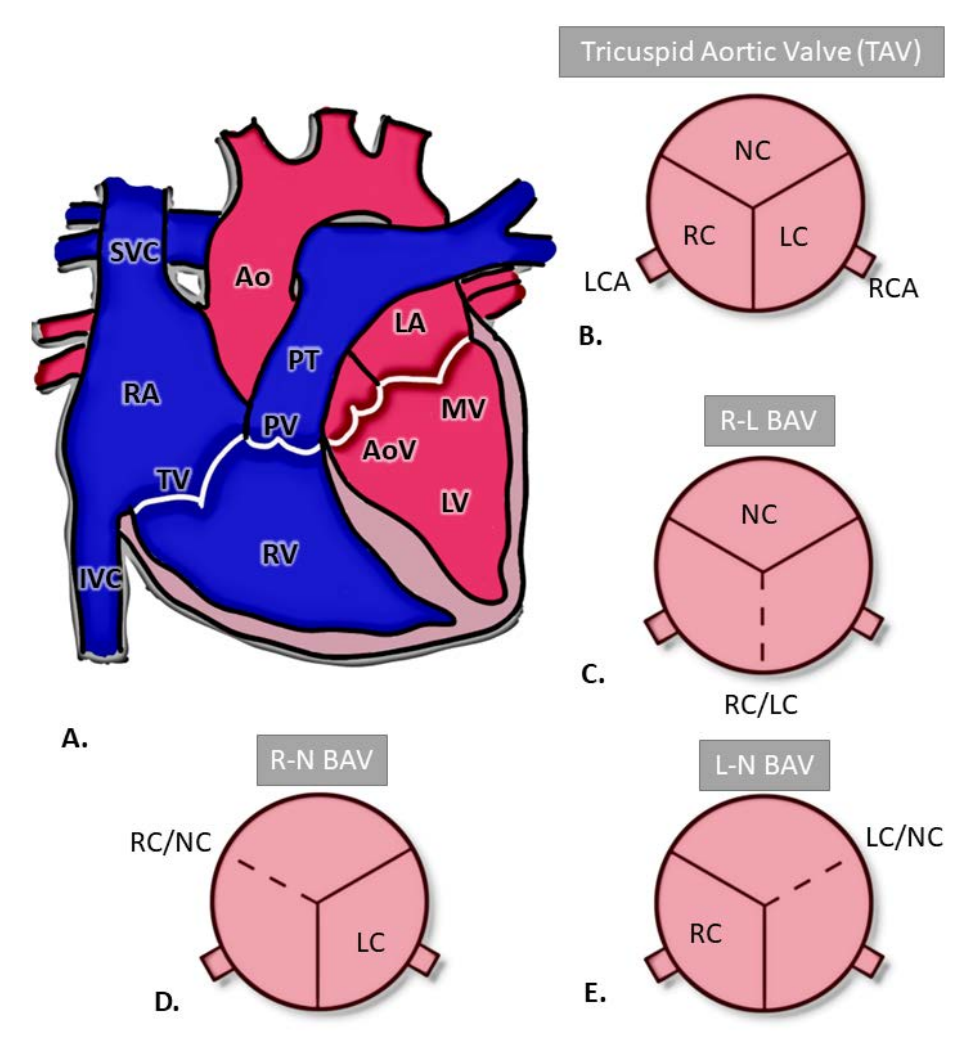


Figure 1.1 Introduction to BAV. A: A schematic overview of the human heart. Oxygen deprived blood enters the heart on the right-side (blue). After the blood passes the pulmonary circulation it returns to the heart as richly oxygenated blood from where it continues into the systemic circulation (red). B: The tricuspid aortic valve contains three aortic leaflets, the left coronary cusps (LC) is adjacent to the inlet of the left coronary artery (LCA). The right coronary cusp (RC) is positioned next to the inlet of the right coronary artery (RCA). The non-coronary cusp (NC) is third leaflet and is not situated next to any of the coronary inlets. C: Bicuspid aortic valve (BAV) subtypes can be distinguished on the location of leaflet fusion. R-L type BAV have fused leaflets of the RC and LC. D: A R-N type BAV is observed when the RC is connected to the NC. E: A L-N type BAV can be determined if the LC and the NC are fused. Abbreviations: Ao: Aorta, AoV: Aortic Valve, LA: Left Atrium, LCA: Left Coronary Artery, LC: Left Coronary Cusp, LV: Left Ventricle, MV: Mitral Valve, NC: Non-Coronary Cusps, PV: Pulmonary Valve, RA: Right Atrium, RCA: Right Coronary Artery, RC: Right Coronary Cusps, RV: Right Ventricle, PT: Pulmonary Trunk, TV: Tricuspid Valve, SVC: Superior Vena Cava, IVC: Inferior Vena Cava.

observations have led to a middle ground approach suggesting that BAV aortopathy is less dangerous than previously described, but still requires careful patient monitoring (*Itagaki et al., 2015; Sherrah et al., 2016; Borger et al., 2018; Otto et al., 2021*). Determining the underlying cause of BAV associated aortopathy is thus vital for patient risk stratification and operative management. To achieve this, a detailed understanding of the cellular mechanisms influencing the embryological development of BAV and the aorta is required.

## 1.2 Anatomy of the Human Heart

The heart is a muscular organ which main function is to pump blood with nutrients and oxygen throughout the body (Silverthorn, 2009). It consists of four chambers, four valves, coronary arteries, and the cardiac conduction system. The hearts functionality can be separated in a rightsided pulmonary circulation and a left-sided systemic circulation (Fig. 1.1A). The gatekeepers of these two circulatory systems are known as the semilunar valves which derive their name from their resemblance to a crescent moon. The human heart contains two semilunar valves which are embedded in the cardiac outflow tract. One is the pulmonary valve which connects the heart to the pulmonary trunk. The other is the agric valve which connects the heart to the aorta. The semilunar valves have the important function of maintaining unidirectional blood flow throughout the body. In healthy adults this function is regulated by the synchronized opening and closing of the three cusps (tricuspid) within each valve. When the heart contracts (systole), the ejecting blood from the chambers will drive the cusps into an open position allowing blood to flow into the connected arteries. When the heart dilates (diastole), the sudden change in pressure, enables the valves to close preventing blood in the arteries to leak back into the chambers. During a single heart beat the heart powers both the pulmonary and systemic circulation. The pulmonary circulation starts as deoxygenated blood enters the heart through the caval veins into the right atrium after which it flows into the right ventricle passing the tricuspid atrioventricular (AV) valve. Thereafter, the blood passes the tricuspid leaflets of the pulmonary valve and continues its route into the pulmonary trunk which transports the blood into the lungs via multiple pulmonary arteries. Once the deoxygenated blood passes the pulmonary circuit and the gasses (CO2/O2) have been exchanged, it returns back to the heart as richly oxygenated blood. This oxygen rich blood enters the left atrium via the pulmonary veins. After which it continues into the left ventricle through the mitral AV valve. Upon contraction of the left ventricle the blood exerts a hydrodynamic force large enough to open the aortic semilunar valve, enters the aorta, and continues its journey too supply oxygen to every tissue in the body. The heart is the first to receive oxygenated blood via the coronary arteries. Given that the aorta is the main artery of the human body, changes affecting the vessel wall integrity can have a major influence on homeostasis. A common aortic adaptation which happens during adulthood is the loss of aortic elasticity due to the stiffening of the elastic lamella within the aortic wall. Stiffening of the aortic wall will generally result in increased blood pressure which also increases cardiovascular risk (*Benetos et al., 2010; Safar et al., 2018*). Studies show that increased systemic blood pressure strongly correlates with aneurysm formation (*Kobeissi et al., 2019*) and has been linked to genetic heritability (*Biddinger et al., 1997; Albornoz et al., 2006*).

# 1.3 Cardiac embryology

#### 1.3.1 Formation of the four-chambered heart

Cardiovascular development is a complex but organized process that is highly depended on the correct proliferation, migration and differentiation of various cell types of multiple embryonic origins.

The heart originates from the anterior splanchnic mesoderm of the embryonic plate (Fig. 1.2A). During gastrulation, these mesodermal cells arise from the primitive streak and subsequently migrate cranially and laterally to form the bilateral cardiogenic plates (primary heart fields) which will give rise to the myocardial and endothelial cell lineages (DeRuiter et al., 1992; Lough and Sugi, 2000). The expression of NKX2.5 (Olson and Srivastava, 1996) and GATA4 (Laverriere et al., 1994) within the cardiogenic plates induces the differentiation of early cardiomyocytes. The fusion of the two cardiogenic plates results in the formation of the muscular primary heart tube containing an inner endothelial and outer myocardial layer (DeRuiter et al., 1992). After formation of the primary heart tube, the embryonic heart will perform a number of dynamic changes through a complex looping process. During the looping process the heart tube elongates by addition of cardiomyocytes at both poles of the tube and bends into a s-shape heart tube (Kelly and Buckingham, 2002) (Fig. 1.2B). The curves of the s-shaped heart tube form the primitive atrial and ventricular chambers (Moorman and Christoffels, 2003). These primitive chambers are connected by the atrio-ventricular canal (AVC). The regions of the AVC and the outflow tract (OFT) will develop local tissue swellings within the endocardium, a process known as cushion formation. These regionalized cushions will later develop into the atrioventricular (mitral and tricuspid) and semilunar (aortic and pulmonary) valves. The formation of a four-chambered heart is final when septation of the atria, AVC, ventricles and outflow tract is complete.

#### 1.3.2 Semilunar valve development

As the s-shaped heart tube takes shape a thick basement membrane is formed between the endothelial and myocardial layer at the regions of the OFT, aptly called "cardiac jelly". The cardiac jelly is a hydrophilic substance rich in hyaluronic acid, proteoglycans and extracellular matrix secreted by the myocardium (Eisenberg and Markwald, 1995). Moreover, the myocardial secretion of factors of the TGF $\beta$  super family, such as BMP2 and TGF $\beta$ -2, induces an endothelial to mesenchymal transition (EndMT) within the endothelial cells lining the heart tube (Ma et al., 2005; Kruithof et al., 2012). The process of EndMT results in a morphologic transition of static coble-stone endothelial cells into a mobile spindle mesenchymal cellular phenotype. The mesenchymal cells then migrate into the cardiac jelly populating the OFT cushions. Cells from other lineages such as the second heart field and neural crest cells will also migrate into the cushions resulting in further remodelling forming the septal and parietal cushions of the OFT (Fig. 1.2C). During normal development the septal and parietal cushions will fuse forming part of the aortopulmonary septum separating the aorta from the pulmonary trunk (Fig. 1.2D) and the formation of the aortic and pulmonary valve, each containing 3 leaflets. As the leaflets mature into cusps, three distinct layers become distinguishable within each leaflet, the collagen-rich fibrosa located at the apical (arterial) side of the valve, a spongiosa middle layer composed of fibroblasts, mesenchymal cells, and a mucopolysaccharide-rich matrix, and located at the basal (ventricular) side of the valve is the ventricularis which is high in elastin. These layers provide tensile strength and flexibility to the valves (Freeman and Otto, 2005).

### 1.3.3 Cell lineages contribution to the cardiovascular OFT

#### The First and Second Heart Field

The first heart field (FHF) is an embryonic region located near the cardiac crescent (*Zaffran and Kelly, 2012; Später et al., 2013*). The cells of the FHF form the earliest cardiac progenitor cell population to be observed during development. The cells of the second heart field (SHF) are the second wave of cardiac progenitor cells to form (*Waldo et al., 2001; Kelly, Brown and Buckingham, 2001; Mjaatvedt et al., 2001*). The SHF progenitors are located posteriorly to the heart tube in the pharyngeal mesoderm. The FHF contributes to the formation of the myocardium of the left ventricle and atrial appendages, with a minor contribution to the right ventricle whilst the second lineage gives rise to the myocardium of the OFT, right ventricle, and the posterior wall of the atria, corresponding to SHF-derived parts of the heart (*Meilhac et al., 2004*).

During development, the SHF lineage is multipotent and does not only provide cardiomyocytes

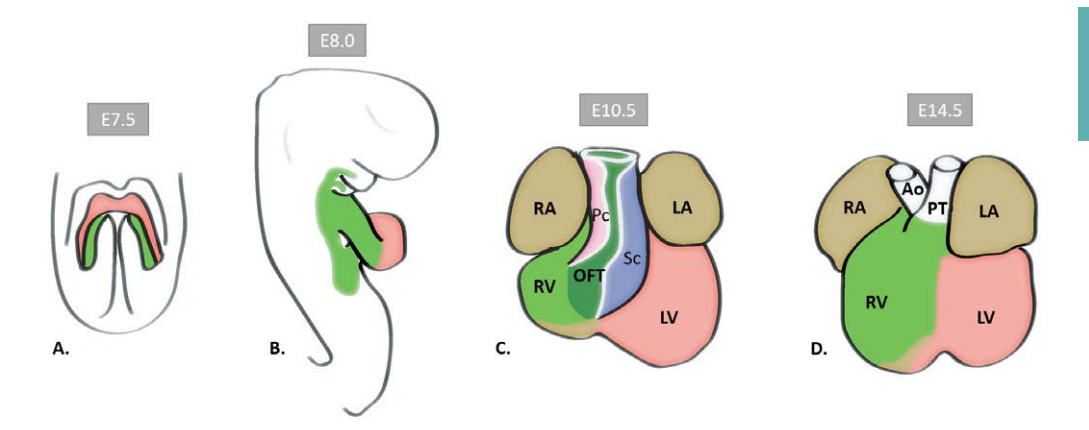


**Figure 1.2 Murine Embryonic Heart development. A**: During heart development early cardiac progenitor populations can be distinguished as cells of the first heart field (red) and second heart field (green). **B**: During the formation of the heart tube the FHF contribute to the formation of the future left ventricle. The SHF cells are added to both poles of the elongating heart tube. As a result the SHF will contribute to the development of the cardiac atria, the right ventricle and the outflow tract (OFT). **C**: At E10.5 the left ventricle is primarily derived from cells of the FHF whilst the right ventricle is mostly derived of SHF cells. At this stage the aorta and pulmonary trunk still share a common outflow tract and two outflow tract cushions, the parietal (pink) and septal cushions (blue) will accommodate cells of endothelial, neural crest and SHF lineages during outflow tract septation. **D**: At E14.5 the process of outflow tract septation is completed. Abbreviations: Ao: Aorta, LA: Left Atrium, LV: Left Ventricle, OFT: Outflow Tract, Pc: Parietal Cushion, Sc: Septal Cushion, PT: Pulmonary Trunk, RA: Right Atrium, RV: Right Ventricle.

(Waldo et al., 2001; Kelly, Brown and Buckingham, 2001; Zaffran et al., 2004) but also contributes to the smooth muscle cells located at the base of the aorta and pulmonary trunk (Waldo et al., 2005; Sun et al., 2007; Sawada et al., 2017) and the valvular interstitial cells within the aortic and pulmonary valves (Eley et al., 2018; Lioux et al., 2020).

#### The endothelial cells

A crucial step for valve development is the formation of endocardial cushions. Studies examining OFT formation describe the formation of regional swellings filled with cardiac jelly between the myocardial wall and the endothelial lining (*Mjaatvedt and Markwald, 1989; Eisenberg and Markwald, 1995; Schroeder et al., 2003*). Endothelial cells lining the cardiac cushions will undergo and populate the aortic cushions. These endothelial derived mesenchymal cells form the bulk of the valvular tissue within the semilunar valve leaflets (*Eisenberg and Markwald, 1995; Sugishita, Watanabe and Fisher, 2004*).

#### The cardiac neural crest cells

The neural crest is a population of multipotent progenitors originating from the neural fold in the region of the otic placode and the posterior border of somite 3 (*Keyte and Hutson, 2012; Keyte, Alonzo-Johnsen and Hutson, 2014*). Early lineage tracing studies using chick-quail models were the first to notice the contribution of the neural crest lineage to the cardiovascular system (*Kirby, Gale and Stewart, 1983; Le Douarin, 2004*). During development the neural crest cells (NCCs) migrate from the neural fold over the arterial arches into to the arterial pole of the heart and induce outflow tract remodelling. The NCCs contribute to the aortopulmonary valves, arterial wall, cardiac ganglia and the aortopulmonary (AP) septum (*Bergwerff et al., 1998; Poelmann, Mikawa and Gittenberger-De Groot, 1998; Waldo et al., 1998*). The AP septum divides the embryonic common arterial trunk into the pulmonary artery and aorta (*Waldo et al., 1998, 1999*). Later lineage tracing studies using the Cre-LoxP system to genetically label the NCCs and its derivatives further substantiated the intricate role of NCCs in mammalian heart development (*Jiang et al., 2000*).

## 1.4 Aortopathy and BAV: a common origin

BAV was historically interpreted as an anomalous congenital variation limited to effect valvular morphology (*Pomerance*, 1972; *Boudoulas*, 2003). Current studies suggested BAV to be a more complex disorder of which the effects are not limited to valvulogenesis (*Ward*, 2000). Evidence suggests that BAV disease could also directly and/or indirectly affect the integrity of the aorta and connected cardiac structures (*Loscalzo et al.*, 2007; *Rajan Jain et al.*, 2011; *Grewal et al.*, 2014). BAV patients were shown to have, throughout their lifetime, an increased risk of developing serious complications, including sudden cardiac death, severe aortic valve dysfunction, endocarditis, aortic aneurysm or dissection and left ventricular dysfunction (*Siu and Silversides*, 2010; *Michelena et al.*, 2011; *Laforest and Nemer*, 2012; *Mordi and Tzemos*, 2012). Most notable in BAV patients are the nonvalvular complications that occur in up to 50% of adults with BAV of which the most common abnormality is a dilation of the aortic root and the thoracic aorta (*Siu and Silversides*, 2010; *Michelena et al.*, 2011; *Mordi and Tzemos*, 2012).

Based on pedigree analysis and familial clustering of BAV patients, researchers suspected a genetic basis for the development of BAV. These early genetic linkage studies found increased prevalence of BAV in patient family members compared with the general population supporting a heritable component of the disease (*Emanuel et al., 1978; Huntington, Hunter* 

and Chan, 1997; Cripe et al., 2004). With the advances in DNA sequencing technologies many gene mutations have been found causal to BAV. Development of knockout murine models allowed for the study of familial BAV. Humans and mice with genetic defects in the TGF-β/BMP signalling pathway such as Smad6 (Gillis et al., 2017) and Alk2 (Thomas et al., 2012) affect the endothelial cell lineage through defects in EndMT resulting in BAV. Patients with defects in genes related to cardiac progenitors such as Nkx2.5 (Qu et al., 2014), Gata4 (Li et al., 2018) Gata6 (Xu et al., 2018) are also known to develop BAV. Similar to these patients, mice with defects in SHF derived lineages such as Gata5 (Laforest, Andelfinger and Nemer, 2011) and Gata6 (Xu et al., 2018) also develop BAV. Moreover, genetic alterations affecting NCC lineages such as Krox20 (Odelin et al., 2017), Pax3 (Rajan Jain et al., 2011), or Hoxb1 (Zaffran et al., 2018) have also been shown to give rise to BAV in mice. Genetic defects affecting these early cardiac lineages may not only affect formation of the aortic valve but also affect development of other cardiac components derived from these same cell lineages (Grewal et al., 2014).

BAV and associated thoracic aortic aneurysms are thought to be manifestations of a common genetic defect. This is supported by observations that BAV patients tend to have a more progressive dilation of the ascending aorta than TAV patients, even after aortic valve replacement (Russo et al., 2002; Yasuda et al., 2003). Moreover, children and young adults with BAV seem predisposed to develop aortic complications as these have larger aortic dimensions of the root and the ascending aorta in conjunction with reduced elastic properties of the aortic vessel wall when compared to children with TAV (Nistri et al., 1999; Basso et al., 2004; Oulego-Erroz et al., 2013; Blais et al., 2020). First degree relatives of BAV patients (with normal functioning TAVs) have an increased likelihood of developing aortic dilations as well as abnormal elastic properties in the aortic wall (Biner et al., 2009). BAV disease is also known to coexist with other congenital vascular defects with cells of common developmental origin; such as coarctation of the aorta. Of all patients diagnosed with coarctation of the aorta, approximately 50% to 75% also have BAV (Sinning et al., 2018). Moreover, BAV is also associated with and genetically related to hypoplastic heart syndrome. There are a number of syndromes whose cardiac involvement includes BAV such as Williams syndrome with supravalvular stenosis, Shone's syndrome with inflow and outflow obstructions, Jacobsen syndrome with various left sided heart lesions and Turner syndrome with coarctation of the aorta and aortic arch abnormalities. Other cardiac malformations that have been associated with BAV include ventricular septal defects (Duran et al., 1995), patent ductus arteriosus (Gelb et al., 1999; Quintero-Rivera et al., 2015), and atrial septal defects (Hor et al., 2008) suggesting extensive genetically induced cell lineage aberrations originating during cardiac development as a basis for BAV related complications.

## 1.5 Thesis Outline

The aim of the research described in this thesis is to advance our current understanding of the impact and mechanisms underlying congenital BAV and BAV related aortopathy. We anticipate that better understanding of congenital BAV could explain the increased susceptibility of aortopathy in patients with BAV and could contribute to the identification of novel parameters to more accurately determine patient risk stratification.

In **Chapter 2** we provide an extended overview of general recognized lineage tracing methodology. Given the large implications of lineage tracing experiments to our current understanding of heart development, this chapter aims to elucidate the technical advances and limitations of cell lineage tracing methods with respect to their roles in cardiac outflow tract development. Here we will address current challenges and discuss emerging opportunities for this field of study.

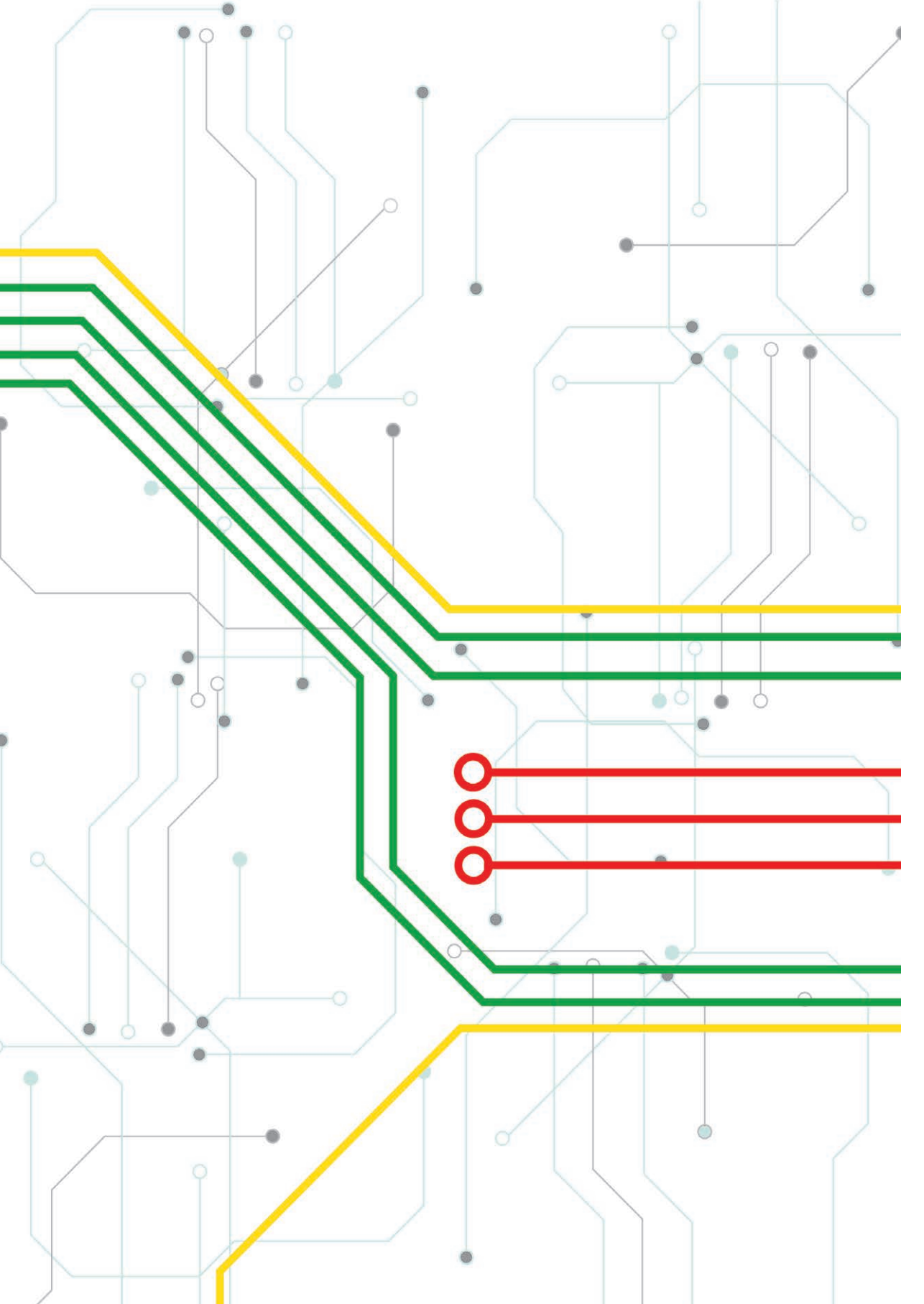
To effectively study cell lineage contributions, a method was required to examine cellular contribution. In **Chapter 3** we demonstrate an analysis method based on fluorescent markers within the boundaries of the tissue of interest. During our studies we developed a method for efficient analysis of cellular contribution using an image analysis pipeline specific to immunofluorescent stained tissues sections.

BAV has been described to result from defects in cushion tissue formation within the outflow tract during development. In **Chapter 4** we explore the formation of BAV in our *Nos3* mutant model and study the contribution of endothelial, neural crest, and second heart field cell lineages to the aortic valve throughout embryonic development. We aimed to identify congenital cell lineage aberrations to that could elucidate the critical processes required for proper valve formation.

In **Chapter 5** we dive deeper in the phenotypical implications of the anomalous cell lineage contributions to the cardiac outflow tract. Observations in BAV patients suggest the possibility of genetic predisposition for BAV related aortopathy. This study aims to examine the role of *Nos3* deficiency on the cell lineages that contribute to the formation of the aortic vessel wall. The dynamics of the neural crest cells and second heart field derived smooth muscle cells is important to cardiac development and formation of the great arteries.

In **Chapter 6** we examine the role of neural crest and second heart field lineages in the formation of pulmonary ductal coarctation and left pulmonary artery interruption.

**Chapter 7** contains a general discussion addressing the current challenges in BAV research within the context of the chapters presented in this thesis, and an outlook on future perspectives.



# Chapter 2

The role of cell tracing and fate mapping experiments in cardiac outflow tract development, new opportunities through emerging technologies

2021

DOI: 10.3390/jcdd8050047

**Journal of Cardiovascular Development and Disease** 

Software: https://github.com/J-PTRson/Cell-Image-Analysis/tree/master/FNMM

Joshua C. Peterson<sup>1,†</sup>, Tim P. Kelder<sup>1,†</sup>, Marie José T.H. Goumans<sup>2</sup>, Monique R.M. Jongbloed<sup>1,3</sup>,

Marco C. DeRuiter<sup>1</sup>

<sup>1</sup>Department Anatomy & Embryology, Leiden University Medical Center, Leiden, The Netherlands <sup>2</sup>Department Cellular and Chemical Biology, Leiden University Medical Center, Leiden, The Netherlands <sup>3</sup>Department of Cardiology, Leiden University Medical Center, Leiden, The Netherlands

† These authors contributed equally to this work

#### **Abstract**

Whilst knowledge regarding the pathophysiology of congenital heart disease (CHDs) has advanced greatly in recent years, the underlying developmental processes affecting the cardiac outflow tract (OFT) such as bicuspid aortic valve, tetralogy of Fallot and transposition of the great arteries remain poorly understood. Common among CHDs affecting the OFT, is a large variation in disease phenotypes. Even though the different cell lineages contributing to OFT development have been studied for many decades, it remains challenging to relate cell lineage dynamics to the morphologic variation observed in OFT pathologies. We postulate that the variation observed in cellular contribution in these congenital heart diseases might be related to underlying cell lineage dynamics of which little is known. We believe this gap in knowledge is mainly the result of technical limitations in experimental methods used for cell lineage analysis. The aim of this review is to provide an overview of historical fate mapping and cell tracing techniques used to study OFT development and introduce emerging technologies which provide new opportunities that will aid our understanding of the cellular dynamics underlying OFT pathology.

#### 2.1 General introduction

The development of the cardiac outflow tract, a region of the heart connecting the ventricles to the great arteries of the heart, has been studied for more than a century (*Thompson*, 1907). Cellular lineage tracing experiments laid the foundation for our knowledge regarding congenital heart disease. Whilst major progress has been made and CHDs as a whole are understood increasingly better, the degree of understanding varies greatly among the individual congenital defects. CHDs affecting the OFT like bicuspid aortic valve, tetralogy of Fallot, transposition of the great arteries, double outlet right ventricle and pulmonary atresia are well known disorders yet it remains challenging to explain such morphological emergences with our current models of OFT development. Common among many of these congenital diseases is a broad phenotypical variation arising from a singular genetic deficiency. Murine knockout models used to study such aforementioned CHDs, such as *Notch1* (*Garg et al.*, 2005), *Gata5* (*Laforest, Andelfinger and Nemer, 2011*) and *Nos3* (*Peterson et al.*, 2018) mutant mice, have been known for their incomplete penetration, yet any agreement addressing such phenotypical variation remains elusive. Whilst lineage tracing studies have contributed significantly to our understanding of a particular cell type heritage, it still falls short to explain, how a cell's lineage

primes cellular behaviour to allow for proper cell adaptation (such as cell maturation) upon environmental cues. Epigenetic modification of chromatin have been described to affect gene expression and could act to consolidate directional developmental gradients (*Perino and Veenstra*, 2016; *Klemm*, *Shipony and Greenleaf*, 2019). As such a cell's identity may arise not only from a genetic component but from a combination of expressed genes and cell lineage epigenetic signatures (*Fisher*, 2002).

A single genetic mutation could give rise to multiple phenotypical outcomes if the imprinted epigenetics are dissimilar among cell lineages (*Peaston and Whitelaw, 2006*). Currently we are limited in our understanding about the role of cell identity in CHD. However given that a cell's identity is highly plastic (*Merrell and Stanger, 2016*), understanding the role of the identity of a cell might explain the broad phenotypical variation observed in these congenital heart diseases and could aid with disease risk stratification. Lineage tracing experiments built the foundation of our current understanding and new developments in methods could provide more detailed definitions of cell types and cell lineage dynamics to better explain how aberrant cell behavior contributes to the multivariate phenotypes seen in CHD.

### 2.1.1 Basic cardiac development and anatomy of the OFT

The heart is formed from the anterior splanchnic mesoderm of the embryonic plate. During gastrulation, mesodermal cells arise from the primitive streak, and migrate cranially and laterally to the notochord to form the cardiogenic plates expressing NKX2.5 (Olson and Srivastava, 1996) and GATA4 (Laverriere et al., 1994). The first sign of cardiomyocyte differentiation is seen in this region at Hamburger and Hamilton (HH) stage 8-9 in chick and between embryonic day (E) 6.5-7.5 in mice, when cardiac troponin-I (cTnI) and sarcomeric myosin (MF20) are first detected. Fusion of the bilateral plates of splanchnic mesoderm establishes the primary heart tube (PHT), that shows peristaltic contraction at 3 weeks of development in a human, E8.0-8.5 in mouse and HH stage 10-11 in chick embryos (DeRuiter et al., 1992; Buckingham, Meilhac and Zaffran, 2005; Abu-Issa and Kirby, 2007; Tyser and Srinivas, 2020). During further development, cells from the splanchnic mesoderm differentiate into cardiomyocytes and are added to the PHT. The splanchnic mesoderm that gives rise to the cardiomyocytes of the cardiac crescent and PHT is called the first heart field (FHF). The FHF will contribute to part of the atria, atrioventricular canal (AVC), inlet of the right ventricle and left ventricle (Buckingham, Meilhac and Zaffran, 2005). In the next phase of heart formation, cells are added to specific structures at the venous (atrial septum and smooth myocardial wall of the atrium) and arterial poles (outflow tract and the

right ventricle). These cells are considered to be derived from a distinct cardiogenic field, the second heart field (SHF) (Buckingham, Meilhac and Zaffran, 2005). How the distinction between FHF and SHF is related to the ultimate phenotype of the left and right ventricular myocardium is an intriguing guestion, but is not the focus of this review. The addition of cells at the arterial and venous poles initiates the process of cardiac looping, the transformation of the linear heart tube into an S-shaped heart tube with primitive ventricular and atrial chambers (Moorman and Christoffels, 2003). These primitive chambers are connected by the AVC. In the AVC and the OFT, the myocardium secretes cardiac jelly, a hydrophilic substance rich in hyaluronic acid, proteoglycans and extracellular matrix. This results in the formation of localized swellings called the endocardial cushions acting as primitive valves, aiding in maintaining unidirectional flow in the heart tube (Kirby, 2007; Combs and Yutzey, 2009). The endocardial cushions of the OFT mature into aortic and pulmonary valves through contribution of cell lineages of neural crest (Waldo et al., 1998; Jiang et al., 2000), endothelial (Eisenberg and Markwald, 1995; Kisanuki et al., 2001) and second heart field cells (Zaffran and Kelly, 2012; Eley et al., 2018; Mifflin et al., 2018), but are also crucial to the development of the interventricular septum (Kirby, 2007; Miguerol and Kelly, 2013). The separation of the aorta and the pulmonary trunk is the result of OFT septation. During OFT septation, extracardiac neural crest cells migrate into the endocardial cushions forming a central mass of condensed mesenchyme, resulting in an aortopulmonary septum followed by invagination of cardiomyocytes. The rotation and elongation of the aortic and pulmonary orifices is the result of the pulmonary push driven by cells of the second heart field lineage (Scherptong et al., 2012). OFT septation is completed when the aortic orifice connects to the left ventricular outflow tract whilst the pulmonary orifice remains connected above the right ventricle (Gittenberger-De Groot et al., 2005). In addition to cardiac growth, several processes, including the outgrowth and remodelling of the different chambers, coronary artery development, and formation of the cardiac conduction system, will establish the mature electro-mechanically functional 4-chambered heart with separated pulmonary and systemic circulations (reviewed in Gittenberger-de Groot et al., 2013, 2014).

### 2.1.2 OFT Development

The OFT can first be observed between E8.0-E8.5 in mice and week 3 of development in humans during formation of the PHT where it connects the primitive ventricle with the aortic sac. During cardiac looping the OFT elongates and remodels forming the OFT cushions. Aortopulmonary septation occurs at the level of: 1. the great arteries; 2. the valvular level and 3. of the outflow tract (*Bartelings and Gittenberger-de Groot, 1991*).

The aortopulmonary septum is formed by contributions of neural crest cells and second heart field cells (*Kirby, Gale and Stewart, 1983; Poelmann, Mikawa and Gittenberger-De Groot, 1998; Poelmann et al., 2017*). The initially unseparated vascular part of the outflow tract is called the aortic sac. For adequate separation of the different levels of the developing outflow tract, development of the aortopulmonary septum and adequate fusion of the outflow cushions are mandatory (*Anderson et al., 2014*). Neural crest cells will be positioned at the level of the aortic sac, as well as in the condensed mesenchyme of the septal outflow tract cushion at and below the orifice level (*Gittenberger-de Groot et al., 2002*). As a result of this process, separation of the aortic sac will extend from the arterial orifice level (i.e. the level of the developing arterial valve) to the myocardial outflow tract.

The aortopulmonary septum will gradually separate the common aortopulmonary trunk into the aorta and pulmonary trunk. At the valvular level this process will also separate the OFT cushions at the aortic and pulmonary orifices giving rise to the semilunar valves. Later the coronary arteries will grow into the aortic sinuses of Valsalva and the myocardial and smooth muscle components of the OFT will mature.

Historically, the developing OFT has been studied using classical light microscopy, histological staining and electron microscopy (*Davis*, 1927; *DeHaan*, 1963; *DeRuiter et al.*, 1992). A comprehensive basis providing insight in OFT development was founded using these techniques. Unfortunately, as cells undergo intrinsic and phenotypical changes during development, analysing the developmental origin of the OFT was not possible using these early methods. To examine cell lineage development, several techniques such as genetic tracing and vital dye labelling of cells have been developed. Extensive lineage tracing experiments examining OFT morphogenesis have revealed an important role for multiple cell types and signaling pathways in OFT development.

# 2.2 Cell tracing techniques applied to OFT development

In the next section, the different techniques used to study OFT development will be described briefly. The main focus of this section will be to review fate mapping experiments that contributed to our current understanding of OFT development.

#### 2.2.1 Vital dye and viral labelling experiments

With vital dye it is possible to directly label clusters of cells. This method is widely used in developmental biology in several species, and has provided essential information on the developmental origin of the OFT.

# Basics of vital dye and viral labelling experiments during heart development

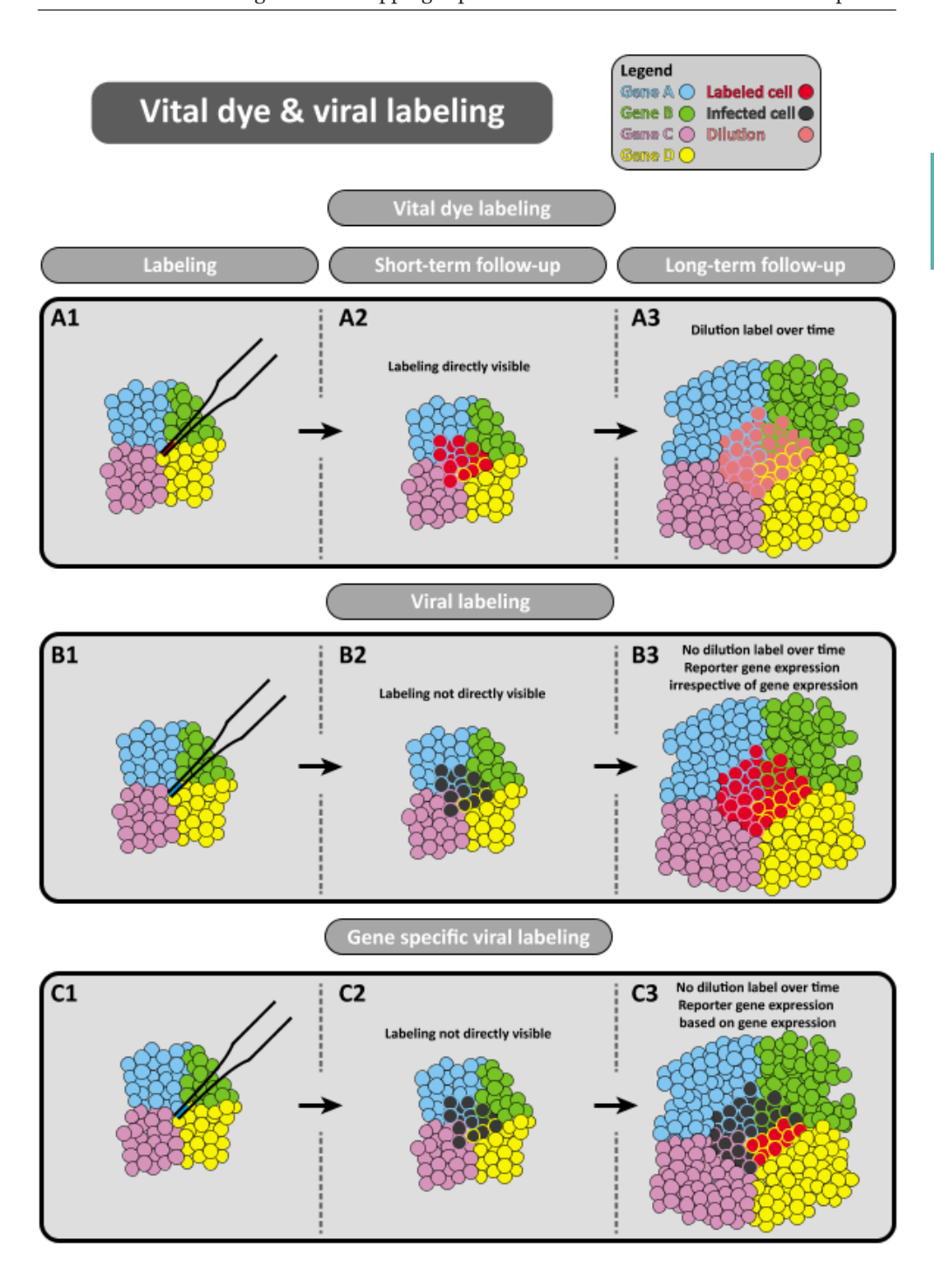
Labelling of cells is performed with a glass capillary mounted to micromanipulators, and a pneumatic micro-injector to inject small amounts of dye or virus in the region of interest.

Vital dye labelling is performed with lipophilic dyes, such as dil-C18-(3) (*Axelrod, 1979*), which can label distinct cell compartments (**Fig. 2.1A**) (*Kelder et al., 2015*). Commercial dyes are available in different colours, which enables simultaneous labelling of different clusters of cells and studying the direction of migration and potential intermingling of different cell clusters. Viral labelling experiments are aimed at induction of reporter gene expression in specific regions of the embryo. This technique utilizes the ability of retroviruses to infect the cell and to incorporate its genome in the genome of the infected cell (*Sanes, Rubenstein and Nicolas, 1986; Price, Turner and Cepko, 1987; Sanes, 1989*). Retroviral vectors driving the expression of a reporter gene (such as *LacZ*) enable cell tracing of the infected cells (**Fig. 2.1B**). More targeted viral tracing can be performed by placing expression of the reporter gene under the transcriptional control of a cell type specific promoter, which enables tracing of cells that express the gene of interest (**Fig. 2.1C**) (*Pacak and Byrne, 2011*).

## Advantages of vital dye labelling experiments

With physical labelling of a progenitor pool, it is possible to select that specific group of cells based on location and to time the exact moment of labelling. An important advantage of this technique is the opportunity to select a cluster of cells without prior knowledge of the cell type. Performing physical labelling experiments is relatively cost efficient and easy, especially

**Figure 2.1 Vital dye and viral labeling techniques. A**: Lipophilic dyes are used to visualize and track distinct cell compartments over time. **B**: Alternatively, retroviral vectors can allow for expression of a reporter gene (such as LacZ) to enable cell tracing of infected cells. **C**: Placing the reporter gene under the transcriptional control of a cell specific promoter allows for increased accuracy in targeting cells through gene specific viral labelling.



in chick, fish and amphibian embryos. Furthermore, labelling can be combined with other microsurgical procedures.

#### Limitations of vital dye and viral labelling

To perform microinjection of minute quantities of either vital dye or viral constructs, the embryo needs to be physically accessible to the researcher. For this reason most labelling experiments examining heart development using micro-injections have been performed in oviparous vertebrates, such as zebrafish (*Stainier, Lee and Fishman, 1993*), xenopus (*Krotoski, Fraser and Bronner-Fraser, 1988*), and chick embryos (*de la Cruz et al., 1977; Kelder et al., 2016*). For use in mice, it is first necessary to extract the embryo from the uterus, followed by reincubation in culture medium, for example in rolling bottles (*Domínguez et al., 2012*).

Physical labelling experiments require a progenitor population of interest to study. Knowledge about the location of a possible progenitor pool is required to correctly target these cells. Moreover, when targeting a progenitor population, the lineage trace is limited to cells solely derived from that original cluster. This complicates examining structures derived from multiple progenitor clusters because non-labelled cell contributions could be interpreted as inefficient labelling.

Furthermore, physically labelling cells is relatively invasive and manipulation of the embryo may induce developmental defects. It is therefore necessary to carefully select embryos that show no macroscopic abnormalities and to include control embryos. Toxicity of the dyes itself appears to be negligible (*Honig and Hume, 1986; Progatzky, Dallman and Lo Celso, 2013*).

With viral labelling, there is random integration of the viral genome in the host cell's DNA, which could result in damage or abnormal functioning of the infected cell (*Buckingham and Meilhac*, 2011). Leakage of dye or infection of cells in the vicinity of the designated progenitor pool could result in incorrect interpretation regarding the fate of the progenitor cell population. It is therefore essential to evaluate the location of dye directly after administration in great detail (*Bressan*, *Liu and Mikawa*, 2013; *Kelder et al.*, 2015). Histological evaluation of embryos directly after labelling is crucial, but this also terminates lineage tracing in those embryos. Live-imaging of vital dyes (*Sipkins et al.*, 2005; *Lo Celso et al.*, 2009; *Progatzky*, *Dallman and Lo Celso*, 2013) could help to minimize this limitation. Furthermore, delay in reporter gene expression with viral labelling omits direct evaluation of the location of labelling. In addition, efficiency of reporter

gene expression in the desired cells has to be tested prior to ascertain activation of expression in the specific cell type within the animal model (i.e. species differences in expression levels in specific cell types). Rapid cell division in early embryos results in dilution of the vital dyes, which complicates long-term follow-up of the labelled cells (*Honig and Hume, 1989*). The extent of dilution is dependent on the rate of proliferation and the amount of dye administered, which therefore necessitates titration of the dye with every new experiment. With retroviral labelling, integration of the reporter gene in the host cell's DNA results in stable and high expression of the reporter gene in the daughter cells (*Mikawa et al., 1996*), which overcomes the problem of dilution. Therefore, a disadvantage of vital dye labelling is dilution, whilst the possibility of direct evaluation after labelling is an important advantage. The opposite is true for viral labelling, where direct evaluation is not possible, but dilution of dye does not occur after stable integration of the viral vector. Therefore, a possible solution to overcome these limitations is to combine vital dye labelling with viral labelling. Finally, to perform viral labelling experiments, advanced biosafety laboratories are crucial to safely perform experiments with potentially hazardous viral constructs.

# Vital dye and viral labelling experiments aimed at understanding OFT development

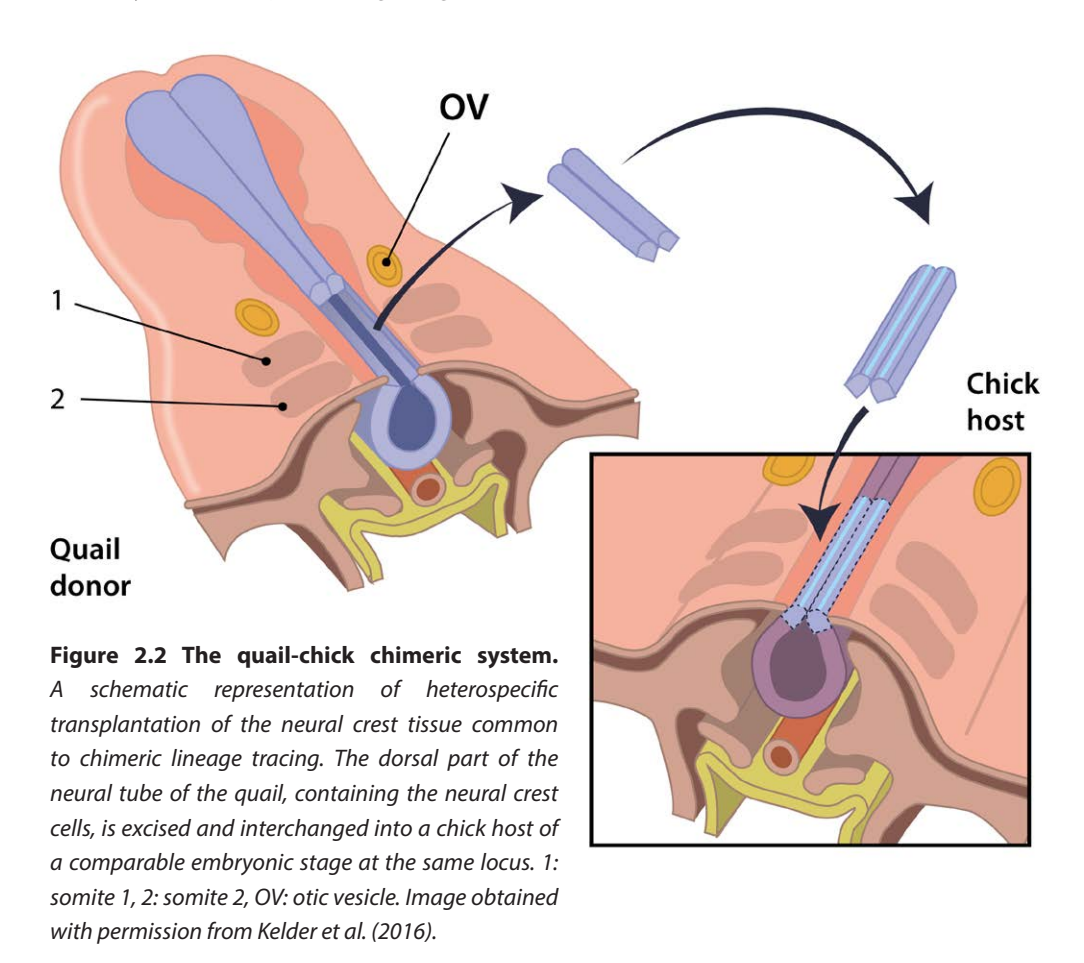
Studies performing dye injected lineage tracing have aided in understanding heart development by carefully fate mapping groups of cardiac precursor cells (*Schaefer et al., 2004*; *Barbosky et al., 2006*). Prior to the concept of vital dye lineage tracing descriptive embryological studies in the early 20<sup>th</sup> century examining human embryos postulated the concept of the primitive cardiac cavities (*Davis, 1927*). These primitive cardiac cavities where demarcated by local folds. Using these folds as fixed borders, the outgrowth of cardiac structures such as the development of the atria and ventricles could be described. The introduction of vital dye injected lineage tracing pioneered by de la Cruz refuted the concept of primitive cardiac cavities and showed that structures such as the primordium of the trabeculated portion of the right ventricle could be determined at the straight heart tube stage prior to the formation of primitive cardiac cavities (*de la Cruz et al., 1977*).

## 2.2.2 Lineage tracing using the quail-chick chimeric system

The use of chimeric models is an alternative lineage tracing approach as compared to the previous mentioned vital dye injections. The quail-chick chimeric system proved a vital tool for understanding cell lineage development.

#### Basics of the quail-chick chimeric system.

The quail chick chimera system was devised in 1969 (*Le Douarin, 1969, 1973, 2004*). In the quail-chick chimera system a subset of cells derived from quail, i.e. cells of the neural fold, are transplanted in stage-matched chick embryos (or vice versa) (**Fig. 2.2**). As a result, the quail derived cells develop into functional tissues resulting in viable chimeric quail-chick offspring. The quail-chick marker system relies on the differences in heterochromatic DNA in the nuclei of chick and quail. With the use of a nuclear Feulgen staining or a donor specific antibody (*Selleck and Bronner-Fraser, 1995*) distinction could be made between host and donor cells, allowing researchers to study embryonic development at later stages as compared to vital dye labelling. Besides the quail-chic chimeric system, xenopus hybrids were also used to study early stages of embryonic development (*Koga, Kageura and Yamana, 1986*).



#### Advantages of the quail-chick chimeric system.

The quail-chick chimera system allows for cell lineage tracing using the genetic footprint of the host cells. As a result, this method of lineage tracing results in a permanent change through which chimeric models overcome the limitation of vital dye dilution mentioned previously. Therefore, chimeric systems allow researchers to examine a specific cell population for longer time periods as compared to injecting cells with vital dyes. Moreover, whilst vital dyes may suffer from dye leakage during injection, chimeric models have no such issues. Another advantage of chimeric models is that it enabled researchers to perform in-vitro cell manipulation prior to transplantation.

#### Disadvantages of the quail-chick chimeric system

Similar to vital dyes, chimeric models require physical access to an embryo favouring oviparous vertebrates over mammalian embryos. Nevertheless, lineage tracing through cell transplantation has often been applied in mice studies examining multilineage differentiation through bone marrow transplantation in irradiated mice but also to study early mammalian development through injection of cells in the developing morula (*Tam and Rossant, 2003*). Moreover, with the recent developments in stem cell biology the study of heart development using mice-rat chimeric models could lead to new insights (*Sereti et al., 2018*). In contrast to vital dye injections, in chimeric models a graft versus host rejection may occur in postnatal studies. Another challenge when making interspecies grafts is the need to perform microsurgery on two stage-matched embryos increasing the experimental complexity. Moreover, chimeric models are generally best used when cells are transplanted superficially, such is the case with cells of the spinal cord or epicardium. Transplantation of difficult to reach mesodermal cells is likely to complicate experimental reproducibility.

### $The \,quail-chick \,chimeric \,system \,and \,in sight \,into \,OFT \,development$

Chimeric models like the chick-quail system were paramount for understanding the role of NCCs in cardiac development. Le Lievre and LeDouarin showed that NCCs formed the tunica media of the great arteries (*Le Lievre and Le Douarin, 1975*). Kirby and Steward used quail-chick chimeras to observe migration of NCCs into the heart, contributing to the aortopulmonary septum and showed how ablation of the NCC population resulted in persistent truncus arteriosus (*Kirby, Gale and Stewart, 1983*). Moreover, transplantation studies using chimeric models made the initial observation of cellular pluripotency because quail NCCs could expand into subsets of totipotent and pluripotent progenitors (*Baroffio, Dupin and Le Douarin,* 

1991). The quail-chick chimera system was also used to determine that neural crest cells were contributing to the formation of semilunar valves (*Takamura et al., 1990*) as well as to elastogenesis in the developing cardiovascular system (*Rosenquist et al., 1988*). A role for NCCs in coronary artery formation was demonstrated by Arima et al which found NCCs contributing to heart development and smooth muscle heterogeneity within a coronary artery using the quail-chick chimeric model (*Arima et al., 2012*).

#### 2.2.3 Genetic lineage tracing

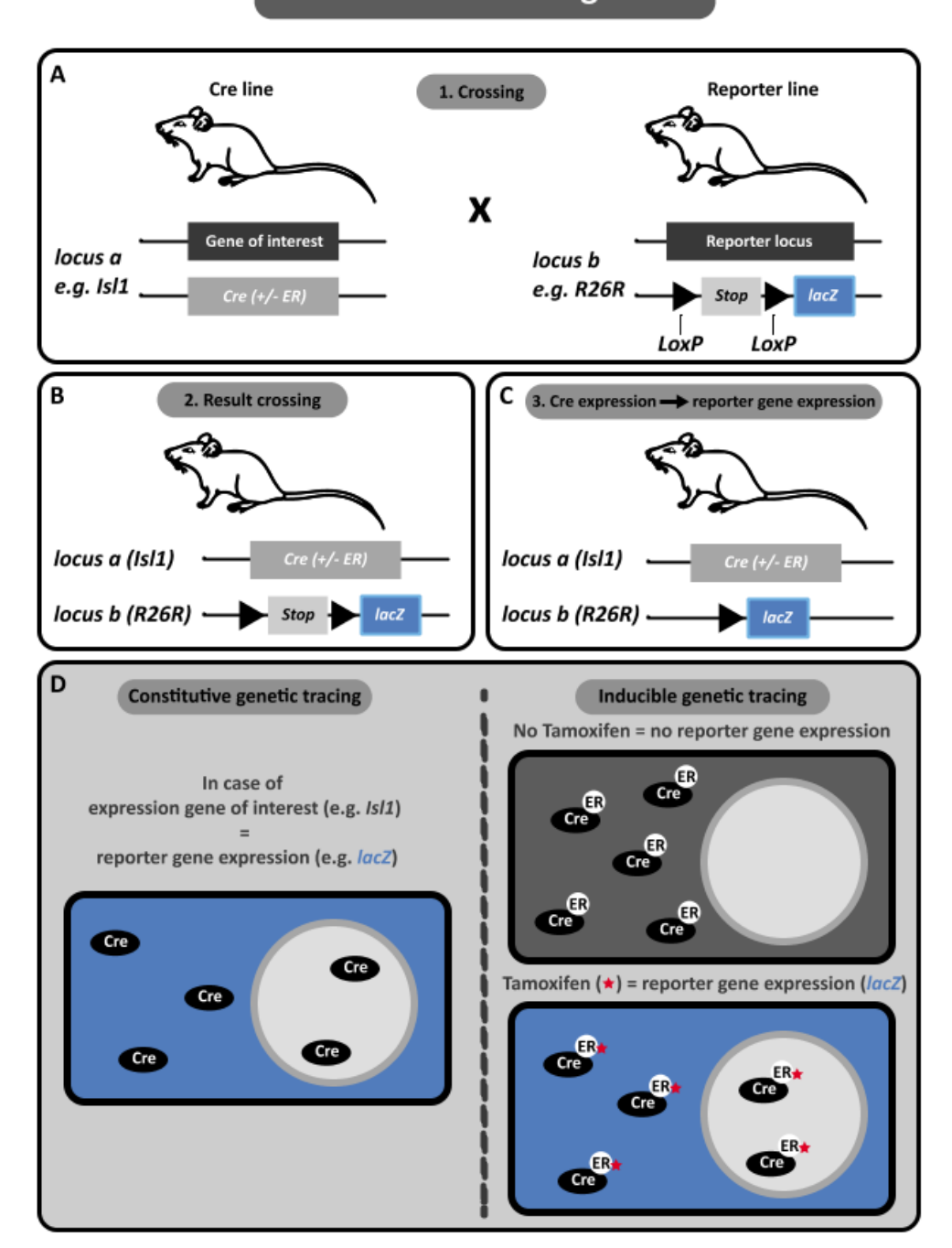
A widely used tool in developmental biology is based on site-specific recombination within the genome. Most mouse models developed for genetic lineage tracing utilize the P1 Bacteriophage derived enzyme Cre-recombinase, which recognizes a 34-bp sequence called the *loxP* site, and induces recombination between pairs of these sites (*Sauer*, 1998). The Cre-*loxP* system, combined with the ability to knock-in sequences at specific sites in the genome has been used to study the origin of the developing OFT.

#### Basics of genetic lineage tracing

To use the Cre-loxP system for genetic tracing, several steps are necessary (**Fig. 2.3**). The basis of the Cre-loxP system is crossing a Cre transgenic mouse strain with a mouse in which a reporter gene is flanked by LoxP sequences ("floxed"). First, the sequence coding for Crerecombinase is knocked into the locus of the gene of interest, for example Isl1. The next step is crossing the Isl1<sup>cre</sup> mouse line with a reporter line (**Fig. 2.3A**). The genetic tracing experiments in this review were mostly performed in reporter lines that utilize the Rosa26 locus (R26R), but different loci (e.g. Gata4 (Ma, Zhou and Pu, 2008)) have also been used in other studies. Important characteristics of a potential reporter locus are ubiquitous expression of the gene and viability and fertility of the mouse strain after homozygous inactivation of the reporter

**Figure 2.3 Genetic lineage tracing. A**: Genetic lineage tracing can be achieved using the Cre-LoxP system. Upon expression, the Cre recombinase specifically targets LoxP DNA motives and allows for excision of DNA elements floxed by LoxP sites. The reporter line contains a stop-cassette inhibiting expression of the reporter gene in the absence of Cre. **B**: Crossing the reporter line with the Cre line results in offspring carrying both constructs. **C**: Cells expressing the gene of interest will express the Cre-recombinase. Cre will then permanently remove the stop-cassette and thus allow expression of the reporter gene, resulting in cell lineage labelling. **D**: Modified Cre-recombinases can be used to allow for more temporal control in genetic labelling. Cre-ER variants can prevent Cre-recombinase activity by restricting mobility to the cells cytoplasm in absence of Tamoxifen. Upon stimulation of Tamoxifen-Cre activity is restored resulting in an inducible system for genetic lineage tracing.

## **Genetic tracing**



locus by insertion of a reporter gene, such as *LacZ* or a single or multiple fluorescent proteins. To control expression of the reporter gene, a floxed sequence preventing transcriptional readthrough (also referred to as a "stop-cassette") is placed before the reporter gene sequence (**Fig. 2.3A**).

Crossing the floxed reporter line with the cell type specific Cre line results in offspring carrying both constructs (**Fig. 2.3B**). Cells expressing the gene of interest will produce Cre-recombinase, which will result in permanent deletion of the stop-cassette and expression of the reporter gene (**Fig. 2.3C**). Since expression is under control of the ubiquitous Rosa26 promoter, these cells and their progeny will retain reporter gene expression, thereby enabling tracing of these cells over a long period of time. The above-described method is referred to as "constitutive" genetic tracing in this review (**Fig. 2.3D**).

A variation of genetic tracing, referred to as "inducible" genetic tracing, enables temporal control of recombination (**Fig. 2.3D**). This system is based on fusion of a mutated ligand-binding domain (LBD) of the human estrogen receptor (ER) and Cre-recombinase. The resulting protein is only sensitive to the anti-estrogen Tamoxifen, not to the endogenously present estradiol (*Feil et al., 1996*). The fusion gene is inserted in the locus of the gene of interest, which results in production of the fusion protein upon expression of the gene of interest. The Cre fusion protein is located in the cytoplasm and is unable to enter the nucleus, due to the presence of the mutated LBD. Administration of Tamoxifen results in binding to the LBD, which enables translocation of Cre-recombinase to the nucleus, where it induces gene specific recombination (*Indra et al., 1999*). Thus, recombination can only occur after administration of Tamoxifen, resulting in temporal control of lineage labelling (**Fig. 2.3D**).

In 2007, multicolour lineage tracing using the Brainbow labelling cassettes was introduced to the genetic lineage tracing toolset (*Livet et al., 2007*). The Brainbow cassettes (Brainbow-1,2 and 3.2) are genetic labelling constructs exploiting the Cre-loxP system to allow for stochastic recombination events to obtain single cell resolution lineage labelling. This method is based on combining multiple fluorescent reporter gene sequences in the Brainbow cassettes flanked by a combination of cis- and trans- *loxP* sites. Upon Cre expression, driven by the gene of interest, the fluorescent reporter genes randomly change configuration within the cassette affecting expression of the cell marker. Because multiple copies of fluorescent reporters are embedded within the Brainbow cassettes (i.e. CFP, YFP, RFP) it allows for multiple fluorescent signatures related to the combination of reporters being stochastically expressed after recombination (i.e.

Expression of a CFP-CFP combination would allow for a "Blue" signal, whilst a RFP-RFP-CFP combination would result in a "Magenta" signal). Combining multicolour lineage tracing with tamoxifen induction can result in a multicolour lineage tracing model with temporal control.

#### Advantages of genetic tracing

The most important advantage of genetic tracing is the ability to visualize the complete heritage of a progenitor population driven by a single marker gene of interest. Combination of these results with previous known expression patterns (e.g. based on immunohistochemical staining patterns) allows for the reconstruction a genetic fate map during development of the OFT.

Furthermore, genetic lineage tracing is non-invasive, as long as insertion of the sequence for Cre does not impair normal development of the embryo. This is an important advantage as compared to performing prospective tracing with microinjection of vital dyes or viral constructs (see section 2.2.1).

Inducible genetic tracing has an important advantage over constitutive genetic tracing, as it allows for temporal control of Cre expression. Constitutive genetic tracing is solely dependent on the natural timing of Cre expression related to the driving promotor. Expression of the gene of interest at any given (and frequently unknown) time point will result in reporter gene expression (if the level of Cre expression is sufficient to induce reporter gene expression, see below). With inducible tracing, reporter gene expression will only occur in the presence of Tamoxifen (*Feil et al., 1996*).

## Disadvantages of genetic tracing

Reporter gene expression in the tissue or structure of interest can result from several scenarios. In the ideal situation, it can show that at time point 0, a certain structure with known expression of the gene of interest is a progenitor for the structure with reporter gene expression at a later time point. However, a possible pitfall can arise from interference resulting from aspecific lineage markers. In scenarios when a gene of interest gives rise to multiple progenitor populations of different origin, interpretation of developing structures would be troubled, which could lead to an inaccurate conclusion regarding the lineage developmental contribution. This difficulty in interpretation of genetic tracing experiments was demonstrated by constitutive genetic tracing of *Tbx18*. *Tbx18* is commonly used as a marker for the sinus

venosus and epicardium. Constitutive genetic tracing was performed with a Tbx18<sup>Cre</sup> in the R26R<sup>LacZ</sup> background and reporter gene expression was found in myocardial cells, which led to the conclusion that these cardiomyocytes derived from epicardial cells (*Cai et al., 2008*). However, later experiments showed active expression of *Tbx18* in cardiomyocytes, which was put forward as an explanation for the observed reporter gene expression (*Christoffels et al., 2009*). Using constitutive genetic tracing, reporter gene expression in cells shows that either these cells have expressed or still actively express the gene of interest.

Even though timing is far more accurately determined using inducible genetic tracing, exact timing of recombination and reporter gene expression remains difficult. It was shown that after intraperitoneal injection of Tamoxifen at E8.5 in pregnant dams, the first signs of *LacZ* activity in the embryos were seen 6 hours after injection, with an increase in expression at 12, 24, and 48 hours (*Hayashi and McMahon, 2002*). Analysis of reporter gene expression after Tamoxifen injection therefore is dependent on the *duration* of Tamoxifen exposure, which complicates exact timing. Furthermore, the *dosage* of Tamoxifen has also been shown to influence reporter gene expression, with higher doses resulting in reporter gene expression in more cells (*Hayashi and McMahon, 2002*). Recent findings also revealed that the basal activity of Tamoxifen induced Cre (CreERT2) can be sufficient to induce genetic recombination even in the absence of tamoxifen induction (*Cai et al., 2003*). Depending on the reporter line this may result in aspecific cell labelling (*Álvarez-Aznar et al., 2020*). This shows that analysis of reporter gene expression and interpretation of these results can be a challenge and might require further substantiation to quarantee efficacy.

The complete absence of reporter gene expression is also difficult to interpret as this can be caused by absence of expression of the gene of interest, or absence of recombination due to sub-threshold levels of Cre expression, not sufficient to induce reporter gene expression.

Recent studies might raise questions regarding the accuracy of using Cre driven genes as a reliable cell lineage markers. In genetic tracing experiments, interpreting specific gene expression can be problematic, but a far more complex problem arises in case of lack of reporter gene expression. A large number of genetic tracing experiments utilize the *R26R* locus, which is also the most commonly used reporter locus described in the current review. Genetic tracing experiments comparing the *R26R* locus with a *Gata4* based reporter system showed differences in reporter gene expression between the two lines (*Ma, Zhou and Pu, 2008*). Constitutive genetic tracing of *Is11* and *Nkx2.5* (both genes are discussed in more detail below)

showed more extensive reporter gene expression in the *Gata4* reporter line, indicating that the *Gata4* locus was more sensitive to recombination then the *R26R* locus (*Ma, Zhou and Pu, 2008*). The difference in reporter gene expression shows that different reporter strains have different thresholds for reporter gene expression, resulting in different conclusions based on the reporter used. An example of the importance of this is shown by reassessment of the fate of *IsI1+* progenitors (*Ma, Zhou and Pu, 2008*). This gene is commonly used as marker for the SHF (*Cai et al., 2003; Sun et al., 2007*). However, the expanded pattern of reporter gene expression in the *Gata4* reporter line showed that nearly all cells (including the LV, which is commonly described as being derived from the FHF) of the heart derive from progenitor cells that did express *IsI1*, albeit perhaps at a low level for a brief period. This suggest that IsI1 is either not specific enough or not reliable as a SHF marker (*Ma, Zhou and Pu, 2008*). mRNA (*Yuan and Schoenwolf, 2000*) and protein (*Kelder et al., 2015*) expression of IsI1 in the cardiac crescent, classically considered to be a FHF structure, further support these observations.

Therefore, when performing constitutive or inducible genetic tracing experiments, one should be cautious with interpretation of the results (**Fig. 2.4** illustrates this in more detail). In constitutive genetic tracing, reporter gene expression demonstrates that labelled cells have expressed or still actively express the promotor driven Cre. It does not provide information on the initial source/location of the progenitor cells. With inducible genetic tracing, temporal control of Cre expression is possible. Expression of the reporter gene shows that Cre is present in the labelled cell between the time of Tamoxifen administration and the moment of analysis. Finally, interpretation of negative results in genetic tracing is challenging and results need to be verified by additional tracing techniques and gene/protein expression experiments at sequential stages of development.

### Using genetic lineage tracing to study OFT development

Genetic lineage tracing has been applied extensively to identify cell lineages contributing to OFT formation. The early observations of neural crest derived cells contributing to the developing heart were further substantiated using the neural crest specific *Wnt<sup>Cre</sup>* transgenic mouse (**Fig. 2.4A**) (*Jiang et al., 2000*). This model, when crossed with a Cre-specific reporter line, allowed for lineage tracing of NCCs revealing their role in semilunar valve development as well as the cardiac conduction system (*Nakamura, Colbert and Robbins, 2006*). The appearance of the OFT cushions and a role for endothelial cells was observed in early studies using electron microscopy (*Bolender and Markwald, 1979*). However, the development of the *Tie2<sup>Cre</sup>* transgenic

model was essential for the study of endothelial cell lineages in vivo (**Fig. 2.4B**) (*Kisanuki et al., 2001*). Other genetic markers have been extensively used to define cell lineages such as the IsI1+ SHF (*Cai et al., 2003*; *Sun et al., 2007*) and the  $Mef2c^{Cre}$  SHF lineage model (**Fig. 2.4C**) (*Verzi et al., 2005*). **Table 2.1** shows an overview of genetic lineage tracing models that are often used in OFT studies, the morphological structures these lineages contribute to, and the possible conflicts arising from the genetic lineage interpretations.

Recent developments in genetic lineage tracing have introduced a dual genetic tracing system to address the dynamic origins of cardiac valve mesenchyme (*Liu et al., 2018*). Dual genetic tracing allows for the study of multiple cell lineages simultaneously by using multiple site-specific recombinases such as Nigri-nox to complement the Cre-loxP system (*Liu, Jin and Zhou, 2020*). Dual genetic lineage tracing could aid in addressing the specificity concerns of traditional Cre-loxP lineage tracing systems.

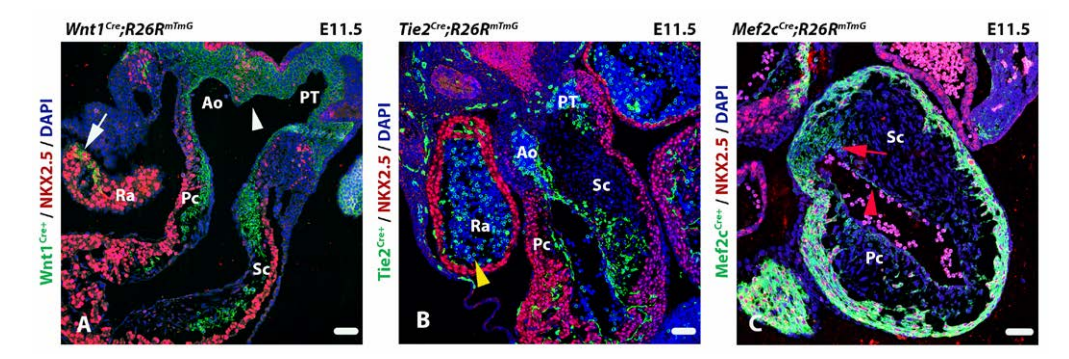


**Figure 2.4 Transversal sections of immunofluorescent outflow tracts show challenges with genetic lineage tracing. A**: A Wnt1<sup>Cre</sup>;R26R<sup>mTmG</sup> embryo showing neural crest cell derived cells (green). Interestingly, Wnt1 derived cells with NKX2.5 stained nuclei can also be observed at the so-called flow divider (Baardman et al., 2016), in front of the primitive foregut which is the central part of the second heart filed contribution (white arrowhead) as well as in the atrial myocardium (white arrow). **B**: a Tie2<sup>Cre</sup>;R26R<sup>mTmG</sup> embryo showing endothelial derived cells (green). Endothelial cells undergoing epithelial to mesenchymal transition give rise to cells within the septal and parietal cushions. Cells derived from myeloid lineages also express Tie2 resulting in lineage positive blood cells (yellow arrowhead). **C**: A Mef2c<sup>Cre</sup>;R26R<sup>mTmG</sup> embryo showing second heart field derived cells (green). Cre positive endothelial cells can also be found lining the heart (red arrowhead). Mef2c derived cells also contribute directly to the septal cushion (red arrow). Ra: Right atrium, Ao: Aorta, PT: Pulmonary trunk, Pc: Parietal cushion, Sc: Septal cushion. Scalebar: 50µm.

### 2.2.4 Retrospective clonal analysis

The aforementioned techniques can all be described as prospective fate mapping techniques. Knowledge on gene and protein expression profile, timing of expression and/or location of progenitors is essential to perform subsequent prospective labelling of this progenitor pool (*Buckingham and Meilhac*, 2011). The following section focuses on retrospective clonal analysis.

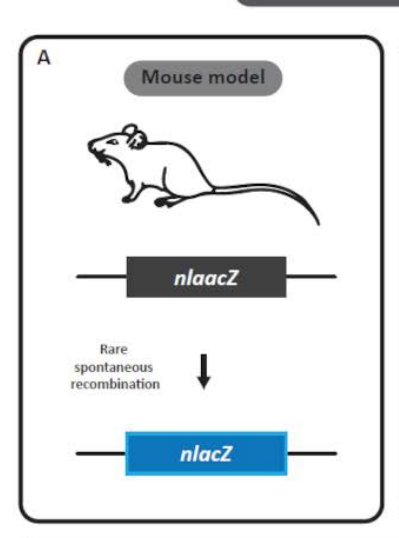
### Basics of retrospective clonal analysis

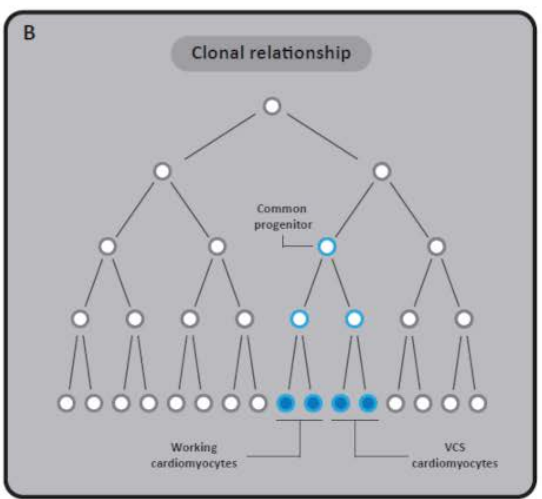
Retrospective clonal analysis is based on infrequent and spontaneous recombination of the nLaacZ reporter ( $Bonnerot\ and\ Nicolas,\ 1993$ ). This reporter gene encodes the LacZ gene, with an inactivating duplication inserted in the reading frame, thereby inhibiting transcription of functional  $\beta$ -galactosidase. A spontaneous and rare recombination event can result in removal of the duplication and subsequent production of  $\beta$ -galactosidase (**Fig. 2.5A**) ( $Bonnerot\ and\ Nicolas,\ 1993$ ). Reporter gene expression can be followed in progeny of cells in which spontaneous recombination of the nLaacZ construct occurred ( $Bonnerot\ and\ Nicolas,\ 1993$ ). Targeting of this construct to an allele which is highly expressed in cardiac muscle, (e.g.  $\alpha$ -cardiac-actin) enables retrospective clonal analysis of cardiac cells, irrespective of gene expression ( $Meilhac\ et\ al.,\ 2003;\ Miquerol\ et\ al.,\ 2010,\ 2013$ ).

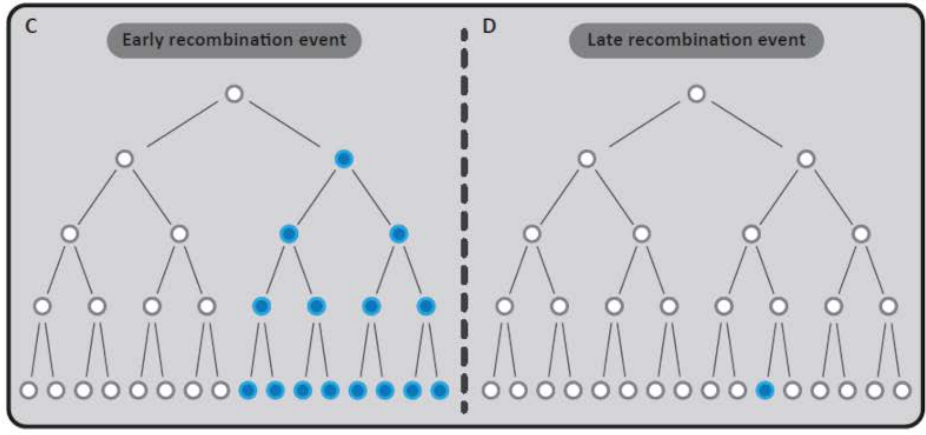
Clonal analysis is based on statistical evaluation of the chance that reporter gene expression in different cells is based on separate spontaneous recombination events, or that these different cells are progeny of one recombination event (and thus share a common progenitor during development). A statistical method commonly used is the fluctuation test of Luria and Delbrück (Luria and Delbrück, 1943). This famous experiment showed that mutations in bacteria occur spontaneously (not induced by selection) and at a constant rate, which was used to formulate a probability distribution (Luria and Delbrück, 1943). This distribution is used to calculate the probability of one or more recombination events, and will therefore determine whether cells showing reporter gene expression are most likely clonally related or are derived from different recombination events (Fig. 2.5B) (Bonnerot and Nicolas, 1993; Meilhac et al., 2003; Miquerol et al., 2010; Lescroart et al., 2012). Early recombination (i.e. during early stages of development) will give large clusters of cells with reporter gene expression (Fig. 2.5C), while late spontaneous recombination will give smaller clusters of LacZ positive cells (Fig. 2.5D).

Recent studies performing retrospective clonal analysis have been adopting next-generation sequencing techniques to study lineage tracing. Recent advances in single cell sequencing

### Retrospective clonal analysis







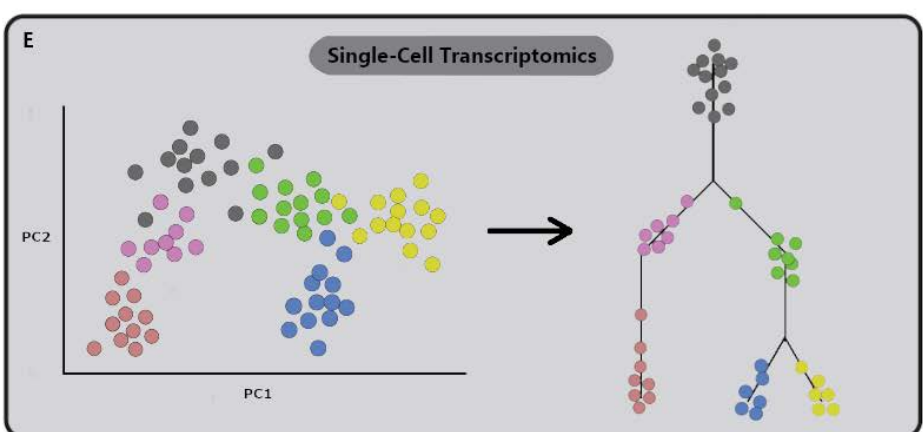


**Figure 2.5 Retrospective lineage tracing. A-B**: Traditional retrospective lineage tracing exploits spontaneous and rare recombination events. The nlaacZ sequence was designed to be inactive by default but increase the odds of recombination events within the region. Upon spontaneous recombination, β-galactosidase is expressed resulting in a lineage label. **C-D**: Early recombination (i.e. during early stages of development) will give large clusters of cells with reporter gene expression, whilst late spontaneous recombination results in smaller clusters of LacZ positive cells. **E**: Modern retrospective lineage tracing derives lineage hierarchy from single cell transcriptomics data. Principle component analysis (PC) aids in clustering groups of cells based on similarity in gene expression profiles. Follow up algorithms can then produce a phylogenetic lineage tree derived from expressional gradients among cell clusters to reconstruct cell lineage development.

technologies allow transcriptome profiling of thousands of single cells. This allowed for the collection of large datasets detailing cellular expression profiles with unprecedented resolution. Alongside advances in sequencing technologies, computational methods designed to examine lineage trajectory reconstruction based on single-cell transcriptomics data have also evolved (*Cannoodt, Saelens and Saeys, 2016; Todorov et al., 2019*). Single-cell transcriptomics allows for the investigation of the transcriptional state of thousands of individual single cells. As a result, cell-type diversity in heterogeneous samples can be reliably captured. As cells transition between different states during embryologic development, their expression profiles give insight into their lineage fate and cellular identity.

If sufficient amounts of cells in these transition states are captured, differentiation trajectories through which tissues are derived can be reconstructed through hierarchical clustering of cells based on the gradient in expressional similarities (**Fig. 2.5E**).

### Advantages of retrospective clonal analysis

To perform prospective lineage tracing, some basic knowledge on the progenitor population that will be traced is required. This information is not necessary when performing retrospective clonal analysis. Studying whether certain structures or clusters of cells are clonally related is done independent of gene expression or any other preconceived idea of a possible progenitor pool. Retrospective clonal analysis can therefore establish clonal relationships that are less apparent at first sight, such as the clonal relationship between head musculature and cardiomyocytes from the outflow tract and right ventricle (*Bredman et al., 1992; Lescroart et al., 2010*).

Furthermore, as described previously, prospective genetic tracing is hampered by the difficulty

to draw conclusions from the absence of reporter gene expression. With the retrospective clonal approach, analysis is based on *LacZ* positive cells. *LacZ* expression in different structures or tissues is mapped and statistical analysis is performed to calculate whether these different tissues or structures are clonally related (*Bonnerot and Nicolas, 1993*). Moreover, as with genetic tracing, retrospective clonal analysis is non-invasive.

When performing retrospective lineage tracing using single-cell sequencing, an advantage is the ability to perform lineage tracing using naturally occurring somatic mutations or copy number variations (CNVs). CNVs can be used as genetic markers to link clones of cells to a common progenitor. This approach allows for lineage tracing without manual labelling or genetic modification. Although CNVs are relatively uncommon in healthy tissue, they are highly abundant in cancerous tissue and have been used to study tumour evolution (*Navin et al., 2011; Wang et al., 2014*). Alternatively to CNVs is lineage tracing using single-nucleotide variations (SNVs) and genomic insertion/deletions (indels). Both SNVs and Indels are often present in non-coding regions of the genome and have been used for the reconstruction of phylogenetic trees of tumours from bulk DNA (*Abbosh et al., 2017*). This technique, however, is not limited to tumour lineage analysis as lineage tracing using somatic SNVs in mitochondrial DNA can be performed with any eukaryotic cell (*Xu et al., 2019*). Moreover, combining the genetic variation in non-coding regions of DNA with the RNA expression profiles when performing lineage tracing has recently been successfully demonstrated (*Ding, Lin and Bar-Joseph, 2019*).

### Limitations of retrospective clonal analysis

The retrospective approach has several drawbacks. Since data is analysed retrospectively, it is not possible to locate the common progenitor, either in time or space. Therefore, it is not possible to perform further experiments with these progenitors (e.g. characterization or ablation). Retrospective clonal analysis has to be performed in conjunction with other fate mapping techniques to build the complete lineage tree of a structure or organ. In this sense, the most important advantage of this technique is also its most important drawback. Starting with a certain progenitor pool based on timing, location and/or gene/protein expression profile excludes contributions from other (sometimes unexpected) progenitors, but does directly pinpoint a possibly important progenitor pool for the structure/tissue of interest. Furthermore, spontaneous recombination of the *nlaacZ* gene is rare and it is therefore necessary to obtain a large library of embryos with *LacZ* positive clones and as a result, large quantities of embryos or adult mice will have to be analysed. A challenge when performing single cell sequencing for

lineage tracing lies in the sparse distribution of SNVs and CNVs within the genome. To achieve confident detection of SNVs, large quantities of reads will have to be generated to achieve adequate sequencing depth. A large portion of the generated data is unsuitable for lineage tracing as these would contain identical sequences. However, enrichment of regions of DNA with greater odds of developing nucleotide variations such as microsatellites could apprehend these challenges.

## Retrospective clonal analysis aimed at the development of the OFT

Many of the cardiac lineages contributing to OFT development have been found using prospective lineage tracing techniques (**Table 2.1**). However, a recent study examining cell populations at the aortic root and pulmonary trunk determined a novel SHF derived cell population called arterial mesothelial cells (AMC) populating a local niche at the base of the great arteries (*Lioux et al., 2020*). Whilst AMCs have first been observed as a distinctive cell type using chick-quail chimera's (*Gittenberger-De Groot et al., 2000*), the study of Lioux et al used a clonal analysis strategy based on the ubiquitous, low-frequency random recombination of two independent reporters to distinguish this population from the frequency of colour matching between labelled cells in different clusters or different cell types within single clusters (*Arques et al., 2007*). This approach allowed for an unbiased characterization of the fate of SHF precursors at the base of the great arteries and detailed the contribution of SHF to the coronary lymphatic vasculature (*Lioux et al., 2020*). Moreover, another study examining the cardiac outflow tract using single cell RNA sequencing found convergent development of the vascular smooth muscle cell lineage suggesting a method of myocardial-to-VSMC differentiation or mesenchymal-to-VSMC differentiation (*X. Liu et al., 2019*).

# 2.3 New Technologies for Lineage Tracing in OFT Development

Lineage tracing has contributed greatly to our understanding of OFT development. Nevertheless, there is still much to be learned regarding multifactorial CHDs. To advance our understanding of phenotypical variation, research efforts should be aimed at understanding the relation between cell lineage and cellular identity. The methods previously described in this review are inadequate to address such issues, as this would require detailed description of the variation among single cells within a lineage population. The introduction of novel analysis methods which combine lineage tracing and single cell analysis could provide new

**Table 2.1** An overview of common genetic lineage tracing models used in OFT studies.

Transgenic mouse lines	Commonly used as cell lineage marker for:	Observed tissue expression	Possible Lineage Conflicts
Hcn4 <sup>Cre-ert2</sup>	First heart field ( <i>Liang et al., 2013</i> )	Cardiac conduction system ( <i>Liang et al., 2013</i> ) Myocardium ( <i>Liang et al., 2013</i> )	Second heart field
Hoxa1 <sup>Cre</sup>	Cardiac precursors (Makki and Capecchi, 2010)	Aortopulmonary septum (Makki and Capecchi, 2010) Cardiac conduction system (Makki and Capecchi, 2010) Coronary arteries (Makki and Capecchi, 2010) Endothelial lining (Makki and Capecchi, 2010) Myocardium (Makki and Capecchi, 2010) Semilunar valves (Makki and Capecchi, 2010)	Endothelial Neural Crest Second heart field
Isl1 <sup>Cre</sup>	Second heart field (Cai et al., 2003)	Atrioventricular valves (Ma, Zhou and Pu, 2008) Cardiac conduction System (Liang et al., 2013) Cushion mesenchyme (Ma, Zhou and Pu, 2008) Endocardium (Ma, Zhou and Pu, 2008) Myocardium (Yang et al., 2006) Proepicardium (Zhou et al., 2008) Semilunar Valves (Ma, Zhou and Pu, 2008)	Endothelial Epicardial First heart field Neural Crest
Krox20 <sup>Cre</sup>	Neural Crest (Odelin et al., 2017)	Endocardium ( <i>Odelin et al., 2017</i> ) Semilunar valves ( <i>Odelin et al., 2017</i> )	Endothelial
Mef2c <sup>Cre</sup>	Second heart field (Verzi et al., 2005)	Ascending aorta ( <i>Crucean et al., 2017</i> ) Coronary arteries ( <i>Tian et al., 2013</i> ) Cushion mesenchyme ( <i>Crucean et al., 2017</i> ) Endocardium ( <i>Crucean et al., 2017</i> ) Myocardium ( <i>Verzi et al., 2005; Crucean et al., 2017</i> ) Semilunar valves ( <i>Crucean et al., 2017</i> )	Endothelial Epicardial
Nkx2.5 <sup>Cre</sup>	First and Second heart field (Moses et al., 2001)	Ascending aorta (Harmon and Nakano, 2013) Coronary artery (Harmon and Nakano, 2013) Endocardium (Ma, Zhou and Pu, 2008) Epicardium (Zhou et al., 2008) Myocardium (Moses et al., 2001), Semilunar valves (Harmon and Nakano, 2013)	Endothelial Epicardial
Pax3 <sup>Cre</sup>	Neural Crest (Epstein et al., 2000)	Aortopulmonary septum ( <i>Epstein and Buck, 2000</i> ) Ascending aorta ( <i>Epstein et al., 2000</i> ) Cushion mesenchyme ( <i>Epstein and Buck, 2000</i> ) Semilunar valves ( <i>Epstein and Buck, 2000</i> )	
Tbx18 <sup>Cre</sup>	Proepicardium/ epicardium ( <i>Cai et</i> <i>al., 2008</i> )	Cardiac conduction system ( <i>Liang et al., 2013</i> ) Epicardium ( <i>Cai et al., 2008</i> ) Myocardium ( <i>Cai et al., 2008</i> )	First heart field Second heart field
Tbx2 <sup>Cre</sup>	Proepicardium/ epicardium ( <i>Greulich et al.,</i> 2016)	Cardiac conduction system (Aanhaanen et al., 2009) Coronary arteries (Greulich et al., 2016) Epicardium (Greulich et al., 2016) Myocardium (Singh et al., 2012; Greulich et al., 2016)	First heart field Second heart field

Tie2 <sup>Cre</sup>	Endothelium (Kisanuki et al., 2001)	Atrioventricular valves ( <i>Kisanuki et al., 2001; De Lange et al., 2004</i> ) Coronary arteries ( <i>Payne, Val and Neal, 2018</i> ) Cushion mesenchyme ( <i>Kisanuki et al., 2001; De Lange et al., 2004</i> ) Endocardium ( <i>Kisanuki et al., 2001; De Lange et al., 2004</i> ) Hematopoietic cells ( <i>Tang et al., 2010</i> ) Semilunar valves ( <i>De Lange et al., 2004</i> )	Hematopoietic
Tnnt2 <sup>Cre</sup>	Myocardium ( <i>Jiao</i> et al., 2003)	Ascending aorta ( <i>Mifflin et al., 2018</i> ) Myocardium ( <i>Jiao et al., 2003; Mifflin et al., 2018</i> ) Semilunar valves ( <i>Mifflin et al., 2018</i> )	
Wnt11 <sup>CreER</sup>	Cardiac precursors (Sinha et al., 2015)	Endocardium ( <i>Sinha et al., 2015</i> ) Epicardium ( <i>Sinha et al., 2015</i> ) Myocardium ( <i>Sinha et al., 2015</i> ) Semilunar valves ( <i>Sinha et al., 2015</i> )	First heart field Endothelial Epicardial Second heart field
Wnt1 <sup>Cre</sup>	Neural Crest (Jiang et al., 2000)	Aortopulmonary septum (Jiang et al., 2000) Ascending aorta (Jiang et al., 2000) Cardiac conduction system (Poelmann et al., 2004) Coronary arteries (Arima et al., 2012) Cushion mesenchyme (Jiang et al., 2000) Epicardium (Stottmann et al., 2004) Myocardium (Stottmann et al., 2004; Hatzistergos et al., 2020) Semilunar valves (Jiang et al., 2000)	Epicardial Second heart field
WT1 <sup>Cre</sup>	Proepicardium/ epicardium ( <i>Zhou</i> and <i>Pu</i> , 2012)	Coronary arteries ( <i>Zhou and Pu, 2012</i> ) Epicardium ( <i>Zhou et al., 2008</i> ) Myocardium ( <i>Zhou et al., 2008</i> )	Endothelial lineage First heart field Second heart field

opportunities to examine cell lineage plasticity and phenotypical variation in CHD. These methods will be discussed in the following section.

### 2.3.1 Spatially resolved transcriptomics

Current lineage tracing techniques, such as genetic lineage tracing, rely primarily on spatial information to reconstruct OFT development over multiple embryonic stages. The tracking of cell lineage movements can give insight into the environment in which these cells function. However, evaluating the internal cellular state of these cells within such environments can be challenging. Single cell RNA sequencing (scRNA-seq) is a technique which can be used to examine a cell's innerworkings because it allows for quantification of all the RNA molecules

within a single cell. This cellular transcriptome can be used to examine gene expression patterns and to make cell type specific expression profiles. By collecting expression profiles of multiple cells of the same cell type, it is possible to examine the cellular variation in gene expression within a specific cell population. This allows researchers to evaluate the variation in cell states within a particular cell lineage, and reconstruct subclusters structural to a cell lineage population. Whilst scRNA-seg can be used to obtain genome-wide expression data of cells allowing for unprecedented cell type identification, it does not provide any spatial resolution to determine where these cells were located within the embryo. As a result, experiments using scRNA-seg to identify new cell types and cell states still require the use of visualisation techniques such as in-situ hybridization using the genetic markers found during sequencing. However, in-situ hybridization can only provide spatial information regarding a few genes at any given moment. Tomo-seg is a technique which combines genome-wide expression data with spatial information (Junker et al., 2014; Kruse et al., 2016). This is achieved by performing RNAseg on individual cryosections of an embryo or tissue allowing the generation of genome-wide spatial expression maps in 3D. By sequencing sequential tissue sections, spatial information regarding the head to tail axis can be maintained. As a result, gene expression data can be projected with respect to the head to tail axis. Performing this approach using multiple axis (dorsal-ventral, right-left) allows for the reconstruction of gene expression patterns in 3D in the developing embryo (Junker et al., 2014). Although Tomo-seg allows for 3D expression pattern analysis, one limitation is that it is unable to provide single cell resolution in 3D. An alternative method called transcriptome in vivo analysis (TIVA) does allow for single cell sequencing whilst maintaining single cell spatial resolution. TIVA is a non-invasive tool enabling capture of mRNA from single spatially defined cells in living and intact tissue for transcriptome analysis (Lovatt et al., 2014). This is achieved by addition of a cell permeable TIVA tag to the tissue sample which upon photo activation is able to capture cellular mRNA. This technique is an excellent advance over more traditional laser capture techniques or pipette cell isolation adapted for scRNA-seq due to the non-invasive design. The limited throughput, however, might restrict explorative research to specific cases in which the number of cells of interest might be relatively low. A practical example in which TIVA might prove very valuable for OFT studies, is to examine the properties of valvular interstitial cells (VICs) contributing to the aortic and pulmonary valves. VICs may derive from multiple cell lineages such as SHF, NCC or endothelial lineages and VIC dysfunction has been suggested to underly valvular diseases such as calcification (Rutkovskiy et al., 2017). TIVA could enable researchers to examine how cell lineage background influence VIC formation and how cell lineage deficiencies could relate to valvular disease by assigning a spatial criterium to scRNA-seq.

### 2.3.2 Lineage tracing through DNA barcoding

DNA-barcoding technologies are another potential tool for lineage tracing. Lineage tracing using DNA barcoding is a technique that combines aspects of both prospective an retrospective lineage tracing. Similar to genetic lineage tracing using fluorescent reporters, DNA-barcoding technologies introduce genetic modifications into progenitor cells to study cell lineage development. But whilst lineage tracing using fluorescent reporters is limited to only a number of reporter genes, DNA barcodes allow for more complex labelling methods. Techniques such as scGESTALT (Raj et al., 2018) ScarTrace (Alemany et al., 2018) and LINNAEUS (Spanjaard et al., 2018) have demonstrated how the CRISPR-Cas9 system could be used to generate genetic barcodes to perform whole-organism lineage tracing in zebrafish embryos. The CRISPR-Cas9 system allows genomic editing on a specific DNA locus determined by the supplied guide RNA. In the absence of a template for homologous repair, Cas9 may introduce short DNA insertions or deletions at the targeted site (Junker et al., 2016). These genetic aberrations, which vary in size and position, can then be used as a genetic barcoded label to evaluate a cell's offspring. If the guide RNA was designed specific to a region within a constitutive expressed gene, then scRNA-seq can capture the barcode within the transcriptome of a cell. Since the process of barcoding is randomly determined, a cell's lineage can only be evaluated after single cell sequencing. This can be achieved through computational reconstruction of full lineage trees from the single cell level. Although these methods still rely on microinjection of Cas9 and guide RNAs in an early stage zebrafish embryos, DNA-barcoding has also been achieved using retroviral integration (Weinreb et al., 2020) or polylox recombination (Pei et al., 2017) in mice. For an in dept comparison of barcoding techniques, the reader is referred to a recent review of Wagner and Klein (Wagner and Klein, 2020). Lineage tracing using barcodes could be an excellent method to examine cell lineage commitment because it allows to retrospectively evaluate cell lineage branching events. The differences in lineage trajectories among FHF and SHF lineages would be an interesting topic to be evaluated using such methods. Moreover, if barcoding events are temporally restricted and multiple stages of embryonic development are analysed, then it could enable reconstruction of all cell lineage trajectories contributing to heart development simultaneously. Genetic mutations or epigenetic influences affecting cellular identity could also be examined as these would influence the relative distributions among (sub)populations of cell lineages. As such, these methods could aim to elucidate the relationship between phenotypical variation and cell lineage variation.

### 2.3.3 Multi-omics lineage tracing

Whilst barcoding techniques for lineage tracing require aspects of an prospective approach to lineage tracing, recent technological developments using a multi-omics sequencing approach for lineage tracing could allow for complete retrospective lineage tracing. RETrace is an example of a recent lineage tracing technique which captures both DNA microsatellite loci and methylation-informative cytosines from a single cell in order to simultaneously characterize both lineage and cell type (Wei and Zhang, 2020). The utilization of microsatellite regions as markers for retrospective lineage tracing was successfully demonstrated at single cell level (Biezuner et al., 2016). However, enabling DNA methylation profiling of the same cell allows for better cell characterization than either method alone. Although still in early development, a multi-omics approach to lineage tracing would ideally combine the cell lineage identification capability using natural occurring CNV and SNVs captured using whole genome sequencing whilst allowing for accurate cell type identification through gene expression analysis using scRNA-seg and also include epigenetic profiling techniques such as methylome analysis (Y. Liu et al., 2019) or include histone signatures (Ku et al., 2019) to investigate cellular identity and cell lineage dynamics. Multi-omics lineage tracing would enable researchers to investigate the relations between cellular variation, epigenetic modification and disease susceptibility related to CHD. This knowledge could potentially translate to novel methods of treatment and therapy aimed at influencing the epigenome of patients.

### 2.3.4 Reference maps for lineage tracing

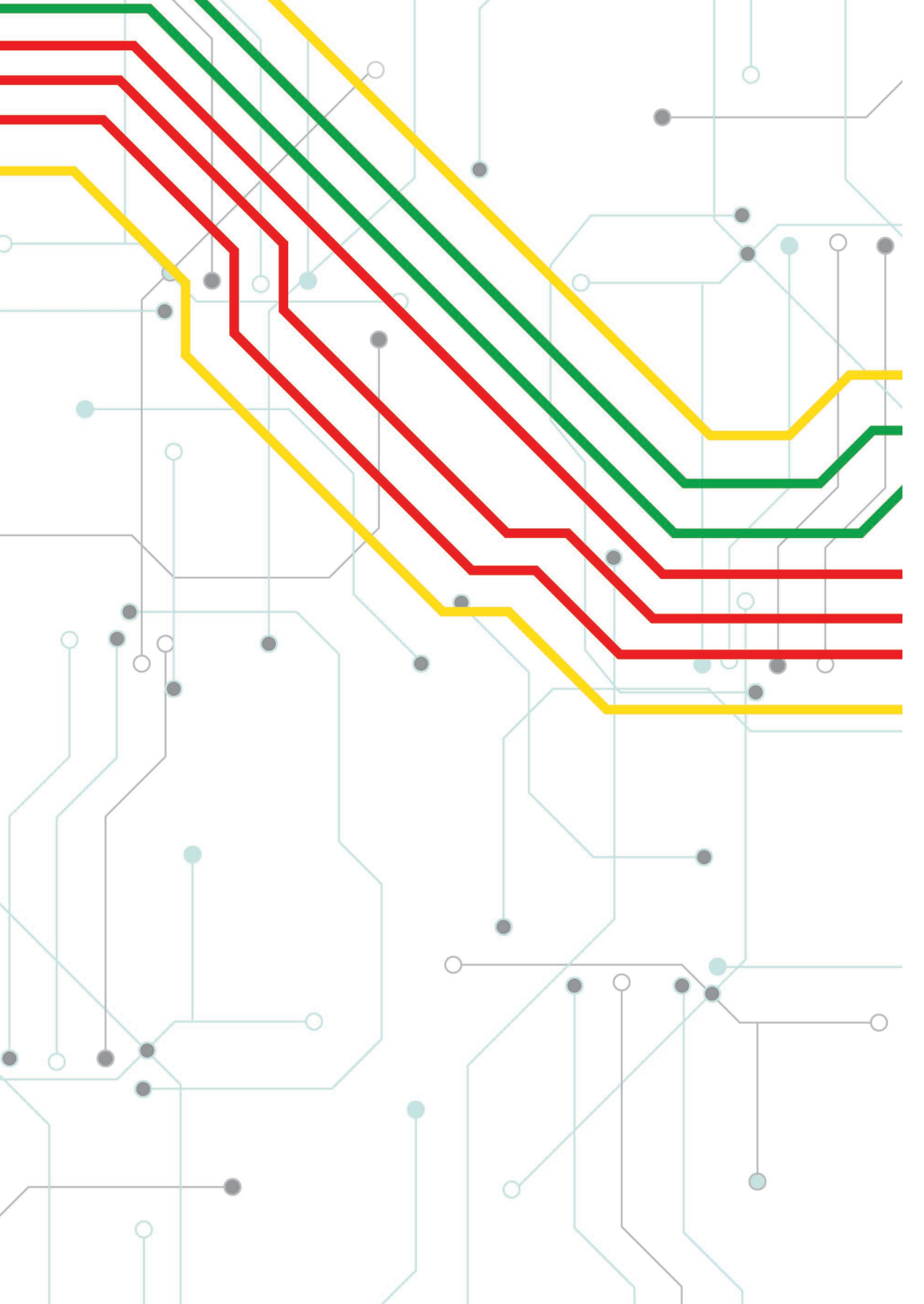
The large amounts of data derived from lineage tracing using transcriptomics are likely to extent the depth at which sub-lineages and cell states will be defined. To facilitate accurate definitions of such sub lineages and intermediate cell states, large quantities of single cell data could be combined. A project called the Human Cell Atlas (HCA) aims to characterize all human cell types using scRNA-seq and single cell transposase accessible chromatin sequencing (scATAC-seq), and combine it with data regarding cell lineage, location and cell states (*Regev et al., 2017*). The scope extents to unify single cell sequencing data towards common reference models similar to the efforts of the Human Genome Project (*Pullen, 2018*). Having the infrastructure to navigate cell lineage development will greatly contribute to the understanding of human health and treatment of disease. (For more information regarding the HCA project, the reader is referred to the HCA white paper (*Regev et al., 2018*)). Initiatives such as these could allow for the comparison of many cell lineage populations among the various types of CHD to determine key processes critical to human cardiovascular development.

# **2.4** Future Perspectives, Combining Old Strengths with New Technologies

With the advances in lineage tracing, new insights regarding cell fate came forth and the role of prospective lineage tracing paved the way for modern developmental biology. In this review we describe the use of lineage tracing techniques and their limitations with respect to OFT development. The recent technological methods described in the final section of this review have the potential to allow more fateful reconstruction of lineage dynamics than previous methods.

The development of next-generation sequencing technology has enabled new and exciting research opportunities for lineage tracing experiments. From our perspective we expect that results obtained from retrospective lineage tracing using naturally occurring mutations and single cell transcriptomics will challenge our current definitions of cell lineages and advance our understanding of cellular dynamics and lineage plasticity. Assuming technological improvements will continue to be developed in the coming years, we can expect an integration of (epi)genetics signatures with single cell sequencing to aid with tracing cellular heritage. Continued development and a multi-omics approach will allow future research to expand the scope of cellular identity and resolve the mechanisms explaining congenital variation in more detail and with better accuracy than current available methods. As a result, a multi-omics approach will help to elucidate the mechanisms for normal OFT development and aid in understanding the pathophysiological pathways leading to the multivariate phenotypes common to OFT diseases. As sequencing techniques become more and more accessible, multi-omics sequencing approaches combined with single cell resolution will become the new frontier for future lineage tracing studies.

**Acknowledgments:** We are very grateful for all the support provided by Adriana C. Gittenberger-de Groot. Her work fuelled our passions for cardiac development and congenital heart disease. The rigorous scientific discussions carry warm memories and helped pave the road to academic excellence. We thank her for all her support throughout the years and the care she took for all her colleagues and collaborators.



## **Chapter 3**

### Fluorescent Nuclei Measurements Macro (FNMM), a tool for automated cell quantification in ImageJ

2020

**DOI**: 10.1016/j.simpa.2020.100030

**Software Impacts** 

**Software**: <a href="https://github.com/J-PTRson/Cell-Image-Analysis/tree/master/FNMM">https://github.com/J-PTRson/Cell-Image-Analysis/tree/master/FNMM</a>

Joshua C. Peterson<sup>1</sup>, Marco C. DeRuiter<sup>1</sup>

<sup>1</sup> Dept. Anatomy and Embryology, Leiden University Medical Center, Leiden, The Netherlands

#### **Abstract**

A common requirement, in field of life sciences, is the quantification of specific cells in a given fluorescent microscopy image. ImageJ is a popular tool for researchers to develop custom scripts for automated cell quantification. Validating the quality of cell quantification measurements is a common challenge for such researchers. The Fluorescent Nuclei Measurements Macro (FNMM) was developed to assist researchers performing cell quantification by presenting the results in an intuitive manner whilst simultaneously facilitating processed data collection and measurement assurance.

### 3.1 Introduction

Since the introduction of digital microscopy the methods for image analysis have been evolving continuously. Advanced microscopes can now generate large amounts of multichannel fluorescence images of cells. Although analytical methods have changed over time, most questions in cell biology are still based on accurate cell quantification. Software tools like ImageJ (Rueden et al., 2017) allow researchers to quickly develop custom methods for automated image analysis. Even though the flexibility of ImageJ allows for highly sophisticated method development, researchers new to software development may struggle to incorporate the collection of data to review such scripts. Around 90% of scientists developing software are self-taught (Wilson et al., 2014) and as a result often fall short to ensure the standards required for reproducibility and reusability of technical analysis (Jiménez et al., 2017). Whilst methodological instruments and laboratory equipment is often validated, ensuring technical accuracy and reliability of developed software can be challenging (Roberts, 1994). There are many online tutorials available to aid researchers in performing automated cell counting using ImageJ, yet these often fail to introduce the aspects of measurements assurance to validate analytical performance. A key conclusion from the cell counting workshop by the National Institute of Standards and Technology and US Food And Drug Administration recommends users to consider the purpose of their cell counting measurement and design the most appropriate method, including measurement assurance strategies as there is currently no single approach for obtaining high quality cell count measurements (Lin-Gibson, Sarkar and Elliott, 2018).

For this reason, we have developed a software script specific to ImageJ to facilitate collection of process-data for measurement assurance and simultaneously aid researchers in exercising

good research practices. This script was designed with a very relatable research question in mind. That is, given any fluorescent microscopic image, how many green fluorescent protein (GFP) positive cells are there relative to all cells in that image. In our situation we have used this macro to examine fluorescent cell lineage distributions throughout embryonic development (*Peterson et al., 2018*). However, this macro has been built to allow for easy adaptation for use in any situation which addresses questions regarding multi-channel fluorescent cell populations.

### 3.2 Description

The Fluorescent Nuclei Measurements Macro (FNMM) was designed to estimate a measure of GFP positive cells within a given cell population using Fiji (*Schindelin et al., 2012*) (ImageJ). This is accomplished by analysing the area of 4',6-diamidino-2-phenylindole (DAPI) positive nuclei enveloped by cytoplasmic GFP versus the total area of all DAPI positive nuclei within a given region of interest (ROI).

The macro facilitates and standardizes image analysis of fluorescent images by allowing users to apply regional masks to define a specific region of interest to perform the analysis. To achieve cell type analysis, this macro analyses multichannel composite images and depends on the presence of a general nuclear cell staining, like the commonly used DAPI staining, embedded in a dedicated image channel, in combination with a cytoplasmic cell staining (like GFP) in a secondary image channel. A user defined threshold is used to identify positive cells in the DAPI channel which creates a mask of all positive cell nuclei. A similar process is performed to determine the areas of GFP positive cytoplasm in the GFP channel. By combining the results of both the DAPI and GFP masks an image filter is constructed to identify the DAPI positive nuclei within GFP positive cell bodies. Using this filtered image, area measurements are performed to calculate the nuclear area of all GFP positive cells. This result is offset to the nuclear area of all DAPI positive cells to derive a ratio of GFP positive cells within the selected ROI.

All results are recorded in .CSV format and visual representations of the labelled area measurements are exported to a local folder for measurement assurance and peer inspection (**Fig. 3.1**). This approach ensures data collection of original input images, as well as the labelled output images to allow for more transparent cell image quantification.

### 3.3 Impact

The quantification of certain cell types using fluorescent imaging is a common explorative procedure during biomedical research. Current microscopes can collect a large volume of high resolution images of cells in a single day. Whether it is for optimizing transfection efficiencies in vitro, ex vivo morphologic analysis, in vivo expression analysis or high throughput compound analysis the need to label and quantify cells persist (**Fig. 3.1, Fig. 3.2**). Nevertheless, there remain bottlenecks at the image analysis stage. Automated cell image quantification presents a solution to increase analytical throughput. Yet accurate validation of automated quantification results is still a challenge. This script allows researchers looking to perform cell quantifications to address the measurement uncertainty related to automated image

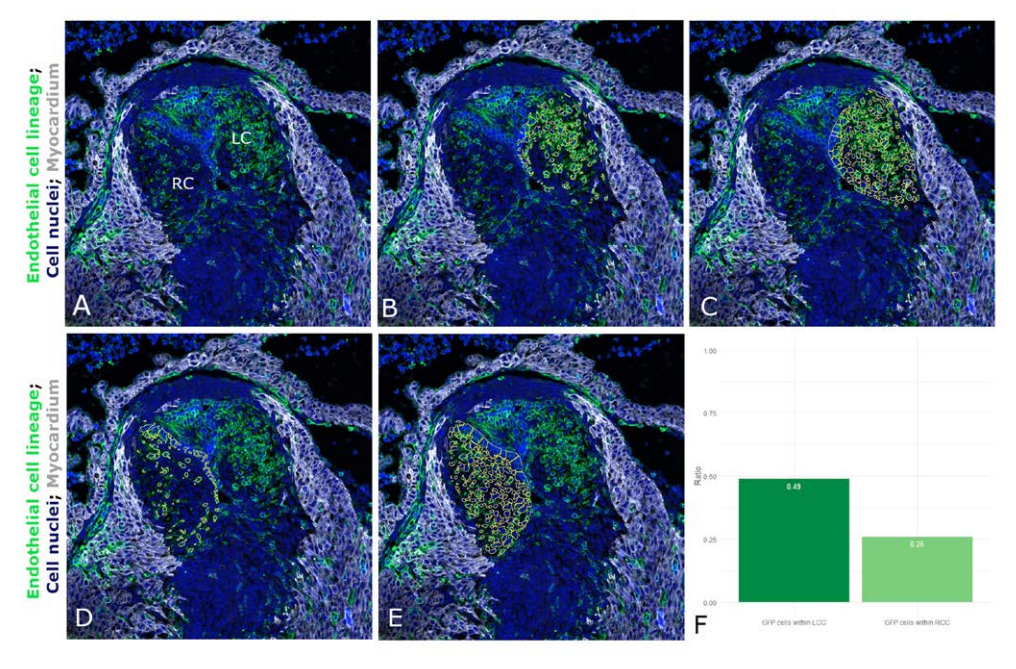


**Figure 3.1 Using FNMM to examine cell lineage distribution within the aortic valve. A**: The original input image is a transversal section of the aortic valve in an embryonic day 13.5 bl6. Tie2Cre;mTmG mouse embryo showing the right coronary cusp (RC) as well as the left coronary cusp (LC). **B**: The LC was selected for analysis, here the cell nuclei (blue) of endothelial derived cells (green) have been quantified and outlined in yellow for visual examination. **C**: Here, all nuclei within the LC were quantified based on the cell nuclei staining. **D-E**: Similar output files as B and C, however, analysis was performed on the RC. **F**: Comparing the ratio of green to blue cells allows for rapid analysis of relative cell distributions in morphological structures.

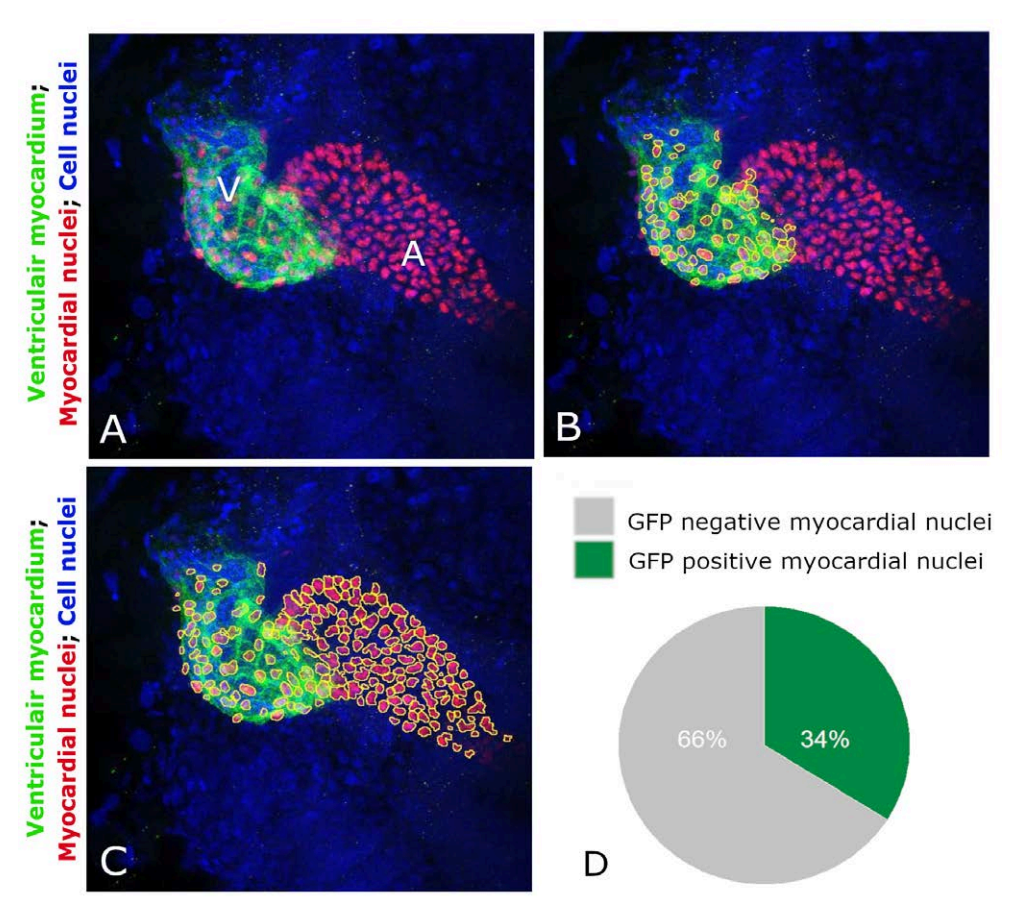


**Figure 3.2 Using FNMM to quantify myocardial cell contribution to the atrium and ventricle during development. A**: Original input image of a 48 hours post fertilization zebrafish heart showing the ventricle (V) and atrium (A). **B**: Myocardial nuclei (red) within the ventricle (green) were quantified and outlined in yellow. **C**: Here, the total area of myocardial cells is measured. **D**: Following this approach, it can be determined that 34% of myocardial cells in the heart contribute to the ventricle whilst 66% of cells contribute to the atrium at this developmental stage.

analysis. This script presents the analytical results in an intuitive manner whilst simultaneously facilitating processed data collection and measurement assurance. This allows users to more easily evaluate the effects of variation in input parameters on the accuracy and reliability of the intended cellular measurements. Knowing that the analysis performed according to expectation improves the pursuit of the existing research questions as concerns regarding measurement error is minimized and can be retrospectively reviewed by multiple peers if required. Moreover, the general-purpose design of this script allows researchers to easily pursue new research questions through reuse of public datasets derived from other studies, like those published

at the Image Data Resource (IDR) (https://idr.openmicroscopy.org/). Studies examining in-vivo cell dynamics such as the work of Duim et al. (2015) or Ge et al. (2020) could benefit from cell quantification scripts like ours as the heterogeneous morphology of cardiac tissue following myocardial infarction requires dynamic selection of ROIs due to local tissue adaptation. The dynamic application of this script and easy customization options provided through ImageJ may be more advantageous than customization options provided by other Image analysis tools such as CellProfiler (*Carpenter et al., 2006*). A comparison of 15 free image analysis tools published by Wiesmann et al. describes that tools such as ImageJ include more functionality but lack more usability due to less user guidance compared to the CellProfiler (*Wiesmann et al., 2015*). Our script addresses this user guidance through an interactive workflow with optional dialog requests for researchers less comfortable with automated cell quantification. An early version of this script has already been successfully used to enable the study of developmental changes in cell lineage distribution in *Nos3*<sup>-/-</sup> mice (*Peterson et al., 2018*). In our ongoing research we are deploying this script for cell analysis of congenital heart disease in mice.

### 3.4 Limitations and potential improvements

The main limitation is that this script currently only supports 2D image analysis. Nevertheless, the basic premise on which this script was build allows for rapid customization by its users. Another potential limitation is that this script was designed solely for fluorescence cell analysis. Histological staining such as hematoxylin eosin (HE) are incompatible using this method. As such, one of our goals is to continue development for efficient analysis of histological images in the future.

Code metadata description			
Current Code version	V2.0.0		
Permanent link to code / repository used of this code version	https://github.com/SoftwareImpacts/SIMPAC		
Legal Code License	MIT License		
Code Versioning system used	Git		
Software Code Language used	пм		
Compilation requirements, Operating environments & dependencies	Fiji (ImageJ v1.52p)		
If available Link to developer documentation / manual	https://github.com/J-PTRson/Cell-Image-Analysis/ tree/master/FNMM		
Support email for questions	j.c.peterson@lumc.nl		



### **Chapter 4**

### Nos3 mutation leads to abnormal neural crest cell and second heart field lineage patterning in bicuspid aortic valve formation

2018

**DOI**: 10.1242/dmm.034637

**Disease Models & Mechanisms** 

Joshua C. Peterson<sup>1</sup>, Mary Chughtai<sup>1</sup>, Lambertus J. Wisse<sup>1</sup>, Adriana C. Gittenberger-de Groot<sup>2</sup>, Qingping Feng<sup>3</sup>, Marie-José T.H. Goumans<sup>4</sup>, J. Conny VanMunsteren<sup>1</sup>, Monique R.M. Jongbloed<sup>1,2</sup>, Marco C. DeRuiter<sup>1</sup>

<sup>1</sup> Dept. Anatomy and Embryology, Leiden University Medical Center, Leiden, The Netherlands <sup>2</sup> Dept. Cardiology, Leiden University Medical Center, Leiden, The Netherlands <sup>3</sup> Dept. Physiology and Pharmacology, Schulich Medicine & Dentistry, Western University, London, Ontario, Canada <sup>4</sup> Dept. Molecular Cell Biology, Leiden University Medical Center, Leiden, The Netherlands

#### **Abstract**

The bicuspid aortic valve (BAV), a valve with two instead of three aortic leaflets, belongs to the most prevalent congenital heart diseases in the world occurring in 1-2% of the general population. We aimed to understand how changes in early cellular contributions result in BAV and impact cardiovascular outflow tract development.

Detailed 3D reconstructions, immunohistochemistry and morphometrics determined that during valvulogenesis the non-coronary leaflet separates from the parietal outflow tract cushion instead of originating from an intercalated cushion.

*Nos3*<sup>-/-</sup> mice develop a BAV without a raphe as a result of incomplete separation of the parietal outflow tract cushion into the right and non-coronary leaflet.

Genetic lineage tracing of endothelial, second heart field and neural crest cells revealed altered deposition of neural crest cells and second heart field cells within the parietal outflow tract cushion of *Nos3*. embryos. The abnormal cell lineage distributions also affected the positioning of the aortic and pulmonary valves at the orifice level.

The results demonstrate that the development of the right and non-coronary leaflets are closely related. A small deviation in the distribution of neural crest and second heart field populations affects normal valve formation and results in the predominant right-non type BAV in *Nos3*<sup>-/-</sup> mice.

### 4.1 Introduction

The tricuspid aortic valve (TAV) has a crucial role in maintaining the unidirectional blood flow from the left ventricle into the systemic circulation. Abnormalities in aortic valve morphology, as seen in case of the bicuspid aortic valve (BAV), have been linked to valvular regurgitation, stenosis and progressive thoracic aortic aneurysm development (*Ward*, 2000; *Verma and Siu.*, 2014; *Sievers et al.*, 2015; *Merkx et al.*, 2017). BAV is currently accepted as a congenital anomaly with a high incidence, occurring in 1-2% of the Western population (*Roberts*, 1970; *Ward*, 2000; *Hoffman and Kaplan*, 2002).

BAV is generally considered to be an abnormal fusion of aortic leaflets which occurs during

embryonic development (Fernandez et al., 2009; Theron et al., 2015; Odelin et al., 2017). Although leaflet fusion might be a valid mechanistic explanation, there is currently no unequivocal data supporting this mechanism in BAV mouse models.

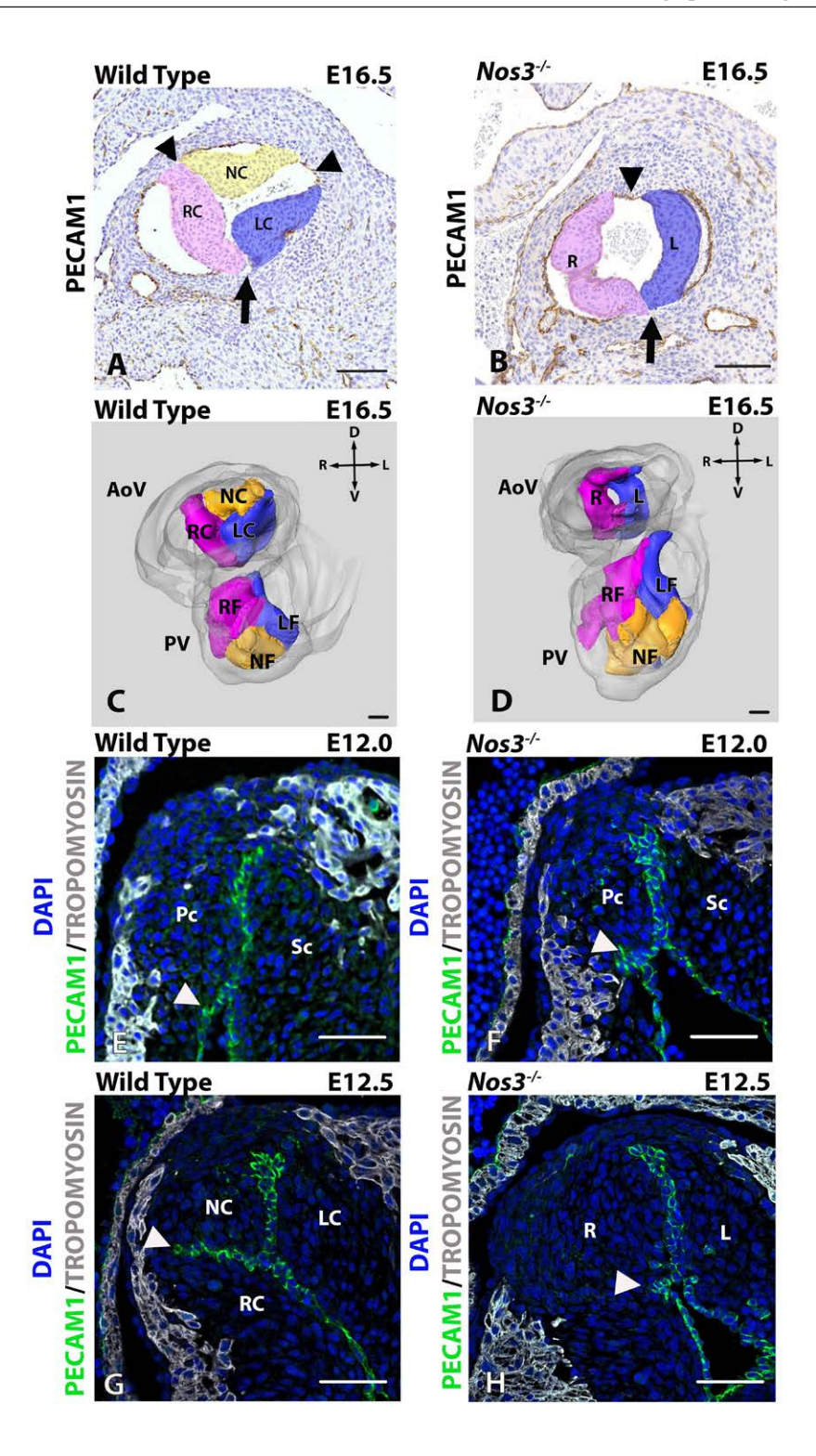
During embryonic development the heart starts as a single heart tube consisting of an outer layer of myocardium and an inner lining of endocardium. These layers are separated by a thick hydrophilic region of cardiac jelly, rich in extracellular matrix, hyaluronic-acid, glycosamino-and proteoglycans, produced by cardiomyocytes (*Manasek*, 1968). The primitive myocardium secretes factors, like Bmp2, in the cardiac jelly which induce the transition of endothelial cells into mesenchymal cells (EndMT) (*Sugi et al., 2004*). This process results in an invasion of endothelial-derived mesenchymal cells into the cardiac jelly (*Eisenberg and Markwald*, 1995; *Kisanuki et al., 2001*). In the cardiac outflow tract (OFT) EndMT results in the formation of a septal and a parietal cushions, the primordia of the myocardial OFT septum and the semilunar valves. Defects in cardiac jelly synthesis result in severely hypoplastic cushions due to failed EndMT (*Baldwin, Lloyd and Solursh, 1994; Camenisch et al., 2000*). Failure of EndMT has been shown to result in bicuspid aortic valves (*Thomas et al., 2012; Mommersteeg et al., 2015*). BAV in *Nos3*<sup>-/-</sup> has also been suggested to be caused by early defects in EndMT resulting in reduced mesenchyme populations in the outflow tract cushions (*Fernandez et al., 2009; Y. Liu et al., 2013*).

Migration of cardiac neural crest cells from the neuroectoderm into the OFT cushions induces the formation of the aortopulmonary (AP) septum, which divides the common OFT at the cardiac to vascular border into an aortic and pulmonary orifice and more proximally intracardiac into a right and left ventricular OFT (Waldo et al., 1998; Jiang et al., 2000; Gittenberger-De Groot et al., 2005). During further development, the parietal cushion gives, at orifice level, rise to the right facing leaflets of the aortic and the pulmonary valve, while the septal cushion will develop into the left facing leaflets of both valves. Finally, the non-facing aortic leaflet and pulmonary leaflet are considered to be derived from separately developing intercalated cushions on the posterior and anterior sides of the OFT, respectively (Kramer, 1942; Lin et al., 2012). Although the development of the septal and parietal cushion has been studied intensively, the role of these intercalated cushions during development remains a challenging concept despite recent progress (Anderson et al., 2003; Lin et al., 2012; Eley et al., 2018; Mifflin et al., 2018). For clarity of description of the valve leaflets and the correlation with the terminology used for the aortic leaflets in human patients with BAV we will refer to the aortic leaflets as right coronary (RC), left coronary (LC) and non-coronary (NC) leaflets (Sievers and Schmidtke, 2007). For the pulmonary semilunar valve leaflets we have chosen to use right facing (RF), left facing (LF) and

a non-facing (NF) leaflets (Fig. 4.1A-D).

It is well established that the aorta and aortic valve are developmentally related. Neural crest (Waldo et al., 1998; Jiang et al., 2000), endothelial (Eisenberg and Markwald, 1995; Kisanuki et al., 2001), epicardial cell lineages (Gittenberger-de Groot et al., 2012) and second heart field (SHF) (Zaffran and Kelly, 2012) derived cells contribute to both the ascending aorta, the aortic valve (Eley et al., 2018; Mifflin et al., 2018) and the various components of the aortic root (valvular leaflets, annulus, sinuses of Valsalva) (de la Cruz et al., 1977; Kirby, Gale and Stewart, 1983; Waldo et al., 2001). Mouse models of BAV show cushion formation to be an essential process during valve formation and defects in contributing cell lineages are known to result in BAV (Biben et al., 2000; Lee et al., 2000; Macatee, 2003; Laforest and Nemer, 2011; Makki and Capecchi, 2012; Thomas et al., 2012; Mommersteeg et al., 2015). In the present study, we examined the contributions of neural crest, endothelial and SHF lineages in aortic valve development of wild type and Nos3<sup>-/-</sup> mouse embryos to identify novel congenital aberrations involved in the formation of BAV. Understanding the fundamental embryology of these early cardiac lineages is crucial to address the challenges in BAV.

Figure 4.1 Failure of cushion separation results in bicuspid aortic valves. A-B: Anti-PECAM1 labelled histological antibody staining depicting the left coronary leaflet (LC), right coronary leaflet (RC) and non-coronary leaflet (NC) in E16.5 tricuspid aortic valve (TAV) wild type ( $\mathbf{A}$ ) and left (L) right (R) leaflets in bicuspid aortic valve (BAV) Nos3<sup>-/-</sup> mice (**B**). Position of the facing L-R commissure was similar between wild type and Nos3<sup>-/-</sup> mice (indicated by arrows in A and B). Bicuspid Nos3<sup>-/-</sup> developed a commissure opposite to the facing commissure whereas tricuspid wild type mice developed three commissures equilateral between the leaflets. (arrowheads in A and B). C-D: 3D reconstruction of the aortic and pulmonary valves (AoV and PV respectively) showing individual and connected leaflets within the aortic root in wild type ( $\mathbf{C}$ ) and Nos3- $^{\perp}$  ( $\mathbf{D}$ ) mice. Note that in Nos3- $^{\perp}$  mice leaflets of the PV developed normally. E-H: Anti-PECAM1 (green), anti-TROPOMYOSIN (grey) immunofluorescent stained paraffin sections of the aortic valve at E12.0 wild-type (**E**) and Nos3.(**F**) embryos show the parietal (Pc) and septal cushion (Sc). Wild type embryos develop tricuspid leaflets as a result of separation of the parietal cushion into the right- and non-coronary leaflets at E12.5 (G). Failure of separation of the parietal cushion resulted in the formation of bicuspid aortic valves (H). Location of endothelial infolding is indicated by white arrowheads. The endothelial distribution within the leaflets showed no indication of leaflet fusion as the result of the merging of two individual leaflets, as no endothelial lined raphe is present in bicuspid Nos3-- mice. Nuclei were stained with DAPI (blue). AoV: aortic valve, PV: pulmonary valve, Pc: Parietal cushion, Sc: Septal cushion, RC: right coronary, LC: left coronary, NC: non-coronary, RF: right facing, LF: left facing, NF: non-facing, R: right, L: left, V: Ventral, D: Dorsal. Scale bars: 50µm.



### 4.2 Methods

#### 4.2.1 Embryonic Material

Cardiac outflow tract and aortic leaflet development was studied in a series developmental stages of Nos3<sup>-/-</sup> mice and compared to wild type mice of the same age. The following mice have been used in this study: Nos3<sup>-/-</sup> B6.129P2-NOS3tm1Unc/J mice (purchased from Charles River Laboratories, Maastricht, Netherlands), Mef2C-Cre mice were kindly provided by Dr. QuinPing Feng (Ontario, Canada) (Verzi et al., 2005). B6.Cg-Tg(Wnt1-cre)2Sor/J (purchased from Jackson laboratories, JAX stock #022501, Bar Harbor, USA), Tie2-Cre mice were kindly provided by Dr. Bernd Arnold, (Heidelberg, Germany), B6.129(Cg)-Gt(ROSA)26Sortm4(ACTB-tdTomato,-EGFP)Luo/J, (mT/mG) (purchased from Jackson laboratories, JAX stock #007576, Bar Harbor, USA). A breeding strategy was carried out to generate Nos3<sup>-/-</sup>;mT/mG, Nos3<sup>-/-</sup>;Tie2Cre;mTmG, Nos3<sup>-/-</sup>;Wnt1Cre;mT/mG; and Nos3<sup>-/-</sup>;Mef2cCre;mT/mG transgenic mouse lines mice which were used for lineage analysis. All mice were back crossed to the Black6 background using C57BL/6JLumc mice (purchased from Leiden University Medical Center, Leiden, Netherlands).

Adult mice were bred overnight and embryonic age was determined according to the presence of a vaginal plug the following morning. Noon of the day which the plug was first observed was taken as embryonic day (E)0.5. Embryos were isolated through hysterectomy at E10.5-E16.5 following dissection in phosphate buffer solution pH 7.4 (PBS). Tail biopsies were used for the isolation of genomic DNA for genotyping by polymerase chain reaction (PCR) targeted at *Cre* transgenes as for *Nos3* (**Table S.4.1**). All mice were handled according to the Guide for Care and Use of Laboratory Animals, as published by the NIH and the experiments were approved by the local LUMC animal welfare committee (dec14184).

Fwd_Cre	ATG-GAT-TTC-CGT-CTC-TGG-TG
Rev_Cre	TTG-CCC-CTG-TTT-CAC-TAT-CC
Nos3_Mut_oIMR8963	AAT TCG CCA ATG ACA AGA CG
Nos3_WT_oIMR9357	AGG GGA ACA AGC CCA GTA GT
Nos3_Common_olMR9358	CTT GTC CCC TAG GCA CCT CT
mTmG_WT_olMR9021	CCG AAA ATC TGT GGG AAG TC
mTmG_Mut_22163	CGG GCC ATT TAC CGT AAG TTA T
mTmG_Common_oIMR9020	AAG GGA GCT GCA GTG GAG TA

**Supplemental Table S.4.** *Primers used for genotyping.* 

#### 4.2.2 Immunohistochemistry

For histological examination, embryos were fixed in 4% paraformaldehyde (0.1M, pH 7.4) for 24h at 4°C. Subsequently, they were embedded in paraffin, sectioned serially (5 μm), and mounted on glass slides. Samples were deparaffinized with xylene followed by a series of graded ethanol steps for rehydration into PBS. Endogenous peroxidase activity was inhibited by exposure of 0.3% H<sub>2</sub>0<sub>3</sub> for 20 minutes. Slides were subjected to microwave antigen retrieval in citric acid buffer (10 mM Citric Acid, 0.05% Tween 20 pH=6.0) for 12 minutes at 97°C. Sections were incubated with primary antibodies against NKX2.5, eGFP, TROPOMYOSIN and PECAM1. Primary antibodies were diluted in PBS-Tween-20 with 1% bovine serum albumin (BSA, A8022; Sigma-Aldrich, St. Louis, MO, USA) to prevent non-specific binding. Between subsequent incubation steps all slides were rinsed twice in PBS followed by a single rinse in PBS-Tween-20. Thyramide signal amplification (TSA PLUSbiotin kit, NEL749A001KT, Perkin Elmer, Waltham, MA, USA) was used in NKX2.5 staining through addition of HRP labelled antibodies followed by thyramide amplification according to the TSA PLUS biotin kit manual. Primary antibodies were visualized by incubation with fluorescently labelled secondary antibodies, diluted in PBST for 60 minutes. Detailed antibody descriptions can be found in the supplementary table (Table **5.4.2**). DAPI (D3571, 1/1000; Life Technologies) was used as a nuclear stain and the slides were mounted with Prolong gold (Life Technologies).

**Supplemental Table S.4.2** *Antibodies used in this study.* 

Primary Antibodies	Manufacturer	Dilutions
Nkx2.5	Santa Cruz SC-8697	1/4000
eGFP	Abcam ab13970	1/500
Tropomyosin	Sigma-Aldrich Chemie T9283	1/500
PECAM1	Santa Cruz sc-1506-R	1/500
ΑΡ2α	GeneTex GTX62588	1/2000
Secondary Antibodies	Manufacturer	Dilutions
Horse Anti-Goat-Biotin	Vector labs BA-9500	1/200
HRP~Streptavidine - (PO)	Agilent P039701	1/200
Alexa Fluor488~Goat anti-Chicken IgY (H+L)	Thermo Scientific A-11039	1/200
Alexa Fluor 594~Donkey Anti-Mouse IgG (H+L)	Life technologies A-21203	1/200
Alexa Fluor 555~Donkey Anti-Rabbit IgG (H+L)	Life technologies A-31572	1/200
Cy5-Biotin	LifeSpan Biosciences ab6975	1/200

### 4.2.3 Microscopic analyses and three-dimensional reconstructions

3D reconstructions of the embryonic hearts were made with Amira software 6.3 (Template Graphics Software Inc., Houston, TX, USA) using a selection of Nos3\*;Tie2Cre;mTmG, Nos3\*;Wnt1Cre;mTmG and wild type embryos respectively between E10.5 and E16.5 (Table S.4.3). Tissue sections (5µm) were collected from paraffin embedded embryos and immunostaining was preformed against NKX2.5, GFP, TROPOMYOSIN, PECAM1 and DAPI. Slides were scanned using the panoramic 250 flash III slide scanner (3DHISTECH Ltd., Budapest, Hungary) and images of identical scale and exposure were exported using Histech Panoramic Viewer (3DHISTECH Ltd., Budapest, Hungary). Subsequently, the photos were stacked and semi-automatically aligned in Amira. Relevant cardiac structures were labeled, based on morphology and stains. Surface views were executed to PDF formats by using Adobe Acrobat 9.5 software package.

### 4.2.4 Myocardial and endocardial cushion morphometry

The ventricular myocardium and the endocardial OFT cushion volumes were measured at ages E10.5 − E13.5 by using the stereological method described by Gundersen et al (1988). This method uses the random placement of evenly distributed points (grid) on to stained sections. Points within a tissue of interest are then counted on at least 10 sections after which a reliable estimation of the real tissue volume can be made. The measured ventricular myocardium and endocardial cushion volumes were compared between wild type (E10.5 N=3, E11.0 N=5, E11.5 N=5, E12.5 N=5) and Nos3<sup>-/-</sup>(E10.5 N=3, E11.0 N=4, E11.5 N=7, E12,5 N=6) embryos. A 100 mm² grid was used to measure the ventricular myocardium (E10.5-E13.5) and endocardial cushion (E10.5-12.5) volumes. At older ages (E12.5) a 225 mm² grid was used for the ventricular

Experimental Evaluation						
	Total embryos		Immuno-staining		3D Reconstructions	
Age	Wild Type	Nos3-/-	Wild Type	Nos3-/-	Wild type	Nos3 <sup>-/-</sup>
E10.5	3	4	3	4	2	2
E11.0	7	6	7	6	1	0
E11.5	11	11	11	11	5	3
E12.0	4	2	4	2	1	0
E12.5	20	16	20	16	4	4
E13.5	14	11	14	11	2	1
E14.5	8	8	8	8	2	4
E15.5	3	8	3	8	0	0
E16.5	4	12	4	12	2	1

**Supplemental Table S.4.3** Number of embryos used in this study.

myocardium morphometry. The distance between two subsequently measured sections was 0,05 mm when measuring the myocardium and 0,025 mm for the endocardial cushions morphometry. An Olympus microscope was used with either a 40 or 100 times magnification, depending on the size of the heart.

### 4.2.5 Cell Lineage Analysis

Fluorescent images were collected using the panoramic 250 flash III slide scanner (3DHISTECH Ltd., Budapest, Hungary) or Leica Sp8 confocal microscopy (Leica Microsystems, Buffalo Grove IL, USA). Measurements were performed on aortic valves from transverse sections (5μm) of wild type C57BL/6JLumc (N=8), Tie2Cre;mTmG (N=5), Wnt1Cre;mTmG (N=4) and Nos3<sup>-/-</sup> B6.129P2-NOS3tm1Unc/J (N=8), Nos3<sup>-/-</sup>;Tie2Cre;mTmG (N=4), Nos3<sup>-/-</sup>;Wnt1Cre;mTmG (N=4). For each embryo all sections containing the heart were imaged. Image analysis was performed using a macro designed in Fiji (Schindelin et al., 2012). The macro was designed to measure the nuclear volume of DAPI+ nuclei bound by cytoplasmic GFP as for DAPI+ nuclei lacking cytoplasmic GFP for each individual leaflet. Briefly, collected images (8-bit) were contrast stretched until 0.4% saturation was reached ensuring identical spectral intensity for all images. Leaflet perimeter of LC, RC and NC were manually selected and DAPI+ nuclei found within a boundary of cytoplasmic GFP were measured as lineage specific nuclei. DAPI+ nuclei lacking cytoplasmic GFP were added to the total volume of DAPI+ nuclei in that individual leaflet. In case of BAV, leaflet perimeters between RC and NC would be defined following the shortest straight path from the observed endothelial infolding to the myocardial wall. Manual image threshold for GFP+ cytoplasm was set at a pixel intensity of 120 and DAPI+ thresholds were automatically detected using imageJ "default" algorithm. Following complete leaflet measurement, volumetric calculations were processed in Excel 2007 (Microsoft, Redmond, Washington, USA). Additional calculations as well as graphic and statistical analysis was performed in GraphPad Prism 7.0 for Windows (GraphPad Software, La Jolla California USA).

### 4.2.6 Angle measurement aorta and pulmonary trunk

Angle measurements of the aorta and pulmonary trunk were performed on wild type TAV (N=12), Nos3<sup>-/-</sup> TAV (N=12), and Nos3<sup>-/-</sup> BAV (N=10). Serial slides stained with Resorcin Fuchsin were stacked and aligned with the Amira software version 6.3. Two planes were created through the top of the three commissure attachments of the aorta and pulmonary valves. In case of BAV the plane was set at the top of the two commissures and the plane perpendicular was determined by the smallest diameter of the aorta. The plane normal of both the aortic

valve (dot vector  $v_{aorta}$ ) and pulmonary valve (dot vector  $v_{pulm}$ ) could then be determined. The angle between the aorta and pulmonary valves was calculated using the formula

$$Cos(\alpha) = \frac{V_{aorta} * V_{pulm}}{|V_{aorta}| * |V_{pulm}|}$$

### 4.2.7 Extracardial lineage analysis

Extracardial lineage analysis was performed on wild type C57BL/6JLumc (N=3) and *Nos3*<sup>-/-</sup> B6.129P2-NOS3tm1Unc/J (N=3) embryos at stage E11.5. Immunostainings were performed using anti-NKX2.5 and anti-AP2α antibodies to visualize SHF and neural crest cells respectively. Detailed antibody descriptions can be found in the supplementary table (**Table S.4.2**). 3D reconstructions and volumetric measurements of the extracardiac region adjacent to the cardiac outflow tract up to but not including the pharyngeal endoderm were made using Amira software 6.3 (Template Graphics Software Inc., Houston, TX, USA) and further processed in GraphPad Prism 7.0 for Windows (GraphPad Software, La Jolla California USA).

### 4.2.8 Statistical analysis

Results are represented as mean  $\pm$ SD of at least three independent experiments. Comparisons were made using unpaired two tailed Student's t-test or One-way ANOVA test if data comparison involved more than two groups followed by Tukey's multiple comparisons test. Significance was assumed when p < 0.05. Statistical analysis was performed in GraphPad Prism 7.0 for Windows (GraphPad Software, La Jolla California USA).

### 4.3 Results

### 4.3.1 Morphological landmarks in bicuspid Nos3<sup>-/-</sup> mice

Seventy-three percent of *Nos3*<sup>-/-</sup> embryos had a normal TAV while 27% develop a BAV (**Table 5.4.4**). In *Nos3*<sup>-/-</sup> embryos, the bicuspid valve had two similar sized leaflets in a left-right leaflet orientation without a visible raphe that indicated the position of a possible third commissure (**Fig. 4.1A-B**). The lack of a raphe did not allow for discrimination between a R-N (a fusion/confluence of RC and NC leaflets) or L-N (a fusion/confluence of LC and NC leaflets) type BAV solely on the basis of morphological aspects. In wild type mice the three parabolic-shaped leaflets are embedded within the aortic root. Distally, at the sinotubular junction, these structures formed three interleaflet commissures. In contrast to wild type, bicuspid *Nos3*<sup>-/-</sup> mice

**Supplemental Table S.4.4** Percentage of BAV found in wild type (WT) and Nos3.<sup>-/-</sup>.

Age	BAV in WT	BAV in Nos3-/-	Other cardiovascular anomalies in WT	Other cardiovascular anomalies in <i>Nos3</i> -/-
E12.5	0/20	4/16	0/20	0/16
E13.5	0/14	0/11	0/14	0/11
E14.5	0/8	2/8	0/8	0/8
E15.5	0/3	5/8	0/3	0/8
E16.5	0/4	4/12	0/4	0/12
Mean	0/49 (0%)	15/55 (27.27%)	0/49 (0%)	0/55 (0%)

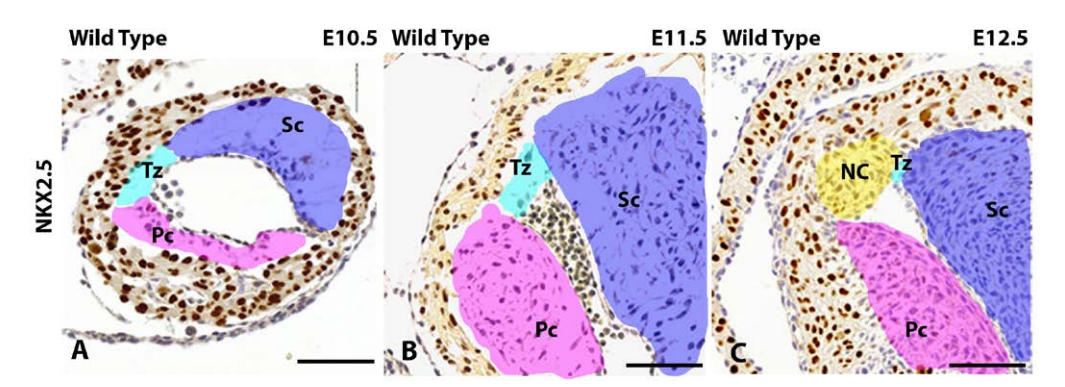
developed a commissure (arrowheads, **Fig. 4.1A-B**) opposite to the facing commissure (arrow, **Fig. 4.1A-B**).

## 4.3.2 Incomplete separation of the parietal cushion leads to R-N BAV in *Nos3*-/- embryos

The first indications of leaflet formation could be observed at E12.0 at which the putative aortic valve leaflets consisted of the parietal and septal cushions and a slight indentation of endothelial cells was present in both wild type and *Nos3*<sup>-/-</sup> embryos (**Fig. 4.1E-F**, arrowheads). At E12.5 a marked separation of the parietal cushion was observed in wild type embryos. The RC and NC leaflet could be distinguished by the presence of an endothelial infolding into the cushion (**Fig. 4.1G**, arrowhead). Bicuspid *Nos3*<sup>-/-</sup> embryos did not develop this marked endothelial infolding causing an incomplete separation of the parietal cushion into a NC and RC leaflet (**Fig. 4.1H**). This resulted in the formation of a single right valvular leaflet, leading to a R-N BAV. Moreover, there was no indication of intercalated cushion development in wild type embryos between the parietal and septal cushion between E10.5 and E12.5. (**Fig. S4.1**).

# 4.3.3 Aortic leaflets develop solely from the parietal and septal cushions

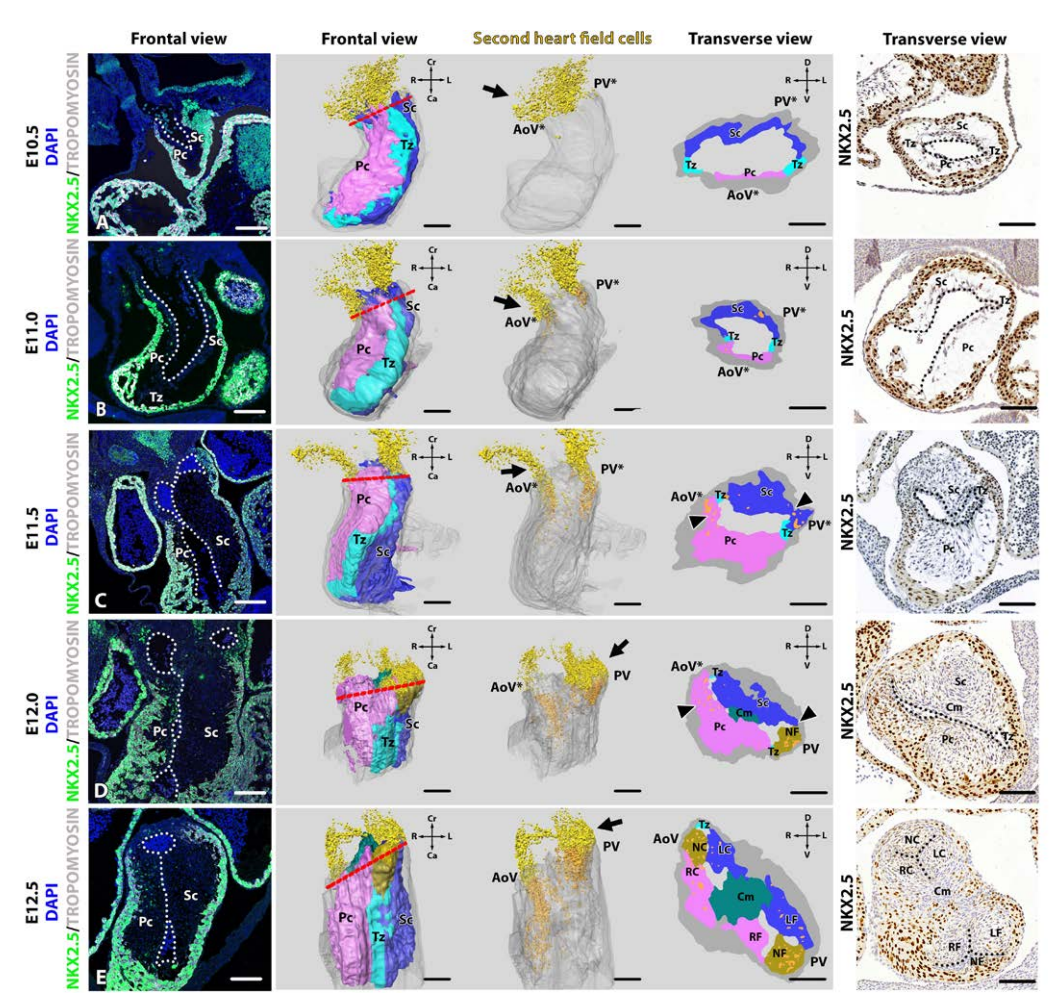
The early OFT cushion formation started around E10.5 in wild type mice with the production of cardiac jelly within the interstitial space between the outer myocardial wall and inner endocardial lining, followed by migration of endocardial derived cells into two compartments resulting in the two OFT cushions, the parietal and septal cushions (**Fig. S4.1**). During cellularization the two cushions remained interconnected by two thin transitional zones. The



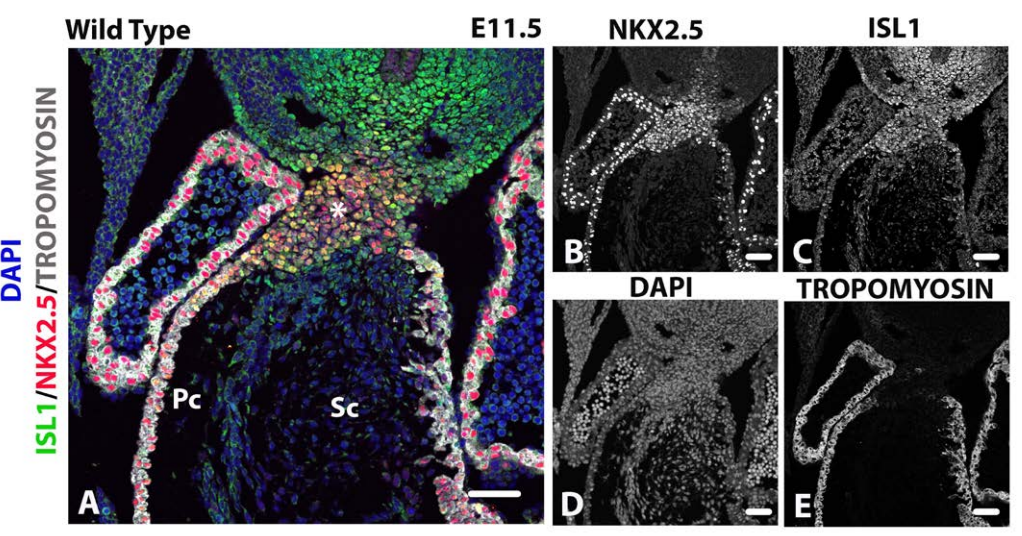
Supplemental Figure S.4.1 Endocardial cushion development in wild type embryos. A: At E10,5 endocardial cells have migrated into the septal cushion (Sc) (blue) and parietal cushion (Pc) (purple). These cushions remained connected by a transitional zone (Tz) (cyan), a thin region of cardiac jelly sparsely populated by cells. B: The Pc and Sc enlarged at E11.5 whereas the transitional zone remained sparsely populated. C: At E12.5 the transitional zone was positioned at the site of the commissure between the left coronary leaflet (LC) and non-coronary leaflet (NC). The NC (yellow) was separated from the Pc. Myocardial cells were NKX2.5 positive (brown). Scale bar is 50µm.

transitional zones are two distinct regions which connect the parietal and septal cushion over the complete length at both ends and are characterized by their composition of mostly cardiac jelly, virtually devoid of cells (**Fig. 4.2A, Fig. S4.1**). At E10.5 and E11.0, the parietal cushion was positioned ventrolateral in the cardiac outflow tract whereas the septal cushion was located more dorsomedial (**Fig. 4.2A-B**). Extracardiac SHF cells could be observed immunohistochemically as non-myocardial (TROPOMYOSIN (TM) negative) cells expressing nuclear NKX2.5 (*Waldo et al., 2001*) (**Fig. S4.2**). NKX2.5+/TM- SHF cells (yellow) migrated via the pharyngeal arteries into the distal parts of the parietal and septal cushions into the cardiac outflow tract (orange) (**Fig. 4.2, S4.3**). From E11.5 onwards the future pulmonary outflow tract changed from a left medial position to a more ventral position with regard to the future aortic ostium, corresponding to a clockwise rotation (**Fig. 4.2C-E, S.4.3C-E**). This phenomenon has

Figure 4.2 Aortic and pulmonary leaflets develop from the parietal and septal cushions. First column depicts frontal fluorescent images of embryonic septal (Sc) and parietal cushions (Pc) within the cardiac outflow tract (OFT) of wild type embryos age E10.5-12.5 using anti-NKX2.5 (green), anti-TROPOMYOSIN (grey) and DAPI as a nuclear marker (blue). Column 2 and 4 show frontal view on and transverse sections through 3D reconstructions of the OFT that can be divided into the myocardial outer wall (grey) and the Pc and Sc (purple and dark blue, respectively). The parietal and septal cushions were connected by a thin transitional zone (Tz) of cardiac jelly sparsely populated by cells (cyan). Column 3 is similar to the reconstructions in column 2 but without the reconstructed Pc, Tz and Sc to demonstrate the intracardiac SHF cells. The 5th column depicts an immunostaining of NKX2.5 at the location of the

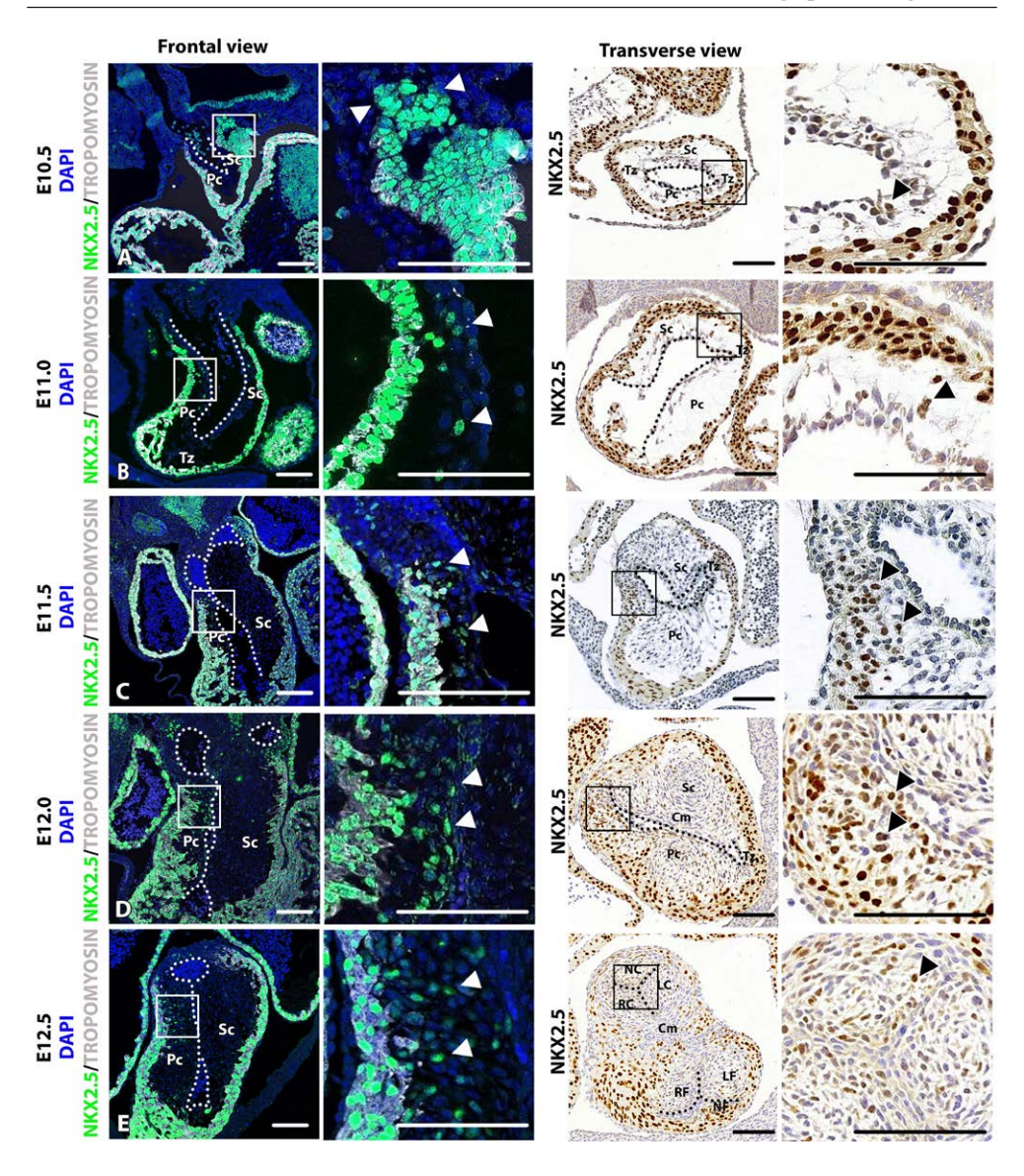


transverse plane (red dotted line). **A**: NKX2.5+/TROPOMYOSIN: second heart field (SHF) cells (yellow) were located at the proximal outflow tract outside the heart tube at E10.5 (Arrows). **B**: NKX2.5+/TROPOMYOSIN: SHF cells that were positioned in the septal and parietal cushions at opposing poles of the OFT at E11.0 have been reconstructed in orange. **C**: Due to OFT rotation the NKX2.5+ cells (orange) could be found within the parietal and septal cushions where the non-facing (NF) and non-coronary (NC) leaflets would form (arrow heads). **D**: At E12.0, condensed mesenchyme (Cm) (dark green) indicated the formation of the AP-septum in the transverse view. At the pulmonary orifice, the NF leaflet dissociated from the septal cushion whilst the NC leaflet remains connected (arrow heads). **E**: Complete separation of valve leaflets was established at E12.5 at which the NC leaflet dissociated from the parietal cushion. AoV\*: future aortic valve, PV\*: future pulmonary valve, AoV: aortic valve, PV: pulmonary valve, Pc: Parietal cushion, Sc: Septal cushion, Tz: Transitional zone, Cm: Condensed mesenchyme, RC: right coronary leaflet, LC: left coronary leaflet, NC: non-coronary leaflet, RF: right facing leaflet, LF: left facing leaflet, NF: non-facing leaflet D: dorsal, V: ventral, Cr: Cranial, Ca: Caudal. White and black dotted line indicate endothelial lining. Scale bar: 100µm.



Supplemental Figure S.4.2 NKX2.5\*/TROPOMYOSIN cells represents ISL1\* second heart field cells contributing to the outflow tract. A-E: Immuno-fluorescent images showing co-expression of NKX2.5 and ISL1 in second heart field cells contributing to the formation of the outflow tract in E11.5 wild type embryos. Colour scheme: Anti-NKX2.5 (red), Anti-ISL1 (green), Anti-TROPOMYOSIN (grey), DAPI was used as a nuclear staining (blue). Scale bar: 50µm.

been described to result from the asymmetric addition of SHF cells to the pulmonary side of the OFT, the so called "pulmonary push" (*Scherptong et al., 2012*). The parietal cushion became positioned more dorsal and the septal cushion more ventral (**Fig. 4.2D-E**). At this stage, the NKX2.5+/TM- SHF cells form a distinct group of cells in the septal and parietal cushions close to the transitional zones (cyan) (**Fig. S.4.3D-E**). The transitional zones in between the septal and parietal cushions remained sparsely populated by cells. The interleaflet commissures of the LC and NC aortic leaflets as well as the LF and NF pulmonary leaflets developed at these transitional zones. The pulmonary NF leaflet also derived from a main OFT cushion. In this case the septal cushion. The timing is somewhat different in that this occurred at E12.0 (**Fig. 4.2D**), whilst the separation of the aortic NC leaflet from the parietal cushion occurred, somewhat later, at E12.5 (**Fig. 4.2E**). The septal cushion therefore gave rise to three leaflets being the LC aortic leaflet as well as the LF and NF pulmonary leaflets. The parietal cushion also gave rise to three leaflets being the RC and NC aortic leaflets as well as the RF pulmonary leaflet (**Fig. 4.2E**).



**Supplemental Figure S.4.3 Direct NKX2.5**+/TROPOMYOSIN- second heart field cells contribution to the aortic valve. A-E: NKX2.5+/TROPOMYOSIN-second heart field cells migrate into the cushions during development and contribute directly to the formation of the aortic leaflets. Colour scheme immunofluorescent images: Anti-NKX2.5 (green), Anti-TROPOMYOSIN (grey), Nuclei were stained with DAPI (blue). Colour scheme imunnohistological images: Anti-NKX2.5 (brown), nuclei are counterstained using hematoxine eosine (HE). Scale bar: 50µm.

## 4.3.4 The volume of the myocardium and the outflow tract cushions are not affected in the *Nos3*-/- embryos

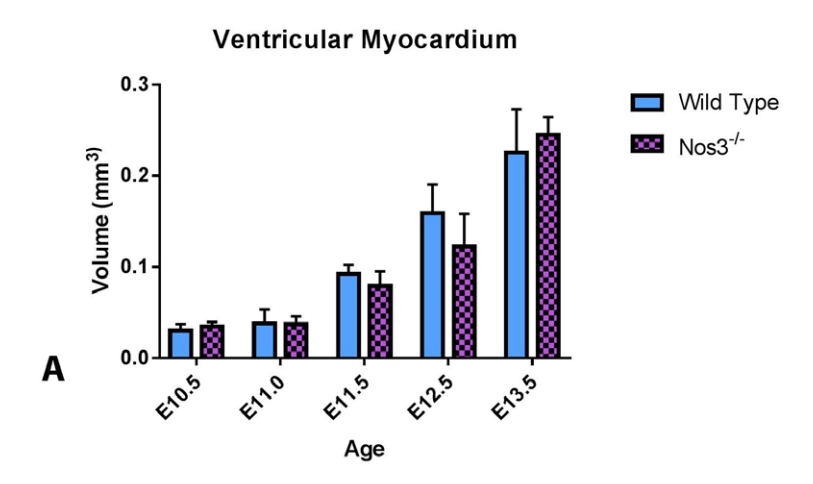
Developmental growth of the OFT cushions could be determined by a decrease in acellular fraction volume (as a measure for the amount of cardiac jelly) and an increase in cellular fraction volume containing cell bodies. Histological image examination determined no difference (p>0.05) in cushion composition of the septal and parietal cushions between *Nos3*<sup>-/-</sup> and wild type embryos from stages E10.5-E12.5 (**Fig. S4.4A-B**). These findings indicate that defects in *Nos3*<sup>-/-</sup> embryos were not caused due to a reduction in total cell volume or changes in cardiac jelly production. Furthermore, no differences were found in heart size based on ventricular myocardial volume measurements between wild type and *Nos3*<sup>-/-</sup> embryos at embryonic age E10.5- E13.5 indicating that the myocardial growth rate is unaffected by the *Nos3* mutation (**Fig. S.4.4C**).

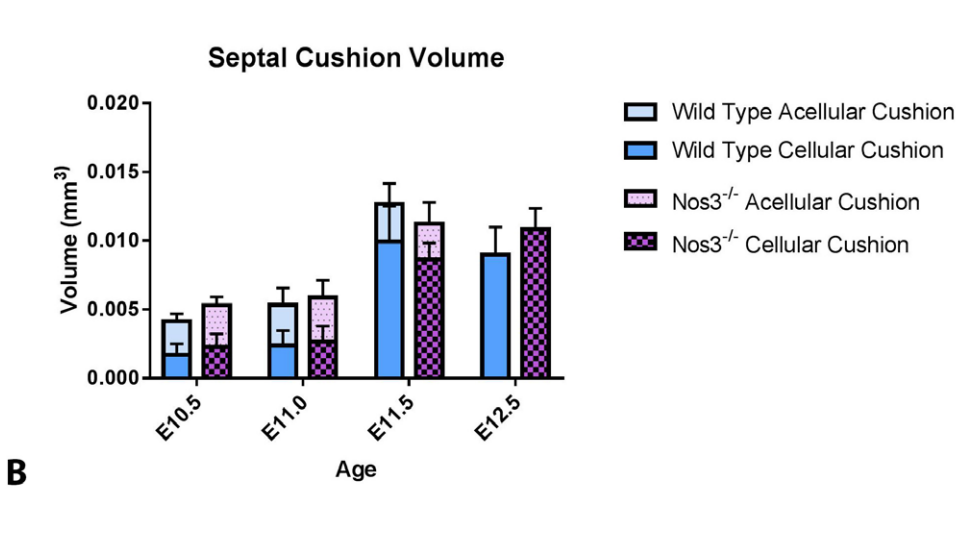
### 4.3.5 Aortic and pulmonary leaflets harbour unique cell lineage distributions

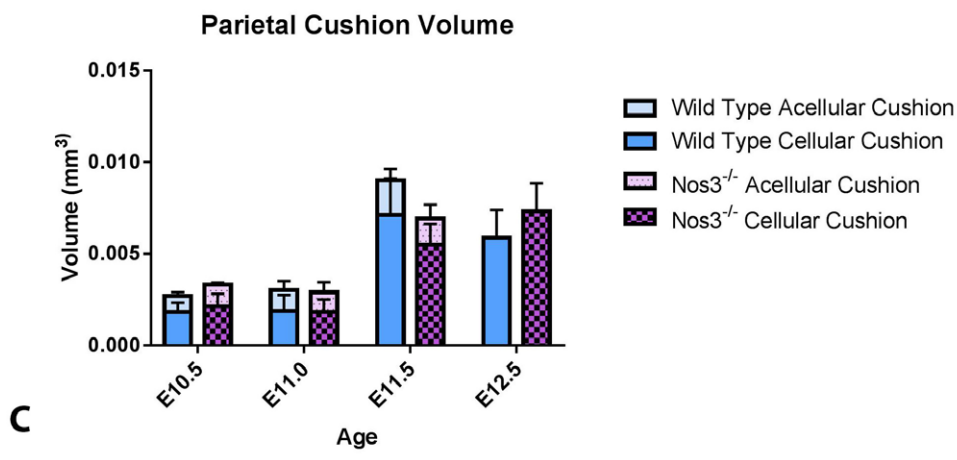
The use of the Cre-loxp system allowed the study of cellular offspring by genetically labelling original progenitor cells (*Sauer and Henderson, 1988; Nagy, 2000*). By combining genetic lineage tracing and antibody staining it was confirmed that the NKX2.5<sup>+</sup>/TM<sup>-</sup> population within the NC leaflets of the aorta are of SHF descent and that these do not colocalize with endothelial (**Fig. S.4.5A**) or neural crest derived populations (**Fig. S.4.5B**), but are a subpopulation of the *Mef2c*-derived SHF cells (**Fig. S.4.5C**). These NKX2.5<sup>+</sup>/TM<sup>-</sup> SHF populations are also found in the NF leaflet in the pulmonary orifice (**Fig. S.4.5D-F**). Recently a study by Mifflin et al. (*2018*) and Eley et al. (*2018*) have identified similar populations in the NC leaflet of the aorta.

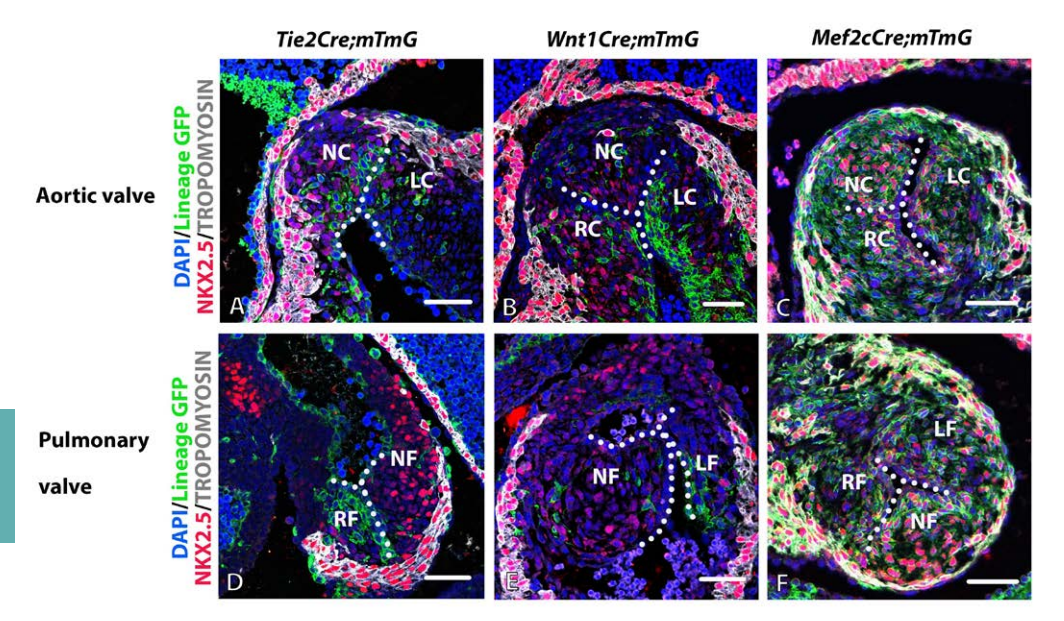
Cell lineage image quantification determined specific regions in the aortic valve to which early cardiac cell lineages contributed. In wild type embryos, the majority of NKX2.5<sup>+</sup>/TM<sup>-</sup> SHF cells contributed to the NC leaflet (**Fig. 4.3A, D**), whereas cells of neural crest origin primarily

**Supplemental Figure S.4.4 Cushion volume is not affected in Nos3**<sup>-/-</sup> **embryos during stages E10.5 to E12.5 of embryonic development. A,B**: Total cushion volume analysis indicated no differences (p > 0.05) in total volume of septal (**A**) and parietal (**B**) cushions between wild type and Nos3<sup>-/-</sup> embryos during development. Close examination also showed no difference in the cellular fractions of the septal and parietal cushions nor the acellular fractions between wild type and Nos3<sup>-/-</sup> embryos at stages E10.5 to E12.5. **C**: Myocardial volume analysis established that Nos3<sup>-/-</sup> embryos have an equal heart size compared to wild type embryos. Data are mean  $\pm$ SD. Analysis was performed using two tailed student T test.



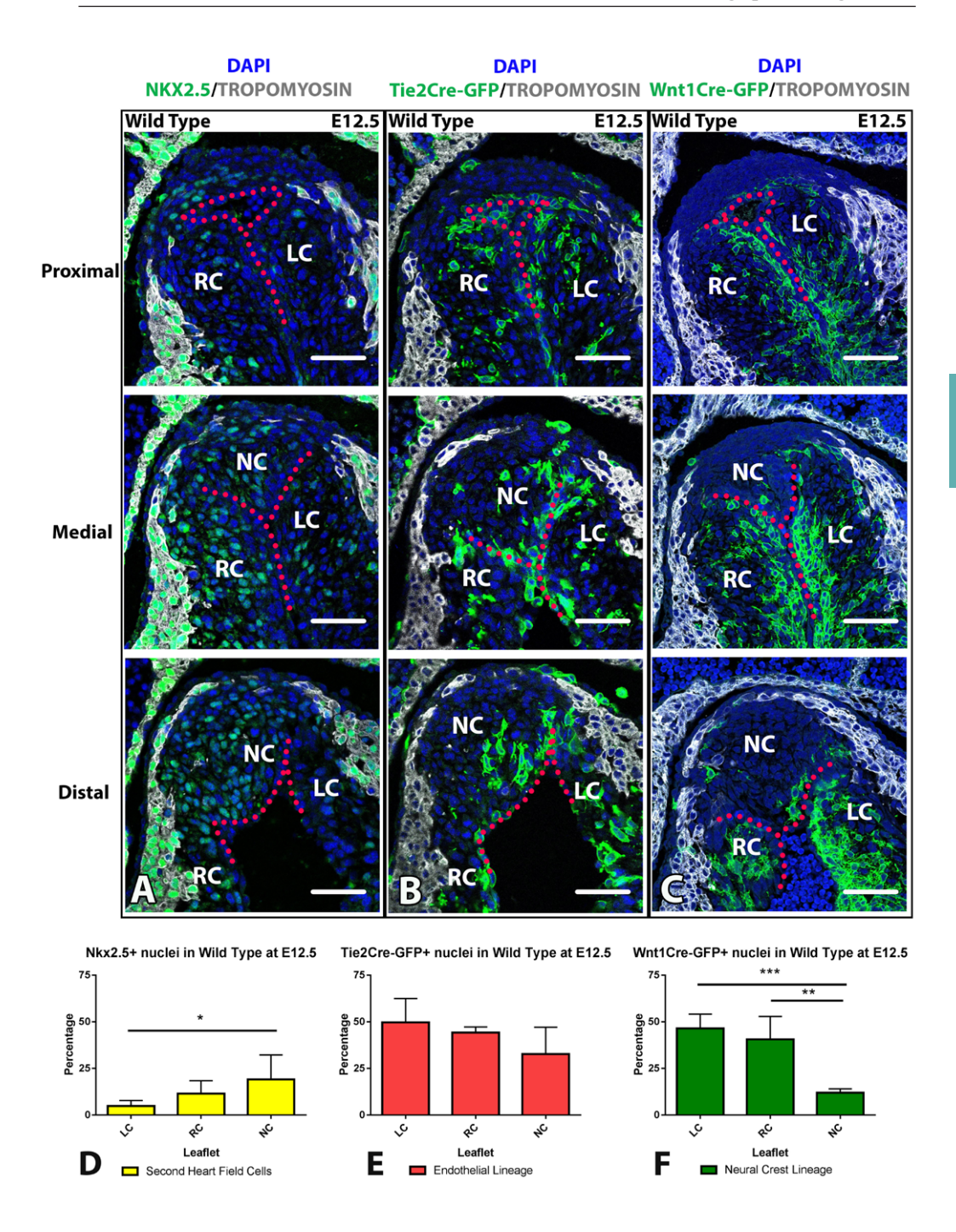






Supplemental Figure S.4.5 Aortic leaflets have unique cell lineage distributions. A-F: Detection of NKX2.5 positive cells negative for TROPOMYOSIN indicated direct contribution of second heart field cells to the non-coronary aortic and non-facing pulmonary leaflet in wild type embryos at E12.5. NKX2.5+/TROPOMYOSIN cells show no overlap with the Tie2Cre endothelial (**A, D**: green) or Wnt1Cre neural crest (**B, E**: green) lineages but do overlap with Mef2cCre second heart field derived cells (**C, F**: green). Dots indicate endothelial lining(white). Color scheme: TROPOMYOSIN (grey), DAPI (blue), NKX2.5 (red), Lineage-Cre derived GFP (green). Scale bar: 50μm.

Figure 4.3 Aortic valve leaflets harbour unique cell lineage distributions in wild type embryos at E12.5. A: Top to bottom pictures represent NKX2.5+/TROPOMYOSIN second heart field (SHF) (green) cell distribution from proximal to distal regions within the aortic valve. Note that the SHF populations within the valve are localized at medial and distal positions. **B**: Depiction of Tie2Cre-GFP+ endothelial *lineage (green) contribution throughout the aortic valve.* **C**: *Wnt1Cre-GFP*<sup>+</sup> *neural crest lineage (green)* cell contribution to the aortic valve is primarily organized in the right and left coronary (RC and LC) leaflets but not the non-coronary (NC) leaflet. D: Cell lineage leaflet analysis of NKX2.5+/TROPOMYOSIN-SHF showed significantly more contribution to the NC leaflet than to the LC leaflet of the aortic valve in wild type embryos (N=8) at E12.5 (P<0.05). E: Tie2CreGFP+ endothelial derived cells showed no bias to which leaflet is populated and distributed equally among individual leaflets in wild type embryos (N=5)at E12.5. F: In wild type embryos, Wnt1Cre-GFP+ neural crest derived cells contributed more to the RC (P<0.01) and LC (P<0.001) leaflets but specifically less to the NC leaflet at E12.5 (N=4). Data are mean  $\pm$ SD. \*, \*\* and \*\*\* indicate P<0.05, P<0.01, and P<0.001 respectively, determined by one-way ANOVA. colour scheme: DAPI (blue), TROPOMYOSIN (grey), Lineage markers (green), Endothelial lining represented with red dotted line. RC: right coronary leaflet, LC: left coronary leaflet, NC: non-coronary leaflet, Scale bar: 50μm.



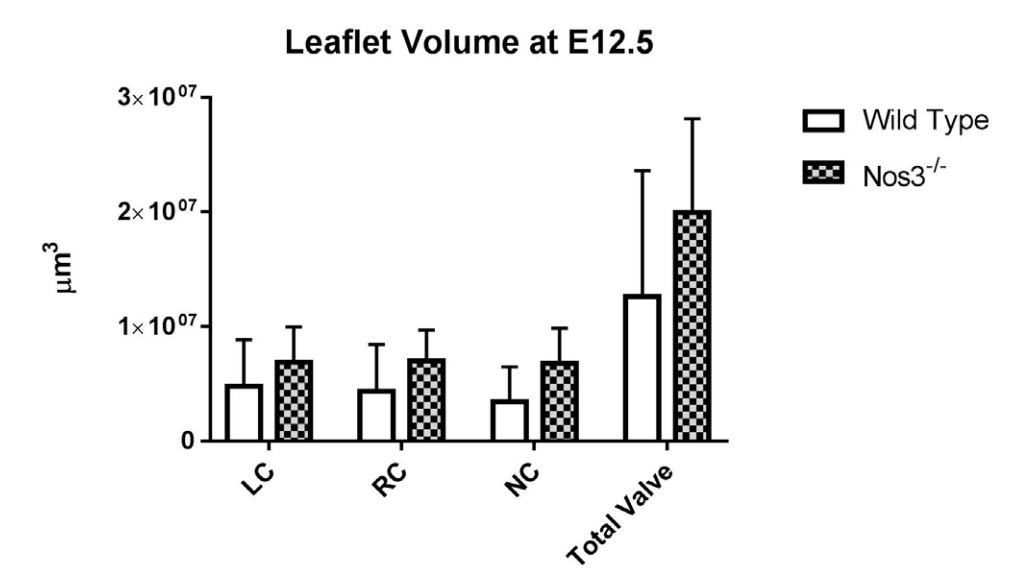
contributed to the LC and RC leaflets (**Fig. 4.3C, F**). Similar neural crest patterns have also been reported in other studies (*Phillips et al., 2013; Odelin et al., 2017*). Interestingly, endothelial derived cells were equally distributed among the aortic leaflets in wild type embryos (**Fig. 4.3B, E**).

### 4.3.6 The distribution of the SHF and NCC in cardiac outflow tract is affected in the *Nos3*-/- embryos

The total leaflet volume between wild type and *Nos3*<sup>-/-</sup> embryos did not differ (**Fig. S.4.6**). *Nos3*<sup>-/-</sup> embryos had a significantly reduced population of in neural crest derived cells in the RC leaflet when compared to aged matched wild type embryos (**Fig. 4.4A**). Moreover, larger contribution of NKX2.5<sup>+</sup>/TM<sup>-</sup> SHF cells was observed in the LC (**Fig. 4.4B**) and NC (**Fig. 4.4C**) leaflet in *Nos3*<sup>-/-</sup> embryos. Although all *Nos3*<sup>-/-</sup> embryos had defects in neural crest and SHF populations, only 27% of *Nos3*<sup>-/-</sup> embryos develop a BAV, as reported in earlier studies of *Nos3*<sup>-/-</sup> mice (**Table S.4.4** and *Fernandez et al., 2009*).

These results show that an altered distribution of neural crest and SHF populations is present in the developing abnormal leaflets of BAV (**Fig. 4.4D-I**). Three dimensional reconstruction of the neural crest and SHF populations within the leaflets showed that these regional lineage disturbances were accompanied by rotational anomalies within the annulus impacting commissure positioning in *Nos3*<sup>-/-</sup> embryos (**Fig. 4.4J-L**). As a result the left commissure developed more dorsal in *Nos3*<sup>-/-</sup> BAV when compared to wild type TAV and *Nos3*<sup>-/-</sup> TAV embryos (**Fig. 4.4J-L**). Measurement of extracardial SHF and neural crest populations showed equal volume outside the heart which indicates that these cell populations are most probably not affected prior to their homing into the cardiac cushions (**Fig. S4.7**).

The aortic and pulmonary valve developed at an angular offset within the OFT of tricuspid wild type embryos (**Fig. 4.5A**). NKX2.5<sup>+</sup>/TM<sup>-</sup> SHF cells (**Fig. 4.5D**) and neural crest derived cells (**Fig. 4.5G**) were located deep within the OFT cushions in wild type embryos. These neural crest derived cells contributed to the formation of the AP septum located centrally between the aortic and pulmonary valves (asterisk, **Fig. 4.5G**). In the OFT of *Nos3*<sup>-/-</sup> embryos NKX2.5<sup>+</sup>/TM<sup>-</sup> SHF and neural crest derived cells were located more proximal to the semilunar valves in both *Nos3*<sup>-/-</sup> TAV (**Fig. 4.5B, E, H**) and *Nos3*<sup>-/-</sup> BAV (**Fig. 4.5C, F, I**). *Nos3*<sup>-/-</sup> TAV embryos showed proper leaflet separation but slight changes in the position of the AP septum were observed (asterisk, **Fig. 4.5B, E, H**). These effects were more pronounced in BAV *Nos3*<sup>-/-</sup> embryos where the aortic valve was oriented more dorsally with regard to the pulmonary valve and changes in position



Supplemental Figure S.4.6 Total leaflet volume is not affected in Nos3 $^{-}$  embryos. Volume analysis of aortic leaflets in the aortic valve shows equal volume in wild type and Nos3 $^{-}$  embryos. LC: left coronary leaflet, RC: right coronary leaflet, NC: non-coronary leaflet. Data are mean  $\pm$ SD. Analysis was performed using two tailed student T test.

of the AP septum were exacerbated (Fig. 4.5C,F,I).

Measurement of the position of the aortic valve in relation to that of the pulmonary valve (protractor, **Fig. 4.5A-C**) revealed that the angle between the aortic and pulmonary valves was significantly smaller in both tricuspid  $Nos3^{-/-}$  and bicuspid  $Nos3^{-/-}$  when compared to wild type mice (P<0.01 and P<0.0001, respectively) (**Fig. 4.5J**). Moreover, TAV  $Nos3^{-/-}$  and BAV  $Nos3^{-/-}$  embryos were also found to be significantly different (P<0.05), indicating that the underlying changes in cell distribution may also affect annulus formation in tricuspid  $Nos3^{-/-}$  mice.

#### 4.4 Discussion

Patients with a BAV are at an increased risk of developing aortopathy. The great vessels and the aortic valve have a similar developmental origin involving contributions of endothelial, neural crest and second heart field lineages. Understanding the exact role of these early cell lineages during leaflet development and outflow tract formation may lead to more accurate patient risk stratification and improved treatment strategies.

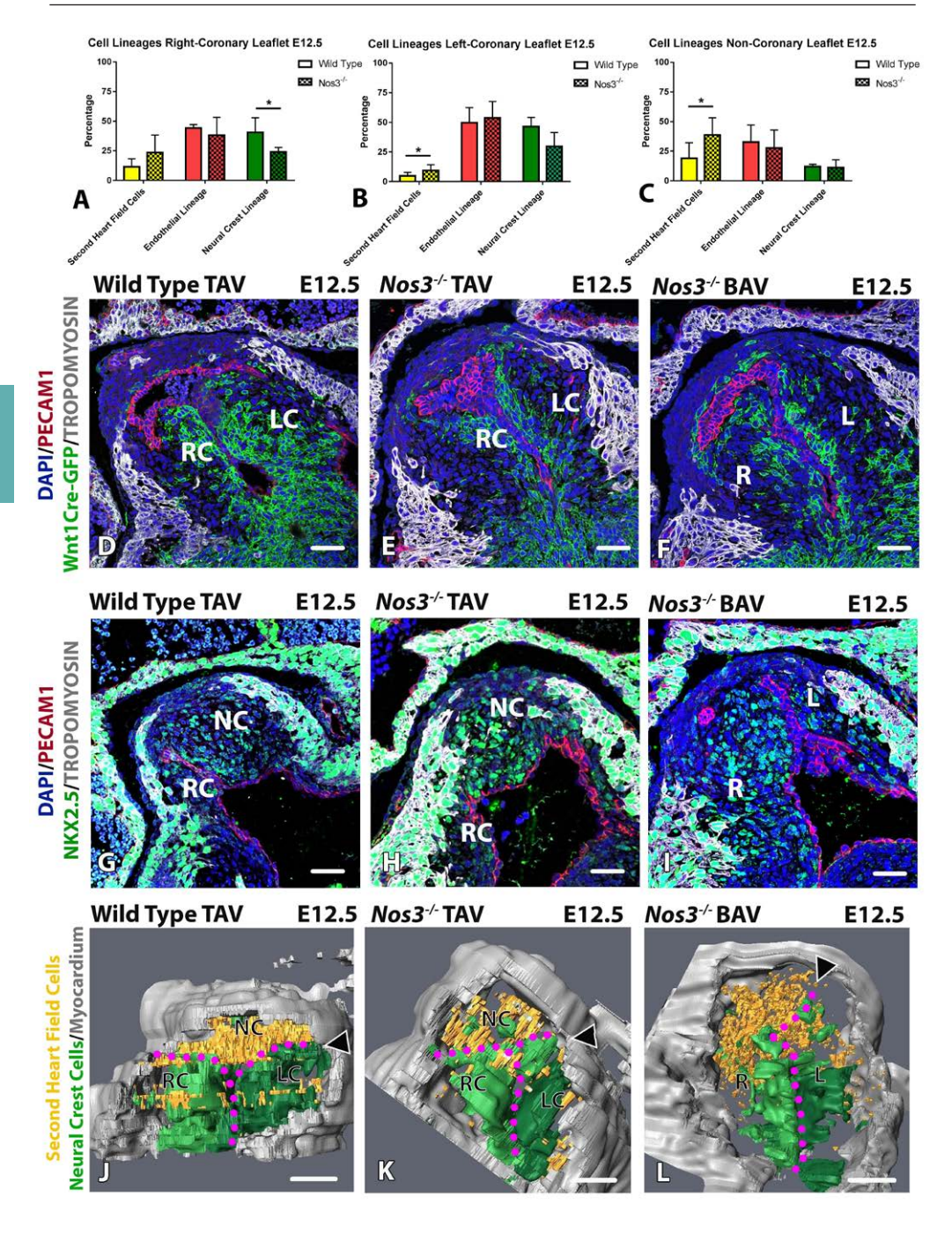
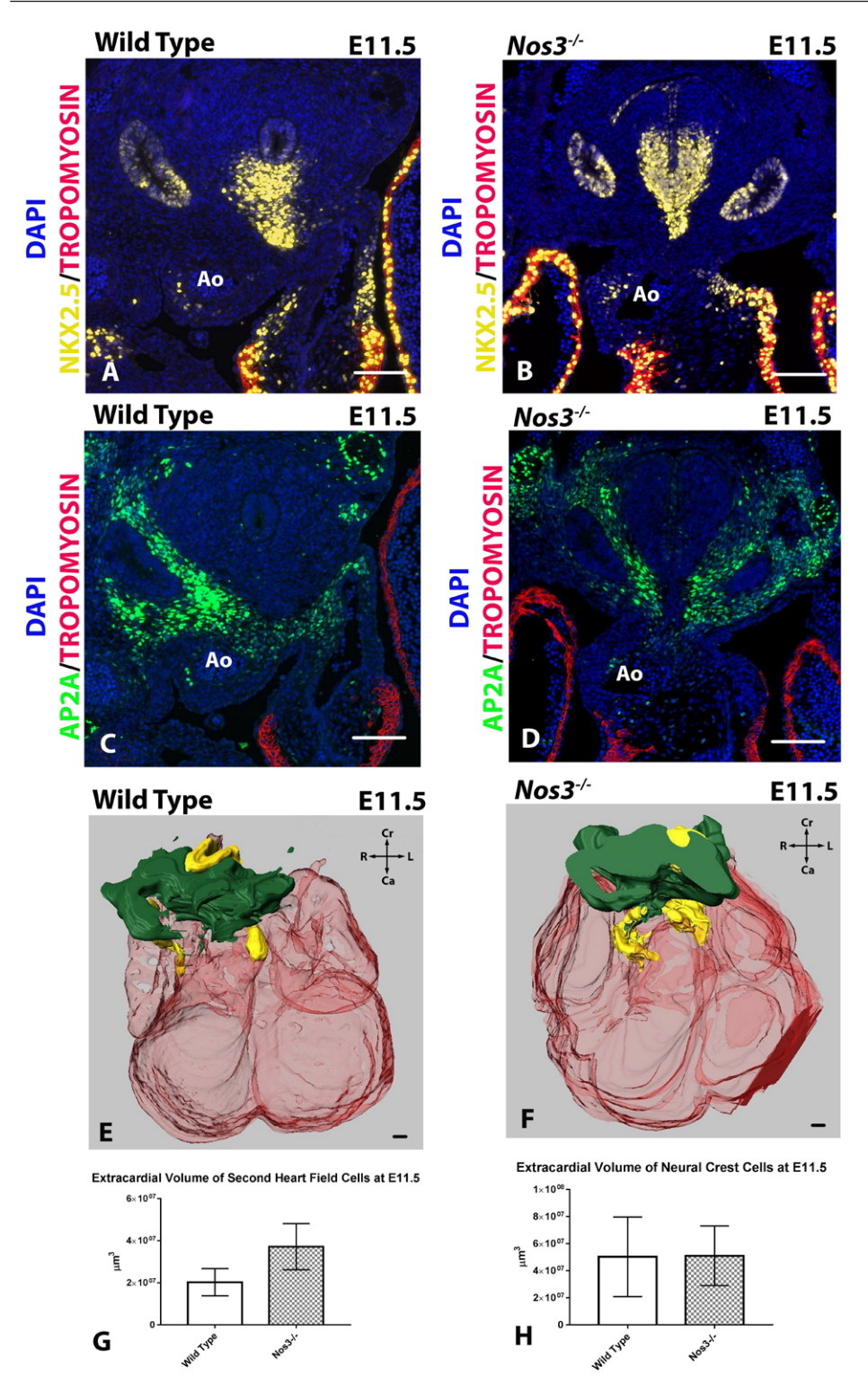


Figure 4.4 Aberrant neural crest and second heart field lineage distribution in Nos3\* embryos. A: Cell lineage analysis in Nos3<sup>-/-</sup> embryos showed significantly less neural crest derived cells contribute to the right coronary (RC) leaflet in Nos3<sup>-/-</sup> than wild type embryos at E12.5 (P<0.05). **B**: Increased contribution of NKX2.5+/TROPOMYOSIN SHF cells were observed in the left coronary (LC) leaflet in Nos3<sup>-/-</sup> embryos as compared to age matched wild type embryos (P<0.05). C: The NC leaflet of Nos3-- contains a significantly larger NKX2.5+/TROPOMYOSIN SHF population than those found in wild type embryos at E12.5 (P<0.05). **D-F**: Immunofluorescent images of Wnt1-Cre:mTmG tricuspid aortic valve (TAV) wild type (D), Nos3<sup>-/-</sup> TAV (E), and bicuspid aortic valve (BAV) Nos3<sup>-/-</sup> (F) embryos at E12.5 showed diminished neural crest populations (green) in the leaflets of the aortic valve in Nos3 $^{-}$  embryos. **G-I:** Immuno-fluorescent images of wild type TAV (G), Nos3<sup>-/-</sup> TAV (H), and Nos3<sup>-/-</sup> BAV (I), show increased NKX2.5⁺/TROPOMYOSIN¹ second heart field cells in the aortic leaflets of Nos3⁺ embryos. Colour scheme: Anti-PECAM1 (red), anti-TROPOMYOSIN (grey), Lineage marker (green), nuclei were stained with DAPI (blue). **J-L**: 3D reconstructions showed that the NKX2.5+/TROPOMYOSIN second heart field cells (orange) primarily localize in the NC leaflet in wild type TAV and Nos3<sup>-/-</sup> TAV whereas in Nos3<sup>-/-</sup> BAV the majority of SHF cells were located in the right (R) leaflet. BAV embryos developed the position of the left commissure more posterior than wild type TAV and Nos3<sup>-/-</sup> TAV (arrowheads). Data are mean ±SD for n≥4 mice per group. \* indicate P<0.05 determined by two tailed student T test. RC: right coronary leaflet, LC: left coronary leaflet, NC: non-coronary leaflet. Scale bar: 50µm.

In this study the formation of the aortic valve in wild type and *Nos3*<sup>-/-</sup> mouse embryos was studied to identify congenital cell lineage aberrations involved in the formation of bicuspid aortic valves.

To the best of our knowledge, we describe for the first time that the non-facing leaflets of the aortic and pulmonary valves arise from a process of cushion separation of the parietal and septal cushions during development. This finding contradicts previous studies which argued that the formation of the non-facing leaflets developed from separate intercalated cushions (*Kramer, 1942; Qayyum et al., 2001; Anderson et al., 2003; Lin et al., 2012; Eley et al., 2018; Mifflin et al., 2018*). The morphological events leading to semilunar valve formation is a challenging concept to represent in a 2D-plane due to complex 3D outflow tract remodelling. Interpretations based on 2D histological sections may result in an incomplete view of the morphological changes throughout development. Moreover these rapid morphological changes require short intervals in between observations and 3D reconstructions for accurate representations of the complete cushions within the context of the cardiac outflow tract remodelling during embryogenesis. The process of leaflet separation requires formation of endothelial infolding within the cushion. Fernández et al. reported fusion of the NC and RC (R-N BAV) as the underlying mechanism for BAV in *Nos3*<sup>-/-</sup> mice (*Fernandez et al., 2009*). However, the absence of a strand of opposed endothelial cells that runs from the lumen to the sinus wall



Supplemental Figure S.4.7 Extracardial neural crest and second hear field population are not affected by Nos3 mutation. A-D: immuno-fluorescent images of extracardial NKX2.5<sup>+</sup>/TROPOMYOSIN⁻ second heart field (SHF) (yellow) and AP2A neural crest cell (green) populations in wild type (A,C) and Nos3<sup>-</sup>/• (B,D) embryos at stage E11.5 when migration into the cushions has been initiated. E-F: 3D reconstruction of extracardial neural crest (green) and SHF populations (yellow) show similar localization in both wild type and Nos3<sup>-</sup>/- embryos. G-H: Volume analysis of extracardial populations shows no difference (P>0.05) between SHF cells (G) and neural crest cells (H) between wild type and Nos3<sup>-</sup>/- at E11.5. Colour scheme: Anti-NKX2.5 (yellow), Anti-AP2A (Green), Anti-TROPOMYOSIN (red), Nuclei were stained with DAPI (blue). Data are mean ±SD. Analysis was performed using two tailed student T test. Scale bars: 50µm.

in the parietal cushion shows that the developmental background of the R-N BAV is not the result of a fusion process between two OFT cushions, but rather the result of an incomplete or absent separation process of the RC and NC leaflets from the parietal cushion during early valve development. We therefore found no indications of endothelial opposition that could support the theory of direct fusion. Recently Eley and co-workers/colleagues links the formation of BAV without a raphe to deficiencies in arterial valve cells from Mef2c-AHF-Cre+;Tnnt2-Cre+ progenitors (*Eley et al., 2018*). Interestingly changes in NKX2.5<sup>+</sup>/TM<sup>-</sup> SHF cell distribution is also observed in the Nos3<sup>-/-</sup> model emphasizing the importance of correct cell lineage distributions during valve formation. Moreover the cellular dynamics of NKX2.5+/TM-SHF population during OFT development observed in this study suggest that these cells do not originate from the myocardial wall as proposed by Mifflin et al (2018) but rather migrate from the extra-cardiac pool of SHF cells into the OFT cushions and in agreement with Eley et al (2018). However, the 3D reconstructions developed in our study do not indicate the formation of a detached/isolated developing intercalated cushions as the transitional zone did not develop into the NC or NF leaflets of the aortic and pulmonary valve. The transitional zones did not experience cushion swelling by cellularization as observed in the parietal and septal cushions but remained a thin region of cardiac jelly connecting the parietal and septal cushions during development. The development of the NC and NF from the septal and parietal cushions is further supported by the observations of the NKX2.5+/TM-SHF cells as a distinct group within the parietal and septal cushion which eventually develop into the NC and NF leaflets of the aortic and pulmonary valve development, respectively.

The asymmetric contribution of the NKX2.5+/TM<sup>-</sup> population to the aortic and pulmonary poles of the OFT has been described as the pulmonary push concept (*Scherptong et al., 2012*). The greater number of contributing SHF cells to the pulmonary pole of the outflow tract in relation to that of the aortic pole might explain the susceptibility of *Nos3*-/- embryo to develop BAV unlike

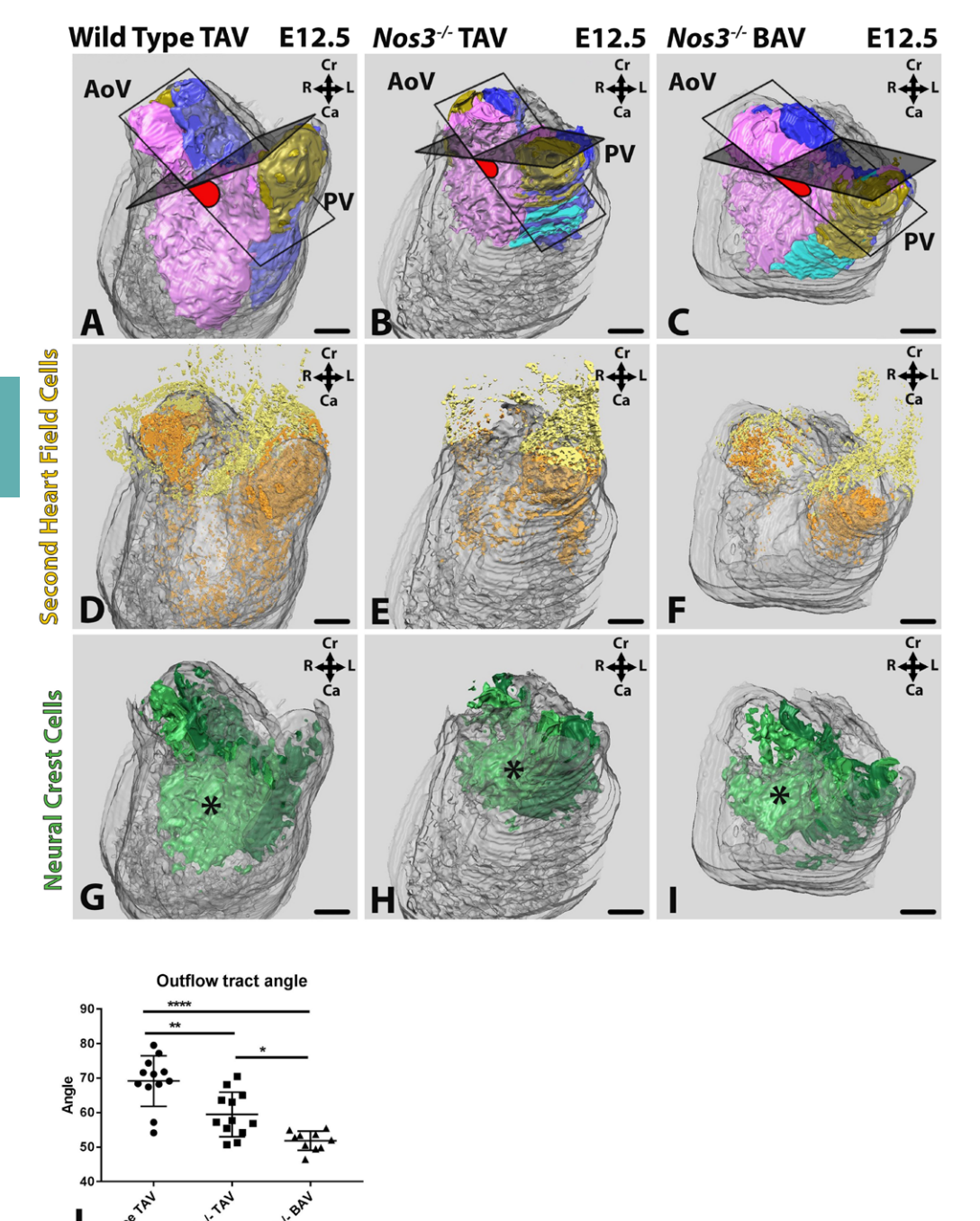


Figure 4.5 Nos3 deficiency results in morphological outflow tract defects in both tricuspid and bicuspid aortic valve mutants. A-I: 3D outflow tract reconstructions depicts myocardium (grey), noncoronary leaflet (gold), transitional region (cyan), parietal (purple), septal (blue) cushions of wild type TAV (A), Nos3-- TAV (B), and Nos3-- BAV (C) embryos at E12.5. Protractor (red) of aortic- and pulmonary valve commissure planes showed smaller angulation in Nos3-f- TAV and Nos3-f- BAV when compared to TAV wild type embryos. NKX2.5+/TROPOMYOSIN second heart field (SHF) cells migrated from outside the cushions (yellow) into the cushions (orange) (**D**). Both tricuspid (**E**) and bicuspid (**F**) Nos3<sup>-/-</sup> mutants showed SHF cell populations restricted to the cushion tissue. **G-I**: In TAV wild type embryos (**G**) neural crest derived cells contributed to the formation of the AP septum in regions of condensed mesenchyme positioned centrally between the aortic and pulmonary orifices indicated by asterisk. AP septum development in Nos3-/- TAV (H) and Nos3<sup>-/-</sup> BAV (I) is located more proximal to the semilunar valves than in wild type, affecting annulus formation and the position of the aortic and pulmonary valves. J: Morphometric measurements between aortic valve and pulmonary valve revealed significant differences between tricuspid wild type and Nos3 $^{+}$  TAV (P=0.0012), as well as between wild type TAV and Nos3 $^{+}$  BAV (P<0.0001). Moreover there were significant differences between Nos3\*- TAV and Nos3\*- BAV (P=0.0159). This indicates a strong relation between outflow tract development and leaflet formation where a small angle between aortic and pulmonary valve indices with BAV. Data are mean ±SD. \*, \*\* and \*\*\*\* indicate P<0.05, P<0.01 and P<0.0001 respectively determined by one-way ANOVA. AoV: aortic valve, PV: pulmonary valve, Ao: aorta, R: right, L: left, D: dorsal, V: ventral, Cr: cranial, Ca: caudal. Colour coding: Myocardium (transparent grey), parietal cushion (purple), Non-coronary leaflet (yellow), septal cushion (light blue), pulmonary artery (dark blue). Nuclear DAPI staining: Blue. Scale bar: 100µm.

bicuspid pulmonary valve. The difference in cellular distribution within the pulmonary valve could possible not reflect that of the aortic valve and could therefore be affected differently by the *Nos3* mutation. This subtle difference in cell lineage distribution might underlie the rarity of a bicuspid pulmonary valve in both mice and human.

Our observations of cushion invagination for valve formation has also been reported in the vertebrate zebrafish model suggesting a conserved mechanism for leaflet separation (*Scherz et al., 2008*). Whether the process of leaflet separation is the result of active endothelial invasion or a result of passive geometric rearrangement, e.g. by outgrowth of the valvular leaflets, is yet to be determined.

NOS3 is a key mediator in the production of nitric oxide (NO) in endothelial cells and plays a role in regulating vascular tone through the L-arginine-NO pathway (*Radomski and Moncada*, 1993). Disruptions in the endothelial NO pathway have been associated with BAV in humans (*Kotlarczyk et al., 2016*). However, the role of NO in outflow tract formation has not been studied in great detail. Signalling pathway analysis in *Nos3*<sup>-/-</sup> mice identified abnormal EndMT

as a cause for BAV (*Fernandez et al., 2009; Y. Liu et al., 2013*). However, these studies did not perform lineage tracing experiments and primarily relied on indirect measurements of EndMT. We used the *Tie2Cre;mTmG* mice to genetically label the endothelial derived cells and showed that the endocardial contribution to the developing leaflets was not affected in *Nos3*<sup>-/-</sup> animals. Interestingly, the *Nos3* mutation did impact cell lineage distribution of neural crest and SHF cells among the leaflets of the aortic valve. This suggest that NOS3 might have an active role in guiding cell migration during development. Both SHF and neural crest cells migrate over the aortic and pulmonary arteries, in close proximity to endothelial cells. There have been reports that interactions between endothelial derived cells and neural crest cell lineages are required for correct leaflet development (*Wu et al., 2011*).

Neural crest cells have been reported to be essential for correct positioning of the developing outflow cushions and patterning of the arterial valve leaflets (*Phillips et al., 2013*). More recently Aghajanian et al. (*2017*) showed that endothelial pdgfrA is an important factor for coordinating neural crest cell migration. The importance of correct lineage distributions of SHF, endothelial and neural crest cells in BAV has also been suggested by other researchers (*Jain et al., 2011*). The findings presented here support the notion that misregulation of these cell lineages can result in BAV in mice.

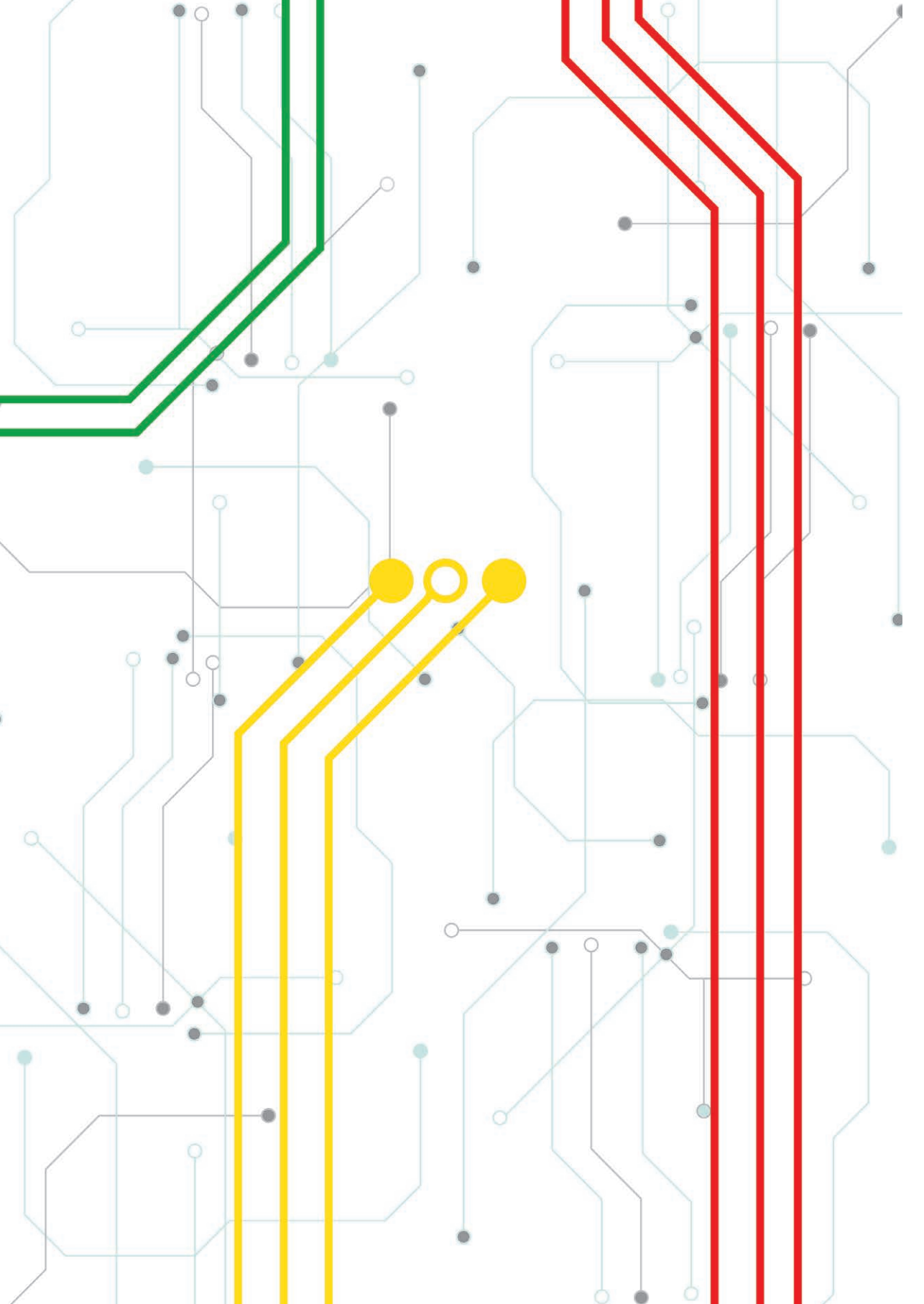
The angular differences in the aortic and pulmonary valve plane between wild type, *Nos3*-- TAV and BAV *Nos3*-- mutants as a result of lineage defects are likely to alter normal flow patterns. Hemodynamic aberrations have been widely supported to contribute to the aortopathy observed in many cases of BAV (*Piatti et al., 2017*).

To examine the exact molecular pathways responsible for the signalling role of *Nos3* influencing neural crest and SHF distribution in outflow tract development further research is required. Interestingly, the advent of RNA-sequencing can shed light on the molecular mechanisms involved in cellular communication among early cell lineages.

#### 4.5 Conclusion

During OFT development the parietal endocardial cushion gives rise to the RC and NC leaflets of the aortic valve as well as to the RF leaflet of the pulmonary valve. The septal cushion gives rise to the LC leaflet of the aortic valve as well as the LF and NF leaflets of the pulmonary valve. This asymmetric leaflet formation leads to non-uniform cell lineage distributions in the aortic valve. The non-coronary aortic leaflet is primarily populated by NKX2.5+/TM-SHF derived cells,

whereas neural crest derived cells primarily populate the RC and LC aortic leaflets. Endothelial derived cell populations contribute to each leaflet equally. However, Nos3<sup>-/-</sup> embryos develop BAV due to defects in endothelial linked separation of the parietal cushion into the NC and RC aortic leaflet accompanied by a different pattern of disposition of embryonic cell lineages. All Nos3<sup>-/-</sup> embryos show increased contributions of SHF cells to the NC and LC leaflets, while a reduction of neural crest cells is observed in the RC leaflet. Moreover, embryonic lineage defects involved in valve formation results in morphometric changes of the outflow tract leading to aberrant positioning of the aortic and pulmonary valve in both tricuspid and bicuspid Nos3<sup>-/-</sup> embryos, albeit it is more pronounced in the latter. These valve alignment anomalies are most probably the result of aberrations in neural crest derived AP-septum formation affected in Nos3<sup>-/-</sup> embryos. These findings suggest that differences in early neural crest and SHF lineage distributions, as seen in BAV, are not limited solely to valve formation but impact complete cardiac outflow tract development.



### Chapter 5

# Disturbed NO signalling gives rise to congenital bicuspid aortic valve and aortopathy

2020

**DOI**: 10.1242/dmm.044990

**Disease Models & Mechanisms** 

Joshua C. Peterson<sup>1</sup>, Lambertus J. Wisse<sup>1</sup>, Valerie Wirokromo<sup>1</sup>, Tessa van Herwaarden<sup>3</sup>, Anke M. Smits<sup>3</sup>, Adriana C. Gittenberger-de Groot<sup>2</sup>, Marie-José T.H. Goumans<sup>3</sup>, J. Conny VanMunsteren<sup>1</sup>, Monique R.M. Jongbloed<sup>1, 2</sup>, Marco C. DeRuiter<sup>1</sup>

<sup>1</sup> Dept. Anatomy and Embryology, Leiden University Medical Center, Leiden, The Netherlands <sup>2</sup> Dept. Cardiology, Leiden University Medical Center, Leiden, The Netherlands <sup>3</sup> Dept. Chemical Cell Biology, Leiden University Medical Center, Leiden, The Netherlands

#### **Abstract**

Patients with a congenital bicuspid aortic valve (BAV), a valve with two instead of three aortic leaflets, have an increased risk of developing thoracic aneurysms and aortic dissection. The mechanisms underlying BAV-associated aortopathy are poorly understood. This study examined BAV-associated aortopathy in Nos3-/- mice, a model with congenital BAV formation. A combination of histological examination and in-vivo ultrasound imaging was used to investigate aortic dilation and dissections in Nos3<sup>-/-</sup> mice. Moreover, cell lineage analysis and single cell RNA sequencing were used to observe the molecular anomalies within vascular smooth muscle cells (VSMCs) of Nos3-/- mice. Spontaneous aortic dissections was found in ascending aortas located at the sinotubular junction in ~13% of Nos3<sup>-/-</sup> mice. Moreover, Nos3<sup>-/-</sup> mice were prone to develop aortic dilations in the proximaland distal-ascending aorta during early adulthood. Lower volumes of elastic fibres were found within vessel walls of the ascending aortas of Nos3<sup>-/-</sup> mice as well as incomplete coverage of the aortic inner media by neural crest (NCC)-derived VSMCs. VSMCs of Nos3<sup>-/-</sup> showed downregulation of 15 genes of which 7 were associated with a ortic aneurysms and dissections in the human population. Elastin mRNA was most markedly downregulated, followed by Fibulin-5 expression, both primary components of elastic fibres. This study demonstrates that disrupted endothelial mediated NO signalling in mice causes next to a congenital BAV also aortic dilation and dissection as a consequence of inhibited elastic fibre formation in VSMCs within the ascending aorta of *Nos3*-/-mice.

#### 5.1 Introduction

Patients with a congenital bicuspid aortic valve (BAV) often develop subsequent aortopathy later in adulthood. Clinical studies show that patients with a BAV have a three-fold increased chance of developing thoracic aortic aneurysms (*Cecconi et al., 2006*). This aortopathy is considered generally as a haemodynamic result from the disturbed flow caused by the narrowed opening and position of the two leaflets. Various studies demonstrate that first degree relatives of BAV patients with a normal tricuspid aortic valve are at increased risk of developing aortic complications (*Biner et al., 2009*) indicating that both BAV and aneurysm formation represent a variable phenotypical expression of a common genetic defect (*Loscalzo et al., 2007*). Remodelling of the extracellular matrix (ECM) has been linked to aortopathy. Patients with aortic aneurysms typically display medial degeneration as a result of elastic fibre fragmentation (*Isselbacher, 2005*). Moreover, reduced collagen disposition has also been observed in patients with ascending aortic aneurysms (*de Figueiredo Borges et al., 2008*).

Aortic vasculature and valve development are closely related and share common embryonic cell populations. Endothelial cells populating the arterial pole of the heart also contribute to the outflow tract cushions from which the aortic valve develops through epithelial mesenchymal transition. Cardiac neural crest cells (NCC) and second heart field derived cell populations both contribute to the interstitial cells of the aortic valves and the medial vascular smooth muscle cells (VSMCs) and adventitial fibroblasts of the aorta. Studies using mice have determined anomalies in embryonic cardiac lineages to result in BAV (*Laforest, Andelfinger and Nemer, 2011; Peterson et al., 2018*), yet much is unknown about how these cell lineages influence ECM composition and contribute to aortic dissections.

In this study, we examined the effects of disrupted NO signalling on the thoracic aorta in Nos3<sup>-/-</sup> mice, which is a genetic BAV model with a ~25% penetrance of the phenotype (*Lee et al., 2000; Fernandez et al., 2009; Peterson et al., 2018*), to identify developmental processes involved in BAV-associated aortopathy. Understanding early aortic vessel formation is crucial to apprehend the risks involved in aortopathy seen in BAV patients and their tricuspid aortic valve (TAV) relatives.

#### 5.2 Material and Methods

#### **5.2.1 Animals**

BAV associated aortopathy was studied in aortic tissue of *Nos3*<sup>-/-</sup> mice and wild type in embryonic and adult stages of development. Mice older than 2 months were considered as adult mice and experiments were performed using a random distribution of male and female mice. The following mice were used in this study: *Nos3*<sup>-/-</sup> B6.129P2-NOS3tm1Unc/J mice (*purchased from Charles River Laboratories, Maastricht, Netherlands*), B6.Cg-Tg(Wnt1-cre)2Sor/J (*purchased from Jackson laboratories, JAX stock #022501, Bar Harbor, USA*), B6.129(Cg)-Gt(ROSA)26Sortm4(ACTB-tdTomato,-EGFP)Luo/J, (mT/mG) (*purchased from Jackson laboratories, JAX stock # 007576, Bar Harbor, USA*). *Nos3*<sup>-/-</sup>;*Wnt1Cre;mT/mG*; and *Wnt1Cre;mT/mG* were generated using a cross breeding strategy. All mice were back crossed to the Black6 background using C57BL/6JLumc mice (*purchased from Leiden University Medical Center, Leiden, The Netherlands*).

Embryos were acquired using timed breeding protocols. Adult mice were bred overnight and examined the next morning for the presence of a vaginal plug. In case a plug was observed, embryonic age would be established at (E)0.5 at noon of that day. Embryos were isolated through hysterectomy at E12.5 and E17.5 following dissection in phosphate buffer solution pH

7.4. Genomic DNA was isolated from tail biopsies for genotyping by polymerase chain reaction targeted at *Cre* and *Nos3* according to previous publication (*Peterson et al., 2018*). All mice were handled according to the Guide for Care and Use of Laboratory Animals, as published by the NIH and experiments were in accordance with relevant local, national and international regulations and guidelines.

#### 5.2.2 Immunostainings and Histochemistry

Embryos and adult aortic tissues were fixed in 4% paraformaldehyde (0.1M, pH 7.4) for 24 hours at 4°C and embedded in paraffin. Samples were sectioned serially (5 µm), and mounted on glass slides. Prior to staining, samples were deparaffinized using xylene followed by a series of graded ethanol steps for rehydration into PBS. In case of immunostainings, slides were subjected to microwave antigen retrieval in citric acid buffer (10mM Citric Acid, 0.05% Tween 20 pH=6.0) for 12 minutes at 97°C. Sections were incubated with primary antibodies against eGFP (Abcam ab13970), ACTA2 (Sigma-Aldrich A2547) or FBLN5 (Abcam ab202977). Primary antibodies were diluted in PBS-Tween-20 (1/500) with 1% bovine serum albumin (BSA, A8022; Sigma-Aldrich, St. Louis, MO, USA) to avoid non-specific binding. Between subsequent incubation steps all slides were rinsed twice in PBS followed by a single rinse in PBS-Tween-20. Primary antibodies were visualized by incubation with fluorescently labelled secondary antibodies (Thermo Scientific A-11039), diluted (1/200) in PBS-Tween-20 for 60 minutes. DAPI (D3571, 1/1000; Life Technologies) was used as a nuclear stain and the slides were mounted with Prolong gold (Life Technologies). Classical histochemistry was used to examine ECM composition. Mayer's Hematoxylin-Eosin (HE) (KLINIPATH VWRK4085-9002) Weigert's Resorcin-Fuchsin (RF) (Sigma-Aldrich 100591), Sirius Red (Sigma-Aldrich 365548) staining were performed according to published protocols (Culling, 1974; Junqueira, Bignolas and Brentani, 1979; Cardiff, Miller and Munn, 2014).

#### 5.2.3 In vivo aortic ultrasound measurements

Wild type (N=8 of which 1 female and 7 males) and *Nos3*. (N=4 of which 1 female and 3 males) mice were selected at 4 months of age. Mice were randomized and ultrasound measurements of systolic and diastolic aortic diameters (AoDs and AoDd respectively) as well as data analysis were executed blinded. Aortic diameters were measured perpendicular to the inner curvature. Mice were anesthetized using isoflurane and monitored for temperature and heart rate during ultrasound measurements. Ultrasound images were collected using Vevo3100 (FUJIFILM Visual Sonics, Toronto, ON, Canada) and the MX400, 20–46 MHz probe with a centre frequency of

30 MHz. Sagittal ECG-gated kHz visualization (EKV) were captured for analysis. Data analysis was performed using Vevo LAB 3.2.0 software. Circumferential Green-Lagrange strain was calculated according to previous publication (Goergen et al. 2010) using the following equation:

$$0.5 * \left[ \left( \frac{AoDs}{AoDd} \right)^2 - 1 \right] * 100\%$$

#### 5.2.4 Three-dimensional reconstructions

Aortic 3D reconstructions of E12.5 *Nos3*<sup>-/</sup>;*Wnt1Cre;mTmG* and *Wnt1Cre;mTmG* embryos were made with Amira software 6.3 (Template Graphics Software Inc., Houston, TX, USA). Tissue sections (5 μm) were collected from paraffin embedded embryos and immunostained using anti-eGFP and DAPI. Slides were scanned using the panoramic 250 flash III slide scanner (3DHISTECH Ltd., Budapest, Hungary) and images of identical scale and exposure were exported using Histech Panoramic Viewer (3DHISTECH Ltd., Budapest, Hungary) and aligned in Amira. Relevant cardiac structures were labelled and surface views were exported to PDF format with the Adobe Acrobat 9.5 software package.

#### 5.2.5 Extracellular matrix quantification

ECM of elastin and collagen were examined in aortic vessel walls of wild type (N=5) and Nos3<sup>-/-</sup> (N=6) mice aged E17.5 as well as in wild type and Nos3<sup>-/-</sup> adult mice (P2 months, N=6 of which 2 females and 4 males, and N=5 of which 3 females and 2 males respectively). Histological sections were scanned using the panoramic 250 flash III slide scanner (3DHISTECH Ltd., Budapest, Hungary). Elastin and collagen was quantified in aortic vessel wall of the proximal-, mid-, and distal-ascending aorta covering a total length of 250 µm and 500 µm in E17.5 and adult mice respectively, corresponding to the same anatomical regions within the aorta. This was achieved with the use of a macro designed in Fiji (Schindelin et al., 2012) which allowed for the quantification of volumetric elastin and collagen respective to the vessel wall. The aortic vessel wall was identified manually in histological images (8-bit RGB) of idential resolution and maginification in wild type and Nos3<sup>-/-</sup> mice. Elastin was detected using the following RGB thresholds: Hue (min=169, max=227) Saturation (min=34, max=255), Brightness (min=17, max=185). Collagen was defined using the following RGB thresholds: Hue (min=0 max=255) Saturation (min=0, max=255), Brightness (min=0, max=199). ECM measurements were presented relative to the volume of aortic vessel wall. Final volumetric calculations were processed in Excel 2016 (Microsoft, Redmond, Washington, USA).

#### 5.2.6 Survival analysis

Events of spontaneous mortality were recorded in breeding colonies of wild type and  $Nos3^{-/-}$  mice up to 1 year of age. The number of spontaneous deaths recorded was 103 in wild type colonies and 133 in  $Nos3^{-/-}$  colonies. Mantel-Cox comparison of survival curves was used to examine the temporal distribution of spontaneous death events between the two groups.

#### 5.2.7 Neural crest lineage analysis

Neural crest lineage analysis was performed similar to previous publication (Peterson et al., 2018). Briefly, fluorescent images were collected using Leica Sp8 confocal microscopy (Leica Microsystems, Buffalo Grove IL, USA). Measurements were performed on aortic vessel walls from transverse sections (5 µm) of Wnt1Cre;mTmG (N=4) and Nos3<sup>-/-</sup>;Wnt1Cre;mTmG (N=4) for stages E12.5 and E17.5. Of each embryo the proximal-, mid-, and distal-ascending aorta were imaged completely covering a total aortic length of 180 µm and 250 µm in E12.5 and E17.5 embryos respectively, corresponding to the same anatomical regions within the aorta. The proximal ascending aorta marks the border of the sinotubular junction and the tubular ascending aorta. The distal ascending aorta marks the border in which the tubular ascending aorta transitions into the proximal aortic arch prior to the brachiocephalic artery. The mid ascending aorta is positioned in the middle of the tubular ascending aorta. Image analysis was performed using a macro designed in Fiji (Schindelin et al., 2012). The macro was designed to differentiate the nuclear volume of Wnt1Cre+ lineage derived nuclei from the nuclear volume of all DAPI+ nuclei within the aortic vessel wall. The regions of the aortic vessel wall were selected manually and DAPI+ nuclei found within a body of cytoplasmic GFP were measured as lineage specific nuclei relative to the total volume of DAPI<sup>+</sup> nuclei in the aortic vessel wall. Image thresholds for GFP+ cytoplasm were set at a pixel intensity of 120 and DAPI+ thresholds were automatically detected using the imageJ "default" algorithm. Final volumetric calculations were processed in Excel 2016 (Microsoft, Redmond, Washington, USA).

#### 5.2.8 Cell sorting and single cell RNA-Seq

E12.5 murine *Nos3*<sup>-/-</sup> (N=4) and wild type (N=4) embryos were collected in cold PBS after which the heart was dissected and the cardiac outflow tract was carefully isolated. Cardiac outflow tracts were incubated with 10% trypsin for 7 minutes at 37°C and resuspended on ice to obtain a single cell suspension. Cells were washed twice with PBS supplemented with 10% of fetal calf serum and transferred over a cell strainer prior to FACS sorting. Dying cells were labelled using DAPI (1/1000) and excluded from further sorting. Single cells were captured using a FACSAria

III cell sorter (BD Biosciences) and distributed over 384 well plates containing CEL-Seq2 primer solution and mineral oil as described previously (*Muraro et al., 2016*). The 384 well plates were immediately frozen on dry ice and stored at  $-80^{\circ}$ C.

CEL-Seq2 primers and ERCC Spike-in RNA (0.02 µL of 1:50.000 dilution) were dispensed with the Mosquito HTS (TTPlabtech). Cell lysis was performed using heat shock incubation of cells for 5 minutes at 65°C. RT and second strand synthesis reagents were dispensed using the Nanodrop II (GC biotech) to generate barcoded cDNA libraries unique to each cell. The barcoded cDNA libraries in all wells were pooled prior to linear amplification in vitro. To generate Illumina sequencing libraries TruSeq small RNA primers (Illumina) were used for library PCR. Libraries were sequenced using 75 bp paired end sequencing using an Illumina Nextseq500 platform. Paired end reads were mapped to the reference genome GRCm38/mm10 using the Burrows-Wheeler Aligner tool (version 0.7.17) (*Li and Durbin, 2010*).

The RaceID3 algorithm was used to cluster cells based on K-medoids clustering as described previously (Herman, Sagar and Grün, 2018). RaceID3 analysis was performed using an criteria of mintotal=1000, excluding cells that had lower than 1000 unique transcripts. Further analysis used default parameters. Mitochondrial and ribosomal genes were excluded as the abundant expression interfered with downstream clustering. Cell clusters were visualized using t-distributed stochastic neighbor embedding (t-SNE) and differential expression of genes between subgroups of cells was calculated using the DESeq2 package in the R platform (*Love, Huber and Anders, 2014; Grün et al., 2015*).

The R-code and documentation of RacelD3 is available for download at <a href="https://github.com/dgrun/RacelD3">https://github.com/dgrun/RacelD3</a> StemID2 package (Herman, Sagar and Grün, 2018).

#### 5.2.9 RNA isolation and quantitative real-time PCR (Q-PCR)

P6 month adult mice were euthanized using cervical dislocation after which the heart and aortic arch were isolated. Aortic samples were carefully dissected from the ascending aorta minimizing any external tissue contamination. Whole tissue RNA isolation of *Nos3*<sup>-/-</sup> (N=5, of which 2 females and 3 males) and wild type mice (N=5, of which 2 females and 3 males) was performed using TRIzol reagent (Invitrogen) RNA isolation and gDNA removal using the TURBO DNA-Free kit (Invitrogen) followed by reverse transcription to obtain cDNA using Iscript cDNA synthesis kit (Bio-rad) according to manufacturer's protocols.

Quantitative PCR was performed with SYBR Green (Bio-rad) on the CFX384 Touch Real-Time PCR Detection System (Bio-rad). The PCR program ran a single cycle of 50°C (10 minutes) and by 95°C (5 minutes) followed by 40 cycles of 95°C (10 seconds) and 60°C (1 minute). Primers used in qPCR are described in **Table S1**. qPCR was performed in triplicates and average Ct score was quantified relative to housekeeping gene *Rpl32* and *Gapdh*. Differential gene expression in ascending aortas of wild type and *Nos3*-/- mice was presented using Log2 fold change.

#### 5.2.10 Statistical analysis

Results are represented as mean  $\pm$ SD of at least three independent experiments. Statistical analyses were performed using unpaired two tailed Student's t-test. Significance was assumed when p < 0.05. Statistical analysis was performed in GraphPad Prism 8.0 for Windows (GraphPad Software, La Jolla California USA).

#### **5.3 Results**

#### 5.3.1 Observation of aortic dissection in Nos3<sup>-/-</sup> mice

The aortic vessel wall is primarily composed of radial sheets of elastin in between layers of VSMCs in the tunica media (**Fig. 5.1**). Extracellular collagen contributes mostly to the fibrous structures found in the adventitia of the aortic vessel wall (**Fig. 5.5.1**). Histological examination of aortic vessel walls in *Nos3*<sup>-/-</sup> mice revealed morphological signatures of spontaneous aortic dissections as a result of local disruptions within the aortic vessel wall (**Fig. 5.1,Fig. 5.5.1**). The aortic dissection was located slightly above the sinotubular junction in *Nos3*<sup>-/-</sup> mice. Adventitial tissue remodelling low in elastin and collagen content in response to aortic dissection was

ELN_FWD	CCC ACC TCT TTG TGT TTC GC
ELN_REV	CCC AAA GAG CAC ACC AAC AAT
FBLN5_FWD	GTG CTT GGG GTT GGT TTT GA
FBLN5_REV	TCA GTT CCC CAT CTT TTG CCA
ACTA2_FWD	GCT ACG AAC TGC CTG ACG G
ACTA2_REV	TAG GTG GTT TCG TGG ATG CC
RPL32_FWD	CAC CAC TCA GAC CGA TAT GTG AAA A
RPL32_REV	TGT TGT CAA TGC CTC TGG GTT T
GAPDH_FWD	TTG ATG GCA ACA ATC TCC AC
GAPDH_REV	CGT CCC GTA GAC AAA ATG GT

**Supplemental Table S.1** Primers used for qPCR.

observed in the dissected aortic vessel wall of *Nos3*<sup>-/-</sup> mice (**Fig. 5.1G**, **Fig. S5.1**).

The spontaneous development of aortic dissections seen in *Nos3*<sup>-/-</sup> mice have been sparsely distributed within the dataset occurring in ~13% of *Nos3*<sup>-/-</sup> mice (4/31 *Nos3*<sup>-/-</sup> mice) ranging in stages from 1 month to 11 months of age. Dissection occurred in both BAV (N=1) (**Fig. S.5.1**) and TAV (N=3) *Nos3*<sup>-/-</sup> mice. Survival analysis indicated no difference in the temporal distribution of spontaneous death events between wild type and *Nos3*<sup>-/-</sup> populations (**Fig. S.5.2**).

#### 5.3.2 Nos3<sup>-/-</sup> mice develop aortic dilation early into adulthood

To examine whether the aortic dissections coincide with an increased aortic diameter, ultrasound imaging was used to visualize the aorta of wild type and *Nos3*. mice in vivo (**Fig. 5.2A-D**). Careful measurements of the proximal-, mid-, and distal-ascending aorta were made to determine aortic diameters during systole and diastole (**Fig. 5.2E-F**). Aortic ultrasound measurements in 4 month-old adult mice showed no difference in aortic diameter during peak systole (**Fig. 5.2E**). However, peak diastolic aortic measurements determined significant larger aortic diameters in the prox- and distal-ascending aorta of *Nos3*. mice (**Fig. 5.2F**). Moreover, aortic strain calculations determined significant reductions in circumferential strain in the prox-ascending aorta of *Nos3*. mice (**Fig. 5.2G**).

### 5.3.3 Reduced elastic fibres in ascending aortic vessel walls of *Nos3*<sup>-/-</sup>mice

The morphologic structure of the ECM within the ascending aorta was analysed at adult as well as embryonic (E17.5) stages of development to examine onset of vascular wall pathology (**Fig. 5.3**). Volumetric quantification of elastic lamellae within the vessel wall of the ascending aorta showed significant reductions in the volume of elastic fibres within vessel walls of *Nos3*. mice at embryonic as well as adult stages. Morphological comparison of the elastic lamellae in aortic vessel walls indicated that disruptions in elastic fibres impacted the inner medial region of the aortic vessel wall. The aortic vessel wall of wild type mice consisted of an inner media of densely packed sinuous elastic lamella and an outer media of smoothly aligned elastin lamellae (**Fig. 5.3A**). In contrast, the aortic vessel wall of adult *Nos3*. mice solely developed smoothly aligned elastin lamellae throughout the complete aortic vessel wall (**Fig. 5.3B**).

In addition to elastin, collagen disposition was also examined in aortic vessel walls of adult

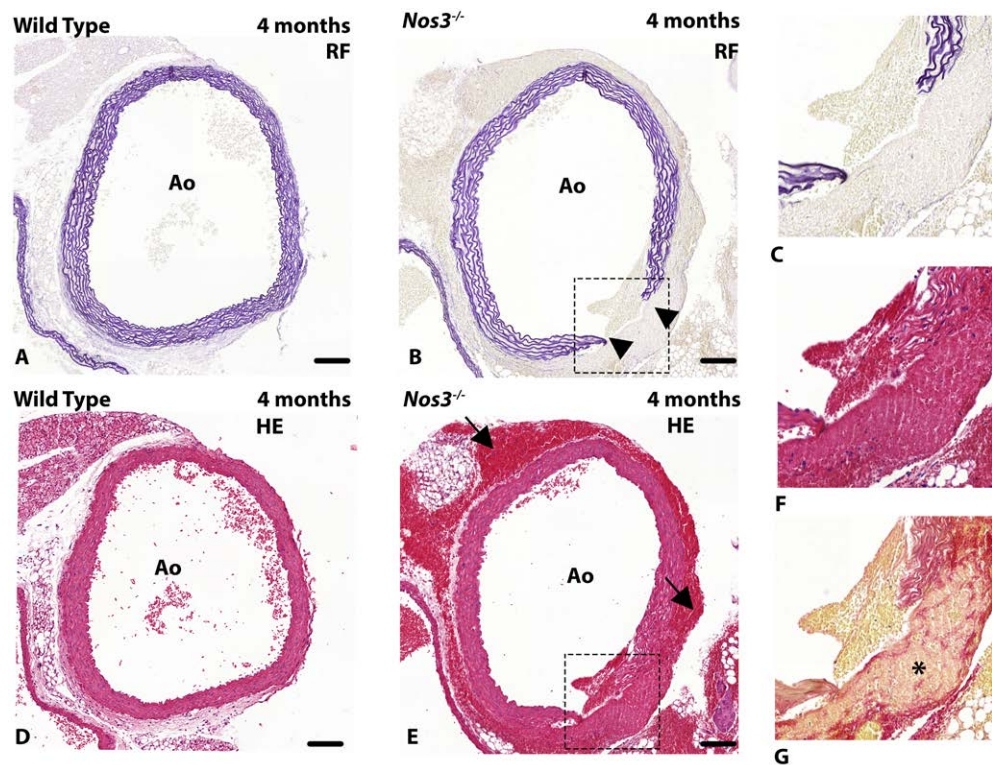
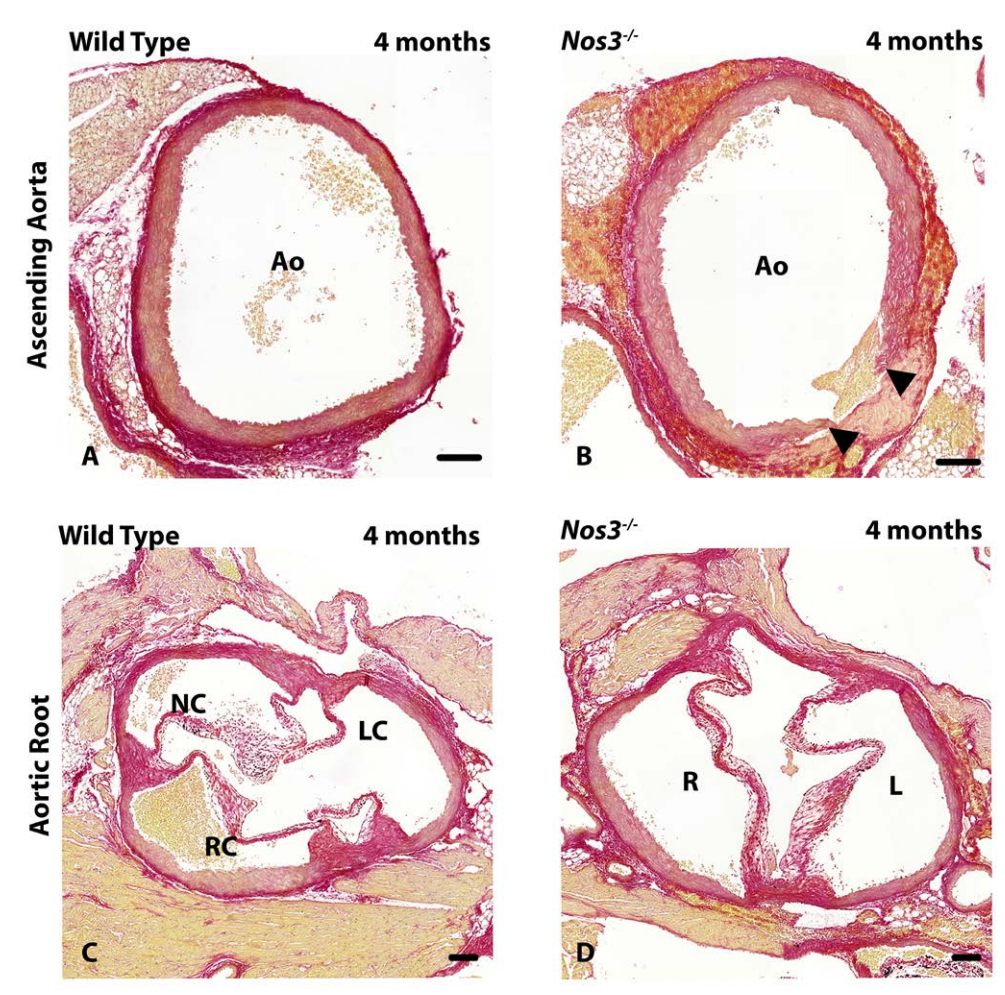


**Figure 5.1 Aortic dissection in Nos3**<sup>-/-</sup> **mice. A-F**: Transverse histological section of the ascending aorta in (**A**) wild type and (**B-C**) Nos3<sup>-/-</sup> mice stained with Resorcin-Fuchsin (RF) and Haematoxylin-Eosin (HE). **D-F**: The Nos3<sup>-/-</sup> mice reveal rupture (arrow heads) of the elastic lamellae in the ascending aortic vessel wall located at or slightly above sinotubular junction. **G**: Adjacent section stained for a combination collagen (red) and elastin (pink). Tissue remodelling of the adventitia can be observed in aortic vessel walls of dissected Nos3<sup>-/-</sup> mice (asterix). Blood deposits are present in the adventitia and subepicardial space (black arrows). Ao: Aorta. Scale bar: 100 μm.

and embryonic mice (**Fig. S.5.3**). Volumetric collagen analysis of medial and adventitial aortic collagen deposition determined no significant indicating that the *Nos3* mutation does not impact collagen deposition within ascending aortic walls of embryonic or adult mice but specifically affects formation of elastic lamellae in the aortic vessel wall (**Fig. S.5.3E-H**).

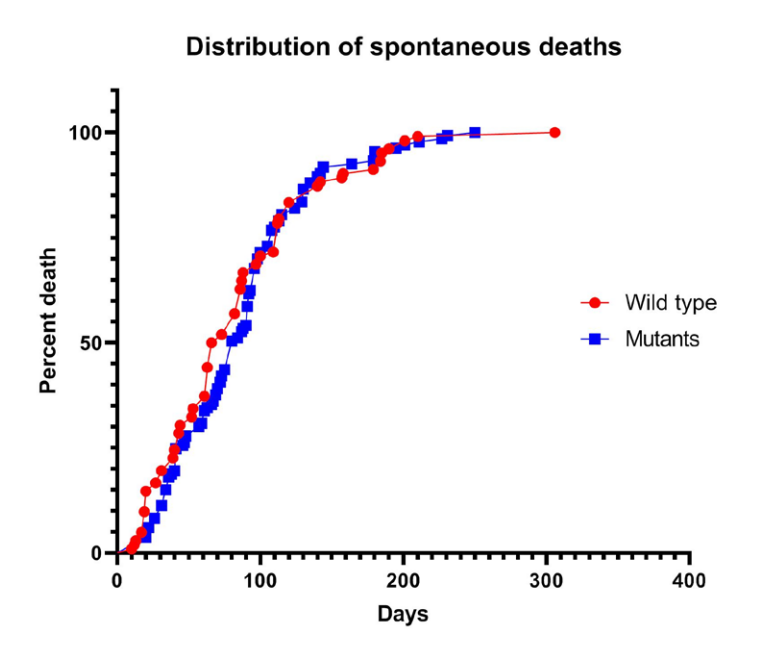
#### 5.3.4 NCC populations are reduced in a ortic vessel walls of $Nos3^{-/-}$ embryos

The observation of elastin disruption within the inner media suggested a possible role of the NCC lineage in aortopathy. Previous findings from our lab already established NCC lineage disruption in aortic valves during cushion development in *Nos3*<sup>-/-</sup> embryos (*Peterson et al.*,



Supplemental Figure S.5.1 Aortic dissection in Nos3 $^{-}$  mice is associated with BAV. Additional histological staining of wild type and Nos3 $^{-}$  mice presented in figure 5.1 stained with a combination of collagen (red) and elastin (pink) showing the ascending aorta (**A-B**) and aortic root (**C-D**). This case of aortic dissection developed in conjunction with a bicuspid aortic valve (**D**). Aortic dissection is apparent in the aortic vessel wall of the Nos3 $^{-}$  mouse (arrow heads). Ao: Aorta, NC: Non-coronary leaflet, RC: Right coronary leaflet, LC: Left coronary leaflet, R: Right leaflet, L: Left leaflet, Scale bar: 100  $\mu$ m.

2018). Genetic lineage tracing using Wnt1Cre;mTmG and Nos3<sup>-/-</sup>;Wnt1Cre;mTmG embryos (E17.5 and E12.5) showed NCC-derived VMSCs line the entire inner media of the ascending aorta (**Fig. 5.4, Fig. S5.4**). Comparison of the NCC-derived cell populations in the ascending aortic vessel wall between wild type and Nos3<sup>-/-</sup> embryos showed a significant reduction of NCCs in the aortic vessel wall of Nos3<sup>-/-</sup> embryos at both E17.5 and E12.5 (**Fig. 5.4C, F**). Close morphological examination revealed incomplete coverage in the inner media of the ascending aorta by NCCs-



Supplemental **Figure** S.5.2 Temporal distribution of spontaneous death events. Wild type (N=103) and Nos3-/- (N=133) in which spontaneous death observed was were examined for the chronologic distribution of death events. No sianificant (P>0.05)difference was observed between wild type and mutant populations using Mantel-Cox comparison of survival curves.

derived cells in *Nos3*<sup>-/-</sup> embryos. Three-dimensional reconstruction of the E12.5 outflow tract indicates the reduction in NCCs derived cells to be limited to the ascending aorta (**Fig. 5.4G**, **H**).

## 5.3.5 Single cell RNA sequencing reveals downregulation of genes associated with aortopathy in VSMCs of $Nos3^{-/-}$ mice

To investigate the effects of the *Nos3* mutation on a transcriptional level, single cell RNA-seq was used on the murine outflow tract of E12.5 embryos. K-medoids clustering using the Race-ID3 algorithm (*Herman, Sagar and Grün, 2018*) defined 16 cell clusters based on similarities in cellular gene expression in the outflow tract of wild type origin (**Fig. 5.5**). Individual clusters were examined for known marker genes to identify cell types corresponding to each cluster. Using this approach we identified multiple cell types namely, VSMCs, cushion mesenchyme, cardiomyocytes, and leukocytes.

Combined clustering of wild type and *Nos3*<sup>-/-</sup> single cell transcriptomes allowed for an unbiased assessment of cell type differences as clustering depends on cellular likeliness based on gene expression. Two clusters were found in close proximity of each other, in which wild type (cluster 1) and *Nos3*<sup>-/-</sup> (cluster 15) derived cells formed separate near homogenous groups (**Fig. 5.6A-D**).

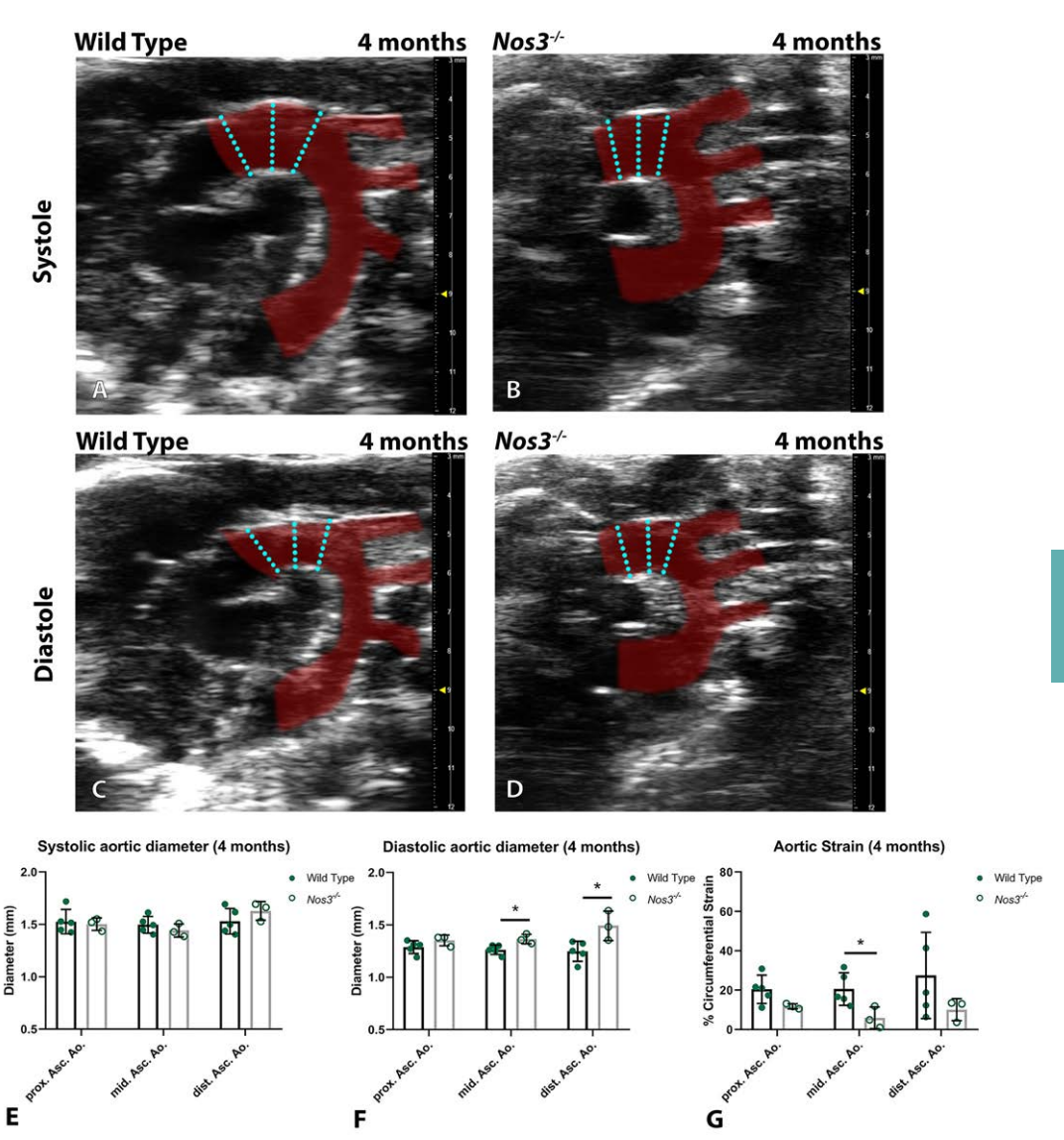


**Figure 5.2 Nos3**<sup>-/-</sup> mice **develop aortic dilation at 4 months.** A-B: Ultrasound image of the aorta (red) during systole in (A) wild type and (B) Nos3<sup>-/-</sup> mice displays peak systolic diameter of the aorta. **C-D**: During diastole aortic diameter reaches maximum constriction in (C) wild type and (D) Nos3<sup>-/-</sup> mice. E-F: Aortic diameter were measured in wild type (N=8) and Nos3<sup>-/-</sup> (N=4) mice at the proximal-, mid-, and distal-ascending aorta (prox. Asc. Ao., mid. Asc. Ao., dist. Asc. Ao. respectively) in 4 months old mice at (E) peak systole and (F) peak diastole. Cyan dotted line indicate measurement locations of proximal, mid, and distal locations of the ascending aorta respectively. Two tailed student T-test showed Nos3<sup>-/-</sup> mice have significant larger diastolic diameters than wild type mice. **G**: Circumferential Green-Lagrange strain of the aorta was found significantly lower in the ascending aorta of Nos3<sup>-/-</sup> mice. \*:P<0.05, \*\*:P<0.01. Data are mean ±SD.

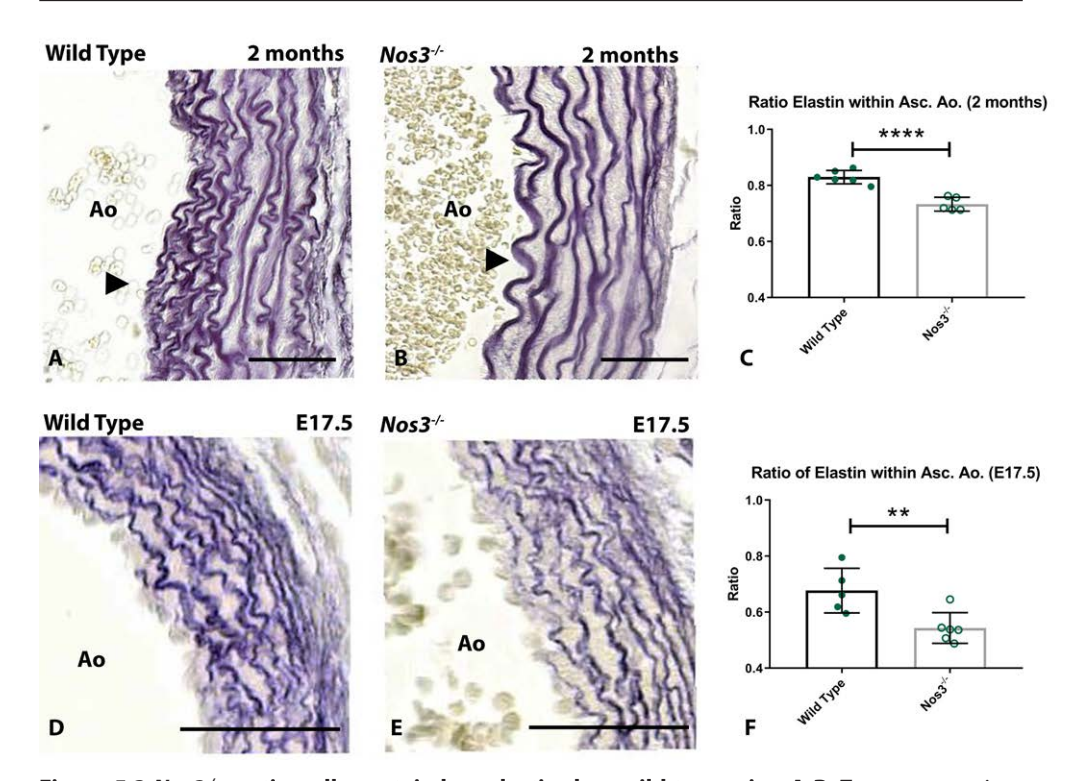
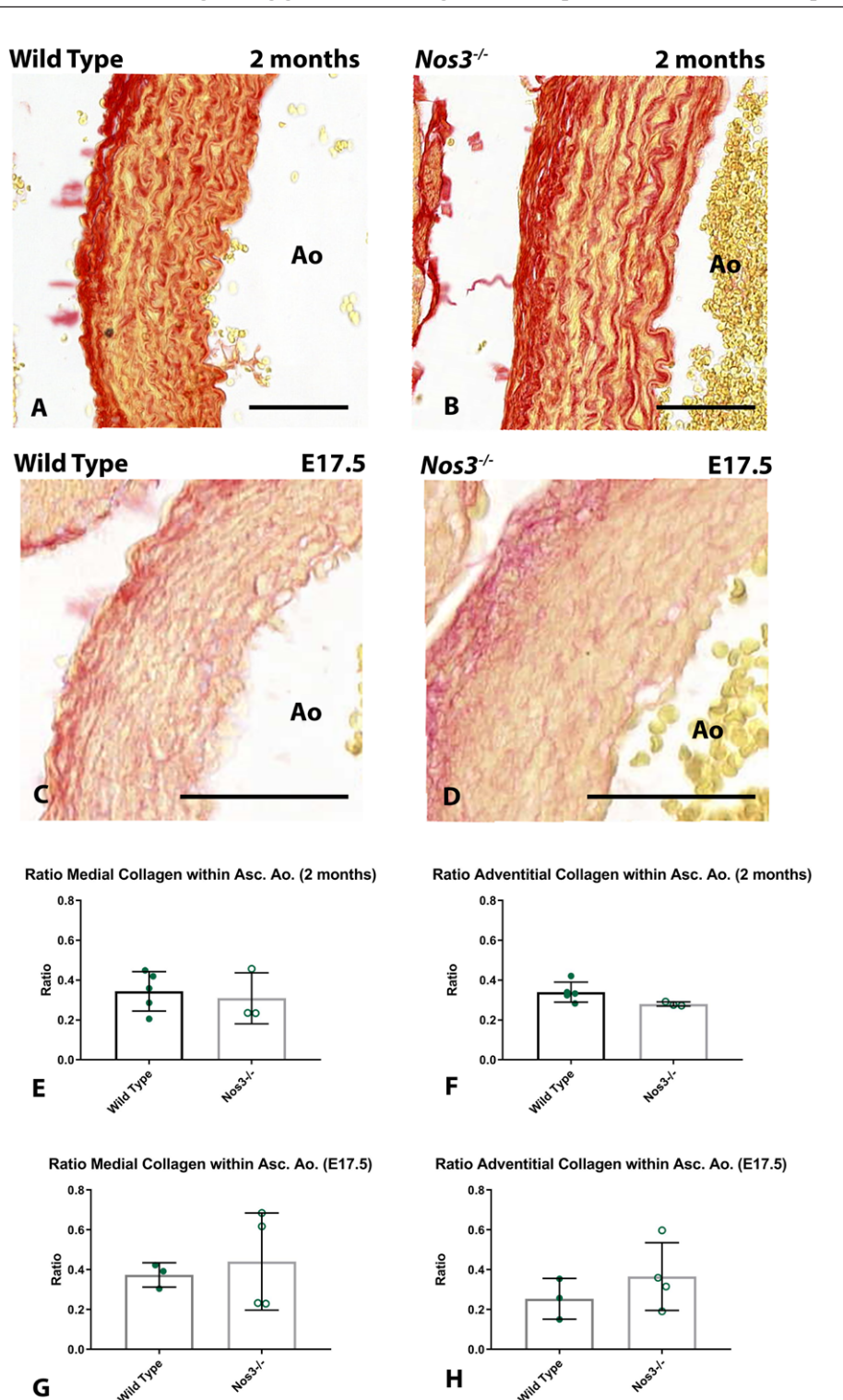


Figure 5.3 Nos3<sup>-/-</sup> aortic walls contain less elastin than wild type mice. A-B: Transverse sections of aortic walls of adult (A) wild type and (B) Nos3<sup>-/-</sup> mice stained with resorcin-fuchsin to visualize elastin deposited as elastic fibres within the ascending aortic vessel wall. C: Volumetric quantification of elastin within the ascending aortic vessel wall of wild type (N=6) and Nos3<sup>-/-</sup> (N=5) adult (2 months) mice shows a reduction of elastin within aortic vessels of Nos3<sup>-/-</sup> mice. D-E: Resorcin-fuchsin staining of ascending aorta vessel walls of embryonic (E17.5). D: wild type and E: Nos3<sup>-/-</sup> mice. F: Volumetric quantification of elastic fibres in wild type (N=5) and Nos3<sup>-/-</sup> (N=6) embryos also shows significant reductions in volume of elastin within the ascending aorta in Nos3<sup>-/-</sup> embryos indicating impaired elastin production during embryogenesis. Morphological smooth elastin fibres, instead of densely packed sinuous lamella are observed within the inner media (arrowheads) of the aortic wall in Nos3<sup>-/-</sup> adult mice. Ao: Aorta, \*\*\*\*: P value <0.0001 \*\*: P value <0.01 were determined by two tailed student T test. Scale bar: 50 µm. Data are mean ±SD.

Supplemental Figure S.5.3 Collagen deposition is not affected in the ascending aortic wall of Nos3<sup>-/-</sup> mice. A-B: Transverse sections of the aortic wall of adult (A) wild type and (B) Nos3<sup>-/-</sup> mice stained with Sirius red to show collagen deposition in the media and adventitia of the ascending aorta. C-D: Sirius red staining of the embryonic aortic wall of (C) wild type and (D) Nos3<sup>-/-</sup> mice at stage E17.5. E-H: Volumetric quantification of collagen staining within the medial (E,G) as well as adventitial layers (F,H) of the adult and embryonic ascending aortic wall show no difference (P>0.05) in the deposition of collagen between wild type and Nos3<sup>-/-</sup> mice. Ao: Aorta. Data are mean ±SD for n≥3 mice per group. Scale bar: 50 μm.



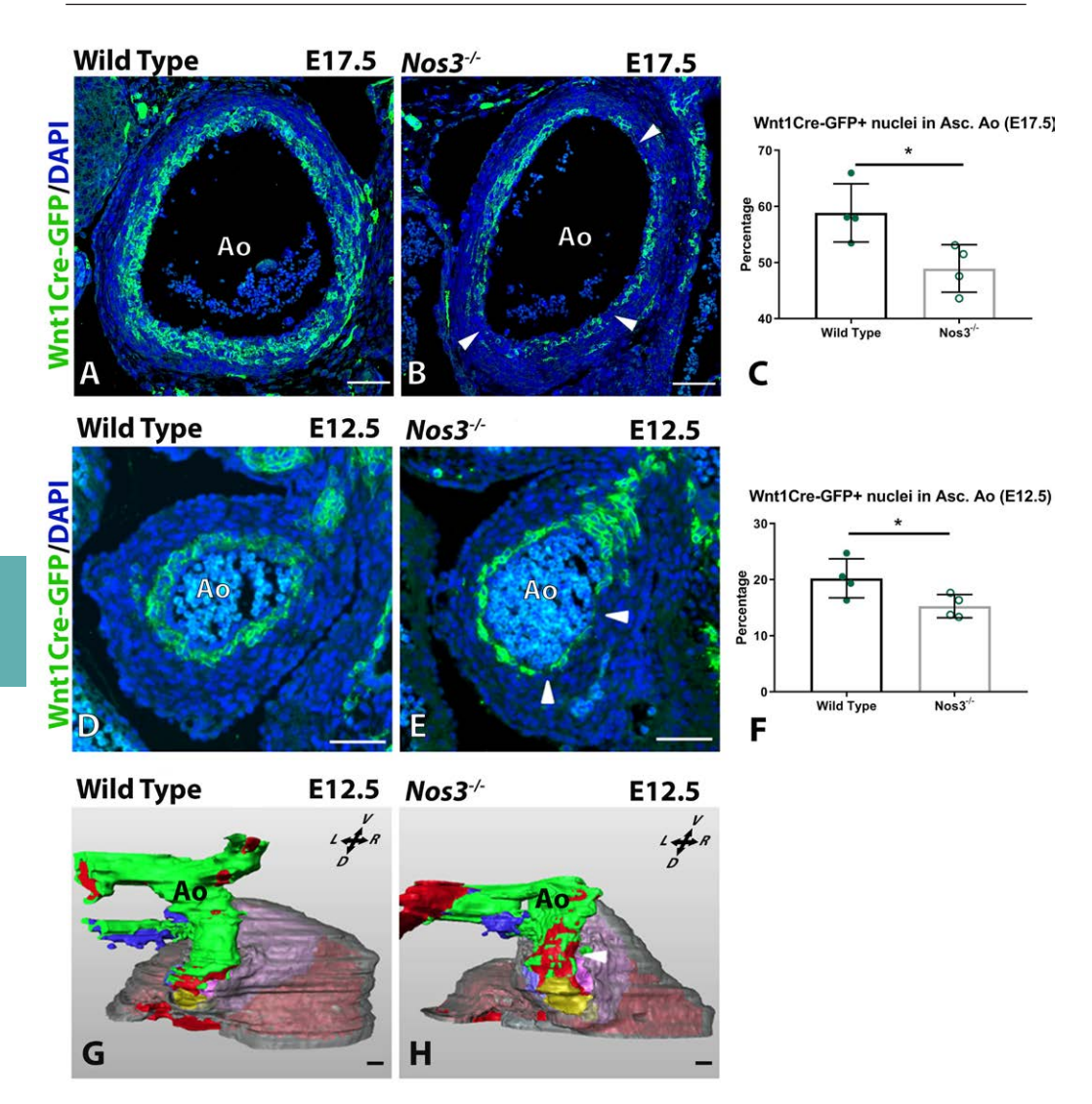


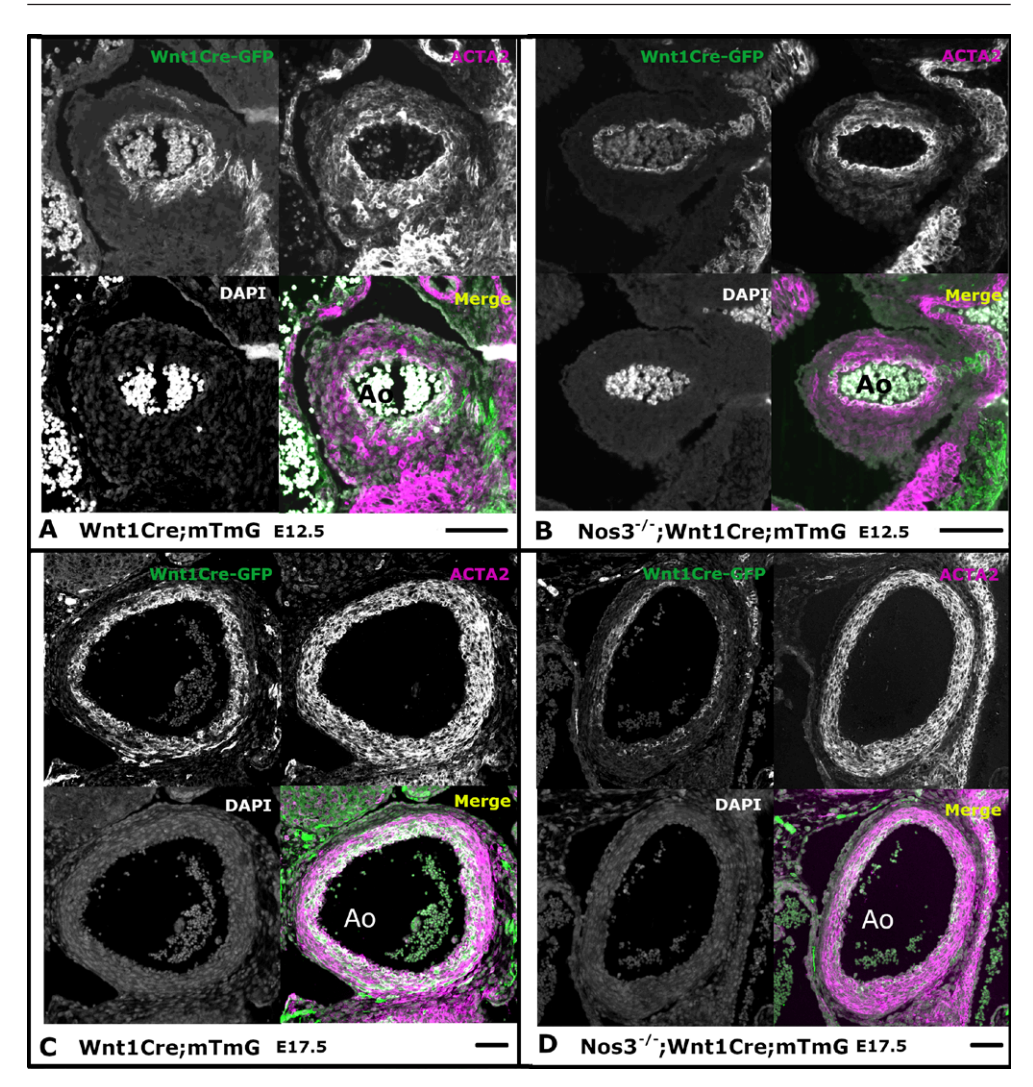
Figure 5.4 Reduction of the NCC population in aortic vessel walls of Nos3<sup>-/-</sup> embryos. A-B: Immunofluorescence staining of NCC-derived cells (green) in transverse sections of the ascending aortic vessel walls of (A) Wnt1Cre+;mTmG and (B) Nos3<sup>-/-</sup>;Wnt1Cre+;mTmG embryos. C: Lineage quantification of NCC-derived cells showed a reduced contribution of NCC-derived cells in the vessel wall of the ascending aorta in Nos3<sup>-/-</sup> (N=4) embryos when compared to wild type embryos (N=4) at E17.5. D-E: Immunofluorescent staining of NCC-derived cells in the ascending aortic vessel wall of E12.5 (D) wild type and (E) Nos3<sup>-/-</sup> embryos. F: Cell lineage analysis at E12.5 also showed reduced contribution of NCC-derived cells within the ascending aorta of Nos3<sup>-/-</sup> (N=4) embryos when compared to age matched wild type (N=4). Incomplete coverage of inner media by NCC-derived cells was observed in the inner media in Nos3<sup>-/-</sup> of both E17.5 and E12.5 embryos (white arrowheads). G,H: 3D reconstruction of E12.5 (G) wild type Wnt1Cre+ hearts showed NCC-derived cells (green) surrounding the complete lumen (red)

of the ascending aorta. In contrast, to wild type, E12.5 (H) Nos3<sup>-/-</sup>; Wnt1Cre<sup>+</sup>;mTmG embryos showed a reduced number of NCCs throughout the ascending aorta as well as an incomplete NCC coverage of the aortic root and proximal ascending aorta. Colour coding: myocardium (transparent grey), parietal outflow tract cushion (purple), Non-coronary leaflet (yellow), septal outflow tract cushion (light blue), pulmonary trunk (dark blue). Nuclear DAPI staining: Blue, \*: P<0.05. Ao: Aorta, R: right, L: left, V: Ventral, D: Dorsal. \* P value <0.05 were determined by two tailed student T-test. Scale bars: 50µm. Data are mean ±SD.

Based on the relative high Acta2 and TagIn RNA expression levels within the clusters these were identified as VSMCs. Differential gene expression analysis between wild type and Nos3<sup>-/-</sup> VSMC clusters revealed significant differences in gene expression of a total of 45 genes (30 upregulated and 15 downregulated genes) of which the top upregulated gene was Acta2, and top downregulated gene was Eln in Nos3<sup>-/-</sup> VSMCs. (Fig. 5.6E-F, Fig. S5.5). This study focused on downregulated genes as BAV and BAV-related aortopathy are often associated with gene mutations resulting in downregulated gene expression (Prakash et al., 2014). The absence of Nos3 induced NO signalling resulted most notably in the down regulation of Eln transcription, a gene encoding for elastin a major component of elastic fibres (Fig. 5.6E, G). VSMCs of Nos3-/- also had decreased expression of FbIn5, which translates to fibulin-5, another important protein which directly interacts with elastin for the formation of elastic fibres in the ECM (Midwood and Schwarzbauer, 2002; Yanagisawa et al., 2002). Interestingly, multiple genes, Eln, Fbln5, Cxcl12, Fn1, Gata6, Mfap4 were found to be downregulated in Nos3<sup>-/-</sup> VSMCs; genes which are all associated with BAV and aneurysm formation (Midwood and Schwarzbauer, 2002; Ogata et al., 2005; Paloschi et al., 2011; Orriols et al., 2016; Girdauskas et al., 2017; Zhang et al., 2018) (Fig. 5.6G). To ascertain that the changes in gene expression were not limited to stages of embryonic development, qPCR was performed for the top 3 differential expressed genes on ascending aortic tissues from adult wild type and Nos3<sup>-/-</sup> mice. qPCR analysis determined similar upregulation of Acta2 and downregulation of Eln and Fbln5 expression as seen in the RNA-seg analysis of E12.5 embryos indicating that these findings persist into adulthood (Fig. 5.6H, Fig. S5.6).

# 5.3.6 Genetic misregulation translates into altered protein expression phenotypes and is most pronounced in NCC-derived VSMCs of $Nos3^{-/-}$ mice

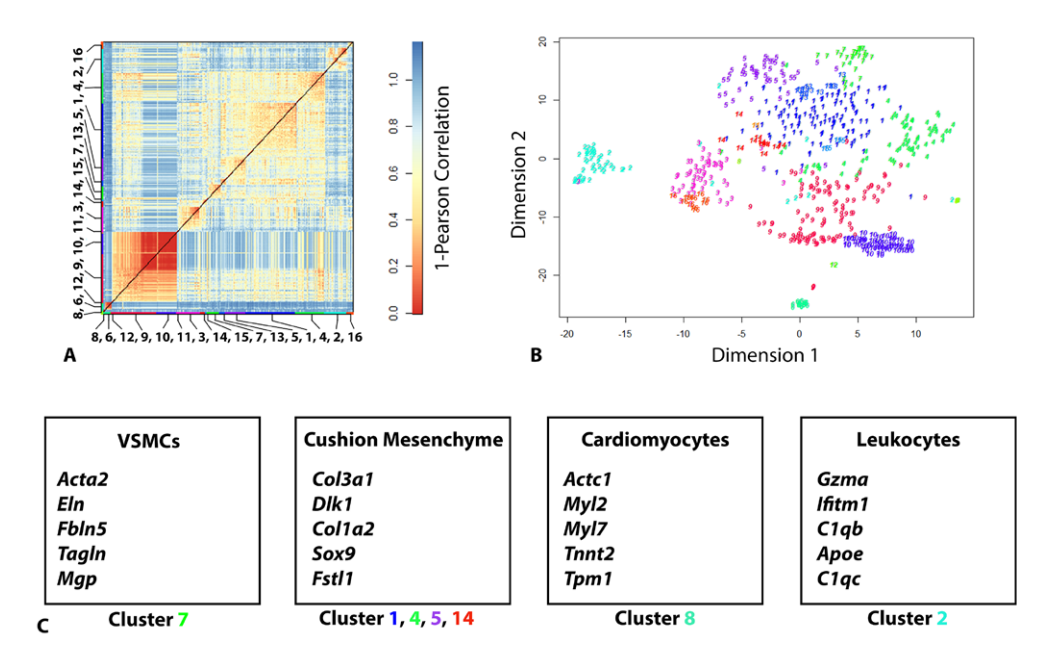
To examine the effects of aberrant RNA expression profiles found in the VSMCs of *Nos3*<sup>-/-</sup> embryos immunofluorescent antibody stainings were performed to examine localized alterations in protein translation within the aortic vessel wall of E17.5 embryos (**Fig. 5.7**). Interestingly,



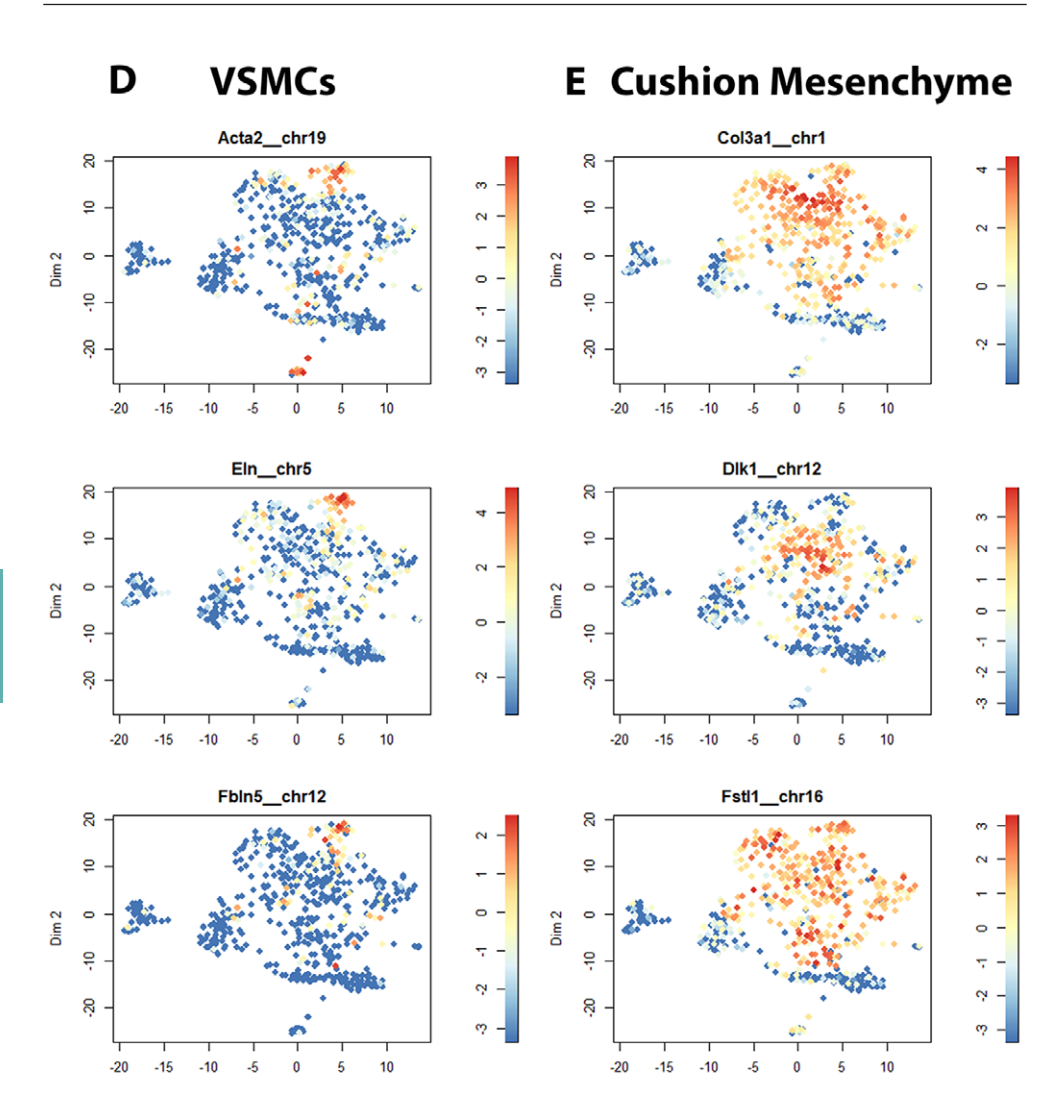
Supplemental Figure S.5.4 Neural crest derived smooth muscle cells populate the inner media of the ascending aortic vessel wall. A-B: Transversal sections of the ascending aorta of Wnt1Cre;mTmG and Nos3+;Wnt1Cre;mTmG embryos at E12.5. Neural crest derived vascular smooth muscle cells (VSMCs) express both Wnt1Cre-GFP (green) and ACTA2 (magenta). C-D: Fluorescent images similar to A and B, but showing embryos of developmental age E17.5. Note that expression of ACTA2 is more pronounced in neural crest derived VSMCs than VSMCs of different origin at E12.5 in both wild type and Nos3+ embryos. Nuclear staining: DAPI (grey). Scale bars: 50µm. Ao: Aorta.

**5.7A, C**). On the contrary, NCC-derived VSMCs *Nos3*<sup>-/-</sup> did not accumulate FBLN5 in accordance to a phenotype of reduced *Fbln5* expression (**Fig. 5.7B, D**). Moreover, ACTA2 expression was also more pronounced in NCC-derived VSMCs in both wild type and *Nos3*<sup>-/-</sup> embryos than VSMCs from a different origin (**Fig. 5.7E-H, Fig. S.5.4**). Nonetheless, the differences in ACTA2 expression between wild type and *Nos3*<sup>-/-</sup> embryos would support a phenotype of *Acta2* overexpression within the NCC-derived VSMCs of *Nos3*<sup>-/-</sup> embryos.

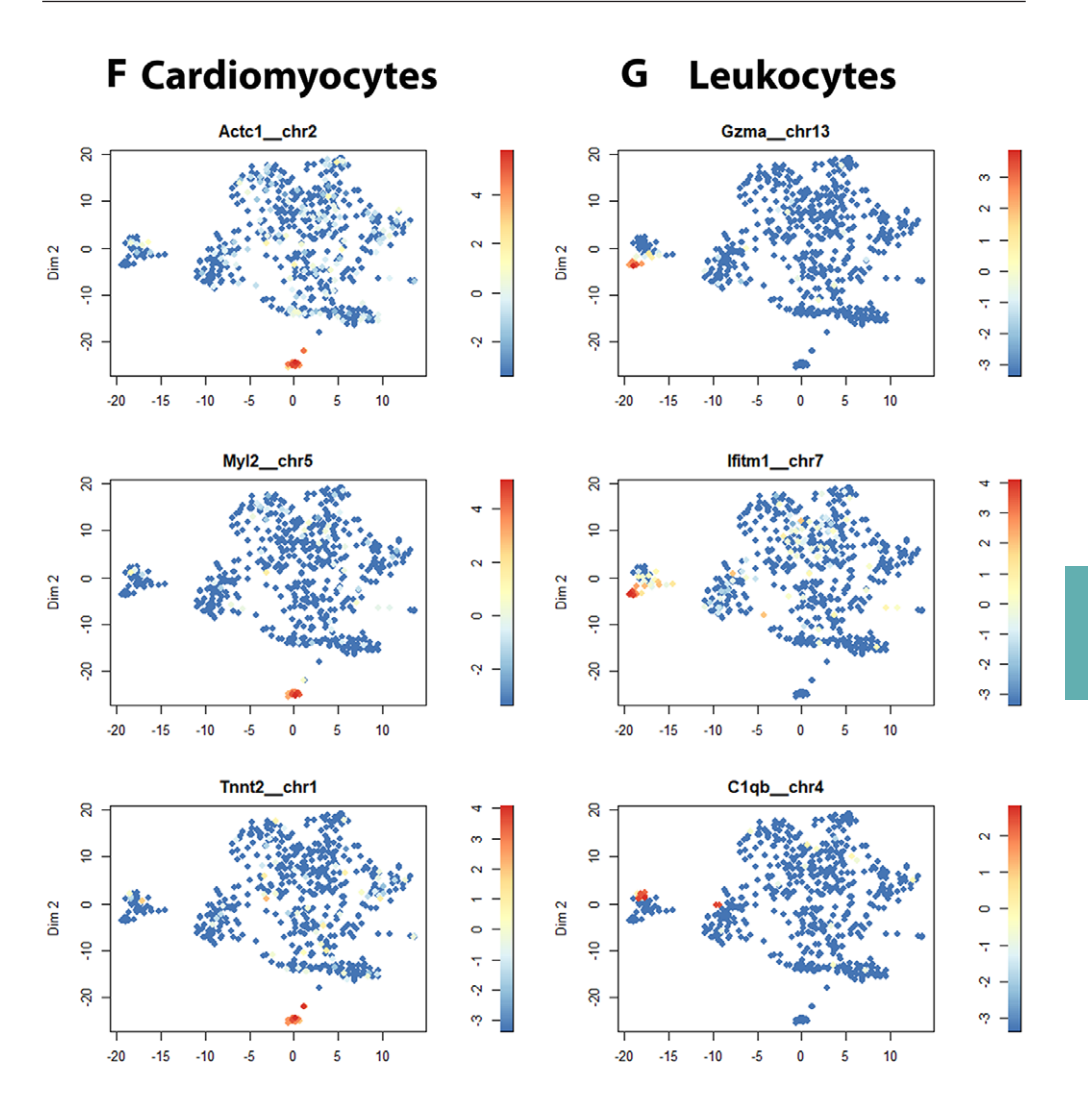
The protein expression dynamics of both FBLN5 and ACTA2 were in agreement to the findings of those predicted by scRNA-seq and qPCR. These findings demonstrate the importance of NO-signalling for maintaining the vessel wall integrity of the ascending aorta.



**Figure 5.5 Clustering of cardiac outflow tract cells based on gene expression. A**: Heatmap depicting distance in cell-to cell transcriptomes of 607 cells obtained from wild type outflow tract tissue at E12.5. K-medoids clustering identified 16 clusters. **B**: t-SNE map showing cell clusters based on affinity in RNA transcriptome profiles corresponding to different cell types. **C**: Tables of established marker genes used to identify cell types corresponding to cluster numbers indicated in B.



**Figure 5.5 Clustering of cardiac outflow tract cells based on gene expression. D-G**: *t-SNE maps showing relative RNA expression of cell specific markers indicating* **D**: *Vascular smooth muscle cells (VSMC),* **E**: *Cushion mesenchyme,* **F**: *Cardiomyocytes,* **G**: *Leukocytes. Data are shown as normalized transcript counts on a colour-coded logarithmic scale.* 



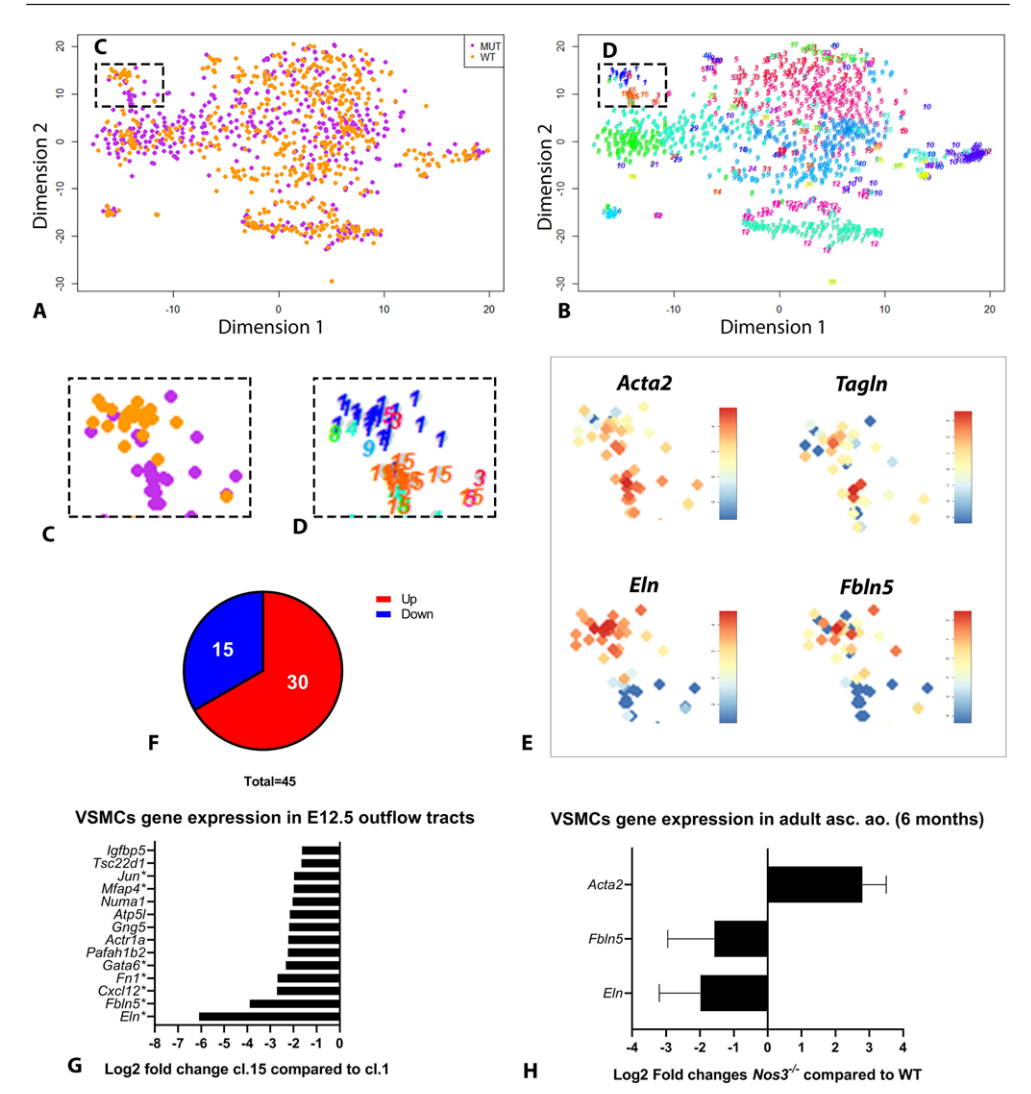
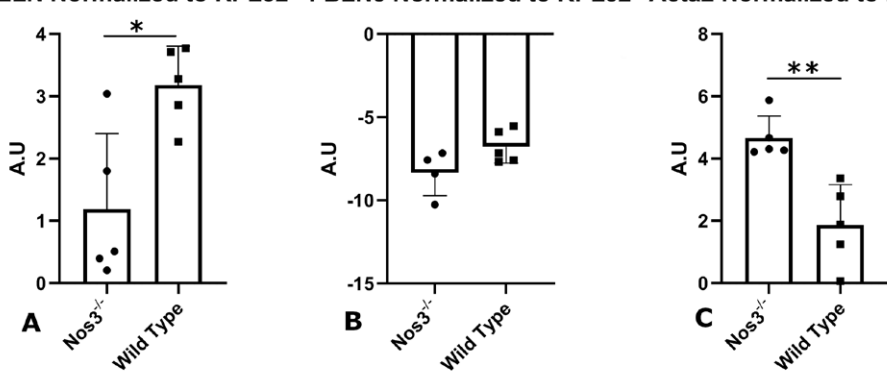
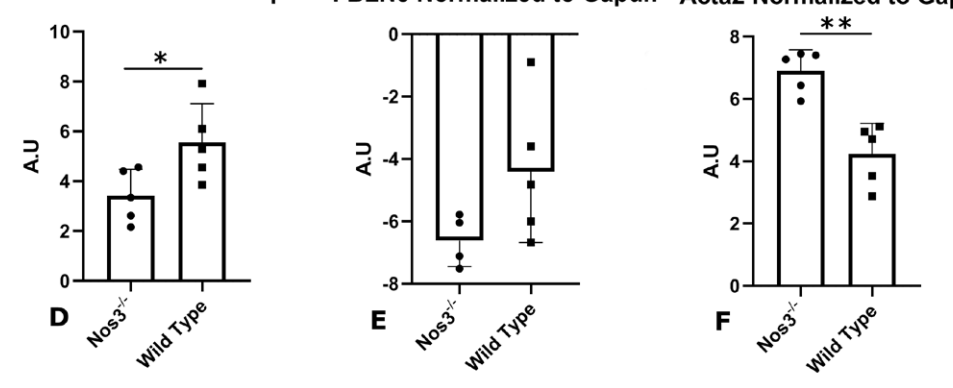


Figure 5.6 Single cell transcriptome analysis of WT and Nos3<sup>-/-</sup> mice. A-B: t-SNE map indicating transcriptome similarities among 1099 single cells. A: Colors highlight the genotype of cells (wild type: orange, Nos3<sup>-/-</sup>: purple). B: Numbers highlight the cluster numbers identified. C-D: Enlargement of the t-SNE map from A and B, focussing on the vascular smooth muscle clusters (VSMCs) showing segregation of wild type and Nos3<sup>-/-</sup> VSMC cells. E: t-SNE maps showing relative RNA expression of VSMC clusters. F: Pie chart showing the number of significantly (P<0.05) up- and down regulated genes in Nos3<sup>-/-</sup> VSMCs (cl.15) compared to wild type VSMCs (cl.1) at E12.5. G: Expression of the 15 significantly downregulated genes in the Nos3<sup>-/-</sup> VSMC cluster (cl.15) compared to the VSMCs in the wild type cluster (cl.1). Known genes linked to aneurysm formation have been marked with an asterix (asterix). H: qPCR of top 3 differential genes found in E12.5 VSCMs by scRNA-seq in adult (P6 months) VSMCs from the ascending aorta (N=5) of wild type and Nos3<sup>-/-</sup> mice (N=5.). Rpl32 was used as reference gene.

#### ELN Normalized to RPL32 FBLN5 Normalized to RPL32 Acta2 Normalized to RPL32



ELN Normalized to Gapdh FBLN5 Normalized to Gapdh Acta2 Normalized to Gapdh



**Supplemental Figure S.5.6 Extended qPCR evaluation normalized to Rpl32 and Gapdh. A-F:** qPCR expression results of 6 month old wild type (N=5) and Nos3 $^{-}$  (N=5) mice using Rpl32 as well as Gapdh as reference genes. Statistical analysis were performed using a two-tailed student T-test, \* and \*\* indicate P<0.05 and P<0.01 respectively. A.U: Arbitrary Units. Data are mean  $\pm$ SD.

## **5.4 Discussion**

Patients with a BAV have a higher risk to develop aortopathy of the ascending aorta. The exact mechanisms through which BAV-associated aortopathy arises are still poorly understood. Knowledge of the underlying processes could advance patient risk assessments and aid in the development of early diagnostic tools.

We examined the impact of NO depletion to identify effects of BAV-associated aortopathy in mice. We describe for the first time that  $Nos3^{-/-}$  mice develop dissections in the ascending aorta

by affecting signalling pathways involved in elastic fibre formation.

Studies by Koenig et al. (2015), have reported evidence of aortopathy in mice with haploinsufficiency of Notch1 in a Nos3<sup>-/-</sup> mixed background. Later studies of the same group, however, reported Notch1 haploinsufficiency in 129SV mice also caused ascending aortic aneurysm making the role of Nos3 in aortopathy less clear (Koenig et al., 2017). Reports examining HPH-1 mice, a mouse model with uncoupled NOS3, showed rapidly developing abdominal aortic aneurysms as well as aortic rupture upon infusion of ANGII (Gao et al., 2012). Moreover, Fan et al. (2014) showed that ANGII infusion could also lead to abdominal aortic dissection through endothelial mediated reactive oxygen signalling in wild type mice. Reports by Kuhlencordt et al. (2001) show that double knockout apoE/Nos3 models develop severe cardiovascular complications including spontaneous abdominal aortic aneurysms and dissection. These studies all suggest Nos3 to be an important gatekeeper of the aortic vessel wall which acts in combination with other factors to maintain aortic stability, yet is unable to result in aortopathy in case singular gene function is lost.

The spontaneous aortic dissections found in *Nos3*<sup>-/-</sup> mice in this study might have been overlooked by previous studies as the age of onset from this study was distributed over a period of 11 months. *Nos3*<sup>-/-</sup> mice in which dissections were found were acquired during routine investigations. Hemorrhages found within dissected mice were limited to the subepicardial space and were not found within the pericardial cavity or the mediastinum. This could suggest that these mice were collected during a window in which the mice were still viable but at high risk to succumb by further aortic deterioration. The mortality rate in humans is known to increase to 70% within 48h after aortic dissection (*Hagan et al., 2000; Criado, 2011*) and *Nos3*<sup>-/-</sup> mice might face an equal rapid increase of mortality rate after the onset of aortic dissection, nevertheless, the observation of aortic remodelling in *Nos3*<sup>-/-</sup> mice might challenge this concept. The survival analysis did not reveal a specific interval at which *Nos3*<sup>-/-</sup> mice spontaneous deaths differed from wild type populations, complicating the acquisition of mice prone to dissect. Future studies should look more specific into the mortality rate related to aortic dissection in *Nos3*<sup>-/-</sup> to better apprehend the timing and risks involved in the development of an aortic dissection.

Ultrasound measurements of the aorta showed increased aortic diameters in 4 months old *Nos3*<sup>-/-</sup> mice. These results suggest that the aortic vessel wall developed structural aortic dilations in adulthood similar to aortic aneurysm development observed in BAV patients

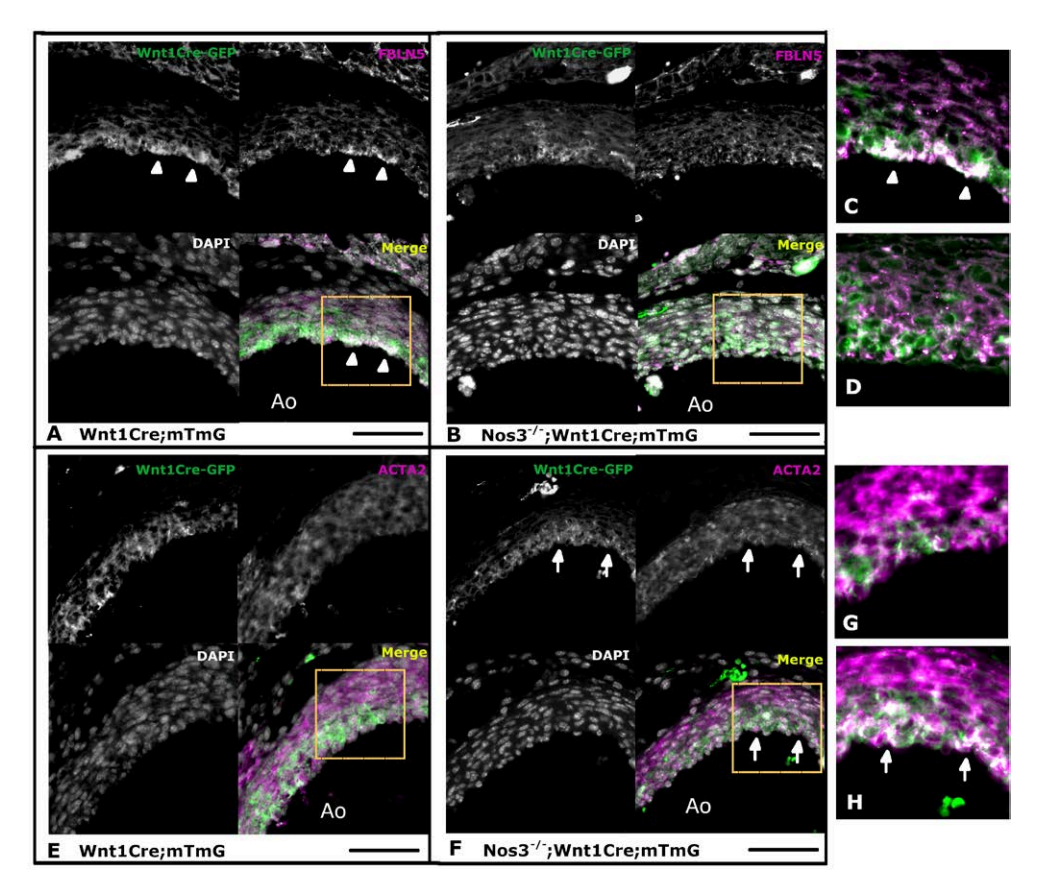


Figure 5.7 Genetic variations translate to misregulated protein expression in neural crest derived vascular smooth muscle cells of Nos3<sup>-/-</sup> embryos. Fluorescent microscopy images of transversal sections of the aortic vessel wall in Wnt1Cre;mTmG and Nos3<sup>-/-</sup>;Wnt1Cre;mTmG embryos age E17.5. A: Neural crest derived vascular smooth muscle cells (VSMCs) (green), line the inner media of the aortic vessel wall and express FBLN5 (magenta) (see arrowheads). B: Nos3<sup>-/-</sup> Neural crest derived VSMCs show reduced accumulation of FBLN5 compared to wild type embryos. C-D: Magnified view of the annotated area for Wnt1Cre-GFP and FBLN5 channels of A and B respectively. E-F: Neural crest derived VSMCs express ACTA2 (magenta) showing increased expression of ACTA2 in neural crest derived VSMCs in Nos3<sup>-/-</sup> embryos (indicated by arrows). G-H: Enlarged view of the squared area for Wnt1Cre-GFP and ACTA2 channels of E and F respectively. Nuclear staining: DAPI (grey). Scale bars: 50µm, Ao: Aorta.

(*Cecconi et al., 2006*). Circumferential aortic strain, a measure of aortic elasticity, is known to decrease with age and has been explored in clinical studies to examine aortic stiffness and is considered an important cardiovascular risk factor for patient health (*Redheuil et al., 2010*). Moreover, in Marfan mouse models circumferential aortic strain has been shown to correlate with elastin fragmentation and reduced elastic lamellae in aortic vessel walls (*Mariko et al., 2011; Chen et al., 2019*).

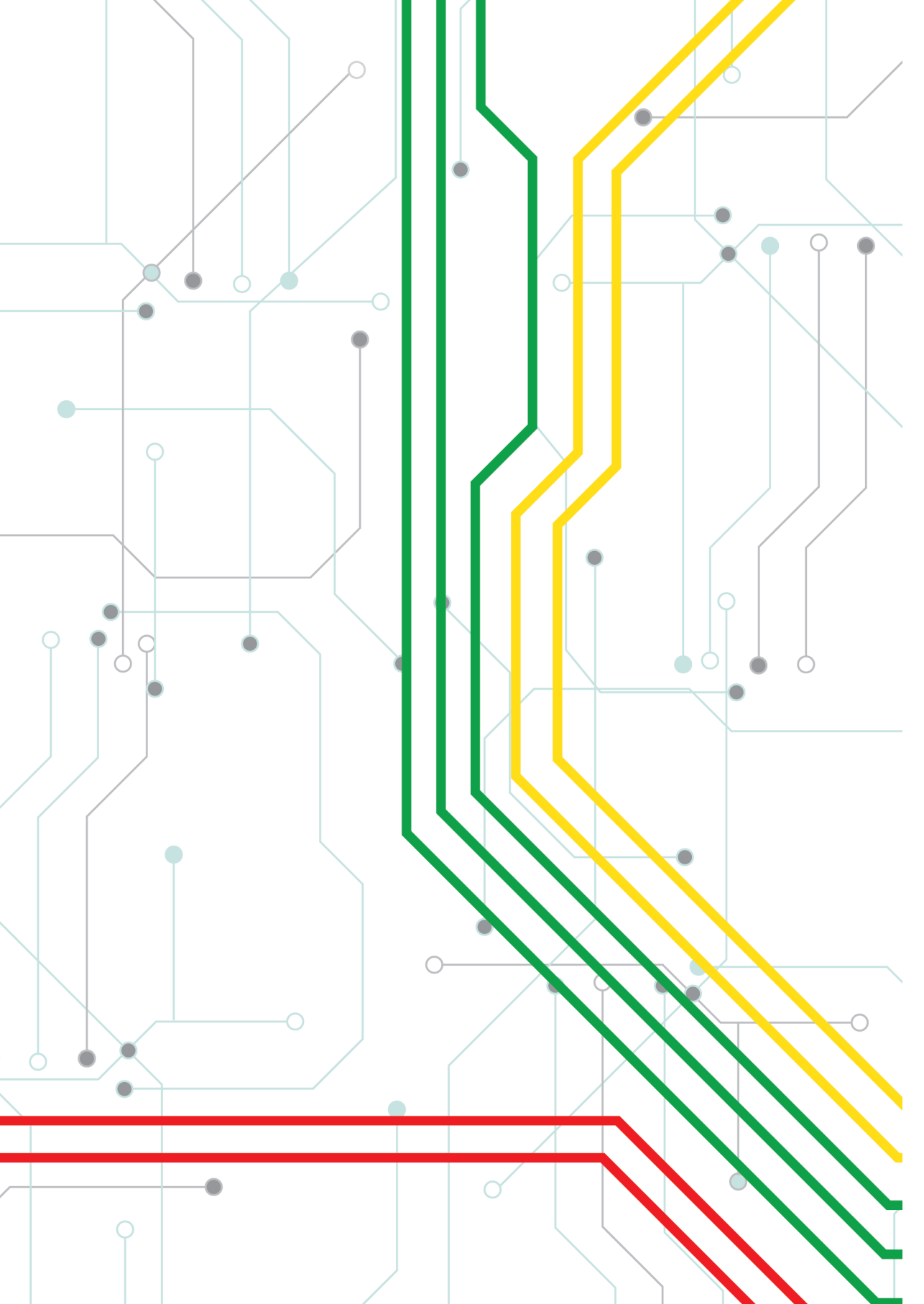
The aorta and the aortic valve have a similar developmental origin involving contributions of endothelial, NCC and second heart field lineages. BAV patients have increased risks to develop aneurysms and dissections of the ascending aorta but not of the descending aorta (Biner et al., 2009). NCCs are known to contribute to the formation of the VSMCs of the aortic root, ascending aorta, and aortic arch. The reduction in the NCC-derived populations was observed in the ascending aorta of E12.5 and E17.5 Nos3<sup>-/-</sup> embryos which was most notable in the region of the commissures. NCCs have been reported to accumulate in the commissures, however their function there is still poorly understood (Badger et al., 2010; Orriols et al., 2016). Previous studies have shown the importance of correct NCC distribution for proper aortic valve and outflow tract formation (Paloschi et al., 2011; Peterson et al., 2018; Zhang et al., 2018). Moreover, BAV patients and their first degree relatives have increased risk aortopathy, suggesting that the underlying mechanisms are not limited solely to BAV cases (Biner et al., 2009). Our findings were derived from Nos3<sup>-/-</sup> which were not selected a priori for BAV or TAV phenotype but Nos3<sup>-/-</sup> mice have been known to develop BAV in ~25% of the cases (Fernandez et al., 2009; Peterson et al., 2018) This study found aortic dissection in both TAV and BAV Nos3<sup>-/-</sup> mice similar to patient observations suggesting a role for NO signalling in aortic development in both human and mice.

This study found the significant downregulation of elastin in VSMCs in both protein and RNA expression to result in aortic dissection in Nos3-/- mice. Interestingly, clinical studies show that the elastin content is generally decreased in the ascending aortic wall of dissected patients when compared to controls (Cattell, Hasleton and Anderson, 1993). Decreased elastin concentrations within the aortic wall is strongly correlated with decreased expression of Fbln5 in patients with ascending aortic dissection similar to results found in Nos3-/- mice (Wang et al., 2005). Whilst elastic fibre degeneration in dissected aortic patients is often attributed to increased activity of metalloproteases (MMPs) (Zhang, Shen and LeMaire, 2011), Nos3-/- mice have decreased NO production inhibiting MMP activity (Ridnour et al., 2007). Elastic fibre degeneration might also be the result of reduced Fbln5 expression as FBLN5 can function as scaffolding protein during elastic fibre assembly (Midwood and Schwarzbauer, 2002). Fbln5<sup>-/-</sup> mice show reduced contractility in the thoracic aorta (Murtada et al., 2016) and develop hypertension (Le et al., 2014) but do not give rise to aortic aneurysms or aortic dissection. Similarly, Eln+/- mice also show reduced aortic contractility and increasing blood pressure (Jiang et al., 2000; Rajan Jain et al., 2011). In humans, hypertension is the single most important risk factor for aortic dissection (Hagan et al., 2000). Interestingly Nos3-/- mice have been described to also exhibit high blood pressure (Huang et al., 1995). The exact mechanisms how Nos3 would give rise to aortic dilation and dissection is not yet fully understood. Given that NCC populations were found reduced within the inner media of Nos3-/- embryos this might suggest a novel role of NO signalling during development. Genetic predisposition of aortic root aneurysm pathogenesis has been observed as a result of lineage-specific events related to NCC derived VSMCs in Loevs-Dietz syndrome, a disease in which BAVs are more frequently observed than in the general population (MacCarrick et al., 2014; MacFarlane et al., 2019). This study also found most changes related to gene expression within the aortic vessel wall to be most prominent in NCC derived VSMCs of Nos3<sup>-/-</sup> mice. The NCC derived VSMCs populate the inner media of the aorta and might depend on the paracrine cues of NO signalling for proper functioning. Interestingly, Kong and colleagues show that inhibition of NO signalling during development affected cranial neural crest patterning, differentiation and convergence in the pharyngeal arch, demonstrating a coordinating role of NO signalling during development (Kong et al., 2014). Moreover, Suvorava and colleagues show that Nos3-/- rescue through additional NO supplementation did not result in reduced hypertension in 3-4 month adult Nos3-/- mice supporting an extra-endothelial role of Nos3 (Suvorava et al., 2015). Effects of NO signalling on cellular function are diverse as NO is known to act on multiple kinase signalling cascades (Schindler and Boadan, 2001) and affect multiple transcription factors through NF-kB, c-Fos/Jun, Sp1, Egr-1, VDR/RXR and HIF-1 interaction (Bogdan, 2001; Hemish et al., 2003). This makes it challenging to interpret primary pathways involved during outflow tract formation. Future studies focusing on the molecular interactions between endothelial cells and NCC during development should provide more insight into the signalling routes through which Nos3 acts during development.

The role of *Nos3* in thoracic aneurysms, aortic dissections and BAV in humans is still poorly understood. In multiple human studies disruptions of *Nos3* signalling in ascending aortic walls of BAV patients (*Ridnour et al., 2007; Zhang, Shen and LeMaire, 2011*). Moreover, a small patient study reported that polymorphisms in *Nos3* were associated with aortic dissections in patients with thoracic aortic aneurysms (*Ekmekç et al., 2014*). These reports suggest that disrupted NO signalling impacts pathologic onset in the human thoracic aorta. Nevertheless, more recently a large cohort study reported no significant associations between *Nos3* and BAV patients with thoracic aneurysms suggesting that *Nos3* polymorphisms might be even protective for of aneurysm development in BAV patients (*Gillis et al., 2017*). Although the exact role of *Nos3* in thoracic aneurysm, aortic dissection and its relation to BAV is not yet fully understood in humans, these reports support an important role of *Nos3* in maintaining vessel wall integrity.

### 5.5 Conclusion

This study examined the developmental processes involved in aortic aneurysm formation and found dissections in ~13% of *Nos3*<sup>-/-</sup> mice aged from 1 to 11 months, of which 25% had a BAV. Ultrasound imaging showed that *Nos3*<sup>-/-</sup> mice develop aortic dilations into adulthood similar to observations in BAV patients. The dissections were a result of disruption in elastin by VSMCs. A reduction in NCC-derived VSMCs which populate the inner aortic media was observed during mid gestation and late embryonic development of *Nos3*<sup>-/-</sup> mice, supporting a congenital predisposition for developing BAV-associated aortopathy. Single cell sequencing of embryonic outflow tracts showed significant downregulation of *Eln* and *Fbln5* mRNA in VSMCs of *Nos3*<sup>-/-</sup> mice which was also confirmed in ascending aortic tissue of adult mice showing that the embryonic disruptions in elastic lamellae formation persisted into adulthood. Downregulation of *Eln* and *Fbln5* translated into reduced ELN and FBLN5 protein translation which primarily affected NCC-derived VSMCs. Disrupted endothelial mediated NO signalling causes congenital BAV-associated aortic dilation and dissection as a result of inhibited elastic lamellae formation in VSMCs in *Nos3*<sup>-/-</sup> mice.



# **Chapter 6**

Pulmonary ductal coarctation and left pulmonary artery interruption; pathology and role of neural crest and second heart field during development

2020

**DOI**: 10.1371/journal.pone.0228478

**PLOS ONE** 

Adriana C. Gittenberger-de Groot<sup>1,2</sup>, Joshua C. Peterson<sup>2</sup>, Lambertus J. Wisse<sup>2</sup>, Arno A. W. Roest<sup>2,3</sup>, Robert E. Poelmann<sup>1,4</sup>, Regina Bökenkamp<sup>3</sup>, Nynke J. Elzenga<sup>2,5</sup>, Mark Hazekamp<sup>6</sup>, Margot M. Bartelings<sup>2</sup>, Monique R. M. Jongbloed<sup>1,2</sup>, Marco C. DeRuiter<sup>2</sup>

Department of Cardiology, Leiden University Medical Center, Leiden, The Netherlands
 Department of Anatomy & Embryology, Leiden University Medical Center, Leiden, The Netherlands
 Department of Pediatric Cardiology, Leiden University Medical Center, Leiden, The Netherlands
 Department of Animal Sciences and Health, Leiden University, Leiden, The Netherlands
 Department of Pediatric Cardiology, University Hospital Groningen, Groningen, The Netherlands
 Department of Cardio-thoracic Surgery, Leiden University Medical Center, Leiden, The Netherlands

#### **Abstract**

**Objectives**: In congenital heart malformations with pulmonary stenosis to atresia an abnormal lateral ductus arteriosus to left pulmonary artery connection can lead to a localised narrowing (pulmonary ductal coarctation) or even interruption We investigated embryonic remodelling and pathogenesis of this area.

**Materials and Methods**: Normal development was studied in WntCre reporter mice (E10.0–12.5) for neural crest cells and Nkx2.5 immunostaining for second heart field cells. Data were compared to stage matched human embryos and a VEGF120/120 mutant mouse strain developing pulmonary atresia.

Results: Normal mouse and human embryos showed that the mid-pharyngeal endothelial plexus, connected side-ways to the 6th pharyngeal arch artery. The ventral segment formed the proximal pulmonary artery. The dorsal segment (future ductus arteriosus (DA)) was solely surrounded by neural crest cells. The ventral segment had a dual outer lining with neural crest and second heart field cells, while the distal pulmonary artery was covered by none of these cells. The asymmetric contribution of second heart field to the future pulmonary trunk on the left side of the aortic sac (so-called pulmonary push) was evident. The ventral segment became incorporated into the pulmonary trunk leading to a separate connection of the left and right pulmonary arteries. The VEGF120/120 embryos showed a stunted pulmonary push and a variety of vascular anomalies.

**Summary**: Side-way connection of the DA to the left pulmonary artery is a congenital anomaly. The primary problem is a stunted development of the pulmonary push leading to pulmonary stenosis/atresia and a subsequent lack of proper incorporation of the ventral segment into the aortic sac. Clinically, the aberrant smooth muscle tissue of the ductus arteriosus should be addressed to prohibit development of severe pulmonary ductal coarctation or even interruption of the left pulmonary artery.

## 6.1 Introduction

Before birth the ductus arteriosus (DA) connects the pulmonary trunk (PT) to the descending aorta, thus bringing oxygen-rich placental blood to the systemic circulation, largely circumventing the still not functioning lungs. In the perinatal period the muscular DA starts physiological closure by contraction followed by anatomical sealing and subsequent ligament formation (*Bökenkamp et al., 2010*). Some heart malformations present with narrowing of

the pulmonary outflow tract (OFT) as in tetralogy of Fallot with severe pulmonary stenosis or pulmonary atresia and a ventricular septal defect (VSD). Here, instead of being in direct continuity with the PT (**Fig. 6.1A**), we can find an abnormal lateral DA to left pulmonary artery connection (*Elzenga and Gittenberger-de Groot, 1986; Brink et al., 2015*). Often a narrowing in the proximal part of the left pulmonary artery, a so-called pulmonary ductal coarctation (PDC), is seen (**Fig. 6.1B**). It is not known whether this leftward positioning of the DA connection is a developmental anomaly or whether it reflects the persistence of a normal embryonic stage as seen in an evo-devo setting in chicken embryos (*Bergwerff, DeRuiter and Gittenberger-De Groot, 1999; van der Sterren et al., 2014; Akaike et al., 2019*). Formation of the pharyngeal arch artery (PAA) system, with merging of ventral and dorsal sprouts to form a complete arch, has been extensively studied in the human embryo (*Congdon, 1922*).

Refinements were brought by acknowledging the special status of the 6th or pulmonary arch artery (*de Ruiter et al., 1989*) in which it was shown that the anlage of the pulmonary arteries, derived from the endothelium of the mid-pharyngeal endothelial strand (MPES), does not grow out towards the lung but connects to the ventral sprout before the completion of the 6th PAA. On the left side the dorsal segment of the 6th PAA persists as the DA while this segment on the

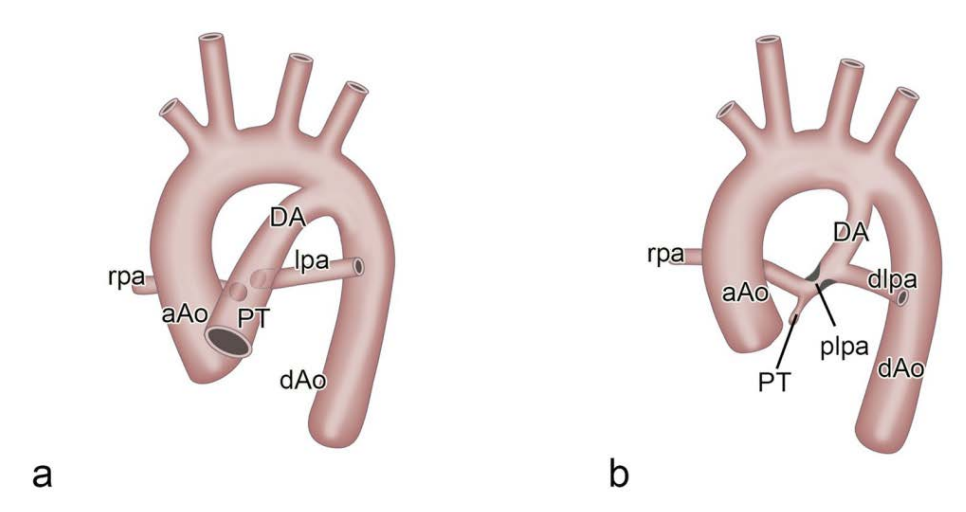


**Figure 6.1 A**: Schematic view of the normal perinatal aortic arch showing the ascending aorta (aAo) and the pulmonary trunk (PT). De ductus arteriosus (DA) connects the PT with the descending aorta (dAo). The left (lpa) and right (rpa) pulmonary arteries are dorsally hooked up to the PT. **B**: Schematic representation of a case with an abnormal lateral DA to lpa connection creating a proximal (plpa) and distal (dlpa) part. Aberrant DA tissue (black indentations), extending into the plpa, create the narrowing hallmark of the pulmonary ductal coarctation.

right side disappears (Congdon, 1922) by a process of selective apoptosis (Molin et al., 2004). To achieve the perinatal situation in which the DA connects directly to the pulmonary trunk (Fig. 6.1A) separately from the adjoining left and right pulmonary arteries, the ventral sprout of the 6th PAA either has to become part of the pulmonary artery or has to disappear. The remodelling in this area has not been adequately studied but is relevant for understanding the abnormal connection of the DA to the left pulmonary artery as encountered in PDC (Fig. 6.1B). The normal remodelling of the PAAs takes place after the endothelium-lined vascular network is consolidated by smooth muscle cells (DeRuiter et al., 1993; Molin et al., 2004) derived from the surrounding mesoderm (second heart field / SHF) and mesectoderm (neural crest cells / NCCs). In order to better understand both normal and abnormal development in this complicated area we have applied in this study the more recent approach of investigating these cellular constituents. Animal models, initially with the chimeric and retroviral tracing techniques in avian embryos and more recently transgenic reporter studies in mouse (Bergwerff et al., 1998; Waldo et al., 1999; Jiang et al., 2000) contribute to our understanding of the importance of the NCC population in PAA formation and OFT septation. Detailed information on the differential contribution of NCC to the wall of the ascending aorta and pulmonary trunk is emerging (Peterson et al., 2018). A relatively novel cell population, that received a hitherto neglected role, is the SHF (Kelly and Buckingham, 2002). This population is actually instrumental in adding myocardium to the right side of the heart (Bajolle et al., 2006; Lazzarini et al., 2018) but it has also been described to contribute to the smooth muscle cells of the aortic and pulmonary wall (Harmon and Nakano, 2013). We have previously shown that the contribution of the SHF is more prominent to the pulmonary side of the OFT, a process dubbed as the pulmonary push (Scherptong et al., 2012), being important for OFT septation and positional shift (often referred to as rotation) of the great vessels. It is of particular interest that this left-sided SHF population encircles the region of the left pulmonary artery-DA connection in which also NCCs are abundantly present. Hardly any attention has been given to the specific contribution of the various cell types to vascular wall formation on boundaries at the merging of the 6th PAA to the pulmonary system. The abnormal lateral DA to left pulmonary artery connection is clinically relevant. In patients with pulmonary atresia and an intracardiac shunt, including cases with tetralogy of Fallot and univentricular hearts, DA closure potentially causes proximal left pulmonary artery stenosis or even interruption of the left pulmonary artery (Elzenga and Gittenberger-de Groot, 1986; Elzenga et al., 1990; Waldman et al., 1996). These additional anomalies complicate the treatment course of the patients seriously. Often it is necessary to address the stenotic proximal left pulmonary artery surgically (Brink et al., 2015) or by repeated catheter intervention because of the somatic growth of the patient. In the present study a combined approach has been adopted to study this problem using both staged mouse embryos (normal, reporter mice and growth factor deficient mice) and stage-matched human embryos. Histopathology and clinical images of human patients will be presented to underscore the clinical importance.

#### 6.2 Materials and methods

### 6.2.1 Embryonic material

The material used to study the development of the pulmonary arterial system consists of mouse embryos of various strains and stages, as well as human embryos from different sources. Reporter mice and immunohistochemistry have been used to study cellular constituents (NCCs, SHF mesoderm and endothelium) in arterial development. Growth factor deficient mice were studied for abnormal development. All mice were handled according to the Guide for Care and Use of Laboratory Animals (NIH), the experiments were approved by the LUMC Animal Welfare Committee (dec14184). The following reporter mice (Black6 background using C57BL/6JLumc mice) derived from breeding strategies (Peterson et al., 2018), have been used in this study (N=3 for each stage): Wnt1Cre;mT/mG for NCC tracing; Mef2cCre;mT/mG for myocardial tracing (generous gift of Dr. Qingping Feng, The University of Western Ontario, London, Ontario, Canada). Furthermore, the VEGF 120/120 mouse (N=49 from which 7 are actually selected for this study), in which vascular endothelial growth factor (VEGF) isoforms 164 and 185 were blocked but an overexpression of soluble VEGF 120 is present (Carmeliet et al., 1996; Van Den Akker et al., 2007), was investigated for PAA pathological phenotypes (Rammeloo et al., 2015). Male and female mice were kept overnight and copulation was determined by the presence of a vaginal plug the following morning. Noon was considered as embryonic day (E) 0.5. Embryos were removed at E10.0-E18.5 following dissection in phosphate buffered saline (PBS), pH 7.4. Using incremental developmental stages of reporter mice (E10.0-14.5) with Wnt/Cre for NCCs, PECAM for endothelium and NKX2.5 staining for SHF-derived cells we reinvestigated the connection of the 6th PAA and the pulmonary arteries to the pulmonary trunk in detail. We consider the Wnt/Cre reporter useful for marking the NCC population and the NKX2.5 and PECAM stainings for SHF and endothelium, respectively, in the constraints of the developmental stages studied and considering heart development. We compared normal mouse development with a series of normal human embryos from 4-24 mm crown -rump length (CR), which are overlapping with the studied mouse stages. As a disease model we used the VEGF120/120 mutant mouse, originally presented as a model for the 22g11 deletion

syndrome (*Stalmans et al., 2003*), with a spectrum of tetralogy of Fallot to pulmonary atresia (*Van Den Akker et al., 2007*). It has already been described that in this mutant mouse initially the left and right 6th PAA are formed and that, depending on the degree PT stenosis to atresia, the DA disappears during further embryonic development. This is accompanied in some cases with development of additional aorto-pulmonary connections (*Rammeloo et al., 2015*). Human embryos (4–24 mm CR length, Carnegie Stages 12-24, N=6) were obtained as described (*Blom et al., 1999; Sizarov et al., 2010, 2012*), with the addition of one embryo from the Viennese department of Anatomy), fixed in 4% formaldehyde and serially sectioned.

#### 6.2.2 Postnatal material

From the human collection of neonatal heart malformations of the Leiden department of Anatomy, macroscopy and histopathology were studied (N=41) in cases with pulmonary atresia and PDC (*Elzenga and Gittenberger-de Groot, 1986*). The (histo)pathology of the human DA to left pulmonary connection of severe PDC is shown in neonatal post-mortem specimen with pulmonary atresia and tetralogy of Fallot. Clinical images of three human patients are presented in addition. The human material belongs to the historical collection of the Leiden University Medical Center, more specifically the Department of Anatomy and Embryology, that falls under the regulations for proper use of human tissues for medical research purposes. These anonymized tissues were collected from 1950 onwards in a period in which informed/signed consent had not come into use. One additional human embryo was provided by Dr. Sizarov (Amsterdam) and that one was collected from medically induced abortions performed for social reasons at the Gynecology Department of the Tartu University Hospital, Estonia. Collection and use for research as presented here was approved by the Medical Ethics Committees of the Universities of Tartu, Estonia, and Amsterdam, the Netherlands.

### 6.2.3 Immunohistochemistry

For histological examination, mouse embryos were processed (*Van Den Akker et al., 2007; Peterson et al., 2018*). In brief, they were fixed in 4% paraformaldehyde (0.1 M, pH 7.4, 24 hours, 4°C), embedded in paraffin, and serial sections (5 μm) were mounted on glass slides. Deparaffinization was followed by ethanol and rehydration. Endogenous peroxidase activity was inhibited and slides were microwaved for antigen retrieval. Sections were incubated with primary antibodies against eGFP (Abcam ab 13970, 1/500), Tropomyosin (Sigma-Aldrich T9283, 1/500), TFAP2α (GeneTex GTX62588, 1/2000), NKX2.5 (Santa Cruz SC-8697, 1/4000), MEF2c (Cell Signaling Technology CST5030), αSMA (A2547 (Sigma-Aldrich, Missouri, USA) and PECAM1

(Santa Cruz SC-1506-R). Diluted primary antibodies (PBS–Tween-20 (PBST), 1% bovine serum albumin; A8022; Sigma-Aldrich, St Louis, MO, USA) prevented non-specific binding. Slides were rinsed twice in PBS and once in PBST. Tiramide signal amplification (TSA PLUS Biotin kit, NEL749A001KT, Perkin Elmer, Waltham, MA, USA) was used in NKX2.5 staining by adding HRP-labelled antibodies followed by amplification according to the manufacturers' manual. For fluorescent microscopy primary antibodies were visualized by incubating in fluorescently labelled secondary antibodies (in PBST, 60 minutes). Secondary antibodies were diluted 1/200 and applied (*Peterson et al., 2018*) DAPI (Life Technologies D3571, 1/1000) was used as nuclear stain while slides were mounted with Prolong Gold (Life Technologies). The human material was stained for standard histology (Hematoxylin-eosin, Azan, Resorcin-fuchsin), furthermore, embryonic human material was stained immunohistochemically for HNK1 and HHF35 [26] and NKX2.5 (SHF) and TFAP2α (NCCs) (*Sizarov et al., 2012*).

#### 6.2.4 Microscopic analyses and 3D reconstructions

3D reconstructions of the arterial poles were made using Amira 6.3 (Template Graphics Software Inc., Houston, TX, USA) of mouse embryos between E10.5 and E16.5. Slides were scanned using the Pannoramic 250 Flash III slide scanner (3DHISTECH Ltd, Budapest, Hungary) and images of identical scale and exposure were exported using Histech Pannoramic Viewer (3DHISTECH Ltd.). Images were stacked and semi-automatically aligned in Amira. Relevant cardiac and arterial structures were labelled based on staining patterns and morphology. Surface views were exported to PDF formats using the Adobe Acrobat 9.5 software package.

## 6.3 Results

## **6.3.1** Normal development in the WntCre reporter mouse embryo

Embryos from E10.0 to E12.5 show the most important development and remodelling with a gradual change in the position and connections of the 4th and 6th PAA to both the aortic sac, later on separated into the ascending aorta and PT, and the dorsal aortae.

### 6.3.2 Pharyngeal arch artery and pulmonary artery remodelling

At E10.0 the 3rd PAA, encased within WntCre positive NCCs, is connected to the aortic sac. Directly caudal of the 3rd PAA, ventral sprouts of the 4th PAA, covered by green labelled NCCs can be detected having a course more parallel to the dorsal aortae instead of the more transverse position of the 3rd arch (**Fig. 6.2A, C, D**). Small indications of dorsal sprouts, covered

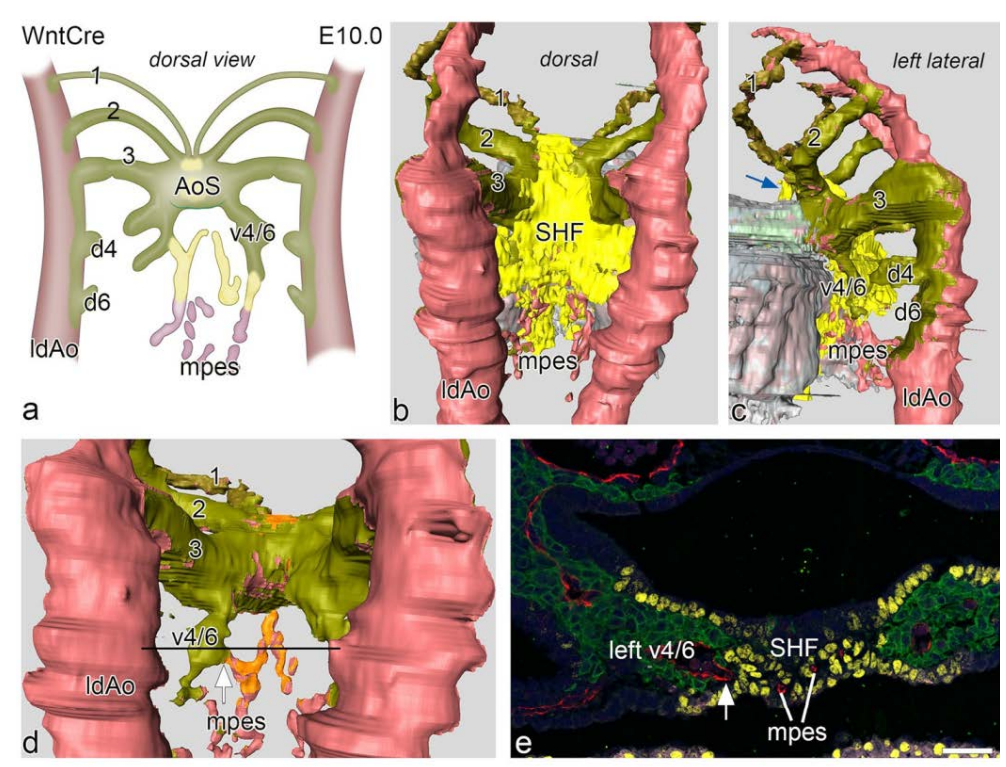


**Figure 6.2 A**: Schematic representation of a dorsal view of the connection of the vasculature of the midpharyngeal endothelial strand (mpes) and connections to the combined ventral sprouts (v4/6) of the right and left 4th and 6th PAA continuous with the aortic sac (AoS) in an E10.0 WntCre mouse embryo. The dorsal sprouts of 4th and 6th PAA (d4 and d6) are connected to the dorsal aorta (indicated is the left one, IdAo). **B-D**: Reconstructions from various angles of relevant structures showing the WntCre positive neural crest cells (olive green) surrounding the continuous PAA arteries (1,2,3) as well as the AoS (out of view in B). The dorsal aortae are on their lateral and dorsal aspect surrounded by NCC. The myocardium is depicted in shades of grey. The mid-line mesenchymal second heart field mass (SHF: yellow) is positioned between the confluence of the 3rd (running anteriorly over the AoS; blue arrow in C) and the developing 4th and 6th PAAs (in B, C). **D**: In this reconstruction the mid-line SHF mesenchymal mass has been removed showing the extent of coverage of the cranial part of the mpes (orange) while more caudally the mpes is not surrounded by SHF (pink). **E**: Transverse section at the level (see black line in D) of the connection (white arrow) of the cranial part of the mpes (white lines) and endothelial cells (stained red for CD31) to the left v4/6 (NCC: green). The NKX2.5 positive SHF cells (yellow) border this connection and surround the endothelial cells here in the midline. Magnification: bar 100 µm.

by green labelled NCCs (**Fig. 6.2C**), are seen but no continuous 4th or 6th PAA is formed yet (**Fig. 6.2A, C-D**). Mid-sagittally between these developing ventral sprouts of the PAAs there is an endothelial network, the MPES. Cranially, the endothelial network is surrounded by yellow labelled NKX2.5 positive SHF while the more caudal extensions of the MPES are surrounded by

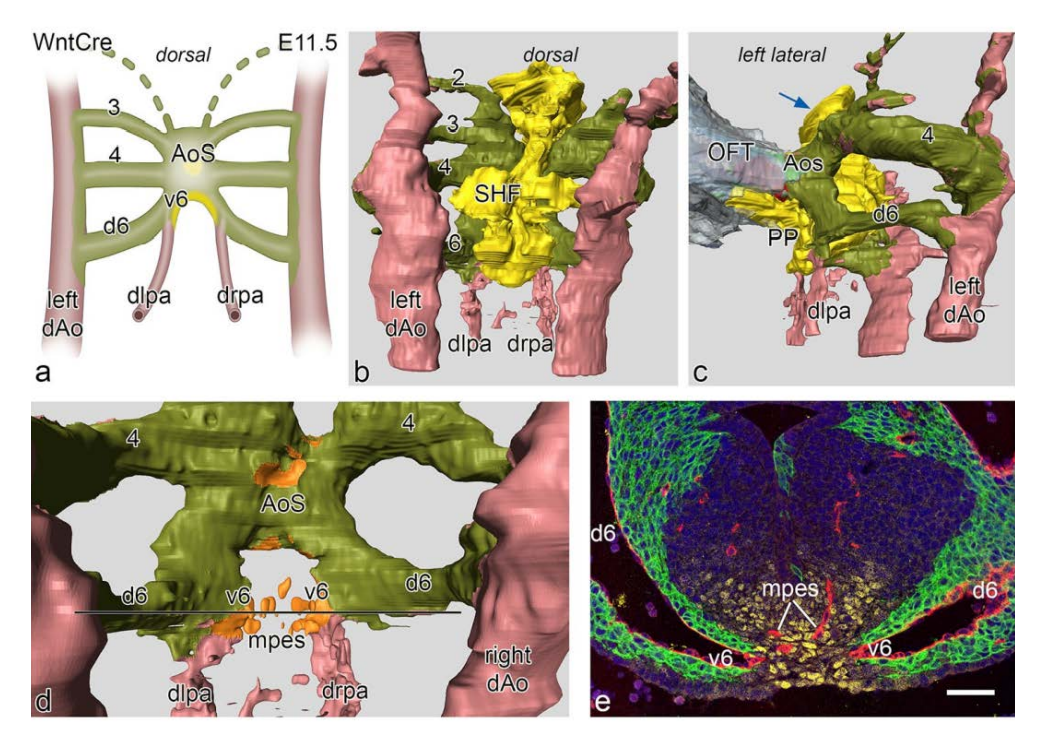
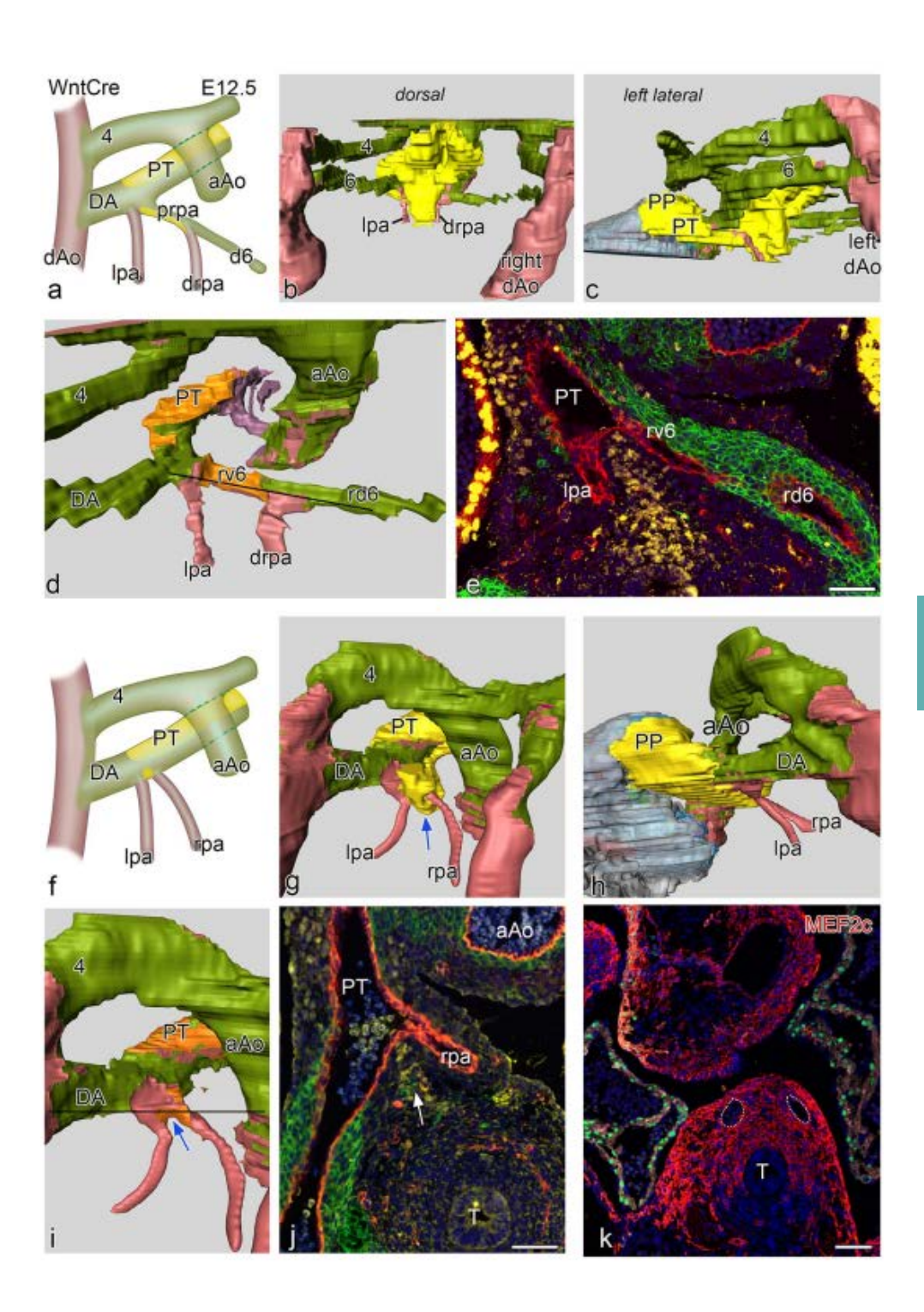


Figure 6.3 A: Schematic representation of a dorsal view of vascular connections in an E11.5 WntCre mouse embryo. In this stage PAA 3, 4 and 6 are complete. The distal left (dlpa) and right (drpa) pulmonary arteries merge sideways with PAA 6 creating a ventral (v6) and a dorsal (d6) segment of the latter. The d6 is completely encircled by neural crest cells (green) while the v6 has a lateral layer of neural crest and a medial layer of second heart field (SHF: yellow). The v6 forms a short proximal pulmonary artery. **B**: Dorsal view of a reconstruction at this stage with now complete 3rd,4th and 6th arches that are lined by neural crest (olive green). The SHF (yellow) forms the mid-line mesenchyme. The dlpa and drpa (pink) are not covered by either NCC or SHF. C: Left lateral view showing the connection of the outflow tract (OFT) myocardium (grey) with the short aortic sac (AoS). The SHF mass has a short extension anteriorly towards the future aortic orifice (blue arrow). More prominent at this stage is the left sided SHF extension that runs underneath the v6 and along the future pulmonary wall of the AoS. This is the so-called pulmonary push (PP). **D**: Dorsal view after removal of the SHF, the double lining of the relatively short v6 (identical to a proximal part of a pulmonary artery (see also a.) is depicted with a NCC (olive green) and a SHF reflected coverage (orange). E: Section of the embryo at the level indicated (black line) in D. The right and left v6 (endothelial cells red) are in part lined by NCCs (green) and NKX2.5 positive SHF (yellow). In the SHF midline mass (yellow) the endothelial plexus (red) of the mid-pharyngeal endothelial strand (mpes) is visible. Magnification: bar 100 µm.

non-NKX2.5 stained pharyngeal mesenchyme (**Fig. 6.2B, D**). Connections of the MPES to both the left and right ventral sprouts of the 4-6th PAA can be discerned (**Fig. 6.2A, D**).

At E11.5 the situation is changed in that the 4th PAAs are now completely developed and connect the aortic sac with the dorsal aortae. Also the 6th PAAs are complete (**Fig. 6.3A-D**). The dorsal sprouts of the 6th PAA are solely surrounded by NCCs and devoid of SHF (**Fig. 6.3A-E**). At this stage the proximal parts of the future left and right pulmonary artery, that at E10.0 are covered by SHF, have disappeared and seem to be incorporated in the short ventral sprouts of the 6th PAA. These are special in that they have a double lining with NCCs of the original 6th PAA ventral sprout laterally, and NKX2.5 positive SHF medially (**Fig. 6.3D, E**) being continuous with the mid-line SHF mass (**Fig. 6.3B**). The distal part of the pulmonary arteries is not surrounded by either SHF or NCC (**Fig. 6.3A, B, D**), but are embedded in Mef2c positive splanchnic mesoderm as shown in a E12.5 embryo (**Fig. 6.4K**).

Figure 6.4 A, F: Schematic representations of two E 12.5 WntCre embryos. Embryo A is slightly less far developed as compared to **F**. In both embryos the ascending aorta (aAo) and the pulmonary trunk (PT) have now been separated. **B-D**: Reconstructions of the younger embryo with a complete 4th and 6th PAA. **C**: Dorsal midline SHF mass (yellow) partly covering the neural crest (green) lined PAA's. **C**: Left-sided view showing the position of the SHF mass (yellow) which has an extension (pulmonary push population: PP) covering the major part of the lumen of the PT towards the myocardial outflow tract (grey), running underneath the 6th PAA to pulmonary artery connection. **D**: Dorsal view after removal of the SHF mass (lumen coverage area: orange). On the left side the dorsal 6th PAA, now referred to as ductus arteriosus (DA) is completely surrounded by neural crest cells, There is no indication of a ventral 6th PAA. The left pulmonary artery (lpa: red) abuts independently on the PT On the right side the situation is less well developed. The dorsal segment of the right 6th PAA (rd6) is regressing and completely surrounded by NCC. The ventral segment of the 6th PAA (rv6) is still present with a lateral wall of NCCs and a medial wall of SHF. The distal part of the right pulmonary artery (drpa) enters side-ways into this right-sided 6th PAA. Thus the proximal rpa is at this stage formed by the rv6. **E**: Section at the level indicated in D (black line) in which it can be seen that the right v6 (rv6: also proximal part of the rpa) has both a lining of SHF (yellow) and NCCs (green). **F**: In the more developed embryo the originally distal parts of the lpa and rpa, embedded in Mef2c positive mesoderm (K) are not covered by NCC and SHF. They enter the PT independent of the DA. G-I: Reconstructions showing similar dorsal views as B-D. Level of section J is indicated by a black line in I. The SHF derived flow divider is still seen between the lpa and rpa (blue arrows in G and I and white arrow in J). The right d6 has regressed completely. There is on both sides no indication anymore of the v6 segments. K: Section of a E12.5 Mef2cCre embryo showing that the distal parts of the lpa and rpa (white dotted vessels) are situated within Mef2c positive splanchnic mesoderm that is not stained by NKX2.5 (green). T: trachea Magnification sections E, J, K. Bars 100 μm.



At E12.5 we present two embryos with a slightly different stage of development (**Fig. 6.4A-J**). In both cases there is an OFT separation of the ascending aorta and the PT. The younger embryo is comparable to the E11.5 case with regard to development on the right side where, next to a regressing right dorsal 6th PAA, the ventral 6th PAA segment show a combined wall of NCC and SHF (**Fig. 6.4A, D, E**). The distal part of the right pulmonary artery, therefore, connect to the 6th PAA between its dorsal and ventral segment (**Fig. 6.4D**). This ventral segment of the 6th PAA present as the proximal part of the right pulmonary artery. On the left side we cannot discern a separate ventral 6th PAA segment anymore as now the distal part of the left pulmonary artery, not being encased by NCC and SHF, enters directly into the PT. The left 6th PAA, also referred to as DA, consists of the dorsal segment being solely surrounded by NCC (**Fig. 6.4A, D**). The mid-line SHF mass show a marked pulmonary push population along the PT.

In the older embryo (**Fig. 6.4F-J**) the ventral segments of the 6th PAA (in the previous stages the proximal pulmonary arteries) are almost completely incorporated in the dorsal wall of the PT. The pulmonary arteries, however, not surrounded by either NCCs or SHF and embedded in Mef2c positive mesoderm (**Fig. 6.4K**), arise separately from the PT and even seem to form part of the dorsal wall of the PT (**Fig. 6.4F, G, I**). The right dorsal segment of the 6th PAA has regressed completely while the dorsal left 6th PAA persists as the definitive DA. The latter, demarcated because being surrounded by NCCs, is now positioned more anteriorly in continuity with the PT. The mid-line SHF mass has now dissolved and is mainly recognisable in the flow divider between the left and right pulmonary arteries as well as its extension as pulmonary push along the PT (**Fig. 6.4G-J**).

# 6.3.3 Role of the midline NKX2.5 positive SHF population and the pulmonary push

The mid-line pre-pharyngeal NKX2.5 positive SHF population, contacting the dorsal wall of the aortic sac, deserves additional attention. At E10.0 these cells extend anteriorly over the 2nd and 3rd PAA towards the aortic side of the outflow tract up to the borderline with the myocardium, reaching the site where the intercalated aortic valve leaflet will develop (**Fig. 6.2C**). Between E11.5 and E12.5 a clear asymmetry develops in the NKX2.5 positive SHF population. This becomes more prominent initially dorsally and thereafter along the left (pulmonary) side of the aortic sac (so-called pulmonary push). At E12.5, after separation of the OFT, the resulting population runs along the left side of the PT and reaches the myocardium at the site of the future pulmonary intercalated valve leaflet area (**Fig. 6.3C, 6.4C, G, H**). This left-

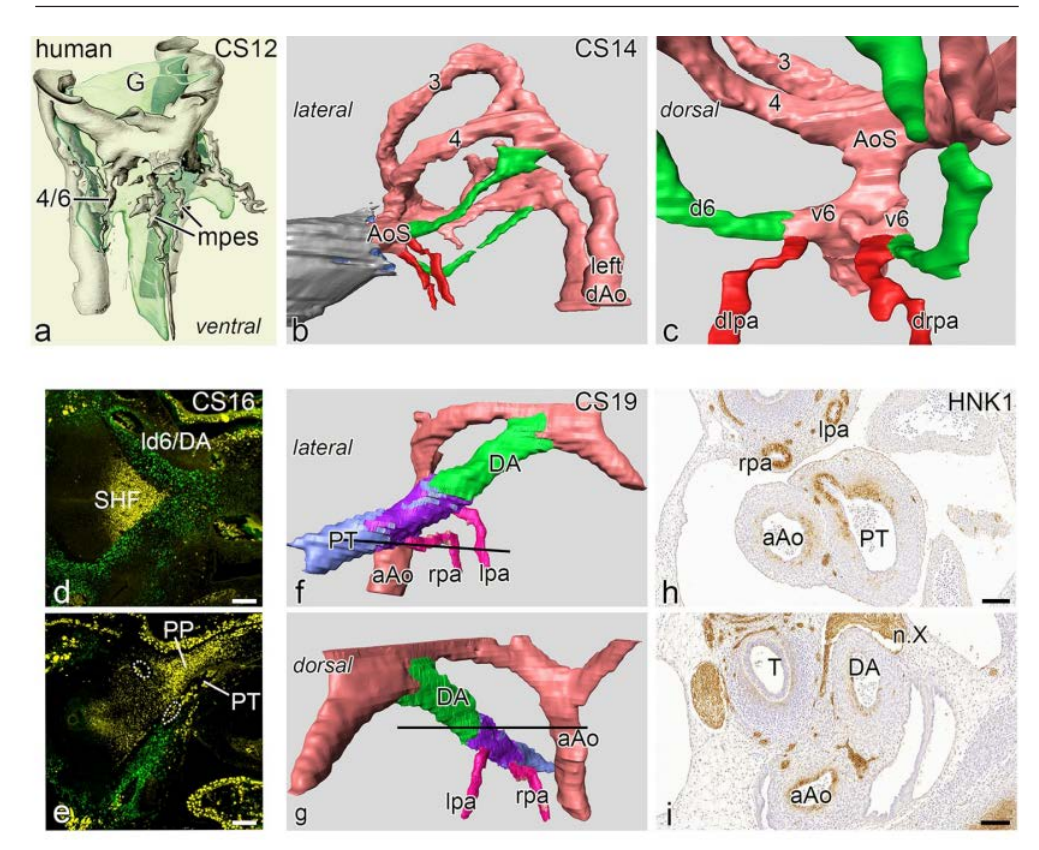
sided pulmonary push population runs below the NCC-surrounded DA. Exactly in the corner of this connection of DA with PT the left pulmonary artery enters the PT at the border of SHF and NCCs (**Fig. 6.4C, G, H**). At the right side, where no pulmonary push SHF is present, the dorsal 6th PAA segment (comparable to the left DA) regresses.

As a consequence the left dorsal segment of the 6th PAA forms the DA while the right dorsal segment, which is already separated from the right pulmonary artery, regresses. Therefore, during normal development there remains after E12.5 no marked length of a ventral segment with a sideway connection of the pulmonary arteries.

#### 6.3.4 Normal development in human embryonic stages

A renewed study of human embryonic stages 4-24 mm CR length (N=5, Carnegie Stages 12-24) confirms the data from the mouse studies showing a similar remodelling and incorporation process of the short ventral sprout of the 6th PAA and the attached left and right pulmonary arteries into the PT. The youngest embryo (4 mm, CS 12 of the Viennese collection) shows the connection of the MPES network to the developing combined 4th and 6th PAA ventral sprouts (Fig. 6.5A). Somewhat more advanced configurations are shown in a 6.5 mm embryo (CS 14, Leiden collection) and a 9.5 mm (CS 16). In these embryos we observed only the morphologic configuration of the vessel lumen as no immunohistochemistry was available at the time of collection of this rare material. We now show, however, that in both embryos the distal pulmonary artery connects sideways to the 6th PAA with a very short ventral 6th PAA segment (Fig. 6.5B-C) comparable with normal mouse embryos. Access to more recently collected valuable embryonic material (CS 16) (Amsterdam UMC), in which immunohistochemistry was performed, confirms the presence of the NKX2.5 pulmonary push population as well as the adjoining, non-overlapping TFAP2a positive NCC cells. The resolution and number of the sections does not allow for detailed reconstruction of this area or decisions on the presence of a ventral 6th PAA segment (Fig. 6.5D-E).

Study of an older embryo (Leiden collection, CS 19, 17mm), in which the boundaries of the pulmonary arteries, PT and the DA were visualized by immunohistochemical staining with an anti-HNK1 antibody, reveals a next stage of development. The differential staining of various SMC types is not primarily related to either NCC or SHF but shows a specific patterning at this stage. The pulmonary arteries are separately connected dorsally to the PT and in continuation with a ring-like part of HNK1 positive SMC between the DA and the PT (**Fig. 6.5F-I**). This area



might be indicative of the incorporated ventral segment of the 6th arch (**Fig. 6.5F, H**). The dorsal sprout of the left 6th PAA (referred to as DA), hardly stained for HNK1 (**Fig. 6.5I**), is more anteriorly in smooth continuity with the, also non-stained main part of the PT (**Fig. 6.5H**). The right 6th PAA has already disappeared thus not encumbering the connection of the right pulmonary artery to the PT (**Fig. 6.5F-G**).

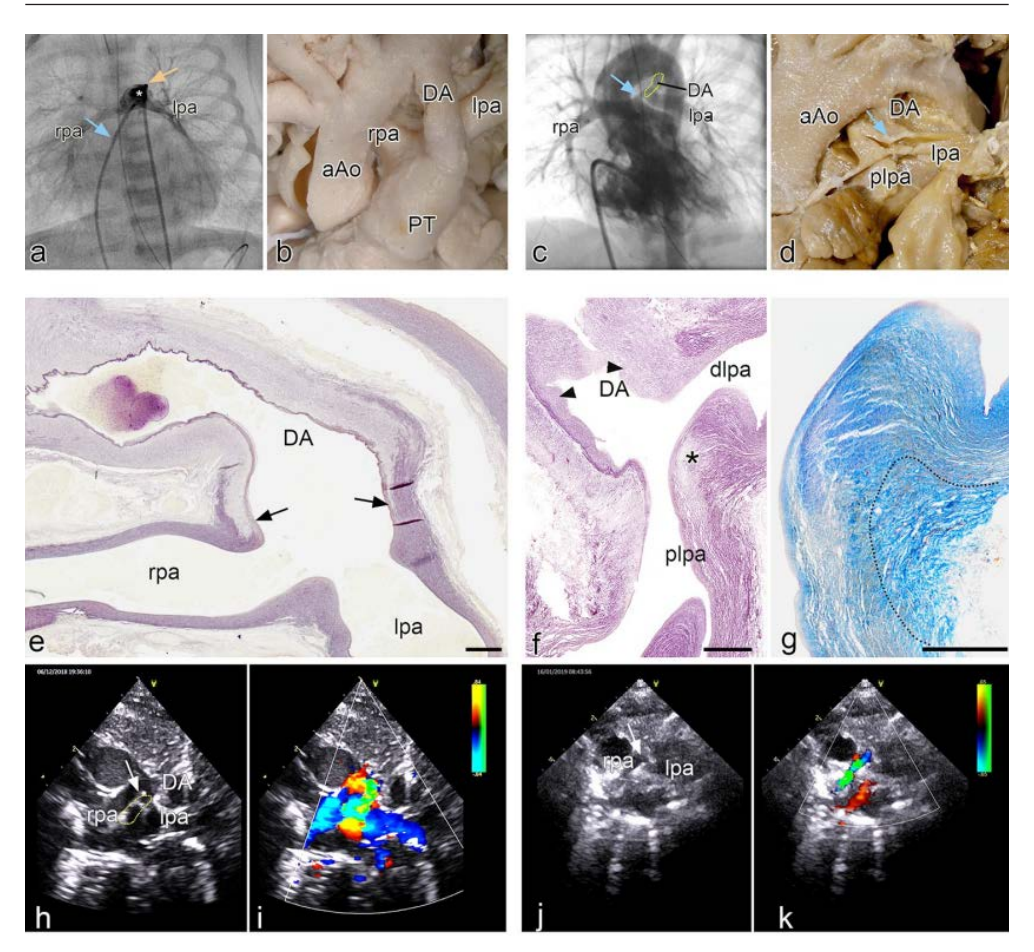
# **6.3.5** Pulmonary ductal coarctation (PDC) and interruption of the proximal left pulmonary artery

In a case of pulmonary stenosis without VSD an angiography frame shows the normal connection of the leftsided DA above and anterior of the left pulmonary artery. The bifurcation of the left and right pulmonary arteries, presenting no indications of narrowing at their origin, (**Fig. 6.6A**) is more posterior. In two clinical cases with PDC there is an abnormal lateral DA to left pulmonary artery (**Fig. 6.6C**). In the first case, a neonate with tetralogy of Fallot with pulmonary atresia and confirmed 22q11 deletion, PDC is demonstrated by angiography (**Fig.** 

Figure 6.5 Human embryos in incremental developmental series. Reconstructions of embryos depicted in A-C have been stained with hematoxylin eosin. A: Reconstruction of a very early human embryo (4 mm, CS 12) with a complete 3rd PAA. The combined ventral sprouts of the 4th and 6th PAA are in contact with the mid-pharynaeal endothelial plexus (mpes) all depicted in arey and surroundina the developing gut (light green, G). **B-C**: Left lateral and dorsal view of a lumen reconstruction of a human embryo (6.5 mm, CS14) with complete 3rd and 4th arches (3,4). The dorsal 6th artery (d6) is indicated in green, the myocardium of the outflow tract in grey and the distal pulmonary arteries in red. The dorsal view the short ventral segments of the 6th PAAs (v6) form a short proximal pulmonary artery. The distal part of the pulmonary arteries (dlpa,drpa:red) are thus in contact with the AoS. **D-E**: Sections of a human embryo (CS16) which is stained for neural crest for TFAP2a (green) which clearly surrounds the Id6/ DA (**D**). In **E** there is a marked extension of NKX2.5 positive SHF (yellow) along the outer side of the PT (pulmonary push population: PP). It cannot be discerned whether the lpa and rpa (white dotted rings) are of proximal or distal order. **F-G**: Reconstruction of an older human embryo (17mm, CS19) stained for HNK1. The ascending aorta (aAo) and the PT have been separated. The right 6th PAA has disappeared. The Ipa and rpa (pink) are connected separately to the dorsal side of the PT, sharing the HNK1 antibody staining (purple) that allows for distinguishing boundaries between the left sided dorsal 6th PAA (ductus arteriosus: DA, green) and the PT (light blue). The DA continues smoothly into the PT with a more anterior position as compared to the lpa and rpa. H-I: Transverse sections (see section levels as black lines in f and q) of the HNK1 stained pulmonary arteries (Ipa and rpa) and the connection of the rpa to the PT, while the main part of the PT and the DA are negative for this staining. Abbreviations: n.X vagal nerve, T trachea. Maanification: bars 100 um.

**6.6C**). The second case with no detected genetic abnormality, shown by echo Doppler (**Fig. 6.6H-K**), concerns a DORV (tetralogy of Fallot type) with pulmonary atresia in whom the development of the severe obstruction of the proximal left pulmonary artery can be observed during the clinical course. The child was born at 31 weeks gestation with a weight of 1075 grams. With a widely patent DA on prostaglandin the left pulmonary artery origin is slightly smaller than the remainder of the branch (**Fig. 6.6H-I**). At term (weight 2100g) a 3,5 mm modified Blalock-Taussig-shunt was connected to the right pulmonary artery and prostaglandin was discontinued. After DA closure the origin of the left pulmonary artery was nearly obliterated (**Fig. 6.6J-K**) and the child needed a second shunt to supply the left pulmonary artery. After uneventful recovery the child is now awaiting corrective surgery.

The macroscopy and histopathology were investigated in 7 selected cases (Leiden congenital heart specimen collection) with a PDC (**Fig. 6.6D, F, G**) and compared with specimen with a normal morphology (**Fig. 6.6B, E**). The pathology specimen have been previously described (*Elzenga and Gittenberger-de Groot, 1986*) and were restudied for details of DA, PT and left pulmonary artery connection. All specimens had a pulmonary atresia (**Fig. 6.6D**) and in 6/7 also a VSD. In all cases the DA inserted sideways into the left pulmonary artery, creating a



proximal (continuous with the PT) and a distal (running towards the lungs) part (**Fig. 6.6D**). The left pulmonary artery was often smaller than the right pulmonary artery (**Fig. 6.6D**). In all seven specimens the ductal tissue formed the major part of the obstructed proximal left pulmonary artery with a variable extension into this arterial segment. It was observed that the elastic lamellae of the media of the proximal and distal pulmonary artery were not continuous at the site of the PDC (**Fig. 6.6F-G**). In 2/7 there was a total occlusion of the left pulmonary artery by this ductal tissue. The lumen of the DA was in open continuity with the distal part of the left pulmonary artery, allowing for filling of the lungs. These histological findings were in marked contrast to the normal neonatal specimen where the elastin-poor DA connected, with a fish tail like construction to the elastic PT and the adjoining left and right pulmonary arteries (**Fig. 6.6E**).

Figure 6.6 A: Angio of a patient with pulmonary atresia without VSD in which the leftsided DA (asterisk) is positioned above and anterior of the left pulmonary artery. The left (lpa) and right (rpa) pulmonary arteries (venous line: blue arrow; arterial line yellow arrow) are not compromised at their origin. **B**: Morphology of the arterial pole of a heart specimen in which the ductus arteriosus (DA) connects anteriorly to the pulmonary trunk (PT), while the rpa and lpa are more dorsally connected. C: Angio of a patient with tetralogy of Fallot with a marked narrowing (blue arrow) of the proximal (origin) left pulmonary artery (DA dotted area). D: Postmortem specimen with atresia of the PT and a confluence of the rpa and lpa, with a smaller diameter of the latter. The DA enters sideways into the lpa which shows a PDC at the site of connection (blue arrow). **E**: Sagittal section of a human fetal (resorcine fuchsine stained for elastin). The elastin poor muscular DA only lined on the lumen side by an internal elastic lamina, connects with a fishtail like construction (arrows) to the elastin rich rpa and lpa. No DA tissue is encountered in the wall of the Ipa and rpa. F: Sagittal section (resorcine fuchsin stained for elastin) of a specimen with severe pulmonary ductal coarctation. The tissue of the elastin poor DA, presenting with intimal cushions (arrowheads), is inserted sideways in the wall of the plpa (asterisk), while the dlpa is still elastic in nature. **G**: Detailed view of the region asterixed in F using a subsequent section stained with Azan. Here it can be seen that the elastic lamellar structure (yellowish) of the dlpa and plpa is interrupted by the adventitia (dotted area) of the DA. H: 2D echocardiographic image of the patient with DORV on prostaglandin. In this high parasternal short axis view the rpa, lpa and DA (dotted area) are indicated. The arrow points to the Ipa origin. I: Same image with Doppler color showing the flow to the rpa and Ipa in blue and the DA flow in orange and green. J: 2D echo of the same patient 10 days later after placement of the right mBT shunt and discontinuation of prostaglandin. Same view as H. The DA has closed. The origin of the lpa is severely stenosed marked by the arrow. **K**: Same image as I with showing the flow to the rpa. Because of the mBTS the rpa the flow is turbulent coded in green. The lpa does not receive flow because of the severe stenosis at its origin. The DA has closed. Magnification: E-G bars: 100 µm.

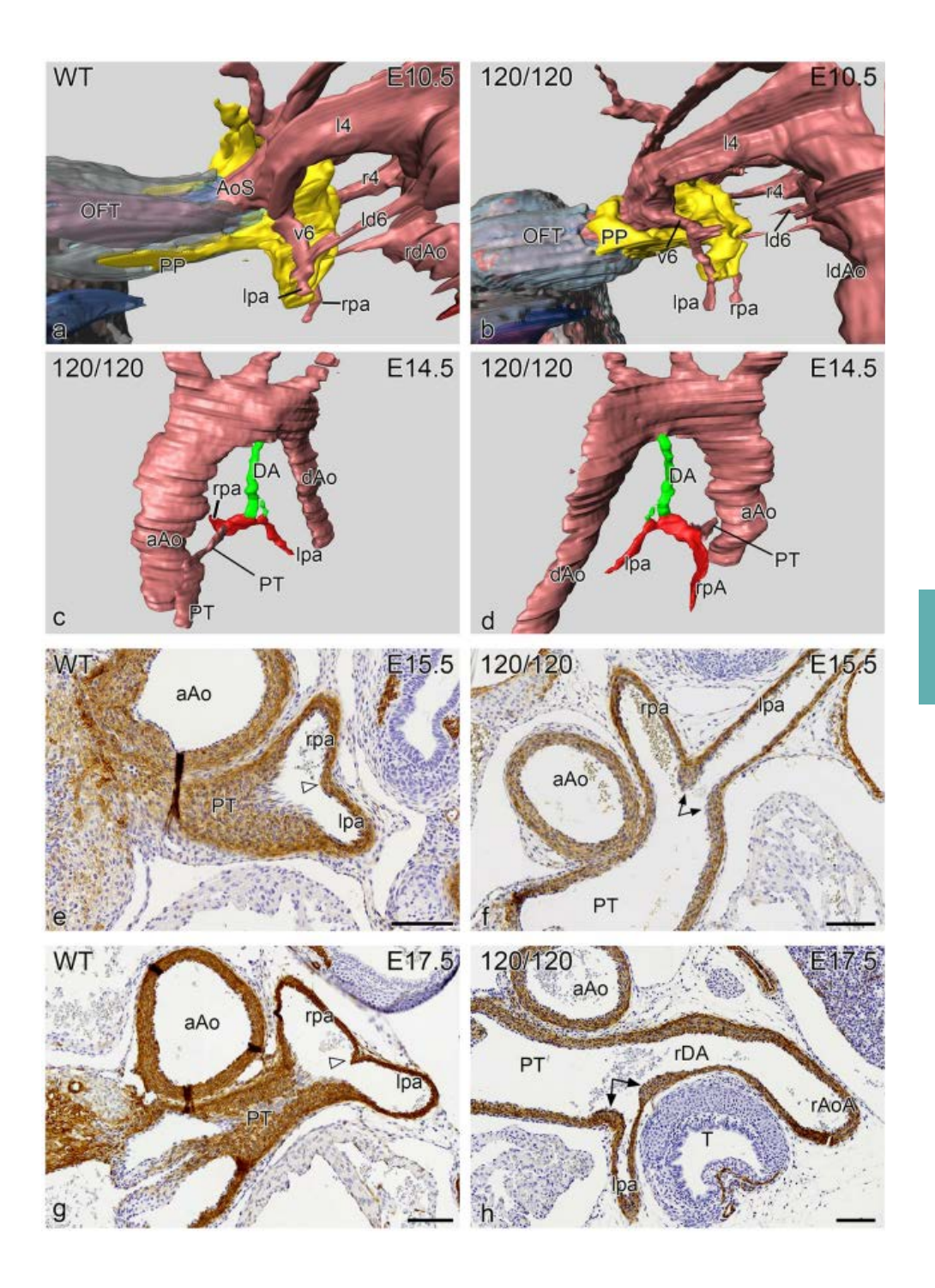
# 6.3.6 Abnormal development of the pulmonary artery, DA and PT connection in the VEGF 120/120 mutant mouse

To obtain more insight in mechanisms underlying aberrant DA to pulmonary artery connections we studied a series of VEGF 120/120 mutant mouse embryos and their development matched wild type embryos. New in this paper compared to the hitherto described VEGF series (*Van Den Akker et al., 2007; Rammeloo et al., 2015*) was the addition of mouse embryos in which we could discern the SHF population by staining for NKX2.5 and thus the possibility to investigate in more detail the connection site of the PT, pulmonary arteries and 6th PAA. The NKX2.5 staining proved to be reliable at E10.5 and E11.5. Older stages from E12.5 onwards the staining was not conclusive anymore because of loss of staining intensity. So, we have focused on these earlier stages to understand more about the possible underlying mechanisms leading to the associated heart malformations. Wild type mouse embryos at E10.5 (N=5, all stained for NKX2.5) showed a marked presence of the dorsal mid-sagittal SHF population with a pulmonary push extension

at the dorsal site of the aortic sac (the future PT side). Both 4th PAAs were complete. The developing pulmonary arteries were connected to the ventral sprouts of the 6th PAA which were not yet connected to the dorsal sprouts to form a complete 6th PAA (**Fig. 6.7A**) and are embedded in this area in the NKX2.5 positive SHF population.

At E11.5 the VEGF wild-type embryos were comparable to older E12.5 WntCre reporter embryos (Fig. 6.4F-J), with a completion of the 6th PAA and separation of the PT and the ascending aorta. The left 6th PAA (now referred to as DA) was complete while the right 6th had already regressed. In the VEGF120/120 E10.5 series (N=5; 3 stained for NKX2.5) the major difference compared to the wild type, was found in the stunted appearance of the SHF population lacking a pulmonary push extension (Fig. 6.7B). The connection of the pulmonary arteries was embedded in the SHF population and connected to the ventral sprouts of 6th PAA like in the wild type embryo. The VEGF120/120 mutant embryos at stage E11.5 (N=7; 3 stained for NKX2.5) all showed a complete 4th and 6th PAA as in the wild type. While at E10.5 the main differences were observed solely in the PP population, this situation had changed at E11.5 showing a variety of abnormalities. The SHF population was stunted and did not show a proper pulmonary push extension. The anlage of the left and right pulmonary arteries bordered the SHF population as in wild types. Both the right ventricular OFT and the PT were stenotic. With regard to the development of the 6th PAA we observed a lack of proper left /right dominance. In 2/7 cases the right pulmonary artery merged sideways with the right 6th PAA, which thus still showed a ventral and a dorsal part. In one case the right dorsal 6th PAA formed a rightsided DA continuing in a right aortic arch. In all cases the left pulmonary artery connected

**Figure 6.7** Reconstruction (left lateral views) of a E10.5 VEGF WT (**A**) and a VEGF 120/120 (**B**) mouse embryo in which the SHF has been stained for NKX2.5 (yellow). There is a marked difference in the pulmonary push (PP) which extends along the future pulmonary side of the aortic sac (AoS) for quite some distance in the WT embryo (**A**), while in the mutant embryo (**B**) the PP is stunted. In both embryos the lpa and rpa connect to the AoS by way of ventral sprout of the 6th PAA (v6) and are embedded in the SHF tissue. **C-D**: Reconstructions of an E14.5 mutant embryo in which the hypoplastic DA (green), arising vertically from the aortic arch, is connected side-ways to the lpa (red). There is atresia of the pulmonary orifice and the pulmonary trunk (PT) is hypoplastic. **E-H**: Sections stained for a smooth muscle actin (1A4) of the site of connection of the lpa and rpa into the PT. **E-F**: E15.5 embryos in which (**E**) the WT shows equal sizes of the lpa and rpa with a small posterior separating ridge (open arrowhead), while in the mutant embryo (**F**) the origin of the lpa, which is relative smaller in diameter as compared to the rpa, is flanked by thickened DA tissue (arrows). In a WT (**G**) and mutant embryo (**H**) of E17.5 we observe a similar phenomenon although in the mutant embryo (h) the small lpa, encircled by thick ductal tissue (arrows) is connected to a right-sided DA (rDA) continuing into a right aortic arch (rAoA). Magnification bars in E-H 100 μm.



already separately to the PT while the left dorsal 6th PAA (the regular left DA) was hypoplastic in 3/7 of these cases although, as yet, still in open connection with the hypoplastic PT. VEGF120 the wild-type embrvos (N=8)showed comparable morphology to F11.5. The VFGF 120/120 embrvos (N=5)showed abnormalities as described for E11.5, complemented by a case with a retroesophageal left subclavian artery and a case with a sling configuration of the arch. In the VEGF embryos of E14.5 –E18.5 (N=15) we specifically looked for cases with an incomplete incorporation of the ventral sprout of the 6th PAA which leads to an abnormal left pulmonary artery-oriented insertion of the DA seen in human patients with PDC (Fig. 6.6E). In one case this was very markedly combined with an hypoplastic left DA (Fig. 6.7C-D). In four other cases we found thickened DA tissue encircling the entrance of the left pulmonary artery into the PT (Fig. 6.7E-H).

### 6.4 Discussion

PDC is relatively common in cases with right ventricular outflow tract stenosis and cyanosis including tetralogy of Fallot with a severe stenosis to a completely atretic pulmonary orifice and trunk (Santos et al., 1980; Presbitero et al., 1984; Elzenga and Gittenberger-de Groot, 1986; Luhmer and Ziemer, 1993; Brink et al., 2015). These anomalies are often seen in combination with the 22q11 deletion syndrome (Momma et al., 1986; Marino et al., 1996; Momma, Kondo and Matsuoka, 1996). PDC has been postulated to be the counterpart of the aortic coarctation (Presbitero et al., 1984) in which DA tissue encircles the inner part of the aortic arch for more than 50%. However, the elastic structure of the aortic wall is always continuous as an outer layer from the aortic arch to the descending aorta (Elzenga and Gittenberger De Groot, 1983). The exact background of the development of a preductal aortic coarctation is still lacking. However a hemodynamic component has regularly been postulated (Presbitero et al., 1984; Elzenga, Gittenberger-de Groot and Oppenheimer-Dekker, 1986; Yokoyama et al., 2017) related to an augmented flow through the DA during development of the stenosis to atresia of the left ventricular outflow tract or aorta (Santos et al., 1980; Presbitero et al., 1984; Elzenga, Gittenberger-de Groot and Oppenheimer-Dekker, 1986). Waldman et al. (1996) studied patients with developing proximal left pulmonary artery interruption including the histopathology of the stenotic/interrupted area. They showed that in PDC the DA tissue could form the complete wall between the proximal and distal part of the left pulmonary artery. Reassessment of the histopathology in our initially described material (Elzenga and Gittenberger-de Groot, 1986) showed this to be correct. At the time we mistook the adventitia of the DA for a continuous outer media and had erroneously postulated a hemodynamic cause, comparable to aortic coarctation. We now realize that the connection of the DA to the proximal part of the left pulmonary artery is a developmental anomaly, as a in general the DA never encroaches on a pulmonary artery but connects separately to the PT forming a continuous arch towards the aorta as we showed in this study for the later stages in both normal human and mouse development.

The above background and findings shed a new light on the development and morphology of the interrelationship of the (left) pulmonary artery, the PT and the DA. First, the investigations in subsequent series of early human embryos and comparable rat and chicken stages refined earlier interpretations. The 6th PAA indeed develops from a ventral sprout from the aortic sac, connecting to the pulmonary artery vasculature, not by sprouting towards the lung parenchyme (Congdon, 1922) but by recruiting endothelial cells from the MPES (DeRuiter et al., 1993). We demonstrated that mouse and human embryos were comparable and that both showed a short period in which there was a ventral and dorsal segment of the 6th PAA. Only in older stages the pulmonary arteries connected directly to pulmonary trunk. The option that the pulmonary arteries directly connect to the aortic sac, as postulated (Rana et al., 2014) are a matter of semantics as in their definition the ventral segments appear to belong to the aortic sac. Second, currently available (transgenic) reporter mouse data, as used in this study, allowed us to investigate in detail the contribution of NCCs and SHF cells (NKX2.5 positive) at the hub of the various involved vessels. The ventral segments of the 6th PAA, which have a dual lining of NCC and SHF, become incorporated in the posterior wall of the pulmonary trunk, after which the definitive pulmonary arteries, embedded in Mef2c positive mesoderm, have an independent connection to the posterior wall of the pulmonary trunk. The right and left dorsal 6th PAA segments are completely surrounded by NCCs as has been shown before (Berawerff et al., 1998). Normal timing of events allows the right 6th PAA to regress, not narrowing the orifice of the right pulmonary artery to PT connection, while the left 6th PAA becomes the DA with a smooth anterior connection to the PT. These data support the recent observation that the mesoderm surrounding the definitive pulmonary arteries lack Tbx1and thus NKX2.5 SHF expression (Mastromoro et al., 2019), explaining the absence of a direct effect of the 22q11 deletion on the development of the left and right pulmonary artery system. The above findings reflect on the (histo) pathology in the human infant with proximal pulmonary artery stenosis. Defective formation of the pulmonary trunk, with absence of proper incorporation of the ventral 6th PAA segment could lead to a situation in which the DA enters side-ways into a pulmonary artery. Most patients with PDC and pulmonary atresia present with a VSD (Luhmer and Ziemer, 1993)

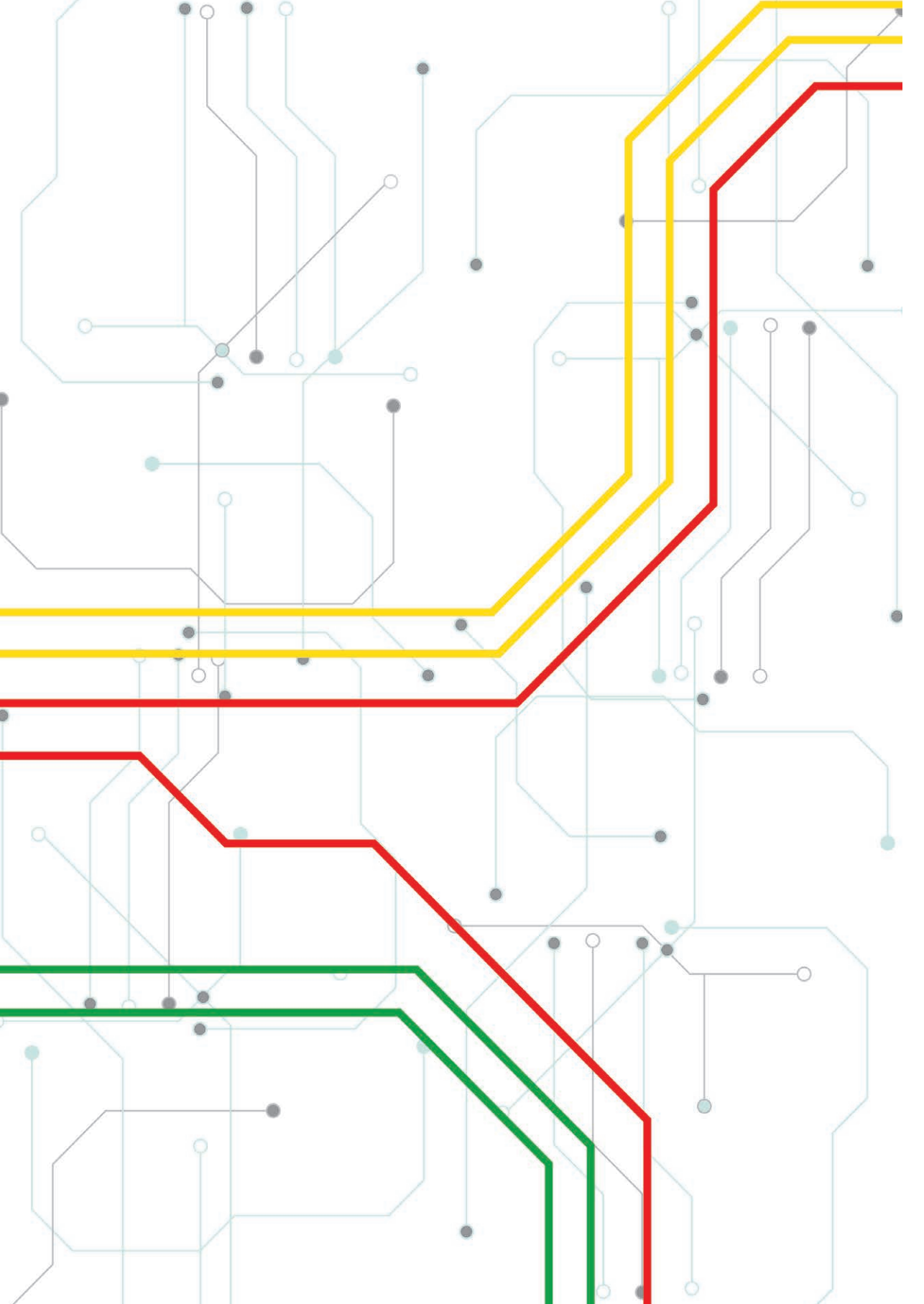
indicating an early embryonic onset of the disease. In case of valvular pulmonary stenosis or atresia without VSD occurrence of PDC is rare (Elzenga and Gittenberger-de Groot, 1986) and the DA is positioned normally between the left and right pulmonary arteries. A number of patients with PDC present with a complete insertion of DA tissue between the proximal and distal part of the pulmonary artery. We considered a possible developmental mechanism, as a simple hemodynamic solution, with preferential retrograde flow from the aorta to the pulmonary trunk during developing stenosis to atresia of pulmonary trunk and orifice, proved not to be adequate. The available VEGF 120/120 mutant mouse model allowed us to study in more detail the DA-PT and pulmonary artery connection. It has already been reported (Rammeloo et al., 2015) that originally both 6th PAA were present and along with the developing PT stenosis to atresia, the left sided DA could also disappear. This was accompanied in some cases with development of additional aorto-pulmonary collateral arteries (MAPCAs). We now added that the most prominent abnormality was a stunted SHF population in early stages of mutant embryos. The PT did not receive the SHF cells as normally contributed by the pulmonary push population (Harmon and Nakano, 2013). Thereafter, we observed lack of proper incorporation of the ventral segments of the 6th PAA together with a loss of normal left-right dominance. This may result in a side-ways connection of a DA to the pulmonary artery. The loss of left-right dominance, with more frequent occurrence of a persisting right DA and a right aortic arch, as encountered in the mutant VEGF embryos, was also described in our human histopathology series (Elzenga and Gittenberger-de Groot, 1986) and also in patients with tetralogy of Fallot, pulmonary artery atresia and the 22q11 deletion syndrome (Momma et al., 1986, 1996; Momma, Kondo and Matsuoka, 1996). However, the anomaly is not exclusive for this syndrome but seems to be linked to development of pulmonary stenosis to atresia in which it is encountered in 40% of the cyanotic infants with right ventricular outflow tract obstruction (Luhmer and Ziemer, 1993; Brink et al., 2015). In case of absent DA no PDC was seen to develop (Luhmer and Ziemer, 1993) as also reported in our (histo)pathology series (Elzenga and Gittenberger-de Groot, 1986) and confirmed in the VEGF model (Stalmans et al., 2003). In both latter studies we observed a diminished diameter of the distal left pulmonary artery. In the VEGF embryos the hypoplasia of the left pulmonary artery occurred relatively late during development when the PT and the DA already showed hypoplastic characteristics. Thus, a secondary hemodynamic influence has been postulated (Van Den Akker et al., 2007). A primary Tbx1 haploinsufficiency (Lindsay et al., 2001) was proposed for the diminished size of the left pulmonary artery in a study of the human 22q11 population, without additional cardiovascular anomalies, supported by data from Tbx1 heterozygous mice (Mastromoro et al., 2019). Relatively recently, a bit of the transcriptional network regarding the formation of the DA seems to be elucidated as TFAP2beta, Endothelin1

and HIF2alpha interact during normal development of the SMC, while disruption of this network results in persistence of the ductus arteriosus (Ivey *et al.*, 2008). Furthermore, TFAP also interacts with Tbx20 resulting in the emergence of ventricular septal defects in patients with tetralogy of Fallot (*Hammer et al.*, 2008). Furthermore, we (*Bökenkamp et al.*, 2014) identified using laser capture microdissection of endothelial and smooth muscle cells of the DA and aorta of fetal rats, vessel-specific transcriptional profiles among which Dlx1, Pcp4 and Tfap2B. As, however, the definitive pulmonary artery (distal anlage) is not surrounded by NKX2.5 positive cells (this study) nor by cells expressing Tbx1 (*Mastromoro et al.*, 2019), or Tbx1–dependent Hox genes (*Rana et al.*, 2014) a secondary hemodynamic cause for this hypoplasia seems more obvious. After removing the obstruction in the proximal pulmonary artery there can be a catch up growth of the left pulmonary artery system (*Brink et al.*, 2015).

## 6.5 Clinical justification

For understanding the clinical presentation of PDC it is very relevant to know that neural crest-derived muscular DA tissue may continue contraction and stenosis formation even after birth. This process can be held responsible for postnatal development of proximal left pulmonary artery interruption. Surgical or (stent) interventions of PDC should ensure that DA tissue is not present anymore or can do no harm (*Elzenga et al., 1990; Waldman et al., 1996; Brink et al., 2015*). Since the majority of patients with PDC will be treated with prostaglandins (PGE1) to maintain DA patency before surgery the development of an interruption will be postponed till PGE1 is withdrawn after surgery. Although stenting of this segment may solve the problem initially it may in the long run be inferior to primary resection of all DA tissue.

**Acknowledgements**: Dr. Aleksander Sizarov (Department of Pediatrics, Maastricht UMC, the Netherlands) and prof. Antoon Moorman (Department of Anatomy, Amsterdam UMC, The Netherlands) provided the human CS16 embryo. The medical illustrator Ron Slagter is acknowledged for his excellent art-work.



# **Chapter 7**

Discussion and Future perspectives

### 7.1 Discussion

The studies presented in this thesis aimed to explain the increased susceptibility of BAV related aneurysms. Our results demonstrate that the developmental processes that give rise to BAV and BAV-related aortopathy can indeed develop from a common cell lineage anomaly that influences cell lineage contribution to the developing valve. Our studies can explain the clinical observations of increased susceptibility among patients of BAV and related aortopathy as our model shows that deviations in cellular contribution of the neural crest to the aortic valves and base of the aorta results in phenotypes that seem to support the observations in clinical patients. The value of these discoveries lies in the explanation of an deterministic model of disease progression. Knowledge of the fact that neural crest cells can affect both the aortic valves as the aortic vessel walls may influence the scope of clinical intervention strategies and support decision making with logical reasoning and increased certainty.

The chapters presented within this thesis address BAV and BAV-related aortopathy as a consequence of cell lineage anomalies occurring during early cardiac development. To examine these developmental aberrations our laboratory primarily studied the *Nos3*<sup>-/-</sup> BAV mouse model. These mice develop BAV as a result of a genetic mutation resulting in defective NO signalling (*Lee et al., 2000*).

Whilst it is very common for researchers to study BAV using well described mutant mouse models of BAV, these models usually represent medical cases of familial BAV. Whether a BAV is familial can be determined by genetic linkage analysis of close relatives (*Cripe et al., 2004*). Familial BAV is often the result of a genetic mutation which propagate through families, such as BAV patients with the NOTCH1 mutation (*Garg et al., 2005*). Such genetic mutations result in a relative high abundance of BAV within a single family. Curiously, familial BAV only represents <10% of clinical BAV cases whilst in >80% of BAV patients there is no prior familial history of BAV (*Prakash et al., 2014*). These later group of patients can be classified as having a sporadic BAV. Performing linkage analysis on sporadic BAV cases is unfeasible given that there are no prior familial observations of BAV. To find a causal explanation for sporadic BAV patients, researchers have instead performed numerous genome wide association studies (GWAS). GWAS studies typically require large populations of patients and controls to attain meaningful results. This is because GWAS identifies indirect associations between the genuine risk variants and genotyped single nucleotide polymorphisms, rather than by direct identification of the causal variants (*Visscher et al., 2012*). Genetic association studies have been able to determine

novel polymorphisms in sporadic BAV patients such as variations in AXIN1/PDIA2 (*Wooten et al., 2010*), Endoglin (*Wooten et al., 2010*), EFGR (*Dargis et al., 2016*), GATA4 (*Yang et al., 2017*), PALMD (*Helgadottir et al., 2018*) and SMAD6 (*Gillis et al., 2017*). Yet, despite the detection of novel variants a common genetic pathway specific to BAV has not been found. Moreover, there often remain many BAV patients within such studies for which a causal genetic explanation remains elusive.

The observation that many sporadic BAV patients do not contain any known mutations for BAV, led to the theory of a non-congenital adaptive/acquired BAV phenotype. Adaptive BAVs are generally considered to result from a valvular adaptation to environmental stress. Evidence for adaptive BAVs can be found in patients with rheumatic heart disease (*Veinot*, 2006). Patients with rheumatic heart disease are generally born with tricuspid aortic valves but can develop fusion of the aortic leaflets in response to inflammation related to rheumatic fever (*Veinot*, 2006). These patients can therefore acquire a BAV phenotype without a genetic component. Nevertheless sporadic BAV patients usually do not suffer from rheumatic heart disease or any other prevalent diseases other than BAV when participating in research studies.

I however, regard that the inability to detect a genetic component in certain sporadic BAV cases is primarily a limitation of genetic association studies. To briefly explain, genetic association studies primarily rely on the premise that an equal phenotype would suggest an equal underlying genotype. That is, when comparing genetic variation within a given population of patients with a certain disease-trait to the genetic variation of the general "healthy" population without said disease-trait. Then that variation that is specific to the disease-trait must be significantly overrepresented within the "diseased" patient population and thus distinct from the genetic variation of the general "healthy" population. This study design will however fail to find meaningful genetic associations when: 1) The disease-trait may originate from a large combination of multiple genetic anomalies, as this could require an impossible number patients to test. 2) The disease-trait has a partial penetrance of less than 50%, which results in a situation where the healthy population could potentially also carry the genetic variation causal to the disease-trait. 3) The disease-trait is not genetic in origin but acquired through environmental stimuli. In the case of BAV there can be raised arguments for all three criteria. One generally recognized challenge with BAV are the large variation of genes which have been linked to BAV. Genetic variations in TGFBR2 (Girdauskas, Schulz, et al., 2011), NOTCH1 (Garg et al., 2005), ACTA2 (Guo et al., 2007), KCNJ2 (Andelfinger et al., 2002), MAT2A (Guo et al., 2015) SMAD6 (Tan et al., 2012; Gillis et al., 2017) FBN1 (Pepe et al., 2014), GATA4/5/6 (Shi et al., 2014; Li et al.,

2018; Xu et al., 2018) and NKX2.5 (Qu et al., 2014) have all been found to result in BAV in human patients. Furthermore gene defects such as, NOS3 (Lee et al., 2000), ROBO1/2 (Mommersteeg et al., 2015), ROBO4 (Gould et al., 2018), ALK2 (Thomas et al., 2012), MATR3 (Quintero-Rivera et al., 2015), HOXA1 (Makki and Capecchi, 2012), KROX20 (Theron et al., 2015) and TBX20 (Cai et al., 2013) are known to give rise to BAV in mice but thus far have not been linked to human patients. However, BAV models such as GATA5/5/6 (Laforest, Andelfinger and Nemer, 2011; Laforest and Nemer, 2011) and NKX2.5 (Biben et al., 2000) knockouts were also identified in mouse prior to discovery of their role in human BAV patients. These observations suggest an even richer palette of possible gene defects to result in BAV for humans than that which is currently described. More interesting is the general acceptance of the limited penetrance of BAV despite our poor understanding regarding these observations. It is well recognized that BAV is a heritable autosomal disease with an incomplete penetrance (Huntington, Hunter and Chan, 1997; Braverman et al., 2005; Loscalzo et al., 2007). This reduced penetrance is also observed within many BAV models of mice (Fernandez et al., 2009; Laforest, Andelfinger and Nemer, 2011; Thomas et al., 2012). As such is the case with the Nos3-/- mouse model in which only ~25% develop BAV whilst 75% of Nos3<sup>-/-</sup>, which are genetically identical, develop TAV (Peterson et al., 2018). Interestingly, a study by Bosse et al shows that introduction of Notch1+/haplodeficiency in the Nos3-/- background increases the penetrance of BAV to ~60% (7 out of 11) and ~30% developed severe dysplastic valves (3 out of 11) (Bosse et al., 2013). Moreover later studies using the Notch1+/-;Nos3-/- model also showed that combinatorial gene variations could exacerbate BAV related aortopathy (Koenig et al., 2015). Our studies show that correct valvular formation requires the careful orchestration of multiple cell lineages and that both BAV and TAV Nos3<sup>-/-</sup> show distinct morphological deviations within the cardiac outflow tract (Peterson et al., 2018). Such observations elucidate the complexity of valve formation and suggest that there are likely subtle cell lineage interactions underlying the severity of morphological anomalies within the OFT. As such, the aortic and valvular complications observed at the outflow tract of BAV patients could derive from a spectrum of cell lineage aberrations.

Whilst there is still little understanding regarding any interactions among these early cell lineages, the outcome of morphological effects could substantiate clinical observations from physicians and thoracic surgeons which first attempted to classify the different etymology's of BAV using phenotypes. There are numerous studies using these classification schemes to identify possible differences among patients (*Koenraadt et al., 2016; Liet al., 2019; Lim, Celermajer and Bannon, 2021; Sillesen et al., 2021*). Yet any formal theory explaining how subtypes of BAV could affect disease progression remains ambiguous. There is currently still little agreement

regarding the practicality of using BAV subtypes for patient risk stratification.

Although there are still many questions regarding the origin of BAV, one common goal of many researchers was to understand BAV-related disease progression. From the study of etymologies of BAV came forth the idea that aortic diseases secondary to BAV might result from accumulated hemodynamic stresses due to altered fluid flow of the bicuspid valve. Studies examining the orifice of the BAV recognized that the asymmetric opening created a nonaxial, turbulent transvalvular flow jet (Robicsek et al., 2004; Girdauskas et al., 2012). As a consequence of the flow jet it was shown that BAV can introduce local regions of high and low shear stress at the aortic wall (Robicsek et al., 2004; Girdauskas et al., 2012). Metrics regarding "cusp opening angle" were introduced by Della Corte and demonstrated prognostic correlations related to aortic growth in BAV patients (Della Corte et al., 2012). Moreover BAV was shown to be associated with altered wall shear stress in the ascending aorta substantiating the difference in hemodynamics among TAV and BAV patients (Barker et al., 2012). The adoption of 4D flow analysis allowed for accurate evaluation of in vivo fluid dynamics (Hope et al., 2010).

Increased hemodynamic mechanical stresses can alter normal VSMCs gene expression patterns and contribute to aortic dilation and dissection in the aortic vessel wall (Isnard et al., 1989; Robicsek and Thubrikar, 1994; Jensen, Bentzon and Albarrán-juárez, 2021). A strong argument for the hemodynamic theory of BAV-associated aortopathy is that many BAV patients tent to develop aortic complications during adolescence (Girdauskas, Borger, et al., 2011). Which suggests that BAV-related aortopathy is independent from the genetic developmental origin of BAV. Congenital defects are generally thought to give rise to complications during childhood development. Nevertheless, there is agreement among researchers that genetic predisposition can influence susceptibility to disease. Studies examining Loeys-Dietz syndrome or Marfan have shown that patient offspring carry increased risk to develop complications at later stages in life (Mariko et al., 2011; MacCarrick et al., 2014). However much is still unclear regarding BAV associated aortopathy, although there is plenty of evidence to suggest that anomalous aortic valve development is intrinsically linked to development of multiple cardiac structures such as the aorta, coronary arteries and aortopulmonary complex (Henderson, Eley and Chaudhry, 2020). Moreover, patients of first degree relatives of BAV often show increased susceptibility for aortic complications independent of having BAV (Biner et al., 2009). Cases of "young adults" developing aneurysms secondary to BAV do suggest that hemodynamics is not the only factor influencing disease progression (Burks et al., 1998; Tzemos et al., 2008; Michelena et al., 2011). Our studies (chapter 5) show cases of Nos3-/- mice developing aneurysms and a case of dissection after 4 months which is similar to *Robo4* deficient BAV mice that develop aneurysms at 20 weeks (*Gould et al., 2018; Peterson et al., 2020*). These observations elucidate that there is currently still a gap in understanding regarding temporal related factors that change during aging but have an implicit role for to the formation of aortic aneurysms.

### **7.2 Future Perspectives**

The current general consensus among cardiovascular researchers is that BAV related aortopathy is a result caused by a combination of both genetic predisposition and hemodynamic adaptation. This explanation, whilst arguably true, holds little value if the impact of genetic predisposition and the magnitude of hemodynamic adaptation cannot be accurately quantified within the same system. Knowing that BAV related aortopathy develops considerably later in life than BAV itself means that secondary effects should take hold before disease onset. A possible approach would be study cellular markers of vascular adaptation to complement current genetic investigations. This could lead to new insight into the temporal relation between early genetic predisposition and later hemodynamic adaptation. Ideally these studies would address the challenge of which mechanisms genetic predisposition affects to increase disease susceptibility and how such effects transition into phenotypical hemodynamic adaptation. One option could be to investigate epigenetic signatures related to vascular aging within the context of BAV related aortopathy. Numerous studies have already been using methylation status of genes such as PTEN (Ma et al., 2018), PDGF (Zhang et al., 2012), MYH11 (R. Liu et al., 2013) as indicators of vascular aging in vascular smooth muscle cells (Xu, Li and Liu, 2021). Given that our Nos3<sup>-/-</sup> mouse model develops both BAV and BAV-related aortopathy as a result of anomalous neural crest contributions, a future direction could investigate both the genetic and epigenetic components of derivative cells during disease progression within the same system. The combination of a cellular methylation mark and a RNA expression profile could reveal insight into the molecular intricacies underlying the phenotypical alterations in BAV disease because age related changes in DNA methylation are known to affect gene expression (Razin and Cedar, 1991; Salameh, Bejaoui and El Hajj, 2020).

Combinatorial genetic and epigenetic profiling would allow for more detailed characterization of the neural crest derived populations than gene expression levels alone. Moreover, this approach could possibly identify cellular signatures characteristic of vascular integrity and disease progression within these cell populations because the combination of an methylation mark and a RNA expression profile could reveal insight into the molecular intricacies underlying the phenotypical alterations in BAV disease. DNA methylation profiling has also been shown

to be successfully applied as biomarker in distinguishing cancer types, such as breast, lung, prostate, and colorectal cancers using blood based cell free liquid biopsies (*Constâncio et al., 2020*). The discovery of novel markers and proxies can facilitate the translation of disease status in BAV patients. Such markers would allow for quantitative measurements to more accurately evaluate the patient risk status, and thus improve clinical decision-making regarding adequate intervention strategies. Future research should therefore focus to resolve the implications and contributions of both genetic and epigenetic influences on the development of BAV and BAV-related aortopathy.

# **Abbreviations**

**AMC**: Arterial mesothelial cells

**AoDd**: Aortic diameter during diastole **AoDs**: Aortic diameter during systole

Ao: Aorta

**AoV**: Aortic Valve **AP**: Aortopulmonary

**AV**: Atrioventricular valve **AVC**: Atrioventricular canal **BAV**: Bicuspid aortic valve

**Cm**: Condensed mesenchyme **CHD**: Congenital heart disease **CNV**: Copy number variations

**CS**: Carnegie stage **DA**: Ductus arteriosus

**DAPI**: 4',6-diamidino-2-phenylindole

E: Embryonic day

**ECM**: Extracellular matrix

**EndMT**: Endothelial to mesenchymal transition

**ER**: Estrogen receptor **FHF**: First heart field

FNMM: Fluorescent nuclei measurements macro

**GFP**: Green fluorescent protein

**GWAS**: Genome wide association study

**HCA**: Human cell atlas

**HE**: Mayer's hematoxylin-eosin **HH**: Hamburger and Hamilton



**IVC:** Inferior vena cava

LA: Left atrium

LBD: Ligand-binding domain

**LC**: Left coronary cusp **LCA**: Left coronary artery

LV: Left ventricle

mT/mG: Membrane-bound Tomato/membrane-bound GFP

**MMP**: Metalloprotease

MPES: Mid-pharyngeal endothelial strand

MV: Mitral balve

NC: Non coronary cusp
NCC: Neural crest cell
NO: Nitric oxide

**OFT**: Outflow tract **Pc**: Parietal cushion

**PAA**: Pharyngeal arch artery **PBS**: Phosphate buffer solution **PCR**: Polymerase chain reaction

**PDC**: Pulmonary ductal coarctation

PHT: Primary heart tube PT: Pulmonary trunk PV: Pulmonary valve R26R: Rosa26 reporter

**RA**: Right atrium

**RC**: Right coronary cusp **RCA**: Right coronary artery

RF: Weigert's resorcin-fuchsin

**ROI**: Region of interest

**RV**: Right ventricle

scRNA-seq: Single cell RNA sequencing

Sc: Septal cushion

SHF: Second heart field

**SNV**: Single nucleotide variation

**SVC**: Superior vena cava

Tz: Transitional zone

A

**TAV**: Tricuspid aortic valve

**TIVA**: Transcriptome in vivo analysis

**TV**: Tricuspid valve

**VIC**: Valvular interstitial cell **VSD**: Ventricular septal defect

**VSMC**: Vascular smooth muscle cell





### References

- Aanhaanen, W. T. J. et al. (2009) 'The Tbx2+ primary myocardium of the atrioventricular canal forms the atrioventricular node and the base of the left ventricle', Circulation Research, 104(11), pp. 1267-1274. doi: 10.1161/CIRCRESAHA.108.192450.
- Abbosh, C. et al. (2017) 'Phylogenetic ctDNA analysis depicts early-stage lung cancer evolution, Nature. doi: 10.1038/nature22364.
- Abu-Issa, R. and Kirby, M. L. (2007) 'Heart field: from mesoderm to heart tube', Annual Review of Cell and Developmental Biology, 23, pp. 45-68. doi: 10.1146/annurev. cellbio.23.090506.123331.
- Aghajanian, H. et al. (2017) 'Pdgfra functions in endothelial-derived cells to regulate neural crest cells and development of the great arteries', Disease Models & Mechanisms, p. dmm.029710. doi: 10.1242/dmm.029710.
- Akaike, T. et al. (2019) 'Transcriptional profiles in the chicken ductus arteriosus during hatching, PLOS ONE, 14(3), p. e0214139. doi: 10.1371/ JOURNAL.PONE.0214139.
- Van Den Akker, N. M. S. et al. (2007) 'Tetralogy of fallot and alterations in vascular endothelial growth factor-A signaling Argues, C. G. et al. (2007) 'Cell tracing reveals a and notch signaling in mouse embryos solely expressing the VEGF120 isoform', Circulation Research, 100(6), pp. 842-849. doi: 10.1161/01.RES.0000261656.04773.39.
- Albornoz, G. et al. (2006) 'Familial thoracic aortic aneurvsms and dissections-Incidence, modes of inheritance, and phenotypic patterns', The Annals of Thoracic Surgery, athoracsur.2006.04.098.
- Alemany, A. et al. (2018) 'Whole-organism clone tracing using single-cell sequencing, Nature. doi: 10.1038/nature25969.

- independent recombination of reporter genes limits lineage tracing and mosaic analysis using CreERT2 lines', Transgenic Research, 29(1), pp. 53-68. doi: 10.1007/ s11248-019-00177-8.
- Andelfinger, G. et al. (2002) 'KCNJ2 mutation results in Andersen syndrome with sex-specific cardiac and skeletal muscle phenotypes', American Journal of Human Genetics, 71(3), pp. 663-668. doi: 10.1086/342360.
- Anderson, R. et al. (2014) 'Myths and realities relating to development of the arterial valves', Journal of Cardiovascular Development and Disease, 1(3), pp. 177-200. doi: 10.3390/ icdd1030177.
- Anderson, R. H. et al. (2003) 'Development of the heart: (3) formation of the ventricular outflow tracts, arterial valves, intrapericardial arterial trunks', Heart, 89(9), pp. 1110-1118.
- Arima, Y. et al. (2012) 'Preotic neural crest cells contribute to coronary artery smooth muscle involving endothelin signalling, *Nature Communications*, 3(1), pp. 1–11. doi: 10.1038/ncomms2258.
  - dorsoventral lineage restriction plane in the mouse limb bud mesenchyme', Development. doi: 10.1242/dev.02873.
- Axelrod, D. (1979) 'Carbocyanine dye orientation in red cell membrane studied by microscopic fluorescence polarization', Biophysical Journal, 26(3), pp. 557-573. doi: 10.1016/ S0006-3495(79)85271-6.
- 82(4), pp. 1400–1405. doi: 10.1016/j. Aydin, A. et al. (2013) 'Ascending aortic aneurysm and aortic valve dysfunction in bicuspid valve disease', International Journal of Cardiology. doi: 10.1016/j. iicard.2011.07.018.
- Álvarez-Aznar, A. et al. (2020) 'Tamoxifen- Baardman, M. E. et al. (2016) 'Common arterial trunk

- and ventricular non-compaction in Lrp2 LRP2 in cardiac development', DMM Disease Models and Mechanisms, 9(4), pp. 413-425. doi: 10.1242/dmm.022053.
- Badger, S. A. et al. (2010) 'Common polymorphisms of Fibulin-5 and the risk of abdominal development', aortic aneurysm Vascular Medicine, 15(2), pp. 113-7. doi: 10.1177/1358863X09355667.
- Baiolle, F. et al. (2006) 'Rotation of the myocardial wall of the outflow tract is implicated in the normal positioning of the great arteries', Circulation Research, 98(3), pp. 421–428. doi: 10.1161/01.RES.0000202800.85341.6E.
- Baldwin, H. S., Lloyd, T. R. and Solursh, M. (1994) 'Hvaluronate degradation affects ventricular function of the early postlooped embryonic rat heart in situ', Circulation Research. 74(2), pp. 244-252. 10.1161/01.RES.74.2.244.
- Barbosky, L. et al. (2006) 'Apoptosis in the developing mouse heart', Developmental Dynamics, 235(9), pp. 2592-2602. doi: 10.1002/dvdy.20885.
- Barker, A. J. et al. (2012) 'Bicuspid aortic valve is associated with altered wall shear stress in the ascending aorta', Circulation: Cardiovascular Imaging, 5(4), pp. 457–466. doi: 10.1161/CIRCIMAGING.112.973370.
- Baroffio, A., Dupin, E. and Le Douarin, N. M. (1991) 'Common precursors for neural and mesectodermal derivatives in the cephalic neural crest', Development. doi: 10.1242/ dev.112.1.301.
- Bartelings, M. M. and Gittenberger-de Groot, A. C. (1991) 'Morphogenetic considerations on congenital malformations of the outflow tract. Part 1: common arterial trunk and tetralogy of Fallot', International Journal of Cardiology, pp. 213-230. doi: 10.1016/0167-5273(91)90329-N.
- Basso, C. et al. (2004) 'An echocardiographic survey of primary school children for bicuspid aortic valve', American Journal of Cardiology. doi: 10.1016/j.amjcard.2003.11.031.
- Benetos, A. et al. (2010) 'Pulse pressure amplification. a mechanical biomarker of cardiovascular risk', Journal of the American College of Cardiology, 55(10), pp. 1032–1037. doi: 10.1016/j.jacc.2009.09.061.
- Bergwerff, Maarten et al. (1998) 'Neural crest cell contribution to the developing circulatory **Implications** system: for morphology?', Circulation research, 82(2),

knockout mice indicate a crucial role of Bergwerff, M., DeRuiter, M. C. and Gittenberger-De Groot, A. C. (1999) 'Comparative anatomy and ontogeny of the ductus

pp. 221-231. doi: 10.1161/01.RES.82.2.221.

- arteriosus, a vascular outsider', Anatomy and Embryology, 200(6), pp. 559-571. doi: 10.1007/S004290050304.
- Biben, C. et al. (2000) 'Cardiac septal and valvular dysmorphogenesis in mice heterozygous for mutations in the homeobox gene Nkx2-5', Circulation Research, 87(10), pp. 888–895. doi: 10.1161/01.RES.87.10.888.
- Biddinger, A. et al. (1997) 'Familial thoracic aortic dilatations and dissections: A case control study', Journal of Vascular Surgery, 25(3), pp. 506-511. doi: 10.1016/S0741-5214(97)70261-1.
- Biezuner, T. et al. (2016) 'A generic, cost-effective, cell lineage scalable analysis platform', Genome Research. doi: 10.1101/ ar.202903.115.
- Biner, S. et al. (2009) 'Aortopathy Is prevalent in relatives of bicuspid aortic valve patients', Journal of the American College of Cardiology, 53(24), pp. 2288-2295. doi: 10.1016/j.jacc.2009.03.027.
- Blais, S. et al. (2020) 'Long-term risk factors for dilatation of the proximal aorta in a large cohort of children with bicuspid aortic valve', Circulation: Cardiovascular Imaging. doi: 10.1161/CIRCIMAGING.119.009675.
- Blom, N. A. et al. (1999) 'Development of the cardiac conduction tissue in human embryos using HNK-1 antigen expression: possible relevance for understanding of abnormal atrial automaticity', Circulation, 99(6), pp. 800-806. doi: 10.1161/01.CIR.99.6.800.
- Bogdan, C. (2001) 'Nitric oxide and the regulation of gene expression', Trends in Cell Biology, 11(2), pp. 66-75. doi: 10.1016/S0962-8924(00)01900-0.
- Bökenkamp, R. et al. (2010) 'Insights into the pathogenesis and genetic background of patency of the ductus arteriosus', *Neonatology*, 98(1), pp. 6–17. doi: 10.1159/000262481.
- Bökenkamp, R. et al. (2014) 'Dlx1 and Rgs5 in the ductus arteriosus: Vessel-specific genes identified by transcriptional profiling of laser-capture microdissected endothelial and smooth muscle cells', PLOS ONE, 9(1), p. e86892. doi: 10.1371/JOURNAL. PONE.0086892.
- vascular Bolender, D. L. and Markwald, R. R. (1979) 'Epithelialmesenchymal transformation in chick

- atrioventricular cushion morphogenesis', Scanning Electron Microscopy.
- Bonnerot, C. and Nicolas, J. F. (1993) 'Clonal analysis in the intact mouse embryo by intragenic recombination', homologous Comptes rendus de l'Academie des sciences. Serie III, Sciences de la vie, 316(10), pp. 1207–17.
- Boodhwani, M. et al. (2014) 'Canadian Cardiovascular Society position statement on the management of thoracic aortic disease', Cai, C. L. et al. (2003) 'Isl1 identifies a cardiac Canadian Journal of Cardiology, 30(6), pp. 577–589. doi: 10.1016/j.cjca.2014.02.018.
- Borger, M. A. et al. (2018) 'The American Association for Thoracic Surgery consensus guidelines bicuspid aortic aortopathy: Full online-only version', Journal of Thoracic and Cardiovascular Surgery. doi: 10.1016/j.jtcvs.2018.02.115.
- Bosse, K. et al. (2013) 'Endothelial nitric oxide signaling regulates Notch1 in aortic valve Cardiology, 60(1), pp. 27-35. doi: 10.1016/j. vimcc.2013.04.001.
- Boudoulas, H. (2003) 'Etiology of valvular Review disease', Expert heart Cardiovascular Therapy, pp. 523-532. doi: 10.1586/14779072.1.4.523.
- Braverman, A. C. et al. (2005) 'The bicuspid aortic Cannoodt, R., Saelens, W. and Saeys, Y. (2016) valve', Current Problems in Cardiology, 30(9), pp. 470-522. doi: 10.1016/j. cpcardiol.2005.06.001.
- Bredman, J. J. et al. (1992) 'Myosin heavy chain during postnatal development', Journal of Anatomy, 180 (Pt 2(Pt 2), pp. 263-274.
- Bressan, M., Liu, G. and Mikawa, T. (2013) 'Early mesodermal cues assign avian cardiac Carmeliet, P. et al. (1996) 'Abnormal blood pacemaker fate potential in a tertiary heart field', Science, 340(6133), pp. 744-748. doi: 10.1126/science.1232877.
- Brink, J. et al. (2015) 'Neonatal pulmonary artery reconstruction during shunting to treat and Carpenter, A. E. et al. (2006) 'CellProfiler: Image prevent juxtaductal coarctation', The Annals of Thoracic Surgery, 99(2), pp. 641-647. doi: 10.1016/J.ATHORACSUR.2014.09.034.
- Buckingham, M. E. and Meilhac, S. M. (2011) 'Tracing cells for tracking cell lineage and clonal behavior', Developmental Cell, 21(3), pp. 394-409. doi: 10.1016/j.devcel.2011.07.019.
- Buckingham, M., Meilhac, S. and Zaffran, S. (2005) 'Building the mammalian heart from two sources of myocardial cells', Nature Reviews Genetics, 6(11), pp. 826–835. doi: 10.1038/ Cecconi, M. et al. (2006) 'Aortic dilatation in patients nrg1710.
- Burks, J. M. et al. (1998) 'Ascending aortic aneurysm

- and dissection in young adults with bicuspid aortic valve: implications for echocardiographic surveillance', Clinical Cardiology, 21(6), pp. 439-443. doi: 10.1002/CLC.4960210615.
- Cai, C. L. et al. (2008) 'A myocardial lineage derives from Tbx18 epicardial cells', Nature. 454(7200), pp. 104-8. doi: 10.1038/ nature06969.
- progenitor population that proliferates prior to differentiation and contributes a majority of cells to the heart', Developmental Cell, 5(6), pp. 877-889.
- valve-related Cai, X. et al. (2013) 'Tbx20 acts upstream of Wnt signaling to regulate endocardial cushion formation and valve remodeling during cardiogenesis', Development. mouse 140(15), pp. 3176-3187. doi: 10.1242/ dev.092502.
- disease', Journal of Molecular and Cellular Camenisch, T. D. et al. (2000) 'Disruption of hyaluronan synthase-2 abrogates normal cardiac morphogenesis and hyaluronanmediated transformation of epithelium mesenchyme', Journal of Clinical Investigation, 106(3), pp. 349–360. doi: 10.1172/JCI10272.
  - 'Computational methods for trajectory inference from single-cell transcriptomics, European Journal of Immunology. doi: 10.1002/eji.201646347.
- expression in rabbit masseter muscle Cardiff, R. D., Miller, C. H. and Munn, R. J. (2014) 'Manual hematoxylin and eosin staining of mouse tissue sections', Protocols. doi: 10.1101/pdb.prot073411.
  - vessel development and lethality in embryos lacking a single VEGF allele', Nature, 380(6573), pp. 435-439. doi: 10.1038/380435A0.
  - analysis software for identifying and quantifying cell phenotypes', Genome Biology. doi: 10.1186/gb-2006-7-10-r100.
  - Cattell, M. A., Hasleton, P. S. and Anderson, J. C. (1993) 'Increased elastin content and decreased elastin concentration may be predisposing factors in dissecting aneurysms of human thoracic aorta', Cardiovascular Research, 27(2), pp. 176–81. doi: 10.1093/cvr/27.2.176.
  - with bicuspid aortic valve', Journal of Cardiovascular Medicine, 7(1), pp. 11–20.

- doi: 10.2459/01.JCM.0000199777.85343.ec. Lo Celso, C. et al. (2009) 'Live-animal tracking of individual haematopoietic stem/progenitor cells in their niche', Nature, 457(7225), pp. 92-6. doi: 10.1038/nature07434.
- Chen, J. Z. et al. (2019) 'Aortic strain correlates with elastin fragmentation in Fibrillin-1 hypomorphic mice', Circulation Reports. doi: 10.1253/circrep.cr-18-0012.
- Christoffels, V. M. et al. (2009) 'Tbx18 and the fate of epicardial progenitors', Nature, 458(7240), pp. E8-9; discussion E9-10. doi: 10.1038/ nature07916.
- Combs, M. D. and Yutzey, K. E. (2009) 'Heart valve development: Regulatory networks in development and disease', Circulation Research. doi: 10.1161/ CIRCRESAHA.109.201566.
- Congdon, E. D. (1922) 'Transformation of the aorticarch system during the development of Washington Publication, 277, p. 47.
- Constâncio, V. et al. (2020) 'DNA methylation-based testing in liquid biopsies as detection and prognostic biomarkers for the four major cancer types', Cells, 9(3). doi: 10.3390/ CELLS9030624.
- Criado, F. J. (2011) 'Aortic dissection: a 250-year Ding, J., Lin, C. and Bar-Joseph, Z. (2019) 'Cell perspective', Texas Heart Institute journal, 38(6), pp. 694-700.
- Cripe, L. et al. (2004) 'Bicuspid aortic valve is Cardiology. doi: 10.1016/j.jacc.2004.03.050.
- Crucean, A. et al. (2017) 'Re-evaluation of hypoplastic left heart syndrome from a developmental and morphological perspective', Orphanet Journal of Rare Diseases, 12(1). doi: 10.1186/ s13023-017-0683-4.
- de la Cruz, M. V et al. (1977) 'Experimental study of the development of the truncus and the conus in the chick embryo', Journal of Anatomy, 123(Pt 3), pp. 661-86.
- Culling, C. F. A. (1974) Handbook of histopathological and histochemical techniques. 3rd ed. doi: 10.1016/c2013-0-04011-x.
- Dargis, N. et al. (2016) 'Identification of genderspecific genetic variants in patients with bicuspid aortic valve', American Journal of Cardiology, 117(3), pp. 420-426. doi: 10.1016/j.amjcard.2015.10.058.
- Davis, C. (1927) 'Development of the human Duim, S. N. et al. (2015) 'Cardiac endothelial cells heart from its first appearance to the stage found in embryos of twenty paired somites', Carnegie Institution of Washington Publication, 19(107), pp. 245-284.

- DeHaan, R. L. (1963) 'Migration patterns of the precardiac mesoderm in the early chick embryo', Experimental Cell Research, doi: 10.1016/S0014-4827(63)80016-6.
- Della Corte, A. et al. (2012) 'Restricted cusp motion in right-left type of bicuspid aortic valves: A new risk marker for aortopathy', Journal of Thoracic and Cardiovascular Surgery, 144(2), pp. 360-369.e1. doi: 10.1016/j. itcvs.2011.10.014.
- DeRuiter, M. C. et al. (1989) 'The special status of the pulmonary arch artery in the branchial arch system of the rat', Anatomy and embryology, 179(4). pp. 319–325. doi: 10.1007/ BF00305058.
- DeRuiter, M. C. et al. (1992) 'The development of the myocardium and endocardium in mouse embryos - Fusion of two heart tubes?', Anatomy and Embryology. doi: 10.1007/ BF00174084.
- the human embryo', Carneaie Institution of DeRuiter, M. C. et al. (1993) 'Development of the pharyngeal arch system related to the pulmonary and bronchial vessels in the avian embryo. With a concept on systemicpulmonary collateral artery formation, Circulation, 87(4), pp. 1306–1319. doi: 10.1161/01.CIR.87.4.1306.
  - lineage inference from SNP and scRNA-Seq data', Nucleic Acids Research. doi: 10.1093/ nar/gkz146.
- heritable', Journal of the American College of Domínguez, J. N. et al. (2012) 'Asymmetric fate of the posterior part of the second heart field results in unexpected left/right contributions to both poles of the heart', *Circulation Research*, 111(10), pp. 1323–35. doi: 10.1161/CIRCRESAHA.112.271247.
  - Le Douarin, N. (1969) 'Particularites du noyau interphasique chez la caille Japonaise (Coturnix coturnix japonica)', Bulletin biologique de la France et de la Belgique.
  - Le Douarin, N. (1973) 'A biological cell labeling technique and its use in experimental embryology', Developmental Biology. doi: 10.1016/0012-1606(73)90061-4.
  - Le Douarin, N. M. (2004) 'The avian embryo as a model to study the development of the neural crest: A long and still ongoing story'. Mechanisms of Development. doi: 10.1016/j. mod.2004.06.003.
  - express Wilms' tumor-1. Wt1 expression in the developing, adult and infarcted heart', Journal of Molecular and Cellular Cardiology. doi: 10.1016/j.yjmcc.2015.02.007.

- Duran, A. C. et al. (1995) 'Bicuspid aortic valves in hearts with other congenital heart disease'. Journal of Heart Valve Disease.
- regulation of atrioventricular valvuloseptal morphogenesis', Circulation Research, pp. 1-6. doi: 10.1161/01.RES.77.1.1.
- Ekmekci A. et al. (2014) 'Association between endothelial nitric oxide synthase intron 4a/b polymorphism and aortic dissection, Turk Kardivoloji Derneaj Arsivi, 42(1), pp. 55-60. doi: 10.5543/tkda.2014.88269.
- Eley, L. et al. (2018) 'A novel source of arterial valve cells linked to bicuspid agrtic valve without Feil, R. et al. (1996) 'Ligand-activated site-specific raphe in mice', eLife, 7(e34110), pp. 1-27. doi: 10.7554/eLife.34110.
- Elzenga, N. J. et al. (1990) 'Juxtaductal pulmonary artery coarctation. An underestimated cause of branch pulmonary artery stenosis in patients with pulmonary atresia or stenosis and a ventricular septal defect'. The Journal of Thoracic and Cardiovascular Surgery, 100(3), pp. 416-424.
- Elzenga, N. J. and Gittenberger-de Groot, A. C. (1986) 'The ductus arteriosus and stenoses of the pulmonary arteries in pulmonary atresia', International Journal of Cardiology, 11(2), pp. 195-208. doi: 10.1016/0167-5273(86)90179-8.
- Elzenga, N. J., Gittenberger-de Groot, A. C. and Oppenheimer-Dekker, A. (1986) 'Coarctation and other obstructive aortic arch anomalies: their relationship to the ductus arteriosus', International Journal of Cardiology, 13(3), pp. 289-308. doi: 10.1016/0167-5273(86)90116-6.
- Elzenga, N. J. and Gittenberger De Groot, A. (1983) 'Localised coarctation of the aorta. An age dependent spectrum', British Heart Journal, 49(4), pp. 317-323. doi: 10.1136/ HRT.49.4.317.
- Emanuel, R. et al. (1978) 'Congenitally bicuspid Gao, L. et al. (2012) 'Role of uncoupled endothelial aortic valves. Clinicogenetic study of 41 families', Heart, doi: 10.1136/hrt.40.12.1402.
- Epstein, J. A. et al. (2000) 'Migration of cardiac neural crest cells in Splotch embryos', Development, 127(9), pp. 1869 LP – 1878.
- Epstein, J. and Buck, C. A. (2000) 'Transcriptional regulation of cardiac development: Implications for congenital heart disease and DiGeorge syndrome', Pediatric Research, pp. 717-724. doi: 10.1203/00006450-200012000-00003.
- Fan, L. M. et al. (2014) 'Endothelial cell-specific Gelb, B. D. et al. (1999) 'Familial patent ductus reactive oxygen species production

- increases susceptibility to aortic dissection, Circulation, 129(25), pp. 2661-72. doi: 10.1161/CIRCULATIONAHA.113.005062.
- Eisenberg, L.M. and Markwald, R.R. (1995) 'Molecular Fedak, P. W. M. et al. (2002) 'Clinical and pathophysiological implications bicuspid aortic valve', Circulation, 106(8), pp. 900-4. doi: 10.1161/01. cir.0000027905.26586.e8.
  - P. W. M. et al. (2005) 'Bicuspid aortic Fedak, valve disease: Recent insights pathophysiology and treatment', Expert Review of Cardiovascular Therapy. doi: 10.1586/14779072.3.2.295.
  - recombination in mice', Proceedings of the National Academy of Sciences of the United States of America, 93(20), pp. 10887-90.
  - Fernandes, S. M. et al. (2004) 'Morphology of bicuspid aortic valve in children and adolescents', Journal of the American College of Cardiology, pp. 1648–1651. doi: 10.1016/j. jacc.2004.05.063.
  - Fernandez, B. et al. (2009) 'Bicuspid aortic valves with different spatial orientations of the leaflets are distinct etiological entities', Journal of the American College of Cardiology, 54(24), pp. 2312-2318. doi: 10.1016/j.jacc.2009.07.044.
  - de Figueiredo Borges, L. et al. (2008) 'Collagen is reduced and disrupted in human aneurysms and dissections of ascending aorta', Human Pathology, 39(3), pp. 437-43. doi: 10.1016/j.humpath.2007.08.003.
  - Fisher, A. G. (2002) 'Cellular identity and lineage choice', Nature Reviews Immunology, pp. 977-982. doi: 10.1038/nri958.
  - Freeman, R. V. and Otto, C. M. (2005) 'Spectrum of calcific aortic valve disease: Pathogenesis, disease progression, and treatment strategies', Circulation. doi: 10.1161/ CIRCULATIONAHA.104.486738.
  - nitric oxide synthase in abdominal aortic aneurysm formation: Treatment with folic acid', Hypertension, 59(1), pp. 158-66. doi: 10.1161/HYPERTENSIONAHA.111.181644.
  - Garg, V. et al. (2005) 'Mutations in NOTCH1 cause aortic valve disease', Nature, 437(7056), pp. 270-274. doi: 10.1038/nature03940.
  - Ge, Y. et al. (2020) 'Human epicardium-derived cells reinforce cardiac sympathetic innervation, Journal of Molecular and Cellular Cardiology. doi: 10.1016/j.yjmcc.2020.04.006.
  - arteriosus and bicuspid aortic valve

- with hand anomalies: A novel hearthand syndrome'. American Journal of Medical Genetics. doi: 10.1002/ (sici)1096-8628(19991119)87:2<175::aidajmg9>3.0.co;2-%23.
- Gillis, E. et al. (2017) 'Candidate gene resequencing in a large bicuspid aortic valve-associated thoracic aortic aneurysm cohort: SMAD6 as an important contributor, Frontiers in Physiology, 13(8), p. 400. doi: 10.3389/ fphvs.2017.00400.
- Girdauskas, E., Borger, M. A., et al. (2011) 'Is aortopathy in bicuspid aortic valve disease a congenital defect or a result of abnormal hemodynamics? A critical reappraisal of a one-sided argument', European Journal of 10.1016/j.ejcts.2011.01.001.
- Girdauskas, E., Schulz, S., et al. (2011) 'Transforming growth factor-beta receptor type II mutation in a patient with bicuspid aortic valve disease and intraoperative Greulich, F. et al. (2016) 'Lack of genetic interaction aortic dissection', The Annals of Thoracic Surgery, 91(5), pp. e70-e71. doi: 10.1016/j. athoracsur.2010.12.060.
- Girdauskas, E. et al. (2012) 'Relation of bicuspid aortic valve morphology to the dilatation pattern of the proximal aorta: Focus on the transvalvular flow', Cardiology Research and Practice. doi: 10.1155/2012/478259.
- Girdauskas, E. et al. (2017) 'Genetic abnormalities in bicuspid aortic valve root phenotype: preliminary resultsdagger', Journal of Cardio-Thoracic Surgery, 52(1), pp. 156-162. doi: 10.1093/ejcts/ezx065.
- Gittenberger-de Groot, A. C. et al. (2002) 'The embryology of the common arterial trunk', Progress in Pediatric Cardiology, 15(1), pp. 1-8. doi: 10.1016/S1058-9813(02)00002-4.
- Gittenberger-de Groot, A. C. et al. (2012) 'The arterial and cardiac epicardium in development, disease and repair', Differentiation, pp. 41-53. doi: 10.1016/j.diff.2012.05.002.
- 'Embryology of the heart and its impact on understanding fetal and neonatal heart disease', Seminars in Fetal and Neonatal Medicine, 18(5), pp. 237-44. doi: 10.1016/j. siny.2013.04.008.
- Gittenberger-de Groot, A. C. et al. (2014) 'Morphogenesis and molecular considerations on congenital cardiac septal defects', Annals of Medicine, 46(8), pp. 640-52. doi: 10.3109/07853890.2014.959557.
- Gittenberger-De Groot, A. C. et al. (2000)

- 'Epicardial outgrowth inhibition leads to compensatory mesothelial outflow tract collar and abnormal cardiac septation and coronary formation'. Circulation Research. doi: 10.1161/01.RES.87.11.969.
- Gittenberger-De Groot, A. C. et al. (2005) 'Basics of cardiac development for the understanding of congenital heart malformations', Pediatric Research, pp. 169–176. doi: 10.1203/01. PDR.0000148710.69159.61.
- Goergen, C. J. et al. (2010) 'In vivo quantification of murine aortic cyclic strain, motion, and curvature: implications for abdominal aortic aneurysm growth', Journal of Magnetic Resonance Imaging: JMRI, 32(4), pp. 847-58. doi: 10.1002/jmri.22331.
- Cardio-Thoracic Surgery, pp. 809–814, doi: Gould, R. A. et al. (2018) 'ROBO4 variants predispose individuals to bicuspid aortic valve and thoracic aortic aneurysm', Nature Genetics 2018 51:1, 51(1), pp. 42-50. doi: 10.1038/ s41588-018-0265-v.
  - between Tbx18 and Tbx2/Tbx20 in mouse epicardial development', PLOS ONE. 11(6), p. e0156787. doi: 10.1371/journal. pone.0156787.
  - Grewal, N. et al. (2014) 'Normal and abnormal development of the aortic wall and valve: Correlation with clinical entities', Netherlands Heart Journal. Bohn Stafleu van Loghum, pp. 363–369, doi: 10.1007/ s12471-014-0576-2.
  - European Grün, D. et al. (2015) 'Design and analysis of single-cell sequencing experiments', Cell, 163(4), pp. 799-810. doi: 10.1016/j. cell.2015.10.039.
    - Gundersen, H. J. et al. (1988) 'Some new, simple and efficient stereological methods and their use in pathological research and diagnosis', APMIS: Acta Pathologica, Microbiologica, et Immunologica Scandinavica, 96(5), pp. 379-94. doi: 10.1111/j.1699-0463.1988. tb05320.x.
- Gittenberger-de Groot, A. C. et al. (2013) Guo, D.-C. et al. (2007) 'Mutations in smooth muscle alpha-actin (ACTA2) lead to thoracic aortic aneurysms and dissections', Nature Genetics, 39(12), pp. 1488-1493. doi: 10.1038/na.2007.6.
  - D. C. et al. (2015) 'MAT2A mutations Guo, predispose individuals to thoracic aortic aneurysms', American Journal of Human Genetics, 96(1), pp. 170-177. doi: 10.1016/j. ajhq.2014.11.015.
  - Hagan, P. G. et al. (2000) 'The International Registry of Acute Aortic Dissection (IRAD): New

- American Medical Association, 283(7), pp. 897-903. doi: 10.1001/jama.283.7.897.
- Hammer, S. et al. (2008) 'Characterization of TBX20 in human hearts and its regulation by TFAP2', Journal of Cellular Biochemistry, 104(3), pp. 1022-1033, doi: 10.1002/JCB.21686.
- Harmon, A. W. and Nakano, A. (2013) 'Nkx2-5 lineage tracing visualizes the distribution of second heart field-derived aortic smooth muscle', Genesis, 51(12), pp. 862-869, doi: 10.1002/ dvg.22721.
- Hatzistergos, K. E. et al. (2020) 'A novel cardiomyogenic role for Isl1+ neural crest 6(49), p. eaba9950. doi: 10.1126/sciadv. aba9950.
- Hayashi, S. and McMahon, A. P. (2002) 'Efficient recombination in diverse tissues by a tamoxifen-inducible form of Cre: a tool for temporally regulated gene activation/ inactivation in the mouse', Developmental Biology, 244(2), pp. 305-18. doi: 10.1006/ dbio.2002.0597.
- Helgadottir, A. et al. (2018) 'Genome-wide analysis yields new loci associating with aortic valve stenosis', Nature Communications, 9(1), pp. 1-10. doi: 10.1038/s41467-018-03252-6.
- Hemish, J. et al. (2003) 'Nitric oxide activates diverse signaling pathways to regulate gene expression', Journal of Biological Chemistry, 278(43), pp. 42321-9. doi: 10.1074/jbc. M308192200.
- Henderson, D. J., Eley, L. and Chaudhry, B. (2020) 'New concepts in the development and malformation of the arterial valves', Journal of Cardiovascular Development and Disease, pp. 1-27. doi: 10.3390/icdd7040038.
- Herman, J. S., Sagar and Grün, D. (2018) 'FateID infers cell fate bias in multipotent progenitors from single-cell RNA-seg data', Nature Methods, 15(5), pp. 379-386. doi: 10.1038/ nmeth.4662.
- Hiratzka, L. F. et al. (2010) '2010 ACCF/AHA/ AATS/ACR/ASA/SCA/SCAI/SIR/STS/ SVM Guidelines for the diagnosis and management of patients with thoracic aortic disease', Journal of the American College of Cardiology. doi: 10.1016/j. jacc.2010.02.015.
- Hoffman, J. I. and Kaplan, S. (2002) 'The incidence of congenital heart disease', Journal of the American College of Cardiology, 39(12), Ivey, K. N. et al. (2008) 'Transcriptional regulation 1890-1900. doi: 10.1016/S0735-1097(02)01886-7.

- insights into an old disease', Journal of the Honig, M. G. and Hume, R. I. (1986) 'Fluorescent carbocyanine dyes allow living neurons of identified origin to be studied in long-term cultures', The Journal of Cell Biology, 103(1), pp. 171–87.
  - Honig, M. G. and Hume, R. I. (1989) 'Dil and diO: versatile fluorescent dves for neuronal labelling and pathway tracing, Trends in Neurosciences, 12(9), pp. 333-5, 340-1.
  - Hope, M. D. et al. (2010) 'Bicuspid aortic valve: Four-dimensional MR evaluation ascending aortic systolic flow patterns', Radiology, 255(1), pp. 53-61. doi: 10.1148/ radiol.09091437.
- cells in the inflow tract', Science Advances, Hor, K. N. et al. (2008) 'The presence of bicuspid aortic valve does not predict ventricular septal defect type', American Journal of Medical Genetics, Part A. doi: 10.1002/ ajmg.a.32609.
  - Huang, P. L. et al. (1995) 'Hypertension in mice lacking the gene for endothelial nitric oxide synthase', Nature, 377(6546), pp. 239-42. doi: 10.1038/377239a0.
  - Huntington, K., Hunter, A. G. W. and Chan, K. L. (1997) 'A prospective study to assess the frequency of familial clustering of congenital bicuspid aortic valve', Journal of the American College of Cardiology. doi: 10.1016/S0735-1097(97)00372-0.
  - Indra, A. K. et al. (1999) 'Temporally-controlled sitespecific mutagenesis in the basal layer of the epidermis: comparison of the recombinase activity of the tamoxifen-inducible Cre-ER(T) and Cre-ER(T2) recombinases', Nucleic acids research, 27(22), pp. 4324-7. doi: 10.1093/nar/27.22.4324.
  - Isnard, R. N. et al. (1989) 'Pulsatile diameter and elastic modulus of the aortic arch in essential hypertension: a noninvasive study', Journal of the American College of Cardiology, 13(2), pp. 399-405. doi: 10.1016/0735-1097(89)90518-4.
  - Isselbacher, E. M. (2005) 'Thoracic and Abdominal Aortic Aneurysms', Circulation, 111(6), pp. 816-828. doi: 10.1161/01. CIR.0000154569.08857.7A.
  - Itagaki, S. et al. (2015) 'Long-term risk for aortic complications after aortic valve replacement in patients with bicuspid aortic valve versus marfan syndrome', Journal of the American College of Cardiology. doi: 10.1016/j.jacc.2015.03.575.
  - during development of the ductus arteriosus', Circulation Research,

- 103(4), pp. 388-395. doi: 10.1161/ CIRCRESAHA.108.180661.
- Jain, R. et al. (2011) 'Cardiac neural crest orchestrates mouse semilunar valves', Journal of Clinical Investigation, 121(1), pp. 422-430. doi: 10.1172/jci44244.
- Jensen, L. F., Bentzon, J. F. and Albarrán-juárez, J. (2021) 'The phenotypic responses of vascular smooth muscle cells exposed to mechanical cues', Cells, 10(9), doi: 10.3390/ CFLLS10092209.
- Jiang, X. et al. (2000) 'Fate of the mammalian cardiac neural crest', Development, 127(8), pp. 1607-1616. doi: 10.1038/ncb3294.
- Jiao, K. et al. (2003) 'An essential role of Bmp4 in the atrioventricular septation of the mouse heart', Genes and Development, 17(19), pp. 2362-2367. doi: 10.1101/gad.1124803.
- Jiménez, R. C. et al. (2017) 'Four simple recommendations encourage to best practices in research software', F1000Research. doi: 10.12688/ f1000research.11407.1.
- Junker, J. P. et al. (2014) 'Genome-wide RNA tomography in the zebrafish embryo', Cell, 159(3), pp. 662-675. doi: 10.1016/j. cell.2014.09.038.
- Junker, J. P. et al. (2016) 'Massively parallel clonal analysis using CRISPR/Cas9 induced genetic scars', bioRxiv, p. 056499. doi: 10.1101/056499.
- Junqueira, L. C. U., Bignolas, G. and Brentani, R. R. (1979) 'A simple and sensitive method for the quantitative estimation of collagen', Analytical Biochemistry. doi: 10.1016/0003-2697(79)90795-4.
- Kelder, T. P. et al. (2015) 'The sinus venosus contributes mvocardium to the atrioventricular canal: potential role during atrioventricular node development?', Journal of Cellular and Molecular Medicine. 19(6), 1375-89. doi: 10.1111/ pp. icmm.12525.
- Kelder, T. P. et al. (2016) 'The avian embryo to study Koenraadt, W. M. C. et al. (2016) 'The extent of the development of the cardiac conduction system', Differentiation, 91(4–5), pp. 90–103. doi: 10.1016/i.diff.2016.01.006.
- Kelly, R. G., Brown, N. A. and Buckingham, M. E. (2001) 'The Arterial Pole of the Mouse Heart Forms from Fqf10-Expressing Cells Koga, M., Kageura, H. and Yamana, K. (1986) 'Use in Pharyngeal Mesoderm', Developmental Cell, 1(3), pp. 435-440, doi: 10.1016/S1534-5807(01)00040-5.
- Kelly, R. G. and Buckingham, M. E. (2002) 'The

- anterior heart-forming field: Voyage to the arterial pole of the heart'. Trends in Genetics. doi: 10.1016/S0168-9525(02)02642-2.
- remodeling and functional maturation of Keyte, A. and Hutson, M. R. (2012) 'The neural crest in cardiac congenital anomalies', Differentiation. pp. 25-40. doi: 10.1016/j. diff.2012.04.005.
  - Keyte, A. L., Alonzo-Johnsen, M. and Hutson, M. R. (2014) 'Evolutionary and developmental origins of the cardiac neural crest: building a divided outflow tract', Birth Defects Research C Embryo Today, 102(3), pp. 309-323. doi: 10.1002/bdrc.21076.
  - Kirby, M. L. (2007) Cardiac Development, Oxford, UK: Oxford University Press.
  - Kirby, M. L., Gale, T. F. and Stewart, D. E. (1983) 'Neural crest cells contribute to normal aorticopulmonary septation, Science. 220(4601), pp. 1059-1061. doi: 10.1126/ science.6844926.
  - Kisanuki, Y. Y. et al. (2001) 'Tie2-Cre transgenic mice: A new model for endothelial celllineage analysis in vivo', Developmental Biology, 230(2), pp. 230-242. doi: 10.1006/ dbio.2000.0106.
  - Klemm, S. L., Shipony, Z. and Greenleaf, W. J. (2019) 'Chromatin accessibility and the regulatory epigenome', Nature Reviews Genetics, pp. 207-220. doi: 10.1038/s41576-018-0089-8.
  - Kobeissi, E. et al. (2019) 'Blood pressure, hypertension and the risk of abdominal aortic aneurysms: a systematic review and meta-analysis of cohort studies', European Journal of Epidemiology. doi: 10.1007/ s10654-019-00510-9.
  - Koenig, S. et al. (2015) 'Evidence of aortopathy in mice with haploinsufficiency of Notch1 in Nos3-null background', Journal of Cardiovascular Development and Disease, 2(1), pp. 17–30. doi: 10.3390/jcdd2010017.
  - Koenig, S. N. et al. (2017) 'Notch1 haploinsufficiency causes ascending aortic aneurysms in mice', JCI Insight, 2(21). doi: 10.1172/jci. insight.91353.
  - raphe in bicuspid aortic valves is associated with aortic regurgitation and aortic root dilatation', Netherlands Heart Journal, 24(2), pp. 127-133. doi: 10.1007/s12471-015-0784-4.
  - of hybrids between Xenopus laevis and Xenopus borealis in chimera formation: Dorsalization of ventral cells: (cell lineage/ chimera/hybrid/Xenopus/dorsalization)',

- Development, Growth & Differentiation. doi: 10.1111/i.1440-169X.1986.00177.x.
- Kong, W. K. F. et al. (2020) 'Sex differences in Cardiovascular Diseases, 63(4), pp. 452–456. doi: 10.1016/j.pcad.2020.06.004.
- Kong, Y. et al. (2014) 'Neural crest development and craniofacial morphogenesis is coordinated by nitric oxide and histone acetylation', Chemistry and Biology, 21(4), pp. 488-501. doi: 10.1016/i.chembiol.2014.02.013.
- Kotlarczyk, M. P. et al. (2016) 'Regional Disruptions Associated With Bicuspid Aortic Valve', The Annals of Thoracic Surgery, 102(4), pp. 1274-81. doi: 10.1016/j.athoracsur.2016.04.001.
- Kramer, T. C. (1942) 'The partitioning of the truncus and conus and the formation of the membranous portion of the interventricular septum in the human heart', American Journal of Anatomy, 71(3), pp. 343-370. doi: 10.1002/aja.1000710303.
- Krotoski, D. M., Fraser, S. E. and Bronner-Fraser, M. (1988) 'Mapping of neural crest pathways in Xenopus laevis using inter- and intraspecific cell markers', Developmental Biology. doi: 10.1016/0012-1606(88)90194-
- Kruithof, B. P. et al. (2012) 'TGFbeta and BMP signaling in cardiac cushion formation: lessons from mice and chicken', Differentiation, 84(1), pp. 89-102. doi: 10.1016/j.diff.2012.04.003.
- genome-wide expression data with spatial resolution', Methods in Cell Biology, doi: 10.1016/bs.mcb.2016.01.006.
- Ku, W. L. et al. (2019) 'Single-cell chromatin immunocleavage sequencing (scChIC-seg) Methods, 16(4), pp. 323-325. doi: 10.1038/ s41592-019-0361-7.
- Kuhlencordt, P. J. et al. (2001) 'Accelerated atherosclerosis, aortic aneurysm formation, and ischemic heart disease in apolipoprotein E/endothelial nitric Li, F. et al. (2019) 'The heterogeneous phenotype of oxide synthase double-knockout mice', Circulation, 104(4), pp. 448-454. doi: 10.1161/hc2901.091399.
- Laforest, B., Andelfinger, G. and Nemer, M. (2011) 'Loss of Gata5 in mice leads to bicuspid aortic valve', Journal of Clinical Investigation, Li, H. and Durbin, R. (2010) 'Fast and accurate long-121(7), pp. 2876-2887. doi: 10.1172/ ici44555.
- Laforest, B. and Nemer, M. (2011) 'GATA5 interacts

- development', Developmental Biology, 358(2), pp. 368-378. doi: 10.1016/j. vdbio.2011.07.037.
- bicuspid aortic valve disease', Progress in Laforest, B. and Nemer, M. (2012) 'Genetic insights into bicuspid aortic valve formation', Cardiology Research and Practice, p. 180297. doi: 10.1155/2012/180297.
  - De Lange, F. J. et al. (2004) 'Lineage and morphogenetic analysis of cardiac valves', Circulation Research. 95(6), pp. 645-654. doi: 10.1161/01. RES.0000141429.13560.cb.
- in Endothelial Nitric Oxide Pathway Laverriere, A. C. et al. (1994) 'GATA-4/5/6, a subfamily of three transcription factors transcribed in developing heart and gut', Journal of Biological Chemistry.
  - Lazzarini, R. et al. (2018) 'The proximal segment of the embryonic outflow (conus) does not participate in a ortic vestibule development, PLOS ONE, 13(12). doi: 10.1371/JOURNAL. PONE.0209930.
  - Le, V. P. et al. (2014) 'Fibulin-5 null mice with decreased arterial compliance maintain normal systolic left ventricular function, but not diastolic function during maturation, Physiological Reports, 2(3), p. E00257. doi: 10.1002/phy2.257.
  - Lee, T. C. et al. (2000) 'Abnormal aortic valve development in mice lacking endothelial nitric oxide synthase', Circulation, 101(20), pp. 2345-2348. doi: 10.1161/01. CIR.101.20.2345.
- Kruse, F. et al. (2016) 'Tomo-seg: A method to obtain Lescroart, F. et al. (2010) 'Clonal analysis reveals common lineage relationships between head muscles and second heart field derivatives in the mouse embrvo', Development, 137(19), pp. 3269-79. doi: 10.1242/dev.050674.
  - to profile histone modification', Nature Lescroart, F. et al. (2012) 'Lineage tree for the venous pole of the heart: clonal analysis clarifies controversial genealogy based on genetic tracing', Circulation Research, 111(10), pp. 1313-22. doi: 10.1161/ CIRCRESAHA.112.271064.
    - bicuspid aortopathy attribute to different dominant pathogenesis', The Annals of Thoracic and Cardiovascular Surgery, 25(5), pp. 265-273. doi: 10.5761/atcs.oa.18-00287.
    - read alignment with Burrows-Wheeler transform', Bioinformatics, 26(5), pp. 589-95. doi: 10.1093/bioinformatics/btp698.
  - with GATA4 and GATA6 in outflow tract Li, R. G. et al. (2018) 'GATA4 loss-of-function

- Mutation and the congenitally bicuspid aortic valve'. American Journal of Cardiology. doi: 10.1016/j.amjcard.2017.11.012.
- Liang, X. et al. (2013) 'HCN4 dynamically marks the first heart field and conduction system precursors', Circulation Research, 113(4), pp. 399-407. doi: 10.1161/ Liu, CIRCRESAHA.113.301588.
- Le Lievre, C. S. and Le Douarin, N. M. (1975) 'Mesenchymal derivatives of the neural crest: analysis of chimaeric quail and chick embryos', Journal of Embryology and Experimental Morphology.
- Lim, M. S., Celermaier, D. S. and Bannon, P. G. (2021) 'Bicuspid aortic valve disease - the influence of valve morphotype on age at and types of surgical treatment, IJC Heart & Vasculature, 34, p. 100786. doi: 10.1016/j. ijcha.2021.100786.
- Lin-Gibson, S., Sarkar, S. and Elliott, J. T. (2018) 'Summary of the National Institute of Standards and Technology and US Food And Drug Administration cell counting workshop: Sharing practices in cell counting measurements', Cytotherapy, doi: 10.1016/j.jcyt.2018.03.031.
- Lin, C.-Y. J. C.-J. Y. et al. (2012) 'Partitioning the heart: mechanisms of cardiac septation and valve development', Development, 139(18), pp. 3277-3299. doi: 10.1242/dev.063495.
- Lindsay, E. A. et al. (2001) 'Tbx1 haploinsufficieny in the DiGeorge syndrome region causes a ortic arch defects in mice', Nature, 410(6824), pp. 97-101. doi: 10.1038/35065105.
- Lioux, G. et al. (2020) 'A second heart field-derived vasculogenic niche contributes to cardiac lymphatics', Developmental Cell. 10.1016/i.devcel.2019.12.006.
- Liu, K. et al. (2018) 'A dual genetic tracing system identifies diverse and dynamic origins of cardiac valve mesenchyme', Development, 145(18). doi: 10.1242/dev.167775.
- Liu, K., Jin, H. and Zhou, B. (2020) 'Genetic lineage tracing with multiple DNA recombinases: A user's guide for conducting more precise cell fate mapping studies', Journal of Biological Chemistry, pp. 6413-6424. doi: Ma, Q., Zhou, B. and Pu, W. T. (2008) 'Reassessment 10.1074/jbc.REV120.011631.
- Liu, R. et al. (2013) 'TET2 is a master regulator smooth muscle cell plasticity', Circulation, 128(18), p. 2047. doi: 10.1161/ CIRCULATIONAHA.113.002887.
- Liu, X. et al. (2019) 'Single-cell RNA-seq of the developing cardiac outflow tract reveals convergent development of the vascular

- smooth muscle cells', Cell Reports. doi: 10.1016/j.celrep.2019.06.092.
- Liu, Y. et al. (2013) 'Nitric oxide synthase-3 promotes embryonic development of atrioventricular valves', PLOS ONE, 8(10), p. e77611. doi: 10.1371/journal.pone.0077611.
- Y. et al. (2019) 'Bisulfite-free 5-methylcytosine detection of and 5-hydroxymethylcytosine base resolution', Nature Biotechnology, 37(4), pp. 424-429. doi: 10.1038/s41587-019-0041-2.
- Livet, J. et al. (2007) 'Transgenic strategies for combinatorial expression of fluorescent proteins in the nervous system', Nature. doi: 10.1038/nature06293.
- Loscalzo, M. L. et al. (2007) 'Familial thoracic aortic dilation and bicommissural aortic valve: A prospective analysis of natural history and inheritance'. American Journal of Medical Genetics, Part A. doi: 10.1002/ajmg.a.31872.
- Lough, J. W. and Sugi, Y. (2000) 'Endoderm and development', Developmental 10.1002/(SICI)1097-Dynamics. doi: 0177(200004)217:4<327::AID-DVDY1> 3.0.CO;2-K.
- Lovatt, D. et al. (2014) 'Transcriptome in vivo analysis (TIVA) of spatially defined single cells in live tissue', Nature Methods, doi: 10.1038/ nmeth.2804.
- Love, M. I., Huber, W. and Anders, S. (2014) 'Moderated estimation of fold change and dispersion for RNA-seq data with DESeq2', Genome Biology, 15(12), p. 550. doi: 10.1186/s13059-014-0550-8.
- Luhmer, I. and Ziemer, G. (1993) 'Coarctation of the pulmonary artery in neonates. Prevalence, diagnosis, and surgical treatment', The Journal of Thoracic and Cardiovascular Surgery, 106(5), pp. 889–894.
- Luria, S. E. and Delbrück, M. (1943) 'Mutations of bacteria from virus sensitivity to virus resistance', Genetics, 28(6), pp. 491-511.
- Ma, L. et al. (2005) 'Bmp2 is essential for cardiac cushion epithelial-mesenchymal transition and myocardial patterning, Development. doi: 10.1242/dev.02156.
- of IsI1 and Nkx2-5 cardiac fate maps using a Gata4-based reporter of Cre activity', Developmental Biology, 323(1), pp. 98–104. doi: 10.1016/j.ydbio.2008.08.013.
- Ma, S. et al. (2018) 'Homocysteine-induced proliferation of vascular smooth muscle cells occurs via PTEN hypermethylation and is mitigated by Resveratrol', Molecular

- Medicine Reports, 17(4), pp. 5312–5319. doi: 10.3892/MMR.2018.8471.
- Macatee, T. L. (2003) 'Ablation of specific expression ectoderm- and endoderm-derived FGF8 during cardiovascular and pharyngeal development', Development, 130(25), pp. 6361-6374. doi: 10.1242/dev.00850.
- MacCarrick, G. et al. (2014) 'Loeys-Dietz syndrome: A primer for diagnosis and management, Genetics in Medicine. doi: 10.1038/ gim.2014.11.
- MacFarlane, E. G. et al. (2019) 'Lineage-specific events underlie aortic root aneurysm pathogenesis in Loeys-Dietz syndrome', Journal of Clinical Investigation. doi: 10.1172/JCI123547.
- Makki, N. and Capecchi, M. R. (2010) 'Hoxa1 lineage tracing indicates a direct role for Hoxa1 in the development of the inner ear, the heart, and the third rhombomere', Developmental Biology, 341(2), pp. 499-509. doi: 10.1016/j. ydbio.2010.02.014.
- Makki, N. and Capecchi, M. R. (2012) 'Cardiovascular defects in a mouse model of HOXA1 syndrome', Human Molecular Genetics, 21(1), pp. 26-31. doi: 10.1093/hmg/ddr434.
- Manasek, F. J. (1968) 'Embryonic development of the heart. I. A light and electron microscopic study of myocardial development in the early chick embryo', Journal of Morphology, 329-365. doi: 10.1002/ 125(3), pp. jmor.1051250306.
- Mariko, B. et al. (2011) 'Fibrillin-1 genetic deficiency leads to pathological ageing of arteries in mice', Journal of Pathology, 224(1), pp. 33– 44. doi: 10.1002/path.2840.
- Marino, B. et al. (1996) 'Associated cardiac anomalies in isolated and syndromic patients with tetralogy of Fallot', The American Journal of Cardiology, 77(7), pp. 505-508, doi: 10.1016/S0002-9149(97)89345-9.
- Mastromoro, G. et al. (2019) 'Left pulmonary Echocardiographic evaluation in patients without cardiac defects and role of Tbx1 in mice', PLOS ONE, 14(4). doi: 10.1371/ JOURNAL.PONE.0211170.
- Meilhac, S. M. et al. (2003) 'A retrospective clonal analysis of the myocardium reveals two phases of clonal growth in the developing mouse heart', Development, 130(16), pp. 3877-3889. doi: 10.1242/dev.00580.
- Meilhac, S. M. et al. (2004) 'The clonal origin of Mjaatvedt, C. H. et al. (2001) 'The outflow tract myocardial cells in different regions of the

- embryonic mouse heart', Developmental Cell, 6(5), pp. 685-698. doi: 10.1016/S1534-5807(04)00133-9.
- domains reveals discrete functions of Merkx, R. et al. (2017) 'Aortic diameter growth in children with a bicuspid aortic valve, The American Journal of Cardiology, 120(1), pp. 131–136, doi: 10.1016/i. amjcard.2017.03.245.
  - Merrell, A. J. and Stanger, B. Z. (2016) 'Adult cell plasticity in vivo: De-differentiation and transdifferentiation are back in style', Nature Reviews Molecular Cell Biology, pp. 413–425. doi: 10.1038/nrm.2016.24.
  - Michelena, H. I. et al. (2011) 'Incidence of aortic complications in patients with bicuspid aortic valves', JAMA - Journal of the American Medical Association. doi: 10.1001/ iama.2011.1286.
  - Michelena, H. I. et al. (2014) 'Bicuspid aortic valve identifying knowledge gaps and rising to the challenge from the international bicuspid aortic valve consortium (BAVCON), Circulation, pp. 2691-2704. doi: 10.1161/ CIRCULATIONAHA.113.007851.
  - Midwood, K. S. and Schwarzbauer, J. E. (2002) 'Elastic fibers: Building bridges between cells and their matrix', Current Biology, 12(8), pp. R279-81. doi: 10.1016/S0960-9822(02)00800-X.
  - Mifflin, J. J. et al. (2018) 'Intercalated cushion cells within the cardiac outflow tract are derived from the myocardial troponin T type 2 (Tnnt2) Cre lineage', Developmental Dynamics, 247(8), pp. 1005-1017. doi: 10.1002/dvdy.24641.
  - Mikawa, T. et al. (1996) 'Retroviral vectors to study cardiovascular development', Trends in Cardiovascular Medicine, 6(3), pp. 79–86. doi: 10.1016/1050-1738(96)00009-6.
  - Miquerol, L. et al. (2010) 'Biphasic development of the mammalian ventricular conduction system', Circulation Research, 107(1), pp. 153–161. doi: 10.1161/CIRCRESAHA.110.218156.
- artery in 22q11.2 deletion syndrome. Miquerol, L. et al. (2013) 'Resolving cell lineage contributions to the ventricular conduction system with a Cx40-GFP allele: a dual contribution of the first and second heart fields', Developmental Dynamics, 242(6), pp. 665-677. doi: 10.1002/dvdy.23964.
  - Miquerol, L. and Kelly, R. G. (2013) 'Organogenesis of the vertebrate heart', Wiley Interdisciplinary Reviews: Developmental Biology. 10.1002/wdev.68.
  - of the heart is recruited from a novel

- heart-forming field'. Biology, 238(1), pp. 97-109. doi: 10.1006/ dbio.2001.0409.
- Miaatvedt, C. H. and Markwald, R. R. (1989) 'Induction of an epithelial-mesenchymal transition by an in vivo adheron-like complex', Developmental Biology, 136(1), pp. 118-128. doi: 10.1016/0012-1606(89)90135-8.
- Molin, D. G. M. et al. (2004) 'Disturbed morphogenesis of cardiac outflow tract and increased rate of aortic arch anomalies in the offspring of diabetic rats', Birth Defects Research. Part A, Clinical and Molecular Teratology, 70(12), pp. 927-938. doi: 10.1002/BDRA.20101.
- Momma, K. et al. (1986) 'Juxtaductal left pulmonary artery obstruction in pulmonary atresia, British Heart Journal, 55(1), pp. 39-44, doi: 10.1136/HRT.55.1.39.
- Momma, K. et al. (1996) 'Cardiac anomalies associated with a chromosome 22a11 deletion in patients with conotruncal anomaly face syndrome', The American Journal of Cardiology, 78(5), pp. 591-594. doi: 10.1016/S0002-9149(96)00374-8.
- Momma, K., Kondo, C. and Matsuoka, R. (1996) 'Tetralogy of fallot with pulmonary atresia associated with chromosome 22q11 deletion', Journal of the American College of Cardiology, 27(1), pp. 198-202. doi: 10.1016/0735-1097(95)00415-7.
- Mommersteeg, M. T. M. et al. (2015) 'Disrupted Slit-Robo signalling results in membranous ventricular septum defects and bicuspid aortic valves', Cardiovascular Research, 106(1), pp. 55-66. doi: 10.1093/cvr/cvv040.
- Moorman, A. F. M. and Christoffels, V. M. (2003) 'Cardiac chamber formation: Development, genes, and evolution', Physiological Reviews. doi: 10.1152/physrev.00006.2003.
- Mordi, I. and Tzemos, N. (2012) 'Bicuspid aortic valve disease: a comprehensive review', Cardiology Research and Practice, p. 196037. doi: 10.1155/2012/196037.
- Moses, K. A. et al. (2001) 'Embryonic expression of mice', Genesis, 31(4), pp. 176–180.
- Muraro, M. J. et al. (2016) 'A Single-Cell Transcriptome Atlas of the Human Pancreas', Cell Systems, 3(4), pp. 385-394. doi: 10.1016/j. cels.2016.09.002.
- Murtada, S.-I. et al. (2016) 'Reduced Biaxial Contractility in the Descending Thoracic Aorta of Fibulin-5 Deficient Mice', Journal of Biomechanical Engineering, 138(5), p. 051008. doi: 10.1115/1.4032938.

- Developmental Nagy, A. (2000) 'Cre recombinase: The universal reagent for genome Genesis. pp. 99-109. doi: 10.1002/ (SICI)1526-968X(200002)26:2<99::AID-GENE1>3.0.CO;2-B.
  - Nakamura, T., Colbert, M. C. and Robbins, J. (2006) 'Neural crest cells retain multipotential characteristics in the developing valves and label the cardiac conduction system', Circulation Research, 98(12), pp. 1547–1554. doi: 10.1161/01.res.0000227505.19472.69.
  - Navin, N. et al. (2011) 'Tumour evolution inferred by single-cell sequencing, Nature. doi: 10.1038/nature09807.
  - Nistri, S. et al. (1999) 'Aortic root dilatation in young men with normally functioning bicuspid aortic valves', Heart, 82(1), pp. 19-22. doi: 10.1136/hrt.82.1.19.
  - Odelin. G. et al. (2017) 'Krox20 defines a subpopulation of cardiac neural crest cells contributing to arterial valves and bicuspid aortic valve', Development. doi: 10.1242/ dev.151944.
  - Ogata, T. et al. (2005) 'Genetic analysis of polymorphisms in biologically relevant candidate genes in patients with abdominal aortic aneurysms', Journal of Vascular Surgery, 41(6), pp. 1036-42. doi: 10.1016/j. jvs.2005.02.020.
  - Olson, E. N. and Srivastava, D. (1996) 'Molecular pathways controlling heart development'. Science. doi: 10.1126/science.272.5262.671.
  - Orriols, M. et al. (2016) 'Down-regulation of Fibulin-5 is associated with aortic dilation: Role of inflammation and epigenetics', Cardiovascular Research, 110(3), pp. 431–42. doi: 10.1093/cvr/cvw082.
  - Otto, C. M. et al. (2021) '2020 ACC/AHA guideline for the management of patients with valvular heart disease: A report of the American College of Cardiology/American Heart Association joint committee on clinical practice guidelines', Circulation, pp. E72-E227. doi: 10.1161/CIR.0000000000000923.
- an Nkx2-5/Cre gene using ROSA26 reporter Oulego-Erroz, I. et al. (2013) 'Ascending aorta children elasticity in with isolated valve', bicuspid aortic International Journal of Cardiology. doi: 10.1016/j. ijcard.2012.11.080.
  - Pacak, C. A. and Byrne, B. J. (2011) 'AAV vectors for cardiac gene transfer: experimental tools and clinical opportunities', Molecular therapy, 19(9), pp. 1582-90. doi: 10.1038/ mt.2011.124.
  - Paloschi, V. et al. (2011) 'Impaired splicing of

- aortic aneurysm formation in patients with bicuspid aortic valve', Arteriosclerosis, Thrombosis, and Vascular Biology. doi: 10.1161/ATVBAHA.110.218461.
- Payne, S., Val, S. De and Neal, A. (2018) 'Endothelialspecific cre mouse models is your cre CREdibile?', Arteriosclerosis, Thrombosis, and Vascular Biology, 38(11), pp. 2550-2561. doi: 10.1161/ATVBAHA.118.309669.
- Peaston, A. E. and Whitelaw, E. (2006) 'Epigenetics and phenotypic variation in mammals', Mammalian Genome, pp. 365-374. doi: 10.1007/s00335-005-0180-2.
- Pei, W. et al. (2017) 'Polylox barcoding reveals haematopoietic stem cell fates realized in vivo', Nature. doi: 10.1038/nature23653.
- Pepe, G. et al. (2014) 'Identification of fibrillin 1 gene mutations in patients with bicuspid aortic valve (BAV) without Marfan syndrome', BMC Medical Genetics, 15, p. 23, doi: 10.1186/1471-2350-15-23.
- Perino, M. and Veenstra, G. J. C. (2016) 'Chromatin control of developmental dynamics and plasticity', Developmental Cell, pp. 610-620. doi: 10.1016/i.devcel.2016.08.004.
- Peterson, J. C. et al. (2018) 'Bicuspid aortic valve formation: Nos3 mutation leads to abnormal lineage patterning of neural crest cells and the second heart field, Disease Models & Mechanisms, 11(10), pp. 655-8. doi: 10.1242/dmm.034637.
- Peterson, J. C. et al. (2020) 'Disturbed nitric oxide signalling gives rise to congenital bicuspid aortic valve and aortopathy', DMM Disease Models and Mechanisms, 13(9), doi: 10.1242/ DMM.044990.
- Phillips, H M. et al. (2013) 'Neural crest cells are required for correct positioning of the developing outflow cushions and pattern the arterial valve leaflets', Cardiovascular Research, 99(3), pp. 452-460. doi: 10.1093/ cvr/cvt132.
- Piatti, F. et al. (2017) '4D flow analysis of BAV-Related fluid-dynamic alterations: Evidences of wall shear stress alterations in absence of clinically-relevant aortic anatomical remodeling', Frontiers in Physiology, 8(JUN). doi: 10.3389/fphys.2017.00441.
- Poelmann, R. E. et al. (2004) 'The neural crest is contiguous with the cardiac conduction system in the mouse embryo: A role in Qu, X. K. et al. (2014) 'A Novel NKX2.5 Loss-ofinduction?', Anatomy and Embryology, 208(5), pp. 389-393. doi: 10.1007/s00429-004-0401-6.

- fibronectin is associated with thoracic Poelmann, R. E. et al. (2017) 'Outflow tract septation and the aortic arch system in reptiles: Lessons for understanding the mammalian heart', EvoDevo, 8(1), p. 9. doi: 10.1186/ s13227-017-0072-z.
  - Poelmann, R. E., Mikawa, T. and Gittenberger-De Groot, A. C. (1998) 'Neural crest cells in outflow tract septation of the embryonic chicken heart: Differentiation and apoptosis', Developmental Dynamics, 212(3), pp. 373-384. doi: 10.1002/ (SICI)1097-0177(199807)212:3<373::AID-AJA5>3.0.CO;2-E.
  - van de Pol, V. et al. (2017) 'Thoracic aortic aneurysm development in patients with bicuspid aortic valve: What is the role of endothelial cells?', Frontiers in Physiology, 8(NOV), p. 938. doi: 10.3389/FPHYS.2017.00938.
  - Pomerance, A. (1972) 'Pathology and valvular heart disease', British Heart Journal, pp. 437–443. doi: 10.1136/hrt.34.5.437.
  - Prakash, S. K. et al. (2014) 'A roadmap to investigate the genetic basis of bicuspid aortic valve and its complications: Insights from the international BAVCon (bicuspid aortic valve consortium)', Journal of the American College of Cardiology, 64(8), pp. 832–9. doi: 10.1016/j.jacc.2014.04.073.
  - Presbitero, P. et al. (1984) 'Absent or occult pulmonary artery', British Heart Journal, 52(2), pp. 178-185. doi: 10.1136/HRT.52.2.178.
  - Price, J., Turner, D. and Cepko, C. (1987) 'Lineage analysis in the vertebrate nervous system by retrovirus-mediated gene transfer', Proceedings of the National Academy of Sciences of the United States of America, pp. 156-160. doi: 10.1073/ 84(1), pnas.84.1.156.
  - Progatzky, F., Dallman, M. J. and Lo Celso, C. (2013) 'From seeing to believing: labelling strategies for in vivo cell-tracking experiments', Interface Focus, 3(3), p. 20130001. doi: 10.1098/rsfs.2013.0001.
  - Pullen, L. C. (2018) 'Human cell atlas poised to transform our understanding of organs', American Journal of Transplantation. doi: 10.1111/ajt.14605.
  - Oavvum, S. R. et al. (2001) 'Septation and valvar formation in the outflow tract of the embryonic chick heart', Anatomical Record, 264(3), pp. 273–283. doi: 10.1002/ar.1162.
  - mutation associated congenital bicuspid aortic valve', American Journal of Cardiology. doi: 10.1016/j.

- amjcard.2014.09.028.
- Ouintero-Rivera, F. et al. (2015) 'MATR3 disruption in human and mouse associated with bicuspid aortic valve, aortic coarctation and patent ductus arteriosus', Human Molecular Genetics. doi: 10.1093/hmg/ddv004.
- Radomski, M. W. and Moncada, S. (1993) 'Regulation of vascular homeostasis by nitric oxide', Thrombosis and Haemostasis, pp. 36–41.
- Raj, B. et al. (2018) 'Simultaneous single-cell profiling of lineages and cell types in the vertebrate brain', Nature Biotechnology. doi: 10.1038/ nbt.4103.
- Rammeloo, L. A. J. et al. (2015) 'Development of major aorto-pulmonary collateral arteries in vegf120/120 isoform mouse embryos with tetralogy of fallot', Pediatric Cardiology, 36(1), pp. 89-95. doi: 10.1007/S00246-014-0969-4.
- Rana, M. S. et al. (2014) 'Development of the human aortic arch system captured in an interactive three-dimensional reference model', American Journal of Medical Genetics. Part A, 164A(6), pp. 1372-1383. doi: 10.1002/AJMG.A.35881.
- Razin, A. and Cedar, H. (1991) 'DNA methylation and gene expression', Microbiological Reviews, 55(3), p. 451. doi: 10.1128/mmbr.55.3.451-458.1991.
- Redheuil, A. et al. (2010) 'Reduced ascending aortic strain and distensibility: Earliest manifestations of vascular aging in humans', Hypertension, 55(2), pp. 319-26. doi: 10.1161/HYPERTENSIONAHA.109.141275.
- doi: 10.7554/eLife.27041.
- Regev, A. et al. (2018) 'The human cell atlas white paper', doi: 10.48550/arXiv.1810.05192.
- Ridnour, L. A. et al. (2007) 'Nitric oxide regulates matrix metalloproteinase-9 activity bv quanvlvl-cvclase-dependent and -independent pathways', **Proceedings** of the National Academy of Sciences, 104(43), pp. 1689–16903. doi: 10.1073/ pnas.0702761104.
- Roberts, A. (1994) 'How Accurate Is Scientific Software?', IEEE Transactions on Software Engineering, doi: 10.1109/32.328993.
- Roberts, W. C. (1970) 'The congenitally bicuspid aortic valve. A study of 85 autopsy cases', The American Journal of Cardiology, pp. 72-83. doi: 10.1016/0002-9149(70)90761-7.
- Robicsek, F. et al. (2004) 'The congenitally bicuspid aortic valve: How does it function? Why does it fail?', The Annals of Thoracic Surgery,

- 77(1), pp. 177-185. doi: 10.1016/S0003-4975(03)01249-9.
- Robicsek, F. and Thubrikar, M. J. (1994) 'Hemodynamic considerations regarding the mechanism and prevention of aortic dissection', The Annals of Thoracic Surgery, 58. pp. 1247-1253. doi: 10.1016/0003-4975(94)90523-1.
- Rosenquist, T. H. et al. (1988) 'Origin and propagation of elastogenesis in the developing cardiovascular system', The Anatomical Record, 221(4), pp. 860-871. doi: 10.1002/ ar.1092210411.
- Rueden, C. T. et al. (2017) 'ImageJ2: ImageJ for the next generation of scientific image data, BMC Bioinformatics. doi: 10.1186/s12859-017-1934-z.
- Russo, C. F. et al. (2002) 'Aortic complications after bicuspid aortic valve replacement: Longterm results', The Annals of Thoracic Surgery, doi: 10.1016/S0003-4975(02)04261-3.
- Rutkovskiy, A. et al. (2017) 'Valve interstitial cells: The key to understanding the pathophysiology of heart valve calcification', Journal of the American Heart Association, 6(9). doi: 10.1161/JAHA.117.006339.
- Safar, M. E. et al. (2018) 'Interaction between hypertension and arterial stiffness an expert reappraisal', Hypertension, pp. 796–805. doi: 10.1161/HYPERTENSIONAHA.118.11212.
- Salameh, Y., Beiaoui, Y. and El Haii, N. (2020) 'DNA methylation biomarkers in aging and agerelated diseases', Frontiers in Genetics, 11, p. 171. doi: 10.3389/FGENE.2020.00171.
- Regev, A. et al. (2017) 'The human cell atlas', eLife. Sanes, J. R. (1989) 'Analysing cell lineage with recombinant retrovirus', Trends in Neurosciences, 12(1), pp. 21-28. doi: 10.1016/0166-2236(89)90152-5.
  - Sanes, J. R., Rubenstein, J. L. and Nicolas, J. F. (1986) 'Use of a recombinant retrovirus to study post-implantation cell lineage in mouse embryos', The EMBO Journal, 5(12), pp. 3133-3142.
  - Santos, M. A. et al. (1980) 'Development of the ductus arteriosus in right ventricular outflow tract obstruction', Circulation, 62(4), pp. 818-822. doi: 10.1161/01.CIR.62.4.818.
  - Sauer, B. (1998) 'Inducible gene targeting in mice using the Cre/lox system', Methods, 14(4), pp. 381–92. doi: 10.1006/meth.1998.0593.
  - Sauer, B. and Henderson, N. (1988) 'Site-specific DNA recombination in mammalian cells by the Cre recombinase of bacteriophage P1', Proceedings of the National Academy of Sciences, 85(14), pp. 5166-5170. doi:

- 10.1073/pnas.85.14.5166.
- Sawada, H. et al. (2017) 'Smooth muscle cells derived from second heart field and cardiac neural crest reside in spatially distinct domains in the media of the ascending aorta - brief report', Arteriosclerosis, Thrombosis, and 10.1161/ATVBAHA.117.309599.
- Schaefer, K. S. et al. (2004) 'Dynamic patterns of apoptosis in the developing chicken heart, Developmental Dynamics, 229(3), pp. 489-499. doi: 10.1002/dvdy.10463.
- Scherptong, R. W. et al. (2012) 'Morphogenesis Sievers, H. H. and Schmidtke, C. (2007) 'A of outflow tract rotation during cardiac development: the pulmonary concept', Developmental Dynamics, 241(9), pp. 1413-1422. doi: 10.1002/dvdy.23833.
- Scherz, P. J. et al. (2008) 'High-speed imaging of developing heart valves reveals interplay of morphogenesis and function', Development, 135(6), pp. 1179-1187. doi: 10.1242/dev.010694.
- Schindelin, J. et al. (2012) 'Fiji: An open source platform for biological image analysis', Nature Methods, 9(7), pp. 676-682. doi: 10.1038/nmeth.2019.Fiii.
- Schindler, H. and Bogdan, C. (2001) 'NO as a signaling molecule: effects on kinases', International Immunopharmacology, 1(8), pp. 1443-55. doi: 10.1016/s1567-5769(01)00089-3.
- Schroeder, J. A. et al. (2003) 'Form and function of by extracellular matrix and growth factor signaling', Journal of Molecular Medicine, pp. 392-403. doi: 10.1007/s00109-003-0456-5.
- Selleck, M. A. and Bronner-Fraser, M. (1995) 'Origins of the avian neural crest: The role of neural plate-epidermal interactions', Development, 121(2), pp. 525 LP – 538.
- Sereti, K. I. et al. (2018) 'Analysis of cardiomyocyte clonal expansion during mouse heart development and injury', Nature Communications, 9(1), pp. 1-13. doi: 10.1038/s41467-018-02891-z.
- Sherrah, A. G. et al. (2016) 'Nonsyndromic thoracic aortic aneurysm and dissection outcomes with marfan syndrome versus bicuspid aortic valve aneurysm', Journal 10.1016/j.jacc.2015.11.039.
- Shi, L. M. et al. (2014) 'GATA5 loss-of-function mutations associated with congenital bicuspid aortic valve', International Journal Sizarov, A. et al. (2010) 'Three-dimensional and of Molecular Medicine, 33(5), pp. 1219-1226. doi: 10.3892/ijmm.2014.1700.

- Shim, C. Y. et al. (2011) 'Central aortic stiffness and its association with ascending aorta dilation in subjects with a bicuspid aortic valve'. Journal of the American Society of Echocardiography, 24(8), pp. 847-852. doi: 10.1016/J.ECHO.2011.04.017.
- Vascular Biology, 37(9), pp. 1722–1726. doi: Sievers, H.-H. et al. (2015) 'New insights in the association between bicuspid aortic valve phenotype, aortic configuration and valve haemodynamics', European Journal of Cardio-Thoracic Surgery. doi: 10.1093/ejcts/ ezv087.
  - classification system for the bicuspid aortic valve from 304 surgical specimens', Journal of Thoracic and Cardiovascular Surgery, 133(5), pp. 1226-1233. doi: 10.1016/j. itcvs.2007.01.039.
  - Sillesen, A. S. et al. (2021) 'Prevalence of bicuspid aortic valve and associated aortopathy in newborns in Copenhagen, Denmark', JAMA - Journal of the American Medical Association, 325(6), pp. 561-567. doi: 10.1001/iama.2020.27205.
  - Silverthorn, D. U. (2009) 'Human physiology: An integrated approach (4 ed)', Regulation.
  - Sinah, R. et al. (2012) 'Tbx2 and Tbx3 induce atrioventricular myocardial development and endocardial cushion formation', Cellular and Molecular Life Sciences, 69(8), pp. 1377-1389. doi: 10.1007/s00018-011-0884-2.
- developing heart valves: Coordination Sinha, T. et al. (2015) 'Mapping the dynamic expression of Wnt11 and the lineage contribution of Wnt11-expressing cells mouse development', early Developmental Biology, 398(2), pp. 177-192. doi: 10.1016/j.ydbio.2014.11.005.
  - Sinning, C. et al. (2018) 'Bicuspid aortic valve and aortic coarctation in congenital heart disease—important aspects for treatment with focus on aortic vasculopathy', Cardiovascular Diagnosis and Therapy. doi: 10.21037/cdt.2018.09.20.
  - Sipkins, D. A. et al. (2005) 'In vivo imaging of specialized bone marrow endothelial microdomains for tumour engraftment', Nature, 435(7044), pp. 969-73. doi: 10.1038/ nature03703.
- of the American College of Cardiology. doi: Siu, S. C. and Silversides, C. K. (2010) 'Bicuspid aortic valve disease', Journal of the American College of Cardiology. doi: 10.1016/j. jacc.2009.12.068.
  - molecular analysis of the venous pole of the developing human heart', Circulation,

- 122(8), pp. 798-807. doi: 10.1161/ CIRCULATIONAHA.110.953844.
- Sizarov, A. et al. (2012) 'Three-dimensional and molecular analysis of the arterial pole of Anatomy, 220(4), pp. 336-349. doi: 10.1111/j.1469-7580.2012.01474.x.
- Spanjaard, B. et al. (2018) 'Simultaneous lineage tracing and cell-type identification using CrlsPr-Cas9-induced genetic scars', Nature Biotechnology, doi: 10.1038/nbt.4124.
- Später, D. et al. (2013) 'A HCN4+ cardiomyogenic progenitor derived from the first heart field and human pluripotent stem cells', Nature Cell Biology, 15(9), pp. 1098-1106. doi: 10.1038/ncb2824.
- Stainier, D. Y. R., Lee, R. K. and Fishman, M. C. (1993) 'Cardiovascular development in the zebrafish: I. Myocardial fate map and heart tube formation', Development, doi: 10.1242/ dev.119.1.31.
- Stalmans, I. et al. (2003) 'VEGF: a modifier of the del22q11 (DiGeorge) syndrome?', Nature medicine, 9(2), pp. 173-182. doi: 10.1038/ NM819.
- van der Sterren, S. et al. (2014) 'Prenatal exposure to hyperoxia modifies the thromboxane prostanoid receptor-mediated response to H2O2 in the ductus arteriosus of the chicken embryo', Journal of Physiology and Pharmacology, 65(2), pp. 283-293.
- Stottmann, R. W. et al. (2004) 'BMP receptor IA is required in mammalian neural crest cells for development of the cardiac outflow tract and ventricular myocardium', Development, 131(9), pp. 2205-2218. doi: 10.1242/ dev.01086.
- Suai, Y. et al. (2004) 'Bone morphogenetic protein-2 can mediate myocardial regulation of atrioventricular cushion mesenchymal cell formation in mice', Developmental Biology, 269(2), pp. 505-518. doi: 10.1016/j. ydbio.2004.01.045.
- Sugishita, Y., Watanabe, M. and Fisher, S. A. (2004) 'The development of the embryonic outflow tract provides novel insights into cardiac differentiation and remodeling, Trends in Cardiovascular Medicine, 14(6), pp. 235-241. doi: 10.1016/j.tcm.2004.06.004.
- Sun, B. J. et al. (2018) 'Clinical characteristics of Korean patients with bicuspid aortic valve Tyser, R. C. V. and Srinivas, S. (2020) 'The first who underwent aortic valve surgery', Korean Circulation Journal, 48(1), pp. 48-58. doi: 10.4070/kcj.2017.0124.
- Sun, Y. et al. (2007) 'Islet 1 is expressed in distinct

- cardiovascular lineages, including pacemaker and coronary vascular cells', Developmental Biology, 304(1), pp. 286-296. doi: 10.1016/i.vdbio.2006.12.048.
- of the developing human heart', Journal Suvorava, T. et al. (2015) 'Sustained hypertension despite endothelial-specific eNOS rescue in eNOS-deficient mice'. Biochemical and Biophysical Research Communications, 458(3), pp. 576-583. doi: 10.1016/j. bbrc.2015.01.152.
  - Takamura, K. et al. (1990) 'Association of cephalic neural crest cells with cardiovascular development, particularly that of the semilunar valves', Anatomy and Embryology, 182(3), pp. 263-272. doi: 10.1007/ BF00185519.
  - Tam, P. P. L. and Rossant, J. (2003) 'Mouse embryonic chimeras: Tools for studying mammalian development', Development, pp. 6155-6163. doi: 10.1242/dev.00893.
  - Tan, H. L. et al. (2012) 'Nonsynonymous variants in the SMAD6 gene predispose to congenital cardiovascular malformation', Human Mutation, 33(4), pp. 720-727. doi: 10.1002/ humu.22030.
  - Tang, Y. et al. (2010) 'The contribution of the Tie2+ lineage to primitive and definitive hematopoietic cells', Genesis, 48(9), pp. 563-567. doi: 10.1002/dvg.20654.
  - Theron, A. et al. (2015) 'Krox20 heterozygous mice: A model of aortic regurgitation associated with decreased expression of fibrillar collagen genes', Archives of Cardiovascular Diseases. doi: 10.1016/j.acvd.2015.10.002.
  - Thomas, P. S. et al. (2012) 'Deficient signaling via Alk2 (Acvr1) leads to bicuspid aortic valve development', PLOS ONE, 7(4). doi: 10.1371/ journal.pone.0035539.
  - Thompson, P. (1907) 'Description of a human embryo of twenty-three paired somites', Journal of Anatomy and Physiology, 41(Pt 3), pp. 159-71.
  - Tian, X. et al. (2013) 'Subepicardial endothelial cells invade the embryonic ventricle wall to form coronary arteries', Cell Research, 23(9), pp. 1075-1090. doi: 10.1038/cr.2013.83.
  - Todorov, H. et al. (2019) 'Network inference from single-cell transcriptomic data', Methods in Molecular Biology. doi: 10.1007/978-1-4939-8882-2 10.
  - heartbeat—origin of cardiac contractile activity', Cold Spring Harbor Perspectives in Biology, 12(7), pp. 1–12. doi: 10.1101/ cshperspect.a037135.

- Tzemos, N. et al. (2008) 'Outcomes in adults with American Medical Association, 300(11), pp. 1317-1325. doi: 10.1001/jama.300.11.1317.
- valvular heart disease', Cardiovascular Pathology, 15(5), pp. 243-251. doi: 10.1016/j.carpath.2006.04.007.
- Verma, S. and Siu, S. C. (2014) 'Aortic dilatation in patients with bicuspid aortic valve', The New England Journal of Medicine, 370(20), pp. 1920–1929. doi: 10.1056/NEJMra1207059.
- Verzi, M. P. et al. (2005) 'The right ventricle, outflow tract, and ventricular septum comprise a restricted expression domain within secondary/anterior heart Developmental Biology, 287(1), pp. 134-145. doi: 10.1016/j.ydbio.2005.08.041.
- Visscher, P. M. et al. (2012) 'Five years of GWAS discovery', American Journal of Human Genetics, pp. 7–24. doi: 10.1016/i. ajhg.2011.11.029.
- Wagner, D. E. and Klein, A. M. (2020) 'Lineage tracing meets single-cell omics: opportunities and challenges', Nature Reviews Genetics. doi: 10.1038/s41576-020-0223-2.
- Waldman, J. D. et al. (1996) 'Spontaneous acquisition of discontinuous pulmonary arteries', The Annals of Thoracic Surgery, 62(1), pp. 161-168. doi: 10.1016/0003-4975(96)00229-9.
- Waldo, K. et al. (1998) 'Cardiac neural crest cells the cardiac outflow tract: aortic sac to ventricular septal closure', Developmental Biology, 196(2), pp. 129–144. doi: 10.1006/ dbio.1998.8860.
- Waldo, K. et al. (1999) 'A novel role for cardiac neural Xu, J. crest in heart development', Journal of Clinical Investigation, 103(11), pp. 1499-1507. doi: 10.1172/jci6501.
- arises from a secondary heart field, Development, 128(16), pp. 3179-3188.
- Waldo, K. L. et al. (2005) 'Secondary heart field contributes myocardium and smooth muscle to the arterial pole of the developing heart', Developmental Biology, 281(1), pp. 78-90. doi: 10.1016/j.ydbio.2005.02.012.
- Wang, X. et al. (2005) 'Decreased expression of Yang, fibulin-5 correlates with reduced elastin in thoracic aortic dissection', Surgery, 138(2), pp. 352–9. doi: 10.1016/j.surg.2005.06.006.
- Wang, Y. et al. (2014) 'Clonal evolution in breast genome sequencing, Nature. doi: 10.1038/

- nature13600.
- bicuspid aortic valves', JAMA Journal of the Ward, C. (2000) 'Clinical significance of the bicuspid aortic valve', Heart, 83(1), pp. 81-5, doi: 10.1136/HEART.83.1.81.
- Veinot, J. P. (2006) 'Pathology of inflammatory native Wei, C. J. Y. and Zhang, K. (2020) 'Retrace: retrospective Simultaneous lineage tracing and methylation profiling of single cells', Genome Research. doi: 10.1101/ ar.255851.119.
  - Weinreb, C. et al. (2020) 'Lineage tracing on transcriptional landscapes links state to fate during differentiation', Science. doi: 10.1126/science.aaw3381.
  - Wiesmann, V. et al. (2015) 'Review of free software tools for image analysis of fluorescence cell micrographs', Journal of Microscopy. doi: 10.1111/jmi.12184.
  - Wilson, G. et al. (2014) 'Best practices for scientific computing', PLOS Biology. doi: 10.1371/ journal.pbio.1001745.
  - Wooten, E. C. et al. (2010) 'Application of gene network analysis techniques identifies AXIN1/PDIA2 and endoglin haplotypes associated with bicuspid aortic valve', PLOS ONE, 5(1). doi: 10.1371/journal. pone.0008830.
  - Wu, B. et al. (2011) 'Nfatc1 coordinates valve endocardial cell lineage development required for heart valve formation', Circulation Research, 109(2), pp. 183-192. doi: 10.1161/CIRCRESAHA.111.245035.
  - provide new insight into septation of Xu, H., Li, S. and Liu, Y.-S. (2021) 'Roles and mechanisms of DNA methylation in vascular aging and related diseases', Frontiers in Cell and Developmental Biology, p. 1695. doi: 10.3389/FCELL.2021.699374.
    - et al. (2019) 'Single-cell lineage tracing by endogenous mutations enriched in transposase accessible mitochondrial DNA', eLife, 8. doi: 10.7554/eLife.45105.
- Waldo, K. L. et al. (2001) 'Conotruncal myocardium Xu, Y. J. et al. (2018) 'GATA6 loss-of-function mutation contributes to congenital bicuspid aortic valve', Gene. doi: 10.1016/j. gene.2018.04.018.
  - Yanagisawa, H. et al. (2002) 'Fibulin-5 is an elastinbinding protein essential for elastic fibre development in vivo', Nature, 415(6868), pp. 168-71. doi: 10.1038/415168a.
    - B. et al. (2017) 'Protein-altering and regulatory genetic variants near GATA4 implicated in bicuspid aortic valve', Nature Communications, 8(1), pp. 1–10. doi: 10.1038/ncomms15481.
  - cancer revealed by single nucleus Yang, L. et al. (2006) 'Isl1 Cre reveals a common Bmp pathway in heart and limb development,

R

- *Development*, 133(8), pp. 1575–1585. doi: 10.1242/dev.02322.
- Yasuda, H. et al. (2003) 'Failure to prevent progressive dilation of ascending aorta by aortic valve replacement in patients with bicuspid aortic valve: Comparison with tricuspid aortic valve', Circulation. doi: 10.1161/01.cir.0000087449.03964.fb.
- Yokoyama, U. et al. (2017) 'Pathology and molecular mechanisms of coarctation of the aorta and its association with the ductus arteriosus', The Journal of Physiological Sciences: JPS, 67(2), pp. 259–270. doi: 10.1007/S12576-016-0512-X.
- Yuan, S. and Schoenwolf, G. C. (2000) 'Islet-1 marks the early heart rudiments and is asymmetrically expressed during early rotation of the foregut in the chick embryo', The Anatomical Record, 260(2), pp. 204–207.
- Zaffran, S. et al. (2004) 'Right ventricular myocardium derives from the anterior heart field', Circulation Research, 95(3), pp. 261–268. doi: 10.1161/01.RES.0000136815.73623.BE.
- Zaffran, S. et al. (2018) 'Ectopic expression of Hoxb1 induces cardiac and craniofacial malformations', *Genesis*. doi: 10.1002/ dvg.23221.
- Zaffran, S. and Kelly, R. G. (2012) 'New developments in the second heart field', *Differentiation*, 84(1), pp. 17–24. doi: 10.1016/j. diff.2012.03.003.
- Zhang, D. et al. (2012) 'Homocysteine activates vascular smooth muscle cells by DNA demethylation of platelet-derived growth factor in endothelial cells', Journal of Molecular and Cellular Cardiology, 53(4), pp. 487–496. doi: 10.1016/J. YJMCC.2012.07.010.
- Zhang, J. et al. (2018) 'Significant association of CXCL12 rs1746048 with LDL-C level in intracranial aneurysms', Current Neurovascular Research, 15(1), pp. 26–33. doi: 10.2174/15672026156661803191536 28.
- Zhang, X., Shen, Y. H. and LeMaire, S. A. (2011) 'Thoracic aortic dissection: Are matrix metalloproteinases involved?', Vascular, 17(3), pp. 147–157. doi: 10.2310/6670.2008.00087.
- Zhou, B. *et al.* (2008) 'Epicardial progenitors contribute to the cardiomyocyte lineage in the developing heart', *Nature*, 454(7200), pp. 109–113. doi: 10.1038/nature07060.
- Zhou, B. and Pu, W. T. (2012) 'Genetic Cre-loxP assessment of epicardial cell fate using

Wt1-Driven cre alleles', *Circulation Research*, p. e276. doi: 10.1161/CIRCRESAHA.112.275784.

### Acknowledgements/ Dankwoord

The work presented in this thesis is the result of a long academic journey with many ups and downs. I am very fortunate that I did not have to walk this path alone. This section is therefore dedicated to all the people which contributed to the completion of this thesis.

The first person that I would like to thank for all of his efforts is my promotor Marco de Ruiter. I am very thankful for the guidance and support he provided during this academic journey through all the morphological complexities of embryonic development.

The next person that I would like to thank for all the contributions and support during my PhD track is my co-promotor Marie-José Goumans. I am convinced that having had my two promotors working together so well as they both did, resulted in an great environment for my personal and academic development.

I would also like to thank all my colleagues which supported me during my time at the department of anatomy and embryology. I particularly want to thank Bert and Conny for all there help and advice during this period. There have been many occasions in which your

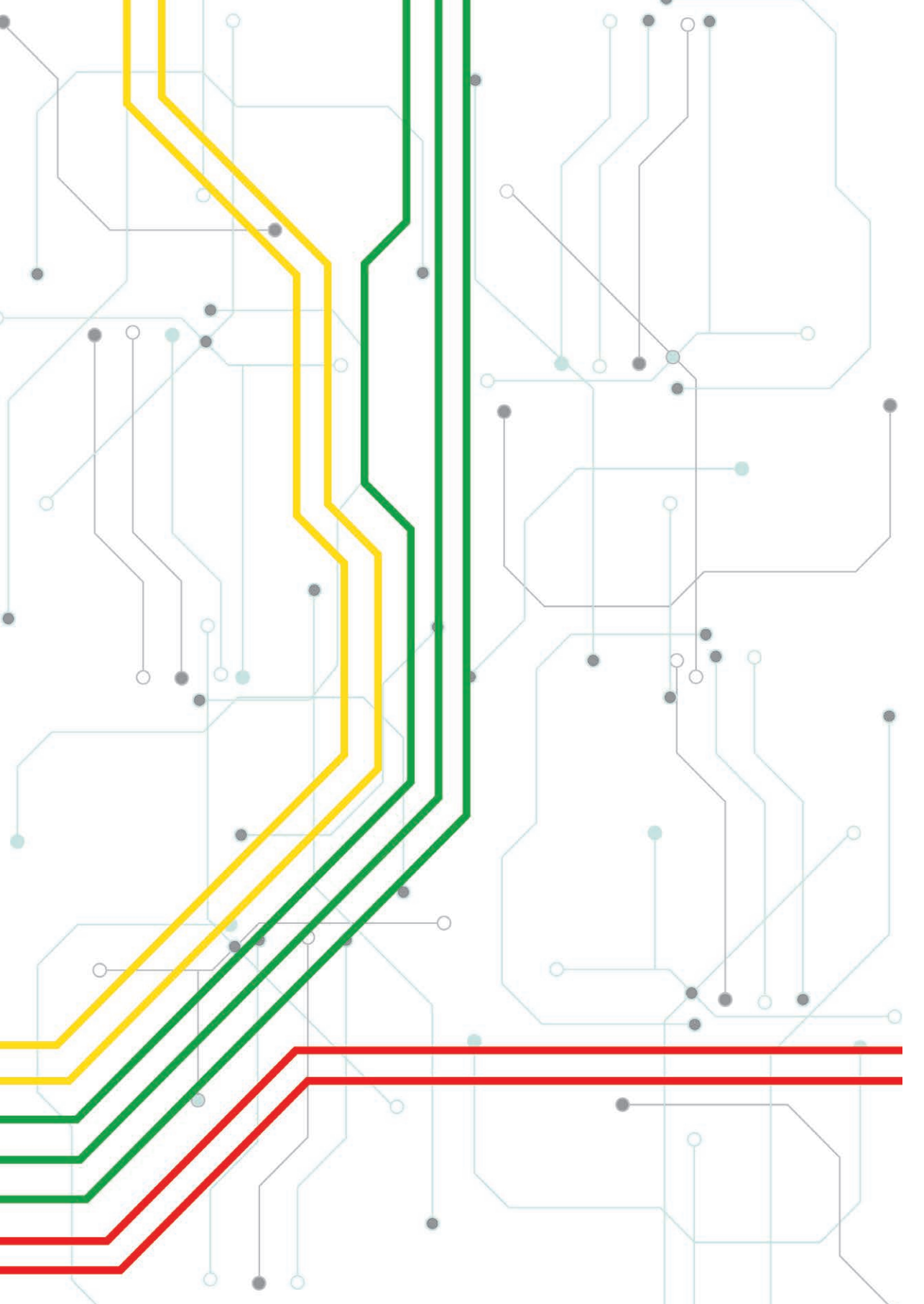
honest opinions have led to more research insights and better experimental designs. I would also like to thank Vera, Tessa, Valerie, Anke and Boudewijn for their help and fruitful discussions. Related to effective discussions, I would also like to thank, Adri, Rob, Monique, Margot, Yang and Friso for the enthusiasm during our weekly Carver meetings. I also would like to thank Tim for his insights and advise threading the roads of cellular lineage tracing. I would like to thank Karina, Berend, Xu, George, Marcello, Oleh, Elisa, Jeroen, Dennis, Michel, Ruben, Claire, Mervyn, Ana, Tom, Lisa, Saskia, Giulia, Maria, Sophia, Lettine, Jasin and all other colleagues of our department for their parts and efforts in this experience.

I would also like to express my gratitude to all my colleagues which supported me during the completion of the final parts of this thesis. Thank you Ashna, Nathalie and Nelleke, Floris-1, Floris-2, Widad, Chiara and Alexander.

Although I have spent much time within the lab during my PhD, I have also received plenty of support from my friends and family outside the lab. As such I would like to give a big thanks to Faiez, Corrie, Willem, Else, Karina, Altug, Riley, Viola, Alberto, Astrid, Gerard, Rita, Ruth, Bea and Joris. Whether it was just hearing my struggles, completing that nice dance, or providing snickers to avoid further drama, all your efforts are really appreciated!

Finally I would like to thank those relatives most closely to me. I would like to thank my parents, Josi and Arnold, for their undying love and support throughout the whole period leading up to and beyond the formation of this dissertation. I also like to thank my brother, for his support and positive distractions from my work. I really appreciate all our random moments as they came and went. Last but not least I would like to thank my wife, Esther. Thank you for having been there for me during this whole journey. I can't begin to summarize all the good that you have brought to my life. Without you, this thesis wouldn't have been what it is today. I thank you so much for your unwavering love, support and pies.





## **Summary/Samenvatting**

#### **Summary**

The bicuspid aortic valve (BAV) is a congenital heart defect which is characterized by the formation of two aortic leaflets instead of the normal three leaflets within the tricuspid aortic valve (TAV). Whilst all BAV patients have a bicuspid valve, extended patient monitoring has revealed a large variation of disease progression trajectories during a patient's lifetime. This large variation troubles clinical decision making due to the uncertain proliferation of BAV disease. More knowledge of the biological mechanisms underlying BAV could address that uncertainty and thus help stratify patient risk with more accuracy. Therefore this thesis aims to advance our current understanding regarding the biological impact and developmental mechanisms underlying congenital BAV and BAV related aortopathy.

In **Chapter 1** information is presented on several aspects of cardiovascular development that are relevant to study the developmental anomalies relating to BAV. Background information regarding the consequences of BAV, aortopathy and the role of cell lineages involved in outflow tract formation is provided along with an outline of the chapters within this thesis.

**Chapter 2** focusses on the role of cell tracing and fate mapping experiments in cardiac outflow tract (OFT) development. Common among many congenital heart diseases affecting the OFT, such as BAV, is a large variation in disease phenotypes. Embryonic fate mapping and lineage tracing experiments have categorized and studied many of the individual cell lineages involved in OFT formation. Nevertheless it remains challenging to relate cell lineage dynamics to the morphologic variation observed in OFT pathologies. In this chapter we provide an overview of historical fate mapping and cell tracing techniques used to study OFT development and introduce emerging technologies which will provide new opportunities to aid our understanding of the cellular dynamics underlying OFT pathology.

**Chapter 3** addresses a common methodological concern involving cellular measurements. Many biological studies highly value the quantification of specific cells within a localized tissue sample or an in-vitro cell culture because this provides quantitative information regarding cell behavior under various circumstances. Numerous methods to address cell quantification have thus been developed to address this issue, ranging from manual cell counting to automated image analysis tools. ImageJ is a popular tool that enables researchers to create custom image analysis scripts to facilitate automated image analysis. Whilst there exist many tutorials on the internet to quickly develop such custom analysis methods, there is often surprisingly little

concern regarding any aspects of measurement validation and process-data collection to ensure experimental reproducibility. Therefore we have developed a software script specific to ImageJ to facilitate collection of process-data for measurement assurance. This script simultaneously aids researchers with exercising good research practices when performing computational image analysis.

In **Chapter 4** we investigate the development of BAV using the *Nos3*<sup>-/-</sup> mouse model. We aimed to understand whether alterations in early cell lineages contributed to the formation of BAV and influenced cardiovascular outflow tract development. To understand the role of early cell lineages during OFT formation lineage tracing experiments were performed to evaluate cell lineage contributions to the heart over multiple developmental stages. A detailed overview was constructed describing a novel interpretation of aortic and pulmonary valve development using high resolution microscopic imaging and 3D reconstruction. Using this approach it was determined that Nos3<sup>-/-</sup> mice develop a BAV without a raphe as a result of incomplete separation of the parietal outflow tract cushion into the right and non-coronary leaflet. Further investigation into the formation of aortic and pulmonary leaflets showed that the individual leaflets harbour unique cell lineage contributions. The right and left leaflets of the aortic valve contains relatively more neural crest derived cells, whereas the non-coronary leaflets contains relatively little neural crest derived cells and more second heart field derived cells. Careful inspection of these lineage populations in Nos3-/- revealed altered deposition of neural crest cells and second heart field cells within the parietal outflow tract cushion of Nos3<sup>-/-</sup> embryos. The effects of these abnormal cell lineage distributions also affected the positioning of the aortic and pulmonary valves at the orifice level. Our results demonstrated a small deviation in the distribution of neural crest and second heart field populations affected normal valve formation and resulted in the characteristic right-non type BAV in Nos3-/- mice.

**Chapter 5** investigates the effects of *Nos3*<sup>-/-</sup> on vascular health. Given that patients with BAV are at increased risk of aortopathy this chapter examines BAV-associated aortopathy in *Nos3*<sup>-/-</sup> mice. Here we used a combination of histological examination and in-vivo ultrasound imaging as an initial step to investigate aortic dilation and dissections in *Nos3*<sup>-/-</sup> mice. We discovered spontaneous aortic dissections in ascending aortas located at the sinotubular junction in ~13% of *Nos3*<sup>-/-</sup> mice. Further analysis showed that *Nos3*<sup>-/-</sup> mice were prone to develop aortic dilations in the proximal- and distal-ascending aorta during early adulthood. To explain these observations we examined the elastic fiber and collagen content within the aortic wall using classical histological stainings. Analysis of the elastic fibers determined that the aortic walls

of *Nos3*<sup>-/-</sup> contained less elastin than those of wild type mice. Interesting is that the vascular smooth muscle cells (VSMCs) which make up the aortic vessel wall are derived from neural crest and second heart field lineages during development. Investigation of the neural crest lineage in the ascending aorta showed a reduction of neural crest derived VSCMs at the inner media of the aortic wall that could be traced back to embryonic development. Using single cell RNA sequencing we compared the gene expression profiles of VSMCs between wild type mice and *Nos3*<sup>-/-</sup>. We found downregulation of 15 genes of which 7 were associated with aortic aneurysms and dissections in the human population. Elastin mRNA was most markedly downregulated, followed by Fibulin-5 expression, both primary components of elastic fibres. This chapter demonstrates that disrupted endothelial mediated NO signalling in mice can give rise to aortic dilation and dissection as a consequence of inhibited elastic fibre formation in VSMCs within the ascending aorta of *Nos3*<sup>-/-</sup>mice.

In **Chapter 6** we address the pathological formation of pulmonary ductal coarctation (PDC) and left pulmonary artery interruption during development. To study this formation a combined approach was adopted using both mouse embryos and stage-matched human embryos. Neural crest and second heart field cell lineages were studied in perspective of the VEGF120/120 mutant mouse strain that develops pulmonary atresia. Careful observations showed that pulmonary stenosis/atresia and a subsequent lack of proper incorporation of the ventral segment into the aortic sac were the result of an anomalous development related the asymmetric contribution of second heart field to the future pulmonary trunk on the left side of the aortic sac, known as, the pulmonary push. These findings explain how neural crest-derived muscular ductus arteriosus (DA) tissue may continue contraction and stenosis formation even after birth leading to the postnatal development of proximal left pulmonary artery interruption. Surgical intervention strategies of PDC should aim to eliminate DA tissue instead of stenting this segment, as this will lead to less complication on the whole.

**Chapter 7** contains a general discussion addressing some of the current challenges in BAV research within the context of the chapters presented in this thesis. Here we discuss the consequence of developmental predisposition theories relative to findings from different research studies. We suggest future directions of research that could address current study limitations to further expand our understanding of the intricacies of cardiovascular development and BAV.

### **Nederlandse Samenvatting**

Het hart is een orgaan dat de mens in leven houdt door bloed in het lichaam rond te pompen. In het hart bevinden zich diverse hartkleppen die ritmisch openen en sluiten bij iedere hartslag. Deze hartkleppen zorgen ervoor dat het bloed op één manier door het hart kan stromen, vanuit de instroom van het hart via de boezems, naar de uitstroom van het hart via de hartkamers, richting de grote slagader van het lichaam (aorta) en de longslagaders. Om te voorkomen dat het bloed van de aorta terug het hart in stroomt is er de aortaklep. De aortaklep heeft drie klepslippen; deze klep wordt daarom ook wel de 'tricuspid aortic valve' genoemd (tri = drie cusp = slip aortaklep, TAV). Het grootste deel van de Nederlandse bevolking wordt geboren met een TAV (98-99%), maar er zijn ook mensen die met een bicuspide aortaklep (BAV) ter wereld komen. De BAV is een aangeboren hartafwijking die wordt gekenmerkt door de aanwezigheid van twee klepslippen in de aortaklep in plaats van de gebruikelijke drie klepslippen.

BAV-patiënten hebben een hoger risico op medische complicaties zoals het optreden van aortaverwijding, dissectie en verkalking van de aortaklep. Het ziekteverloop van deze patiënten verschilt onderling sterk. Sommige patiënten hebben vrijwel geen medische klachten, terwijl er bij andere patiënten ingrijpende operaties moeten worden uitgevoerd. Deze grote variatie in het ziektebeeld van BAV maakt het vanuit klinisch oogpunt uitermate lastig om patiënten de juiste zorg aan te kunnen bieden. Om van te voren het ziekteverloop van een patiënt beter in te kunnen schatten, is er meer kennis nodig van de biologische processen die BAV veroorzaken. Deze kennis kan bijdragen aan een betere profilering van patiënten waardoor er beter kan worden geanticipeerd op toekomstige aandoeningen van de aorta (aortopathie). Dit proefschrift vergroot de kennis die we hebben over de vorming van de bicuspide aortaklep en de BAV-gerelateerde aortopathie.

**Hoofdstuk 1** geeft achtergrondinformatie over de gevolgen van BAV, aortopathie, de embryologische ontwikkeling van het hart en de rol van cel populaties die betrokken zijn bij de vorming van het cardiale uitstroomkanaal. Deze informatie is relevant om het ontstaan van BAV beter te begrijpen. Hoofdstuk 1 bevat ook een overzicht van alle hoofdstukken in dit proefschrift.

**Hoofdstuk 2** is een literatuurstudie over de ontwikkeling van 'cell tracing' en 'fate mapping' methoden die worden gebruikt bij onderzoek naar embryonale ontwikkeling. Veelvoorkomend bij aangeboren hartaandoeningen die het cardiale uitstroomkanaal (OFT) beïnvloeden, zoals

BAV, is de grote variatie in fenotypes. Om het OFT te bestuderen zijn verschillende technieken ontwikkeld om cel populaties te volgen tijdens de ontwikkeling van een embryo. Ondanks onze huidige kennis blijft het een grote uitdaging om de cel dynamiek te relateren aan de fenotypische variatie die wordt waargenomen bij aangeboren afwijkingen. De nieuwe technologieën die dit hoofdstuk voorstelt, bieden meer mogelijkheden om deze cellulaire dynamiek in detail te bestuderen.

**Hoofdstuk 3** behandelt een veel voorkomend methodologisch probleem van cellulaire metingen. Veel biologische studies tellen specifieke cellen in een weefselmonster of een in vitro celkweek om zo iets te kunnen zeggen over het cel gedrag. Er zijn daarom talloze methoden ontwikkeld om cellen te kwantificeren, variërend van handmatig cellen tellen tot geautomatiseerde beeldanalyse. ImageJ is een populaire tool waarmee onderzoekers softwarescripts kunnen ontwikkelen voor geautomatiseerde beeldanalyse. Om betrouwbare beeldanalyses uit te voeren, is het essentieel om data te genereren die inzicht geeft in de kwaliteit van de analyse: metadata. Dit soort metadata is belangrijk omdat het de reproduceerbaarheid van een experiment waarborgt. Momenteel wordt er nog te weinig aandacht besteed aan het verzamelen van metadata bij beeldanalyse. Om het verzamelen van metadata te vergemakkelijken en het belang daarvan te benadrukken, hebben wij binnen ImageJ een script ontwikkeld dat hier een oplossing voor biedt. Dit script helpt onderzoekers bij het implementeren van zogenoemde 'good-research practises' tijdens het uitvoeren van hun beeldanalyse.

In **Hoofdstuk 4** onderzoeken we de ontwikkeling van BAV met behulp van het *Nos3* mutante muismodel. Met hulp van dit muismodel kan er gekeken worden of de embryonale bijdrage van verschillende cel populaties afwijkend is tijdens de vorming van BAV. Om deze cel populaties beter in kaart te brengen zijn cell lineage tracing-experimenten uitgevoerd. Met deze experimenten bestuderen wij de bijdragen van diverse celtype gedurende de ontwikkeling van het hart. Tijdens deze studie is met behulp van microscopische beeldvorming en 3D-reconstructies een nieuw beeld gevormd over de ontwikkeling van aortakleppen. Met behulp van deze benadering is vastgesteld dat *Nos3* mutante embryo's een BAV ontwikkelen door een onvolledige scheiding van het pariëtale uitstroomkussen. Deze onvolledige scheiding ontwikkelt zich in een bicuspide aortaklep waarbij de rechter en de niet-coronaire klep gefuseerd blijven. De klepslippen in de aortaklep zijn opgebouwd uit unieke verhoudingen van bepaalde cellijnen. De *Nos3* mutante embryo's hadden een afwijking in neurale lijstcellen en tweede hartveldcellen. Deze afwijking beïnvloedt de vorming van de hartkleppen, waarbij

de klepvorming zodanig kan worden verstoord dat er een BAV ontstaat.

Uit klinische studies is gebleken dat patiënten met BAV een verhoogd risico hebben op het ontwikkelen van aortopathie. In **Hoofdstuk 5** worden deze risico's in het *Nos3* mutante muismodel bestudeerd. Om afwijkingen in de aorta van de muizen te bekijken, gebruikten we een combinatie van histologische onderzoeksmethoden en echografie. We ontdekten spontane aortadissecties in ~13% van de Nos3 mutante muizen. Daarnaast zagen we ook verwijdingen van de aorta optreden in deze muizen. Om deze verwijdingen van de aorta te verklaren, onderzochten we het gehalte aan elastische vezels en collageen in de aortawand met behulp van klassieke histologische kleuringen. De aortawanden van Nos3 mutante bevatten minder elastine dan de aortawanden van wildtype muizen (zonder mutaties). Hierdoor zou de vaatwand minder rekbaar zijn in de Nos3 mutante muizen. Uit de kleuringen bleek ook dat de aorta vaatwand voornamelijk is opgebouwd uit cellen die zijn afgeleid van de neurale lijst en het tweede hartveld. Nos3 mutante muizen hadden een verminderde bijdrage van neurale lijst afgeleide cellen aan de aorta vaatwand. Met behulp van de laatste ontwikkelingen in genetische analyses vergeleken we de genexpressieprofielen van de aorta vaatwandcellen tussen wildtype muizen en Nos3 mutanten. Hierbij vonden we een verminderde expressie van 15 genen. Van deze genen zijn er 7 geassocieerd met aortadilatatie en dissecties in de mens. Van alle 15 genen was elastine-mRNA het meest gereduceerd in expressie, gevolgd door een verlaagde fibuline-5-expressie. Elastine en fibuline-5 vormen beide primaire componenten voor de structuur van de aorta vaatwand. Dit hoofdstuk laat zien dat een verstoring in neurale lijst afgeleide vaatwandcellen leidt tot een verminderde rekbaarheid van de aorta vaatwand waardoor er aortaverwijding en dissectie kan optreden in de Nos3 mutante muizen.

**Hoofdstuk 6** beschrijft de rol van embryonale cellijnen tijdens de ontwikkeling van de linker longslagader. Hiervoor zijn resultaten van menselijke embryo's vergeleken met VEGF120/120 mutante muismodel embryo's, omdat in deze muizen de pulmonalisklep en de linker longslagader niet goed ontwikkelingen. Het muismodel toont aan dat de groeistoornis in de pulmonalisklep en de afwijkingen in de linker longslagader het resultaat zijn van een verminderde bijdrage van de tweede hartveldcellen. Deze afwijking in het tweede hartveld heeft als gevolg dat de neurale lijst en het tweede hartveld niet goed op elkaar aansluiten tijdens de ontwikkeling van de linker longslagader. Door de verminderde bijdrage van de tweede hartveld afgeleide cellen kunnen de neurale lijst afgeleide cellen een overmaat aan weefsel aanmaken binnen de linker longslagader. Dit 'overtollig' weefsel leidt tot een vernauwing van de linker longslagader. De ontwikkeling van de linker longslagader is dus

afhankelijk van een goede samenwerking tussen cellen van de neurale lijst en het tweede hartveld. Bij de behandeling van patiënten is het daarom noodzakelijk om dit 'overtollige' neurale lijstweefsel te verwijderen. Het verwijderen van het neurale lijstweefsel zal namelijk leiden tot minder complicaties voor de patiënt dan een alternatieve ingreep.

**Hoofdstuk 7** bevat een algemene discussie over de uitdagingen en limitaties van het BAV-onderzoek. Het hoofdstuk richt zich op de gevolgen van de genetische aanleg van BAV-gerelateerde complicaties en stelt ook de toepassing van nieuwe wetenschappelijke technieken ter discussie. Nieuwe vooruitzichten die in grote mate bij kunnen dragen aan nieuwe ontdekkingen rondom cardiovasculaire ontwikkeling en BAV, worden belicht.

### List of publications

**Peterson JC**, Kelder TP, Goumans MJTH, Jongbloed MRM, DeRuiter MC. The Role of Cell Tracing and Fate Mapping Experiments in Cardiac Outflow Tract Development, New Opportunities through Emerging Technologies. J Cardiovasc Dev Dis. 2021 Apr 26;8(5):47. doi: 10.3390/jcdd8050047. PMID: 33925811; PMCID: PMC8146276.

**Peterson JC**, Deruiter MC. Fluorescent Nuclei Measurements Macro (FNMM), a tool for automated cell quantification in ImageJ. Software Impacts. 2020; 6. 100030. doi: 10.1016/j.simpa.2020.100030.

**Peterson JC**, Chughtai M, Wisse LJ, Gittenberger-de Groot AC, Feng Q, Goumans MTH, VanMunsteren JC, Jongbloed MRM, DeRuiter MC. Bicuspid aortic valve formation: Nos3 mutation leads to abnormal lineage patterning of neural crest cells and the second heart field. Dis Model Mech. 2018 Oct 19;11(10):dmm034637. doi: 10.1242/dmm.034637. PMID: 30242109; PMCID: PMC6215433.

**Peterson JC**, Wisse LJ, Wirokromo V, van Herwaarden T, Smits AM, Gittenberger-de Groot AC, Goumans MTH, VanMunsteren JC, Jongbloed MRM, DeRuiter MC. Disturbed nitric oxide signalling gives rise to congenital bicuspid aortic valve and aortopathy. Dis Model Mech. 2020 Sep 28;13(9):dmm044990. doi: 10.1242/dmm.044990. PMID: 32801116; PMCID: PMC7541347.

Gittenberger-de Groot AC, **Peterson JC**, Wisse LJ, Roest AAW, Poelmann RE, Bökenkamp R, Elzenga NJ, Hazekamp M, Bartelings MM, Jongbloed MRM, DeRuiter MC. Pulmonary ductal coarctation and left pulmonary artery interruption; pathology and role of neural crest and second heart field during development. PLOS ONE. 2020 May 15;15(5):e0228478. doi: 10.1371/journal.pone.0228478. PMID: 32413023; PMCID: PMC7228067.

Honkoop H, de Bakker DE, Aharonov A, Kruse F, Shakked A, Nguyen PD, de Heus C, Garric L, Muraro MJ, Shoffner A, Tessadori F, **Peterson JC**, Noort W, Bertozzi A, Weidinger G, Posthuma G, Grün D, van der Laarse WJ, Klumperman J, Jaspers RT, Poss KD, van Oudenaarden A, Tzahor E, Bakkers J. Single-cell analysis uncovers that metabolic reprogramming by ErbB2 signaling is essential for cardiomyocyte proliferation in the regenerating heart. Elife. 2019 Dec 23;8:e50163. doi: 10.7554/eLife.50163. PMID: 31868166; PMCID: PMC7000220.

Gjini E, Jing CB, Nguyen AT, Reyon D, Gans E, Kesarsing M, **Peterson JC**, Pozdnyakova O, Rodig SJ, Mansour MR, Joung K, Look AT. Disruption of asxl1 results in myeloproliferative neoplasms in zebrafish. Dis Model Mech. 2019 May 7;12(5):dmm035790. doi: 10.1242/dmm.035790. PMID: 31064769; PMCID: PMC6550042.

Plomp, E. and Peterson, JC. IsoMAPNL, v1.0.0, Zenodo. 2020. doi: zenodo.3941066.



#### **Curriculum Vitae**

Joshua C. Peterson was born on March 10th, 1990 in Utrecht, The Netherlands. In 2007 he was accepted at the Institute for Life Science & Chemistry at the Hogeschool Utrecht where he specialized in Biomolecular Research. After completing a primary internship at the Dutch Cancer Institute - Antoni van Leeuwenhoek hospital (NKI-AVL) under the supervision of Kees Jalink, and a secondary intership at the Hubrecht Institute in the lab of Niels Geijsen he obtained his BSc in 2011. He continued his studies by enrolling into the master program, Cancer Genomics and Developmental Biology at the University of Utrecht that same year. After completing a secondary research project at the Hubrecht Institute in the group of Jeroen Bakkers, and a minor research project at Dana-Farber Cancer Institute in Boston MA, United States he successfully completed his master program in 2014. Later that year Joshua started a Ph.D. project in the group of Prof. dr. Marco C. de Ruiter at the department of Anatomy and Embryology at the Leiden Medical Center (LUMC), Netherlands. His research focused University understanding the role of developmental cell lineage dynamics that underly bicuspid aortic valve disease. The results of this work are described in this thesis. He took an opportunity to build experience as an executive secretary of the animal welfare body at LUMC. Currently, he is working as an bioinformatician at the lab of Alexander van Oudenaarden at the Hubrecht Institute. The Netherlands.



